

UNIVERSITÀ DEGLI STUDI DI NAPOLI FEDERICO II
DIPARTIMENTO DI FARMACIA



DOTTORATO DI RICERCA IN
“SCIENZA DEL FARMACO”
XXVI CICLO 2011/2014

*Characterization of new bioactive natural products from
marine sources as pharmaceutical tools and lead compounds
in drug discovery processes*

Dott.ssa Filomena D’Aniello

Tutor

Prof.ssa Marialuisa Menna

Coordinatore

Prof. ssa M.V. D’Auria

INDEX

Abstract (English)	page 4
Abstract (Italian)	page 6
Publication of the candidate during the Ph.D. period	page 8
INTRODUCTION	page 9
CHAPTER 1 – THE MARINE ENVIRONMENT	page 13
References	page 17
CHAPTER 2 – METHODOLOGY IN ISOLATING AND CHARACTERIZING MARINE NATURAL PRODUCTS	page 18
2.1. Isolation procedures	page 18
2.2. Structural determination methods	page 19
2.2.1 Mass Spectrometry	page 20
2.2.2 Nuclear Magnetic Resonance	page 22
2.2.3 Circular Dichroism	page 23
2.2.4 Computational methods for configuration determination	page 24
References	page 26

CHAPTER 3 – RESULTS AND DISCUSSION	page 27
3.1. Chemical and pharmacological characterization of new bioactive compounds from marine invertebrates	page 27
3.1.1 Tetracyclic cytotoxic meroterpenes from the Mediterranean ascidian <i>Aplidium conicum</i>	page 29
3.1.2 New bioactive alkyl sulfates from the ascidians <i>Ciona edwardsii</i> and <i>Aplidium elegans</i>	page 36
3.1.3 Phallusiasterols A, B and C: three new sulphated sterols from the Mediterranean tunicate <i>Phallusia Fumigata</i> and their effects as modulators of the PXR receptor	page 41
3.1.4 Phosphoeleganin, a new cytotoxic phosphopolyketide from the ascidian <i>Sidnyum elegans</i>	page 53
3.1.5 . Investigation of the Mediterranean sponge <i>Axinella polypoides</i> : isolation of a new cyclonucleoside and a new betaine	page 58
3.1.6 Conclusions	page 63
3.2. The stereochemistry assignment: a hard challenge in natural products research.....	page 65
3.2.1 Absolute configuration of axibetaine through ab initio calculations.....	page 66
3.2.2 Ab initio calculations to determine the stereochemistry and the regiochemistry of conithiaquinone A	page 68
3.2.3 Determination of phosphoeleganin stereochemistry by NMR and microscale derivatization studies.....	page 70
3.2.4 Conclusions.....	page 74
3.3 Natural quinones as lead compounds in drug discovery processes...page 75	
3.3.1 Synthesis of structurally simplified analogues of aplidinone B	page 77
3.3.2 Potential of quinones as antimalarial agents.....	page 82
3.3.3 Conclusions.....	page 85

3.4. From the macroscopic to the microscopic world: the habitat of microorganisms.....	page 86
3.4.1 History of microbial drug discovery.....	page 86
3.4.2 Cytotoxic quinazolinone isolated from the fungus <i>penicillium sp</i> endogenous with the mangrove <i>Bruguiera gymnorrhiza</i>	page 87
References	page 90

CHAPTER 4 – EXPERIMENTAL.....	page 98
4.1. <i>Aplidium conicum</i>	page 98
4.2 <i>Ciona edwardsii</i> and <i>Aplidium elegans</i>	page 101
4.3 <i>Phallusia fumigata</i>	page 103
4.4 <i>Sydnium elegans</i>	page 108
4.5 <i>Axinella polypoides</i>	page 109
4.6 Synthesis of quinone derivatives.....	page 111
References.....	page 116

CHAPTER 5 – SUPPORTING DATA.....	page 117
5.2 Mass spectra.....	page 118
5.3 NMR spectra.....	page 124
5.4 Computational details of conithiaquinones A and B.....	page 158
5.6 Computational details of compound 28.....	page 166

ABSTRACT

Natural products have historically been a rich source of “lead compounds” in drug discovery. The investigation of terrestrial plants and marine organisms aimed at searching new biologically active compounds is a central issue of this kind of studies, through structure elucidation combined with biological tests. My research activity has been mainly devoted to the discovery and to the chemical and pharmacological investigation of new bioactive natural products as “lead compounds” in the area of antitumor, anti-inflammatory and antimalarial activities. My research work, described in this PhD thesis, was organized in two different topics, i) isolation and structural characterization of bioactive secondary metabolites from marine invertebrates; ii) synthesis of quinones derivatives endowed with cytotoxic and antimalarial activities from natural lead compounds. The fulfilment of my research project required the use of different procedures of isolation and extraction. The chemical characterization of the isolated compounds has been performed through an extensive spectroscopic analysis (UV, IR, ECD, 1D and 2D NMR) together with mass spectrometry and computational methods. I have also used synthetic methods both for the chemical derivatization of the isolated molecules and for the preparation of analogues on the simplified model of natural molecules.

During the course of research conducted during the PhD course and whose results are reported in the following thesis, I have dealt with the extraction and chemical analysis of different species of sea squirts (*Aplidium conicum*, *Ciona edwardsii*, *Aplidium elegans*, *Phallusia fumigata* and *Sidnyum elegans*) and of the sponge *Axinella polypoides*. This analysis led to the isolation of new molecules, which are structurally different, with interesting bioactivity. Among these, two new meroterpenes, conithiaquinones A and B, and three alkyl sulphates with cytotoxic properties. Three sulfated sterols, phallusiasterols A-C, one of them with agonist activity on the pregnane X receptor (PXR) in HepG2 cells. The phosphoeleganin, a potent inhibitor of protein tyrosine phosphatase 1B (PTP1B). An analysis of the metabolic content of the sponge *Axinella polypoides* has provided important chemotaxonomic information about the organism, in addition, led to the isolation of a new

betaine and a new cyclonucleoside. Within the study of compounds with antimalarial activity, in collaboration with the University of Rome La Sapienza and the Department of Public Health, Microbiology and Virology, University of Milan, I have performed the synthesis and evaluation of in vitro on strains of *Plasmodium falciparum* D10 (chloroquine-sensitive) and W2 (chloroquine-resistant) of synthetic analogues of natural quinones, prepared on the pattern of two natural molecules previously isolated from an ascidian. The synthetic derivatives showed significant antimalarial activity and were also highlighted some structural requirements that are critical for the activity. Finally, during the period of research at the Institute of Materia Medica (SIMM) in Shanghai, I started to study lipid-soluble extract of a fungal strain *Penicillium sp*, isolated from the Chinese mangrove *Bruguiera gymnorrhiza*. The analysis showed that the main component of the extract is a cytotoxic alkaloid, 2-(1-hydroxyethyl)-4 (3H) quinazolinone, which is currently subject to a broader drug screening.

ITALIAN ABSTRACT

Le sostanze naturali sono da sempre una ricca fonte di composti guida per la scoperta di nuovi farmaci. Lo studio chimico di piante terrestri e organismi marini attraverso la determinazione stereostrutturale di nuovi metaboliti in combinazione con la valutazione della loro attività biologica costituisce il fulcro della Chimica delle Sostanze Naturali. Durante il corso di Dottorato, la mia attività di ricerca si è sviluppata principalmente nel settore delle sostanze organiche naturali di origine marina. Lo scopo della ricerca è stato l'identificazione di nuovi potenziali "leads" per la terapia antitumorale, antinfiammatoria e antimalarica. L'attività di ricerca si è articolata in due linee parallele, i) analisi chimica di invertebrati marini (tunicati, poriferi) finalizzata all'isolamento ed alla caratterizzazione di nuove molecole bioattive; ii) sintesi di derivati chinonici con attività pro-apoptotica ed antimalarica a partire da lead compounds di origine naturale.

La realizzazione del progetto di ricerca ha comportato l'utilizzo di diverse metodiche di estrazione e di isolamento (es. tecniche cromatografiche quali MPLC o HPLC). La caratterizzazione chimica dei composti isolati è stata realizzata mediante analisi spettroscopica (UV, IR, ECD e, soprattutto, NMR mono- e bidimensionale) combinata con spettrometria di massa e metodi computazionali. Sono state utilizzate metodiche sintetiche sia per la derivatizzazione chimica delle molecole isolate che per la preparazione di analoghi semplificati sul modello di molecole naturali.

Nel corso dell'attività di ricerca condotta durante il corso di Dottorato e i cui risultati sono riportati nella seguente tesi, mi sono occupata dell'estrazione e dell'analisi chimica di diverse specie di ascidie (*Aplidium conicum*, *Ciona edwardsii*, *Aplidium elegans*, *Phallusia fumigata* e *Sidnyum elegans*) e della spugna *Axinella polypoides*. Tale analisi ha portato all'isolamento di nuove molecole, strutturalmente diverse, con interessanti bioattività. Tra queste, due nuovi meroterpeni, i conitiachinoni A e B, e tre alchilsolfati con proprietà citotossiche. Tre steroli solfatati, i phallusiasteroli A-C, di cui uno con attività agonista sul recettore X del pregnano (PXR) in cellule HepG2. La fosfoelegantina, un fosfo-polichetide potente inibitore della proteina tirosin-fosfatasi 1B (PTP1B). L'analisi del contenuto metabolico della spugna *Axinella*

polypoides ha fornito importanti informazioni di natura chemio-tassonomica sull'organismo; inoltre, ha portato all'isolamento di una nuova betaina e di un nuovo ciclonucleoside.

Nell'ambito dello studio di composti ad attività antimalarica, in collaborazione con l'Università di Roma La Sapienza e con il Dipartimento di Sanità pubblica, Microbiologia e Virologia dell'Università di Milano, ho effettuato la sintesi e la valutazione dell'attività in vitro sui ceppi di *Plasmodium falciparum* D10 (cloroquina-sensibile) e W2 (cloroquina-resistente) di analoghi sintetici di natura chinonica, preparati sul modello di due molecole naturali precedentemente isolate da un'ascidia. I derivati sintetici hanno mostrato una significativa attività antimalarica e sono stati messi in evidenza anche alcuni requisiti strutturali che sono critici per l'attività. Infine, durante il periodo di ricerca presso l'Istituto di Materia Medica (SIMM) di Shanghai, ho iniziato lo studio dell'estratto liposolubile di un ceppo fungino *Penicillium* sp, isolato dalla mangrovia cinese *Bruguiera gymnorrhiza*. L'analisi ha evidenziato che il componente principale dell'estratto è un alcaloide citotossico, il 2-(1-idrossietil)-4(3H)chinazolinone, che è attualmente sottoposto ad un più ampio screening farmacologico.

Publications of the candidate during the Ph.D. period

1. Menna, M.; Aiello, A.; D'Aniello, F.; Fattorusso, E.; Imperatore, C.; Luciano, P.; Vitalone, R. Further Investigation of the Mediterranean Sponge *Axinella polypoides*: Isolation of a New Cyclonucleoside and a New Betaine. *Mar. Drugs* **2012**, *10*, 2509-2518.
2. Imperatore, C.; Aiello, A.; D'Aniello, F.; Luciano, P.; Vitalone, R.; Meli, R.; Mattace Raso, G.; Menna, M. New Bioactive Alkyl Sulfates from Mediterranean Tunicates. *Molecules* **2012**, *17*, 12642-12650.
3. Menna, M.; Aiello, A.; D'Aniello, F.; Fattorusso, E.; Imperatore, C.; Luciano, P.; Vitalone, R.; Irace, C.; Santamaria, R. Conithiaquinones A and B, novel tetracyclic cytotoxic meroterpenes from the Mediterranean ascidian *Aplidium conicum*. *Eur. J. Org. Chem.* **2013**, 3241-3246.
4. Menna, M.; Imperatore, C.; D'Aniello, F.; Aiello, A. Meroterpenes from marine invertebrates: structures, occurrence, and ecological implications. *Mar. Drugs* **2013**, *11*, 1602-1643.
5. Imperatore, C.; D'Aniello, F.; Aiello, A.; Fiorucci, S.; D'Amore, C.; Sepe, V.; Menna, M. Phallusiasterols A and B: two new sulfated sterols from the Mediterranean tunicate *Phallusia fumigata* and their effects as modulators of the PXR receptor. *Mar. Drugs* **2013**, *IN PRESS*
6. Imperatore, C.; Aiello, A.; D'Aniello, F.; Luciano, P.; Vitalone, R.; Irace, C.; Santamaria, R.; Jia, L.; Guo, Y.; Menna, M. Isolation, Structure elucidation, and stereochemistry of Phosphoeleganin, a cytotoxic phosphopolyketide from the Mediterranean Ascidian *Sidnyum elegans*, **2014** *IN ELABORATION*

INTRODUCTION

The use of natural products has been up to now the most successful way to the discovery of new medicines. Approximately one-third of the top-selling drugs in the world are natural products or their derivatives; well-known examples of valuable natural products widely used in medical and animal health industries include erythromycin (antibiotic), amphotericin B (fungicidal agent), cyclosporine A and FK506 (immunosuppressive agents), lovastatin (anticholesterolemic agent); as many as 25% of the currently used anticancer drugs are natural chemicals, with another 25% coming from synthetic derivatives of natural products.^{1,2}

Today, with the continuing need for novel drug-like lead compounds against an increasing number of ever-more challenging molecular targets, the availability of rich libraries of chemically diverse molecules is an essential requirement. The remarkable chemical diversity encompassed by the natural products is still relevant in the field of the discovery of new and more effective drugs. In most of the cases the natural metabolite is mainly considered a suitable chemical platform useful to project new molecular entities able to modulate biological activity rather than a real therapeutic agent.

Nowadays, drug discovery has entered a more highly competitive era in which the quality of chemical collections and the time taken from assay to drug development are crucial factors. Thus, although the chemical novelty associated with natural products is higher than that of any other source, this diversity must be accessed more efficiently and effectively. Currently, most of the new drugs are discovered on the basis of a molecular approach, which can be performed not only through the rational drug design aided by computer based techniques or through the manipulation of genetic targets (antisense approach), but also through the pragmatic approach of random screening. This last approach to drug discovery, which is also called combinatorial biology, has been updated by the recent developments in molecular biology, instrumentation technology and information, so that it can now be carried out at high throughputs that could not have been imagined, even a few years ago.³⁻⁶

The increasing availability of new molecular targets, the potential to transform them by genetic engineering, such as the simplification of the de-replication processes

through the use of clones, make random screening a very promising tool to the discovery of novel bioactive compounds; a further not marginal improvement comes from the use of robotics to conduct the assays. Currently, wide-ranging assays can be quickly carried out by using micro plates equipped with numerous wells. Recent advances in random screenings enabled enormous increases in throughput to be achieved, but, on the other hand, they posed some problems in order to be conveniently applied. A high-throughput screening program requires the availability of large numbers of compounds for testing which have to be structurally different in order to increase the chance of finding activity at the molecular target. This requirement cannot be supplied by traditional organic synthesis and so, over the past few years, new approaches, such as combinatorial chemistry and computer-based molecular modelling design have become the source of new levels of chemical diversity. Initially, they seemed to lower the natural products value in drug discovery; however, as the use of these techniques has matured, it became clear that they achieved significant importance mainly in the generation of focused libraries for specific discovery programs.³ Indeed, combinatorial chemistry has failed to supplant natural products programs as the primary source of broad chemical diversity and it is now clear that combinatorial chemistry practiced by Nature is much more sophisticated than that in the laboratory, yielding elaborate structures rich in stereochemistry, concatenated rings and reactive functional groups. As a result, an amazing number of products have been found in nature, with peculiar structures and biological activities.

The present thesis aims to illustrate the results obtained from of my PhD research program, which indeed is grounded in the natural product chemistry field. My research activity has been mainly devoted to the discovery of new bioactive natural products as “lead compounds” in the area of antiviral, antitumor, anti inflammatory and antimalarial activities.

The road map for reaching this goal has been to follow a two-way course. The first one was the isolation and pharmacological characterization of new molecules with biological activity from terrestrial and marine organisms, which have been selected on the basis of their presumed content in bioactive metabolites. The second way was the optimization of natural leads under study through de novo synthesis and/or structural modifications. Our efforts have been directed towards both the total

synthesis, and the design of new simplified analogues obtained through the implementation of innovative synthetic procedures and parallel synthesis approaches. Selected collections of both natural and synthetic compounds have been submitted to pharmacological tests. The synthetic work, the analysis of the structure-activity relationship and the pharmacological evaluation of the new natural compounds and of their synthetic derivatives have been obtained through the active collaborations with selected national or foreign research groups from both industries and academia. This research activity led to the isolation of several bioactive molecules, some of them being new compounds. Their different structures, ranging from simple linear polyfunctionalized alkyl chains to complex polycyclic frameworks, contributed to enlarge the chemical diversity generated into natural products of marine origin. On the other hand, the synthetic studies performed using previously isolated marine natural compounds led to the identification of molecules with significant antimalarial activity and also highlighted some structural requirements critical for this activity. The research exemplified the potential of a natural product to qualify as lead structure for medicinal chemistry campaigns, affording simplified analogues with better bioactivity and easier to synthesize.

References

1. O'Neill, M.; J.A. Lewis in *Human Medicinal agents from Plants*, Kinghorn, A. D., Balandrin, M. F., Eds.; ACS Symposium Series 534; American Chemical Society: Washington, D. C., **1993**, 48.
2. Cragg, G.M.; Newmann, D. J.; Snader K.M. *J. Nat. Prod.*, **1997**, *60*, 52.
3. Silva, C.J.; Brian, P.; Peterson T. *Drugs and the Pharmaceutical Sciences*, **2002**, *114*, 357.
4. Harvey, A.L. *Trends in Pharm. Sci.***1998**, *20*, 196.
5. Strohl, W.R. *Drug Discovery Today*, **2000**, *5*, 39.
6. Harvey, A.L. *Drug Discovery Today*, **2000**, *5*, 294.

CHAPTER 1

THE MARINE ENVIRONMENT.

That nature represents an endless arsenal of new bioactive molecules has been recognized since ancient times and the study of these metabolites has historically proven of immense benefit in the drug discovery process. Some of these bioactive molecules have become life-saving drugs or biomedical tools. The history of terrestrial natural products chemistry can readily be traced back to the beginning of the XIX century with the first investigation of terrestrial plants aimed at finding the molecules responsible of the biological activities of the extracts. This is in distinct contrast to the natural products chemistry associated with marine species which has emerged only over the past 65 years mainly as a result in the improvement of collection techniques, as SCUBA diving. The marine environment contains a number of plants, animals and microorganisms, which, due to the unique adaptations to their habitat, elaborate a wide diversity of natural products with specific bioactivities. These products provide a rich source of chemical diversity that can be used to design and develop new potentially useful therapeutic agents. The exceptional marine reservoir represents a vast chemical and biological diversity of molecules, some without terrestrial counterpart or analogy, and often showing unique biological activities at extremely low concentration.

Assessment of the chemical diversity contained in the oceans thus began in the fifties but now is an established field with a great deal of research focused on extraction of chemicals from sessile invertebrates, such as sponges, molluscs and ascidians. These organisms live in a complex and highly competitive environment and produce a wide variety of toxic chemicals in order to mediate spatial competition as well as to prevent parasitism and predation. All marine organisms have provided a seemingly endless parade of very unusual novel structures; biogenetically, they can be included in the major biosynthetic pathways proposed for terrestrial secondary metabolites whereas, structurally, they often possess functional groups appearing uniquely or predominantly marine. Particularly, ascidians' chemistry is dominated by the presence of nitrogenous metabolites. Through the combined efforts of marine natural

product chemists and pharmacologists, a number of promising compounds have been identified and some of them are either already at advanced stages of clinical trials or have been selected as promising candidates for extended pre-clinical evaluation. Most of these products fall within the area of cancer therapy; the case of the marine alkaloid ecteinascidin 743 (ET-743), an anti-tumour compound especially effective against solid tumours, is an illustrative example.¹

On the other hand, research on molecules of marine origin has evolved relatively slowly, mainly due to the small quantities of the living material which generally could be obtained by collecting the marine species by hand. It is very common to isolate less than one milligram of a bioactive substance from one kilogram of the marine organism. However, more sensitive methods of NMR spectroscopy and mass spectrometry combined with advanced liquid chromatography techniques are currently routinely used for identification and characterization of natural products and, so, also complex molecular structures can be now solved with much less than one milligram of compounds. Chemical identification of the molecules present in biological extracts is just one step of their full investigation; particularly an interesting aspect is the individuation of their real producers. The extremely rich secondary metabolism of some marine invertebrates can be explained in the light of the evidence that marine invertebrates harbour microorganisms, such as bacteria, cyanobacteria and fungi, in their tissues, where they reside in the extra- and intra-cellular spaces. In some cases, associated micro organisms may constitute up to a 40% of the biomass, as it has been evidenced for the Mediterranean sponge *Aplysina aerophoba*.²⁻⁵ In fact, sponges possess amoeboid cells that phagocytose bacteria and, at the same time, are efficient filter feeders; as a result of such a continuous functional activity, a certain amount of transient microorganisms (one ml of seawater contains an estimated one million microbes) are trapped within the vascular system or remain attached to sponge surface. In *A. aerophoba*, the bacterial concentration exceeds that of the surrounding seawater by two or three orders of magnitude. The relations between marine invertebrates and microorganisms living either permanently or temporarily inside have been currently understood to a very limited extent. Recent studies based on feeding experiments with different species of sponge bacteria suggest that the organism can differentiate between commensal bacteria and those permanently associated with the host. Interestingly, 16S rDNA diversity studies

revealed that sponges belonging to the same species but collected from different seas and at different depth showed a significantly uniform microbial community. Several roles are believed to be played by the retained microorganisms: they serve as food and enrich the diet of their hosts through nitrogen and carbon fixation. In addition, quite likely they are involved in the biosynthesis of natural products recovered from the sponges.⁶ Consequently, the permanent bacterial presence is undoubtedly not irrelevant for the exceptional chemodiversity of invertebrates, but the real contribution of the microorganisms to the host secondary metabolism has not yet been fully understood and evaluated; this is essentially due to the failure of most attempts to culturing permanently the sponge-associated bacteria outside their host. However, often there are evidences that suggest the involvement of associated microorganisms in the biosynthesis of compounds collected from the invertebrate host. This happens when one organism is shown to contain an unusual variety of classes of metabolites, when the metabolite concentrations are exceedingly low, or when the structures of the metabolites are reminiscent of bacterial biogenetic pathways. Thus, the major reason for marine natural products unique molecular diversity likely resides in the marine environmental conditions, which favour close and permanent associations between different organisms.

The limited availability of most bioactive compounds elaborated by marine invertebrates currently does not represent a serious obstacle for their structure determination as well as for preliminary biological tests. Problems actually arise when preliminary positive assays refer the product for a more advanced investigation. They can be easily overcome, if the research continues using the molecule as a lead; in this case, preliminary information on the structure-activity relationships often can be obtained taking advantage from the frequent co-occurrence of a series of closely related compounds rather than a single example of a compound type. The presence of a pool of analogues is probably a chemical defence strategy, by which the organism is protected against an array of organisms, since resistance against a broad range of compounds with similar structures is less likely to occur. The various compounds may display synergism in their biological activity and this property may be of interest for drug development.

The limited availability of a natural compound often prevent the research aimed to its direct use in therapy, which develops according to the usual procedure, involving

first the assays *in vivo*, followed by preclinical evaluations and then by clinical trials, where gram quantities are needed. The supply of a natural product becomes a large-sized, very often insoluble, problem, when it is licensed, as drug and an economically convenient synthesis cannot be carried out. The industrial use of marine species requires large amounts of raw material to be collected from natural stocks. This collection will, in the long run, exert significant impacts on the benthic community and will be a severe pressure on the targeted species. The production of sponges, tunicates and bryozoans in specially designed mari-culture plants has been considered. Currently, a number of multidisciplinary researches are targeting the development of new technologies for mari-culture plants of marine invertebrates for the environmentally compatible production of pharmaceutical relevant species. Even if the obtained yields of biomass are still far from those that should be needed for commercial purposes, encouraging progress has been made in this field and now the bryozoan *B. neritina* and the tunicate *E. turbinata*, the sources of ET-743 and of bryostatins, respectively, can be successfully cultured.⁷

The possible microbial origin of bioactive molecules recovered from marine invertebrates recently opened new and interesting perspectives for their synthesis at commercial level. Isolation and cultivation of the suspected microbial producers either from the surrounding seawater or from tissue of invertebrates could provide a more satisfying answer to the pressing supply problem. If bacteria are indeed, the producers of bioactive metabolites of interest, transfer of the gene clusters responsible for the biosynthesis of the respective natural products to a vector suitable for large-scale fermentation could provide an alternative strategy thereby avoiding the foreseeable difficulties in culturing symbiotic bacteria.

In conclusion, it is clear that marine environment will continue to be a major source of new drug leads but effective utilization of these resources will require advances in technologies and the opening of new frontiers in science. The increasing genomic information and progress in molecular biology in general, combined with biochemical studies leading to a comprehensive understanding of complex natural product biosynthesis at the molecular level, as well as technologies exploiting this knowledge, are expected to give marine natural products research a promising future.

References

1. Valoti, G.; Nicoletti, M.I.; Pellegrino, A.; Jimeno, J.; Hendriks, H.; D'Incalci, M.; Faircloth, G.; Gavazzi, R. *Cli. Can. Res.*, **1998**, *4*, 1977.
2. Vacelet, J. *J. Microscop.*, **1971**, *12*, 363.
3. Wilkinson, C.R. *Mar. Bio.*, **1978**, *49*, 161.
4. Wilkinson, C.R. in *Algae and Symbioses*, Reisser, W. Ed., Biopress: Bristol, **1992**, 112-151.
5. Vacelet, J.; Donadey, C. *J. Exp. Mar. Ecol.*, **1977**, *30*, 301.
6. Kobayashi, J.; Ishibashi, M. *Chem. Rev.*, **1993**, *93*, 1753.
7. Mendola, D. in *Drugs from the sea* Fusetani, N. Ed., Kager: Basel, **2000**, 120-133.

CHAPTER 2

METHODOLOGY IN ISOLATING AND CHARACTERIZING MARINE NATURAL PRODUCTS.

The marine environment has many limits, such as the difficulty in the collecting biological material and its identification, but also the necessity to safeguard marine ecology. For these reasons, for the discovery of new compounds from marine source it is important a constant need to separate small quantities of mixture efficiently and then it is necessary to characterize these new compound in a non-destructive way, with sub-milligram samples.

The study of natural compounds consists of some steps:

1. Isolation and purification of new compounds from biologic material;
2. Structural determination of the isolated compounds;
3. Determination of absolute and relative stereochemistry of the new compounds.

2.1. ISOLATION PROCEDURES

The isolation of natural products from natural sources poses numerous problems, because these compounds may only be present in infinitesimal quantities. The nature of separation problems varies considerably, from the isolation of small quantities (milligrams or less) for structure determination purposes to the isolation of very much larger amounts (hundred milligram to gram quantities) for comprehensive biological testing, for semi-synthetic work or even for production of therapeutic agents. For these purposes, a good selection of different techniques and approaches is essential. The problem of separation and isolation of new metabolites from natural sources was solved with the development of refined techniques, such as the various analytical and preparative chromatographic methods. We have successfully performed a procedure of purification. Usually, after biomass extraction with adequate solvents (usually methanol, acetone, and/or chloroform), the first step in the isolation of a natural compound from the main extract consists of a sequential gradient partition with solvents. The fractions so obtained contain compounds

distributed according to their polarity. In the case of bioactive extract, this process can be guided by the appropriate assay to localize the active component. Next, in accordance with the diverse properties of the components of these fractions, different procedures for purification can be followed. Particularly, the fractions of low or medium polarity, usually monitored, contain lipophilic organic compounds that can be usually separated by standard normal or reverse phase column chromatography and/or MPLC and finally HPLC to get individual components.

Medium Pressure Liquid chromatography (MPLC) is a liquid-solid chromatography, in which the liquid mobile phase is forced through the solid stationary phase at medium pressure. MPLC is more efficient in resolution than the open-column and flash chromatography methods and the separation involves a considerable gain in time. The solid stationary phase can be a normal phase, like silica gel or bonded phase (RP-8, RP-18). The technique makes use of pressures of *ca.* 5-40 bar and can easily accommodate much larger sample loads (100 mg-100 g) than are generally applied in other separations. As far as separating power is concerned, MPLC lies somewhere between flash chromatography and semi-preparative HPLC.

High Performance (or High Pressure) Liquid Chromatography (HPLC), both normal-phase and reverse-phase, is the most widely used chromatographic method, and finds application in the preparative separation of samples to “pilot” the preparative isolation of natural products (optimization of the experimental conditions, checking of the different fractions throughout the separation). On the whole, however, HPLC is commonly applied as the last step in purification processes affording pure compounds in high yields, and, in this respect, the quantities involved tend to be at the lower end of the scale.

Finally the compounds, so isolated, are structurally characterized and are submitted to pharmacological assays.

2.2. STRUCTURAL DETERMINATION METHODS

Recently, natural products chemistry has undergone explosive growth due to advances in isolation techniques, synthetic and biosynthetic approaches as well as spectroscopic and chromatographic methods. Structural determination described in this thesis is largely based on spectroscopic techniques, mostly mass spectrometry

(MS) and nuclear magnetic resonance (NMR), and sometimes degradation methods, coupled with circular dichroism (ECD) and computational methods.

2.2.1. Mass Spectrometry

Mass Spectrometry is an analytical technique, particularly used in organic chemistry, which allows to measure molecular masses of unknown compounds and thus to determine their elementary formula. Unlike other spectroscopic techniques, mass spectrometry is a destructive analytical technique, that is not based on the interaction between radiations and matter. Any molecule has first to be ionized and transferred to gas phase in the ion source and then it is transmitted to the mass analyzer where its mass properties are measured. These three fundamental steps of the process occur in three different parts of the mass spectrometer, namely the *ionisation source*, the *analyzer*, and the *detector*. In order to obtain a mass spectrum, in the ion source, must be produced ions in a gas-phase. they are subsequently accelerated, by an electric field, until they get to a specific speed and they are transferred to the mass analyzer, which separate different ions on the base of their mass/charge (m/z) ratio. The separated ions are then measured on the detector and the results displayed.

Most of compounds described in the following chapters have been analyzed by *Electrospray Ionisation* (ESI) mass spectrometry through an *Orbitrap* system.

ESI mass spectrometry allows the determination of non-volatile molecules to be analyzed directly from the liquid phase (**Figure.2.1**). The electrospray process is governed by a large number of chemical and physical parameters that together determine the quality of the process. Its start and end can be defined by an electrical circuit that drives the spray of liquid-charged droplets.

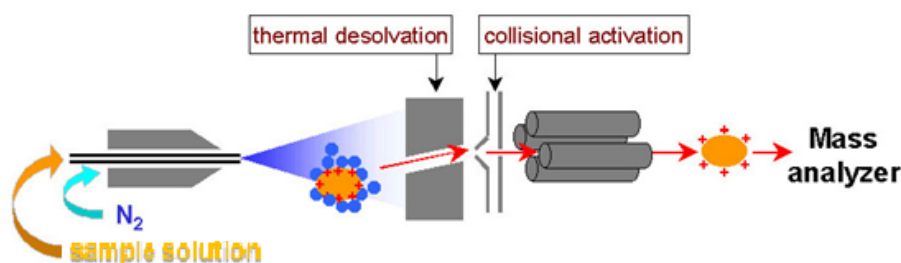


Figure 2.1. ESI mass spectrometry

In this process the biomolecule starts out as an entity or complex, usually charged and dissolved in a water-rich environment. At the end of the process the same biomolecule is represented and harvested through the orifice of a mass analyser as a series of ‘naked’ multicharged ions. In a vacuum, the biomolecular ions then are selectively analysed according to their mass/charge ratio. Because of the electric potential of the capillary, each droplet of the spray carries an excess positive or negative charge, and this causes extensive protonation or deprotonation of the molecules of the sample, which become ions. An uncharged carrier gas such as nitrogen is used to help the liquid to nebulize and the neutral solvent in the droplets to evaporate.

Orbitrap is a new type of mass analyzer introduced by Makarov.¹ The LTQ-Orbitrap combines the most advanced Ion Trap and Fourier Transform technologies into a single instrument with unprecedented analytical power and versatility. The instrument provides a high mass resolution, accurate mass determinations, and MSⁿ for routine high-throughput analysis.

In an orbitrap, ions are injected tangentially into the electric field between the electrodes and trapped because their electrostatic attraction to the inner electrode is balanced by centrifugal forces. Thus, ions cycle around the central electrode in rings. In addition, the ions also move back and forth along the axis of the central electrode. Therefore, ions of a specific mass-to-charge ratio move in rings which oscillate along the central spindle (**Figure 2.2**). The frequency of these harmonic oscillations is independent of the ion velocity and is inversely proportional to the square root of the mass-to-charge ratio (m/z).

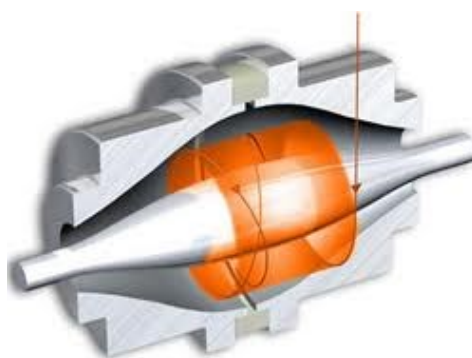


Figure 2.2. Ion trajectories in an Orbitrap mass spectrometer.

By sensing the ion oscillation similar as in the FT-MS (Fourier transform mass spectrometry), the trap can be used as a mass analyzer. Orbitraps have a high mass accuracy (1-2 ppm), a high resolving power (up to 200,000). Currently, there are two commercial LTQ-Orbitrap instruments, the Discovery and XL models. One of the primary differences is that the XL has a linear octopole collision cell (absent in the Discovery model), in which collisional activation and fragmentation can be performed. Although this feature provides additional versatility to MS/MS experiments, the analytical performance and fundamental principles of operation of the Orbitrap analyzers in both instruments are identical.²

2.2.2 Nuclear Magnetic Resonance³⁻⁵

Nuclear Magnetic Resonance spectroscopy is a powerful and theoretically complex analytical tool used for structure elucidation of the isolated secondary metabolites. It involves reorientations of nuclear spins with respect to an applied static magnetic field. In addition to standard ¹H and ¹³C NMR spectra, a large use of 2D NMR experiments has been made in the course of my research activity. They are superior to their 1D NMR counterparts both for the information on the connection of nuclei and for the easier assignment of nuclei resonating in crowded regions of the spectra (signal overlapping is much less likely in two dimensions than in one).

The COSY (COReLation SpectroscopY) experiments allow you to determine the connectivity of a molecule by determining which protons are spin-spin coupled. In spite of the many modifications which have been proposed along the years, the very basic sequence composed of two $\pi/2$ pulses separated by the evolution period t_1 is still the best choice if one is simply dealing with the presence or the absence of a given coupling, but not with the value of the relevant coupling constant.

The HSQC (Heteronuclear Single Quantum Correlation) experiment is 2D NMR heteronuclear correlation experiment, in which only one-bond proton-carbon couplings (¹ J_{CH}) are observed. The HSQC experiment correlates the chemical shift of proton with the chemical shift of the directly bonded carbon.

The HMBC (Heteronuclear Multiple Bond Correlation) experiment is a heteronuclear two-and three-bond ¹H-¹³C correlation experiment; its sequence is less efficient than HSQC because the involved ^{2,3} J_{CH} couplings are smaller (3-10Hz). Moreover, while ¹ J_{CH} are all quite close to each other, ^{2,3} J_{CH} can be very different,

making necessary the optimization of the experiment for each type of coupling. As a consequence, in many HMBC spectra not all of the correlation peaks which could be expected from the structure of the molecule are present. Cross peaks are between protons and carbons that are two or three bonds away while direct one-bond cross-peaks are suppressed. This experiment, finally, allows the connection of the fragments and the assembling of the structure of the molecules.

2.2.3 Circular Dichroism

First-principles calculations of electronic circular dichroism (ECD) are widely used to determine absolute configurations of chiral molecules. Circular Dichroism (CD) is observed when a molecule is optically active, it absorbs right- and left-handed circularly polarized light to different extents. The CD spectroscopy takes advantage of the different absorption shown by chiral compounds of left and right circularly polarized UV/Vis light. Plane polarized light can be viewed as being made up of 2 circularly polarized components of equal magnitude, one rotating counter-clockwise (left handed, L) and the other clockwise (right handed, R). Circular dichroism (CD) refers to the differential absorption of these 2 components (**Figure 2.3**).

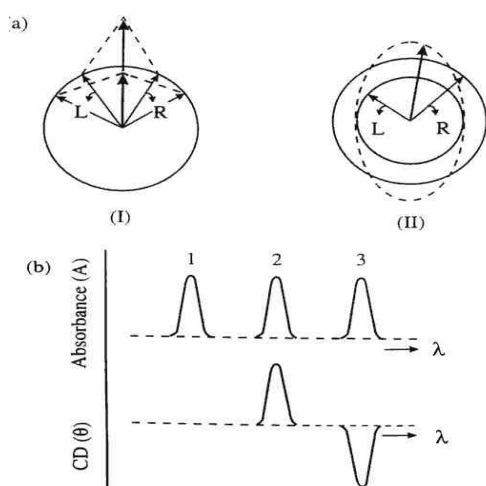


Figure 2.3. Origin of the CD effect. (a) The left (L) and right (R) circularly polarised components of plane polarised radiation: (I) the two components have the same amplitude and when combined generate plane polarised radiation; (II) the components are of different magnitude and the resultant (dashed line) is elliptically polarised. (b) The relationship between absorption and CD spectra. Band 1 is not chiral; band 2 has a positive CD spectrum with L absorbed more than R; band 3 has a negative CD spectrum.

If, after passage through the sample being examined, the L and R components are not absorbed or are absorbed to equal extents, the recombination of L and R would regenerate radiation polarised in the original plane (**Figure 2.3**). However, if L and R are absorbed to different extents, the resulting radiation would be said to possess elliptical polarization (**Figure 2.3**).⁶

In practice, the CD instrument (spectropolarimeter) does not recombine the components but detects the two components separately; it will then display the dichroism at a given wavelength of radiation expressed as either the difference in absorbance of the two components: $\Delta\varepsilon = \varepsilon_L - \varepsilon_R$. $\Delta\varepsilon$ as a function of the incident light frequency ω is called CD spectrum.

The CD of pure enantiomers differs in sign, but not in magnitude. There is no simple relation between the absolute configuration of an enantiomer and the sign of its ECD spectrum: CD depends on details of the electronic and geometric molecular structure. However, *ab initio* electronic structure calculations are nowadays able to predict ECD accurately and thus allow an assignment of the absolute configuration by comparison of experimental and computed ECD spectra.

2.2.4. Computational methods for configuration determination

The increasing improvement of computer performances and the development of methods and algorithms ever more advanced and efficient, has led to the emergence of computational chemistry, a branch of chemistry that uses quantum mechanical principles to get the realistic representation of the three-dimensional structure of a molecule. To determine the conformation of a molecule, using a computer and a process called "minimization", the atoms must be moved from their positions evaluating the resulting changes of the total energy of the system. The geometry corresponding to the minimum energy is the most favored and, therefore, the most representative of the structure in solution. It is thus possible to compare the distances between protons in different stereoisomers and verify which of these corresponds to the spectroscopic data previously obtained. The molecular mechanics provides the force field for every molecule that describe the conformation and behavior of molecules. Force field allows to calculate the energy of each rearrangement of atoms in a system and allows you to evaluate how it changes with the position of the atoms. In this way, it is possible to find the minimum point of this function, determining both conformation and minimum energy.

This process, known as minimization, leads to a relative minimum, while the absolute minimum, in simple cases, can be found with processes known as conformational search (systematic search, random search, simulated annealing). The experimental information on the conformation of the molecule, mainly derived from

NMR experiments (NOE effects) may be included in the force field to "help" to determine the actual conformation at low energy. In simulated annealing method, the molecule is subjected to a molecular dynamics simulation, starting at high temperature and gradually lowering the until get to absolute zero. At low temperatures the molecule is locked the energetically lowest conformer. An alternative and complementary method to molecular dynamics for configuration determination of compounds structurally complex for flexibility or number of stereoisomers, is *ab initio* method that allows the prediction of chemical shifts of protons and carbons by values of coupling constants. Good matching between the calculated chemical shifts for one of the potential structures with the experimental values constitutes an excellent tool to support structural analysis of organic compounds. Density functional theory (DFT) has emerged in recent years as a promising alternative to conventional *ab initio* methods in quantum chemistry. All calculations reported in my thesis have been performed using Gaussian 03.33⁷ while the preliminary conformational search was performed by Simulated Annealing in the INSIGHT II package.

References

1. Hu, Q.; Noll, R. J.; Li, H.; Makarov, A.; Hardmanand, M.; Cooks, R. G.; *J. Mass Spectrom.*, **2005**, *40*, 430–443.
2. Perry, R. H.; Cooks, R. G.; Noll, R. J.; *Mass Spectrometry Reviews*, **2008**, *27*, 661– 69.
3. Bax, A.; Two Dimensional Nuclear Magnetic Resonance in Liquids, Delft University Press, Dordrecht, **1982**.
4. Palmer III, A. G.; Cavanagh, J.; Wright, P. E.; Rance, M.; *J. Magn. Reson.*, **1991**, 151-170.
5. Bax, A.; Summers, M. F.; *J. Am. Chem. Soc.*, **1986**, 2093.
6. Kelly, S. M.; Price, N.C.; *Current Protein and Peptide Science*, **2000**, *1*, 349-384.
7. Gaussian 03-Revision B05: Frisch, M. J.; Trucks, G. W.; Schlegel, H. B.; Scuseria, G. E.; Robb, M. A.; Cheeseman, J. A.; Montgomery, Jr., J. A.; Vreven, T.; Kudin, K. N.; Burant, J. C.; Millam, J. M.; Iyengar, S. S.; Tomasi, J.; Barone, V.; Mennucci, B.; Cossi, M.; Scalmani, G.; Rega, N.; Petersson, G. A.; Nakatsuji, H.; Hada, M.; Ehara, M.; Toyota, K.; Fukuda, R.; Hasegawa, J.; Ishida, M.; Nakajima, T.; Honda, Y.; Kitao, O.; Nakai, H.; Klene, M.; Li, X.; Knox, J. E.; Hratchian, H. P.; Cross, J. B.; Bakken, V.; Adamo, C.; Jaramillo, J.; Gomperts, R.; Stratmann, R. E.; Yazyev, O.; Austin, A. J.; Cammi, R.; Pomelli, C.; Ochterski, J. W.; Ayala, P. Y.; Morokuma, K.; Voth, G. A.; Salvador, P.; Dannenberg, J. J.; Zakrzewski, V. G.; Dapprich, S.; Daniels, A. D.; Strain, M. C.; Farkas, O.; Malick, D. K.; Rabuck, A. D.; Raghavachari, K.; Foresman, J. B.; Ortiz, J. V.; Cui, Q.; Baboul, A. G.; Clifford, S.; Cioslowski, J.; Stefanov, B. B.; Liu, G.; Liashenko, A.; Piskorz, P.; Komaromi, I.; Martin, R. L.; Fox, D. J.; Keith, T.; Al-Laham, M. A.; Peng, C. Y.; Nanayakkara, A.; Challacombe, M.; Gill, P. M. W.; Johnson, B.; Chen, W.; Wong, M. W.; Gonzalez, C.; Pople, J. A. *Gaussian03W, Revision B05*, Inc., Wallingford CT, **2004**.

CHAPTER 3

RESULTS AND DISCUSSION.

3.1 CHEMICAL AND PHARMACOLOGICAL CHARACTERIZATION OF NEW BIOACTIVE COMPOUNDS FROM MARINE INVERTEBRATES

The world of nature provides a never-ending set of fascinating problems for the chemist. Many of the most intriguing problems, however, concern compounds available in only truly minute quantities. One solution is to focus on bioassay-guided separations. In so doing one can isolate compounds with novel structures or unsuspected activities from almost any phylum, including tunicates, sponges, insects, or plants. Moreover, newer spectroscopic techniques, especially fast atom bombardment mass spectrometry and tandem mass spectrometry, enhance one's ability to study compounds present in minute quantities, including those of importance to the host organism. Traditionally, natural product research usually involved isolating the most abundant compound, assigning its structure, and then hoping to find a use for it. Today we are more likely to be guided by biology, that is, by bioassay, to direct our attention to the truly important compounds present in a species. Most bioassays are exceedingly sensitive, so that the active compound may be present in only minute quantities. Fortunately, modern structural techniques require only miniscule quantities of the material.

Part of my research work is collocated within this area and concerns the investigation of the natural products deriving from marine invertebrates, such as sponges and tunicates. Among marine organisms, the chance of finding bioactive compounds is remarkably higher in these invertebrates. Presently, more than 35% of useful medical compounds from the sea are isolated from porifera, well known as sponges.

Sponges, lacking any nervous, digestive, circulatory, muscular systems or any physical defence from their predators, produce secondary metabolites, involved in their chemical defence, which is essential for their survival. In fact many species

contain toxic substances, probably to discourage predators. The chemicals also probably play a role in competition among sponges and other organisms, as they are released by sponges to insure themselves space in the marine ecosystem.

A number of promising compounds have been identified from marine sponges that possess pronounced biological activity and are already at advanced stages of clinical trials, mostly for the treatment of cancer, or have been selected as promising candidates for extended preclinical evaluation.

Recently, ascidians have increasingly become the target of natural products research. In fact, in the last 30 years an incredible surge of interest in ascidian chemistry yielded many new ascidian metabolites. These results, which include structurally unprecedented families of biologically active secondary metabolites, have attracted the attention of both synthetic chemists and pharmacologists.

Ascidians belong to the phylum Chordata, which encompasses all vertebrate animals, including mammals. Therefore, they represent the most highly evolved group of animals commonly investigated by marine natural products chemists. Together with the two other classes included in the subphylum Urochordata (= Tunicata), members of the class Ascidiacea are commonly referred to as tunicates, because their body is covered by a saclike case or tunic, or as sea squirts, because many species expel streams of water through a siphon when disturbed. While adult ascidians are exclusively marine invertebrates and bear little resemblance to the other chordates, their larvae resemble amphibian tadpoles and contain notochords, dorsal hollow nerve cords, and pharyngeal slits, all of which are lost during development. There are roughly 2000 living species of tunicates, of which ascidians are the most abundant. Adult ascidians are sessile filter feeders, either solitary or colonial, and live preferentially in regions which are free from extensive wave shock, but receive considerable freely flowing sea water. Ascidian morphology is diverse. Solitary tunicates may be up to 15 cm in length, or as small as 1 cm. Colonial species are often found encrusting rocks and may be extremely thin and delicate, or as thick as 5 cm. Some are of undefined shape, and so disguised by their tunic that they superficially resemble sponges or fleshy coelenterates, yet the contractions which cause a sea squirt to spray streams of water provide the inexperienced observer with a means to distinguish tunicates from other marine invertebrates.

3.1.1 *Tetracyclic cytotoxic meroterpenes from the Mediterranean ascidian *Aplidium conicum**

Since the discovery by Fenical in 1976 of geranylhydroquinone in an unidentified species of *Aplidium*,¹ many diverse meroterpenes, have been isolated from ascidians. These compounds form a class of complex metabolites derived from a mixed terpenoid-polyketide biosynthetic pathway which display a wide range of structural diversity. A large number of meroterpenes have been isolated so far from marine ascidians, almost exclusively belonging to the *Aplidium* genus; their carbon skeletons originate from intra- and intermolecular cyclizations and/or rearrangements of the terpene chains to give unique polycyclic or macrocyclic structures, often linked with diverse functionalities.² The Mediterranean species *A. conicum* has been extensively studied; the peculiarity of this ascidian is that the nature and/or the abundance of its meroterpenes content apparently depends on the geographical place of collection. Specimens of *A. conicum* collected off Tarifa Island, in Spain, were shown to contain geranyl hydroquinone, a number of its hydroxylated and/or cyclized analogues as well as the relevant chromenols.³ From samples of the same ascidian, collected in Italy along Sardinia coasts, a large group of new meroterpenes, with different polycyclic skeletons but all featuring an unusual dioxo-thiazine ring condensed to a benzoquinone ring have been isolated.⁴⁻⁶ The geographical variation of *A. conicum* metabolic content is now highlighted by the results I obtained by analyzing another specimen of the ascidian collected along southern Italy coasts (Porto Cesareo, Lecce). I have isolated two novel meroterpenes, conithiaquinones A and B (**1** and **2**), in addition to the two chromenols (**3** and **4**) and conicaquinones A and B (**5** and **6**) found in the previously investigated samples of *A. conicum*. The new molecules have been characterized using standard spectroscopic techniques as well as on the basis of quantum mechanical chemical shift calculations, as I will discuss in the paragraph 3.2.2.

Both conithiaquinones A and B were assayed for their effect on human skin keratinocyte (HaCaT line) and human breast adenocarcinoma (MCF-7 line) cells growth and viability in vitro, demonstrating a moderate cytotoxicity but especially directed against the human breast cancer cells (**Figure 3.1**).

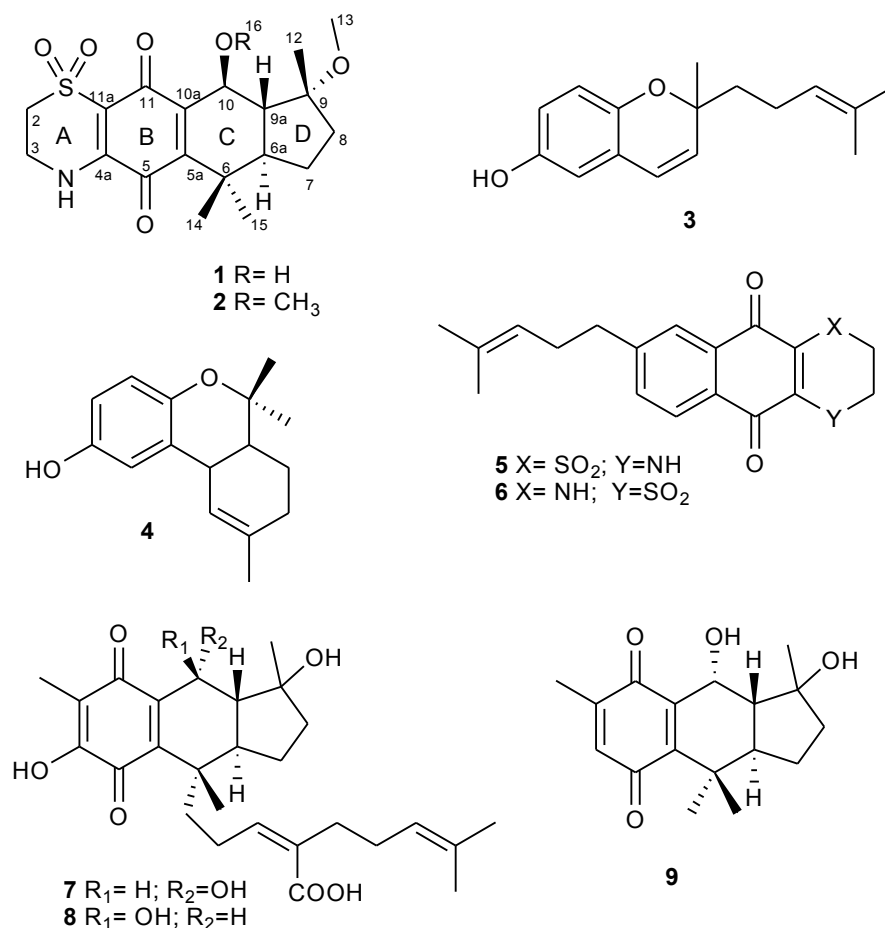


Figure 3.1. Structures of compounds (1-9)

Freshly thawed specimens of *A. conicum* (Olivi, 1792) collected at Porto Cesareo (Lecce, Italy) were exhaustively extracted with methanol and subsequently with chloroform. The concentrated extracts were combined and then partitioned between ethyl acetate and butanol. Medium pressure flash chromatography over a silica gel column of the ethyl acetate soluble portion, followed by extensive HPLC separations of the most polar fractions, afforded conithiaquinones A (**1**) and B (**2**) in the pure state. ESI mass spectrum (positive ion mode) of compound **1** revealed an ion peak at m/z 418.2 corresponding to $[M + Na]^+$. A facile loss of 64 amu was observed in the mass spectrum, attributable to the expulsion of SO₂, and suggested the presence of a sulfone functionality. HRESIMS (positive ions) established a molecular formula of C₁₉H₂₅NO₆S for **1**, indicating eight unsaturation degrees. The ¹³C NMR spectrum

(CD₃OD) revealed the presence of nineteen signals which, on the basis of the data obtained from a HSQC experiment, were sorted as four methyls, four methylenes, three methines, and eight unprotonated carbons. Six carbon resonances were due to sp² quaternary carbons, and two of them, at δ_C 180.5 and 181.5 ppm were assigned to two conjugated carbonyl groups (**Table 3.1**). Thus, **1** must be tetracyclic to satisfy the unsaturation number implied by the molecular formula. The ¹H NMR spectrum of **1** (CD₃OD) was interpreted also on the basis of ¹³C NMR and HSQC information. Besides the resonance of a methoxyl group (δ_H : 3.24, s, 3H; δ_C : 48.5), it contained: i) three upfield shifted methyl singlets at δ 1.23 (δ_C : 18.6, Me-14), 1.24 (δ_C : 25.4, Me-15), 1.40 (δ_C : 21.2, Me-12); ii) three methine protons at δ 1.62 (dd, $J=13.6, 9.1$ Hz, H-9a; δ_C : 51.8), 1.86 (dt, $J=13.6, 9.1$ Hz, H-6a; δ_C : 47.5), and 5.12 (d, $J= 9.1$ Hz, H-10; δ_C : 65.1), this latter presumably being an oxymethine proton; iii) four sp³ methylenes, including two deshielded signals [δ 1.55 (m, Ha-7) and 1.67 (m, Hb-7), δ_C : 21.1; δ 1.44 (m, Ha-8) and 2.09 (m, Hb-8), δ_C : 33.1; δ 3.32 (t, $J= 6.5$ Hz, 2H-2), δ_C : 48.3; 3.94 (m, 2H-3, δ_C : 39.4)]. Moreover, the ¹H NMR spectrum of **1** performed in CDCl₃ showed, in addition to the aforementioned signals, two D₂O-exchangeable broad singlets at δ 6.56 (NH) and 3.65 (OH). Interpretation of COSY map (CDCl₃) revealed that the NH proton was coupled to the multiplet at δ 3.94 (2H-3) which was, in turn, coupled to the multiplet at d 3.32 (2H-2); this spin system was consistent with a -NHCH₂CH₂SO₂- moiety. Since the presence of two conjugated carbonyl signals (δ 180.5 and 181.5) and two tetrasubstituted double bonds (δ 146.1, 110.0, 147.5, and 148.0 ppm) were indicative of a *p*-quinone ring, it was hypothesized that structure of conithiaquinone A contained the same 1,4-benzoquinone/1,1-dioxo-1,4-thiazine bicyclic system (A and B rings) present in the meroterpenes previously isolated from *A. conicum*.⁴⁻⁶

Table 3.1. NMR spectroscopic data for conithiaquinones A and B^[a]

Conithiaquinone A (1)					Conithiaquinone B (2)			
Pos.	δ_c	δ_H , mult.(J in Hz)	HMBC ^[b]	ROESY ^[c]	δ_c	δ_H , mult.(J in Hz)	HMBC ^[b]	ROESY
2	48.3	3.32, t (6.5)	3	3	48.2	3.32, m	3	3
3	39.4	3.94, m	2, 4a	2	39.3	3.95, m	2, 4a	2
4a	146.1	-	-	-	146.4	-	-	-
5	181.5	-	-	-	181.5	-	-	-
5a	148.0	-	-	-	150.0	-	-	-
6	37.5	-	-	-	37.5	-	-	-
6a	47.5	1.86, dt (13.6, 9.1)	6, 7, 9a, 14, 15	10, 7b, 15	48.1	1.77, m	6, 7, 9a, 10, 14, 15	10, 15
7	21.1	H _a : 1.55, m	-	9a, 14	21.7	H _a : 1.51 ^[e]	6	14
		H _b : 1.67, m	6a, 9, 9a	6a, 8b, 15		H _b : 1.68, m	6a, 8, 9, 9a	15
8	33.1	H _a : 1.44, m	-	-	33.7	H _a : 1.52 ^[e]	-	-
		H _b : 2.09, m	6a, 9a, 9	13, 7b		H _b : 2.06, m	6a, 7, 9, 9a	-
9	82.7	-	-	-	82.4	-	-	-
9a	51.8	1.62, dd (13.6, 9.1)	6, 6a, 8, 10, 10a, 12	7a, 12, 14	52.1	1.71 dd (13.7, 8.7)	6, 6a, 9, 10, 12	12, 14
10	65.1	5.12, d (9.1)	5a, 9, 9a, 10a	6a, 13, -OH	74.4	4.84, d (8.7)	5a, 9, 9a, 10a, 11, 16	6a
10a	147.5	-	-	-	149.7	-	-	-
11	180.5	-	-	-	179.7	-	-	-
11a	110.0	-	-	-	110.3	-	-	-
Me-12	21.2	1.40, s	8, 9, 9a	9a	21.6	1.40, s	8, 9, 9a	9a, 13, 16
MeO-13	48.5	3.24, s	9	8b, 10	48.5	3.25, s	9	12
MeO-16	-	-	-	-	58.0	3.51, s	10	12
Me-14	18.6	1.23, s	5a, 6, 6a, 15	7a, 9a	18.4	1.22, s	5a, 6, 6a, 15	7a, 9a
Me-15	25.4	1.25, s	5a, 6, 6a, 14	6a, 7b	25.7	1.25, s	5a, 6, 6a, 9a, 14	6a, 7b
-OH	-	3.65, bs ^[d]	-	10	-	-	-	-
-NH	-	6.56, bs ^[d]	-	-	-	-	-	-

[a] Spectra are recorded in CD₃OD ($\delta_H = 3.34$ ppm and $\delta_C = 49.0$ ppm) at 700 MHz. [b] Carbon atoms coupled with the given proton(s). [c] Overlapped. [d] The chemical shift value was obtained from an ¹H NMR spectrum performed in CDCl₃ ($\delta_H = 7.26$ ppm). [e] Recorded in CDCl₃

This hypothesis was corroborated by a key 3J correlations observed in the HMBC spectrum between the H-3 protons at δ_{H} 3.94 and the quaternary sp^2 carbon at δ 146.1 (C-4a) and supported by comparison of NMR data of **1** with those reported in the literature.⁴⁻⁶ Careful analysis of the HSQC spectrum allowed the chemical shifts of H-9a, 2H-8, and 2H-7 to be determined in the poorly resolved region of the proton spectrum (δ 1.4-2.1). This helped to readily identify a second isolated spin system, including H-10, H-9a, H-6a, 2H-7, and 2H-8 protons, by analysis of COSY connectivities starting at the oxymethine proton at δ 5.12 (H-10). The spin system was enlarged through analysis of COSY spectrum in CDCl_3 , where H-10 was further coupled to the D_2O exchangeable proton at δ 3.65, thus indicating the presence of a hydroxyl substituent linked at C-10. HMBC spectrum showed that methyl singlets at δ 1.40 (Me-12) and 3.24 (MeO-13) were both long range coupled to the quaternary carbon at δ 82.7 (C-9). This quaternary center, bearing both the methyl and methoxyl groups, was connected to C-8 and C-9a carbons through its HMBC correlations with the relevant protons (H-9a and Ha-8), to give the five membered ring D. The remaining two identified methyl groups (Me-14 and Me-15) were judged to be geminal since HMBC spectrum showed mutual correlations as well as three shared carbon correlations for both resonances. They were indeed coupled to the methine carbon at δ 47.5 (C-6a) as well as to the quaternary carbons at δ 148.0 (C-5a) and 37.5 (C-6). This latter carbon was in turn long range coupled to the methine proton at δ 1.86 (H-6a); further diagnostic HMBC correlations were those between H-9a and both C-10 and C-10a as well as between H-10 and both the quaternary sp^2 carbons at δ 147.5 (C-10a) and 180.5 (C-11). These data allowed the ring C to be closed and connected to the *p*-quinone ring, thus delineating the whole skeleton of compound **1** which incorporates the uncommon linearly fused 6, 6, 5-ring core reported in very few natural products. This tricyclic moiety is indeed the skeleton of the plant-derived pycnanthuquinones A and B (**7** and **8**),⁷ of the algal metabolite pycnanthuquinone C (**9**),⁸ and of the ascidian metabolites rossinones.^{9,10} It has been also found incorporated into the larger polycyclic scaffolds of the terrestrial metabolites pinnatal, isopinnatal, and sterekunthal B.¹¹⁻¹³

A $^3J_{\text{H6a-H9a}}$ value of 13.6 Hz implied a *trans*-fused ring junction at C-6a/C-9a. The magnitude of this coupling constant was comparable to that observed for the

relevant protons in pycnanthuquinone C (**9**) (13.9 Hz) and in the other related compounds (pycnanthuquinones A and B, rossinones) having a *trans*-fused 6,5-rings system.⁷⁻¹⁰ On the other hand, structures featuring a *cis* relationship between the protons of the five- and six-membered rings (pinnatal, isopinnatal, and sterekunthal B) displayed clearly smaller coupling constant values.¹¹⁻¹³ Similarly, the magnitude of $^3J_{\text{H9a-H10}}$ in **1** (9.1 Hz) suggested the β -orientation of the OH group at C-10; it was indeed comparable to that reported for **8** (8.8 Hz) but more than the double of those in **9** (4.3 Hz) and **7** (3.6 Hz).^{7,8} Both these conclusions were strongly supported by a number of observed ROESY correlations, listed in Table 3.1, which also allowed the orientation of the substituents at C-9 to be determined. In detail, ROESY spectrum (CDCl_3) of **1** contained cross-peaks from H-6a to H-10, Me-15, and H-7b; further diagnostic cross-peaks were observed from H-9a to Me-12, Me-14, and H-7a. These observations allowed the relative configuration of **1** to be assigned as 6a*R**, 9*R**, 9a*R**, 10*S**

The high-resolution mass spectrum (ESI positive-ion mode) of compound **2** showed an ion peak at m/z 432.1449 corresponding to $[\text{M}+\text{Na}]^+$ (calculated value: m/z 432.1451); the molecular formula of **2** was thus established as $\text{C}_{20}\text{H}_{27}\text{NO}_6\text{S}$. The comparison of NMR spectra of **1** and **2** evidenced a close similarity between the two compounds and indicated that they differed only in the nature of the substituent at C-10. Taking into account the molecular formula and considering the presence of additional signals in ^1H and ^{13}C NMR spectra (δ_{H} : 3.51, s, δ_{C} : 58.0) the substituent in **2** was identified as a methoxyl group. This conclusion was fully corroborated by 2D NMR spectra analysis which also led to the full assignment of all NMR resonances in **2** (Table 3.1).

The significant cytotoxic activity showed by several members of meroterpenes family, probably related to their capacity to interfere with the cellular redox systems,¹¹ prompted us to investigate the effects of **1** and **2** on tumour and non-tumour cell lines cell growth and viability. To this aim, human skin keratinocyte cells (HaCaT line) and human breast adenocarcinoma cells (MCF-7 line) were treated for 48 h with various concentrations of compounds **1** and **2**. Then, the bioscreenings were performed by measuring the level of mitochondrial dehydrogenase activity and by counting the number of live and death cells. The results showed that both **1** and **2** possess a significant and concentration-dependent cytotoxic profile, especially against

mammalian cancer cells, as indicated by the calculated IC₅₀ values reported in Table 3.2.

Table 3.2. Cell growth inhibition (IC₅₀, μM^[a])

Compound	HaCaT cells	MCF-7 cells
1	98.6 ± 4	44.5 ± 3.8
2	162.6 ± 5	125 ± 5
CDDP	6 ± 3	3.5 ± 3

[a] IC₅₀ values are expressed as mean ± SEM (*n* = 24) of three independent experiments

Interestingly, compound **1** displayed an higher toxic effect toward lines, in particular showing an IC₅₀ value against tumour MCF-7 cells within the micromolar range (~45 μM), which is generally considered as a marker of a moderate cytotoxic activity. Positive control for cytotoxicity was performed using cisplatin (CDDP), a well-known antiproliferative drug showing IC₅₀ values lower than 10 μM in the same experimental conditions.¹⁴

In conclusion, conithiaquinones A and B represent a further example of the great structural diversity generated into the meroterpene family. It has been speculated on the origin of some of these molecules; the formation of chromene derivatives and of other cyclized compounds from the relevant quinones/hydroquinones can be also easily rationalized through a sequence of acid-catalyzed cyclizations. However, with the data available, it is not possible to argue whether these transformations occur in the organism, either enzymatically or not, prior to its extraction, or they take place during isolation and/or chromatographic purification. Concerning this, we considered the possibility that conithiaquinones A and B could be artifacts derived from a hypothetical methylation during the extraction procedure. To rule out this possibility, samples of *A. conicum* were extracted with chloroform and acetone and subsequently subjected at the same procedure above reported. The spectrum ¹H NMR of the MPLC fractions eluted with 100% AcOEt was identical to that of corresponding fractions obtained from extraction using methanol. Furthermore there was no evidence of the presence of even small amounts of the putative demethylated conithiaquinones, thus confirming that the conithiaquinones are not artifacts, but genuine metabolites from *A. conicum*.

3.1.2 New bioactive alkyl sulfates from the ascidians *Ciona edwardsii* and *Aplidium elegans*

Ascidians have been an extremely rich source of sulfur-containing molecules which, on the other hand, are quite unusual in marine organisms. A number of sulfides/polysulfides, sulphur heterocycles, sulfoxides, and alkyl sulfates have been isolated from marine ascidians.^{15,16} In particular, these latter compounds, although occasionally reported from marine source,¹⁷⁻²⁰ have shown to be often present in remarkable amounts in solitary ascidians of the families Ascidiidae and Pyuridae, as well in colonial Polyclinidae species.²¹⁻²⁸ They often have quite simple structures, mostly of polyketide derivation even though in some frameworks an isoprenoid origin is clearly recognized; almost all the isolated compounds are endowed with cytotoxic and/or antiproliferative activity. In the course of our program on discovery of cytotoxic metabolites from Mediterranean ascidians,^{29,30} we have analyzed the chemical composition of methanol extracts of two species, *Aplidium elegans* (Monniot & Monniot, 1983) and *Ciona edwardsii* (Roule, 1884), both collected in the Bay of Naples, Italy. This investigation yielded compounds **10** and **11** from *A. elegans*, and compound **12** from *C. edwardsii*, in addition to the known sulfated terpenoids **13** and **14**.²⁴⁻²⁸ (Figure 3.2).

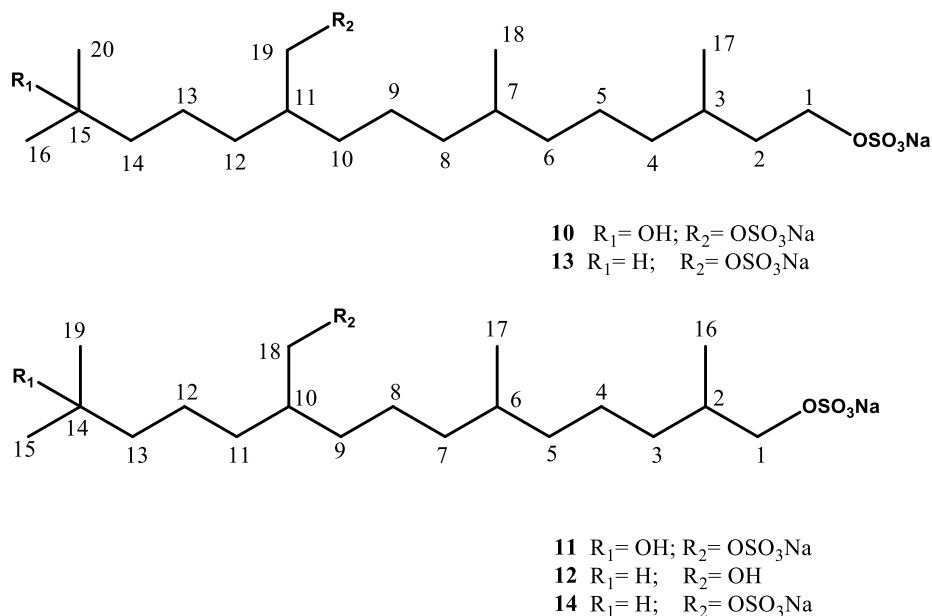


Figure 3.2. Structures of compounds 10–14.

Fresh thawed tissues of both *A. elegans* and *C. edwardsii*, collected in the bay of Naples, immediately frozen, and kept at $-28\text{ }^{\circ}\text{C}$ until extraction, were exhaustively extracted with methanol and, subsequently, with chloroform. For each ascidian sample, the extracts were combined and concentrated; the resulting aqueous suspensions were then partitioned between water and butanol. The butanol extract of *A. elegans* was fractionated by MPLC over a reversed phase C-18 column using stepwise elution with aqueous MeOH. The fractions eluted with 50% aqueous MeOH were further separated and purified by reversed-phase HPLC eluting with 70% aqueous MeOH containing 0.1% TFA, thus affording compounds 10 and 11 in the pure state. The butanol extract of *C. edwardsii* was fractionated by reversed-phase MPLC under the same conditions as described for that of *A. elegans*. Further separation and purification of both fractions eluted with 70% and 50% aqueous MeOH by repeated reversed-phase HPLC yielded compounds 12–14 in the pure state. A first survey of the 1D NMR spectra (CD_3OD) of 10 and the comparison with those of the already known compound 13 readily allowed us to hypothesize that 10 was the 15-hydroxy analogous of 13. The proton spectrum of 10 lacked indeed the signals due to the isopropyl terminus portion of 13, whereas it contained a quite deshielded methyl signal (δ 1.14), resonating as a singlet and integrating for six protons. Likewise, the ^{13}C -NMR spectrum of 10 contained a quaternary carbon resonance (δ 70.8) attributable to an oxygen-bearing carbon while the methine signal at δ 29.1 due to C-15 in 13 was absent. Chemical shifts and coupling patterns of the remaining signals of 10, assigned by aid of COSY, HSQC, and HMBC experiments were very similar to those of 13. Mass data analysis confirmed the assumption made. ESI mass spectrum (negative ion mode) contained an ion peak at m/z 511; an intense fragment at m/z 453 was present and it was interpreted as the result of an α cleavage at C-15. High resolution analysis on the pseudomolecular ion peak gave m/z 511.1987, which was consistent with the molecular formula $\text{C}_{20}\text{H}_{40}\text{NaO}_9\text{S}_2$ corresponding to $[\text{M}-\text{Na}]^-$ (calculated value: 511.2006). The location of the hydroxyl group at C-15 was unambiguously established through 2D-NMR experiments which allowed us also to assign all the proton and carbon resonances of compound 10 (**Table 3.3**). In particular, diagnostic $^3J_{\text{C-H}}$ long-range couplings were observed in the HMBC spectrum between the signal at δ 1.14 (s, 6H, CH_3 -16/20) and

both the oxygenated quaternary carbon at δ 70.8 (C-15) and the methylene carbon at δ 44.4 (C-14).

Table 3.3. ^1H and ^{13}C -NMR data of compounds **10–12** in CD_3OD .

Pos.	10		11		12	
	δ_{H} (mult., J in Hz)	δ_{C}	δ_{H} (mult., J in Hz)	δ_{C}	δ_{H} (mult., J in Hz)	δ_{C}
1	4.02 (m)	66.7	3.80 (H _a , dd, 6.6, 9.1) 3.88 (H _b , dd, 6.6, 9.1)	73.2	3.79 (H _a , dd, 6.6, 9.4) 3.87 (H _a , dd, 6.6, 9.4)	73.6
2	1.42 ^a (H _a) 1.68 (m, H _b)	36.7	1.78 (m)	33.5	1.79 (m)	34.1
3	1.60 (m)	29.9	1.14 (m)	33.7	1.14 (m)	34.3
4	1.10 ^a 1.30 ^a	37.6	1.41 ^a 1.33 ^a	24.5	1.4 ^a 1.32 ^a	25.1
5	1.30 ^a	24.6	1.10 ^a 1.30 ^a	37.6	1.11 ^a 1.30 ^a	38.1
6	1.10 ^a (H _a) 1.28 ^a (H _b)	37.6	1.39 ^a	33.0	1.41 ^a	33.5
7	1.40 ^a	33.1	1.10 ^a 1.30 ^a	37.6	1.11 ^a 1.30 ^a	38.1
8	1.09 ^a (H _a) 1.28 ^a (H _b)	37.7	1.33 ^a	24.5	1.32 ^a	25.1
9	1.29 ^a	24.6	1.31 ^a 1.36 ^a	31.7	1.23 ^a 1.32 ^a	31.9
10	1.30 ^a 1.38 ^a	32.0	1.66 (m)	38.4	1.44 (m)	41.4
11	1.65 (m)	38.4	1.30 ^a 1.38 ^a	31.9	1.23 ^a 1.32 ^a	31.9
12	1.36 ^a	31.7	1.33 ^a	24.5	1.33 ^a	25.2
13	1.30 ^a	24.6	1.42 ^a	44.4	1.19 (m)	40.3
14	1.42 ^a	44.4	-	70.7	1.55 (m)	28.9
15	-	70.8	1.15 (s)	28.3	0.89 (d., 6.4)	22.8
16	1.14 (s)	28.4	0.94 (d, 6.6)	16.3	0.96(d., 6.6)	16.9
17	0.90 (d, 6.6)	18.9	0.86 (d, 6.6)	19.2	0.88(d., 6.4)	19.9
18	0.85 (d, 6.6)	19.2	3.92 (d, 5.4)	70.8	3.44 (d, 5.4)	65.5
19	3.91 (d, 5.4)	70.7	1.15 (s)	28.3	0.89 (d., 6.4)	22.8
20	1.14 (s)	28.4	-	-	-	-

^a Signals overlapped by other resonances.

The negative HRESI mass spectrum (negative ions) of compound **11** displayed an ion peak at m/z 497.1825 corresponding to $[\text{M}-\text{Na}]^-$ (calculated value: m/z 497.1849); the molecular formula of **11** was thus established as $\text{C}_{19}\text{H}_{38}\text{NaO}_9\text{S}_2$. The ^1H - and ^{13}C -NMR spectra of compound **11** displayed a close resemblance to those of

10, and the observed differences were due to the initial segment of the linear skeleton of both compounds (C1-C3/C16 in **11** and C1-C4/C17 in **10**). The multiplet at δ 4.02 due to 2H-1 in compound **10** was replaced by an ABX system at δ 3.80 (1H, dd, $J = 9.1$ and 6.6 Hz, H-1a) and 3.86 (1H, dd, $J = 9.1$ and 6.6 Hz, H-1b). COSY connectivities, which allowed to delineate the large spin system C1-C13 through CH₃-16, CH₃-17 and CH₂-18, as well as HMBC information, clearly evidenced **11** as the 1-nor-derivative of **10** or, alternatively, the 15-hydroxy analogue of **14** (Table 3.3).

The NMR features (CD₃OD) of compound **12** appeared almost identical to those of **14**, except for the chemical shift of the C-18 methylene protons as well as that of the relevant carbon, both showing a significant upfield shift (δ_{H} : 3.94 in **14** vs. 3.44 in **12**; δ_{C} : 73.9 in **14** vs. 65.5 in **12**). The negative ion HRESI mass spectrum of **12** displayed an ion peak at m/z 379.2522 which was consistent with the molecular formula C₁₉H₃₉O₅S⁻, corresponding to [M-Na]⁻ (calculated value 379.2513). These few data readily allowed us to deduce that **12** was the 18-desulfated analogue of **14**; this conclusion was fully corroborated by 2D NMR spectra analysis which also led to the full assignment of all NMR resonances in **12** (Table 3.3).

The cytotoxic effect of compounds **10–12** was evaluated on J774A.1 (BALB/c murine macrophages) and C6 (rat glioma) cell lines *in vitro*. Compounds **10** and **11** induced a concentration-dependent mortality on J774A.1 (Figure 3.3) whereas both drugs were inactive on C6 cells, with a LC₅₀ > of 300 μ M (data not shown). When comparing optical density values of control and treated cells, the cytotoxic effect of compound **10** and **11** was significant at the highest concentrations ($p < 0.05$, compound **10** at 100 μ M; $p < 0.05$ and $p < 0.01$, compound **11** at 30 and 100 μ M, respectively). The LC₅₀ value of compound **11** on J774A.1 cell line was 45.12 μ M, while that of compound **10** was > of 100 μ M (Figure 3.3). The compound **12** was ineffective on both J774A.1 and C6 cells (data not shown). On the basis on these although preliminary data, a sulfate group in R2 and/or a hydroxyl group in R1 seems to be essential for the cytotoxic activity, since they are absent in compound **12** which proved inactive. Nevertheless, previous reports showed that compounds **13** and **14**, possessing exclusively the sulfate group in R2, are still active therefore,^{24,28} we can conclude that only the latter functionality has an obligatory role for the cytotoxic activity showed by compounds **10** and **11** against the macrophagic cell line.

The slightly different potency of compounds **10** and **11** could be ascribed to the different length chain; this hypothesis is supported by cytotoxicity data reported in literature for compounds **13** and **14**, where compound **14**, characterized by a shorter C-chain, resulted more active than its higher analogue **13**.^{24,28}

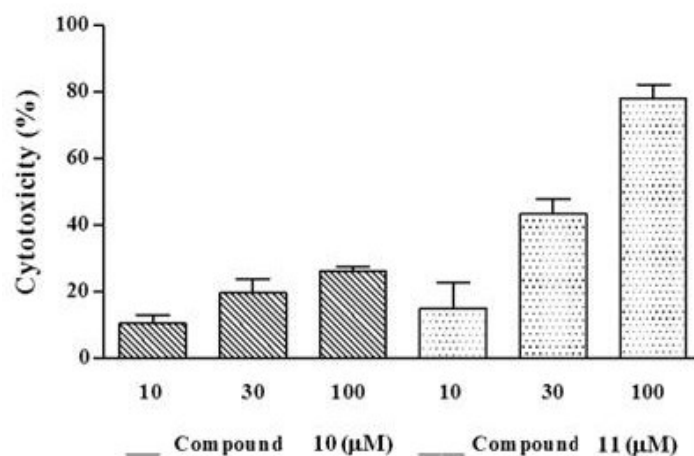


Figure 3.3. Cytotoxic effect of compounds **10** and **11** at increasing concentrations on J774A.1 cells. Each per cent value is the mean \pm SEM of three independent experiments.

In conclusion, the structures of compounds **10–12**, isolated from the Mediterranean ascidians *Aplidium elegans* and *Ciona edwardsii*, have been elucidated using mass spectrometry and NMR experiments and their *in vitro* cytotoxic effects have been evaluated on J774A.1 (BALB/c murine macrophages) and C6 (rat glioma) cell lines. A moderate but selective cytotoxic effect on J774A.1 cell line has been evidenced for compounds **10** and **11**; the inactivity of **12**, as well as further pharmacological data available in the literature,^{24,28} indicated that the hydroxyl group does not confer *per se* cytotoxic activity, while the contribution of the sulfate is of pivotal importance. A slight influence of alkyl chain length on the potency of the active compounds has been also evidenced.

3.1.3 *Phallusiasterols A, B and C: three new sulphated sterols from the Mediterranean tunicate Phallusia Fumigata and their effects as modulators of the PXR receptor*

Marine invertebrates are a prolific source of unconventional steroids. More than 1600 new steroidal structures have been so far isolated^{31,32} with structural modifications including oxygenation, alkylation, esterification, and sulfation of both the nucleus and the side chain, extensive modification of the latter, or bond cleavage in the rings of the tetracyclic nucleus leading to degradation of the conventional carbon backbone.³³⁻³⁶ Steroids of marine origin have exhibited a diverse array of pharmacological activities, such as antimicrobial, cytotoxic, antifouling, ichthyotoxic, and antiinflammatory.³¹⁻³⁴ Nevertheless, the sterol composition of marine ascidians has received much less attention than those of other invertebrates. It has been showed that, in general, tunicates contain Δ^5 sterols bearing conventional side chains with cholesterol as the major component and cholestanol and cholest-7-en-3 β -ol as the minor ones.³¹ Among the minor unconventional sterols isolated from tunicates, 5,8-endoperoxides from several $\Delta^{5,7,9(11)}$ sterols³⁷ together with 24-hydroperoxy-24-vinylcholesterol and the corresponding 24-hydroxy derivative from *Phallusia mamillata* and *Ciona intestinalis*,³⁸ Δ^4 -3-keto steroids, 5 β -stanols, and 4-methyl sterols in addition to endoperoxides from *Ascidia nigra*,^{39,40} two short side chain sterols (C-22 and C-23) from *Polizoa opuntia*,⁴¹ and four 9,11- secosterols from *Aplidium conicum*⁴² have been reported. These findings, although few number, show that ascidians can produce sterols with unique structural features and they could be a good source of interesting novel compound.

As a part of our research program aimed to discover new bioactive metabolites from marine tunicates, we have investigated the Mediterranean ascidian *Phallusia fumigata*.



This study led to the isolation of three new sulfated sterols phallusiasterols A (**15**), B (**16**) and C (**18**) (**Figure 3.4**), which, to our knowledge, represent the first example of sulfated sterols isolated from tunicates. Based on the reported activity of sulfated marine sponge steroids as nuclear receptor ligands, the effects of phallusiasterols A, B and C as modulators of PXR receptor have been investigated in vitro.

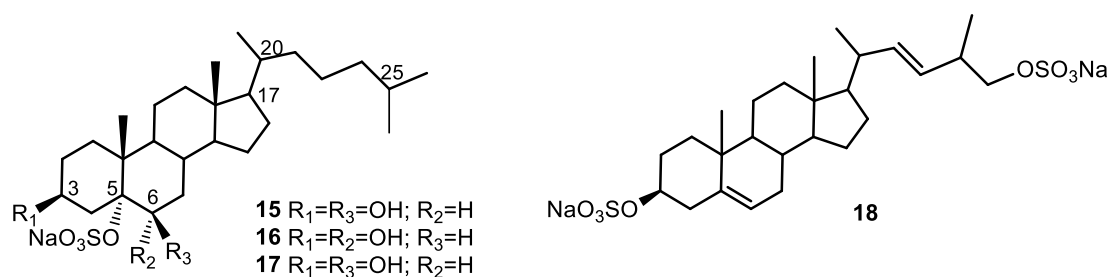


Figure 3.4. Structures of phallusiasterols A-C

These studies revealed that phallusiasterol A induces PXR transactivation in HepG2 cells and stimulates the expression of the PXR target genes CYP3A4 and MDR1 in the same cell line.

PXR is a master gene orchestrating the expression of a wide family of genes involved in uptake, metabolism, and disposal of a number of endo- and xenobiotics, including drugs, bile acids, steroid hormones, and metabolic intermediates in mammalian cells. PXR is almost exclusively expressed in the gastrointestinal tract and liver, with lower levels in the kidney and ovary. PXR dysfunction is associated with immune disorders and inflammatory bowel diseases, including ulcerative colitis and Crohn's disease. Chemical and pharmacological characterization of marine steroid libraries has allowed the identification of a number of selective PXR agonists (natural and synthetic compounds) which have been effective in reducing nuclear factor (NF)- κ B activity and intestinal inflammation. These findings open the possibility of discovering potential leads for the treatment of liver and intestinal disorders.⁴³

A series of subsequent normal-phase chromatographies of the ethyl acetate extract of the ascidian *P. fumigata* collected from the bay of Pozzuoli (Napoli, Italy), allowed the isolation of compounds **15** and **16** (**Figure 3.4**) in pure form.

The high field region of the 1H NMR spectrum (pyridine- d_5) of phallusiasterol A (**15**) contained signals for five methyl groups of a steroidal nucleus: two singlets a δ 0.67

(Me-18) and 1.60 (Me-19) and doublets at δ 0.96 ($J = 6.5$ Hz, H₃-21), 0.89 and 0.88 ($J = 6.6$ Hz, H₃-26 and H₃-27). A pseudomolecular ion at m/z 545.2858 [M+Na]⁺ was observed in the high-resolution ESI mass spectrum (positive ion mode), indicating for **15** a molecular formula of C₂₇H₄₇SO₆Na (calcd. 545.2889). The MS/MS fragmentation pattern of **15** was compatible with the presence of a sulfate group, displaying the peak at m/z 425.3392 [M – NaHSO₄ + Na]⁺. Consistent with the MS data, the ¹H and ¹³C- NMR spectra of **15** contained two hydroxymethine signals [δ_{H} 4.33, bs, δ_{C} 75.3 (CH); δ_{H} 4.79, m, δ_{C} 67.2 (CH)] and a highly deshielded unprotonated carbon (δ 87.8), presumably the locus of the sulfate group. This assumption was verified by acetylation of phallusiasterol A (**15**) which gave the corresponding diacetate **17**, thus confirming, according to MS information, the presence of two secondary alcohols and a quaternary sulfoxy group in **15**.

The whole series of 2D NMR data allowed to locate the hydroxyl groups at C-3, C-6, and the sulfate group at C-5. Analysis of COSY spectrum of **15** (pyridine-*d*₅), assisted by TOCSY information, allowed the sequential assignment of all the protons of the tetracyclic system (**Figure 3.5**) whereas the protonated ¹³C signals were assigned to the relevant protons from HSQC data (**Table 3.4**).

The steroidal skeleton of **15** was assembled on the base of key HMBC correlations of H₃-19 with C-1, C-5, C-9, and C-10 and of H₃-18 with C-12, C-13, C-14, and C-17 (**Figure 3.5**). Information on the side chain were also provided by analysis of 2D NMR data; in the COSY spectrum, the spin system from H-6 to H-17 (through H-14) was extended to the side chain protons through the correlation between H-17 (δ 1.10) and the multiplet at δ 1.36 (H-20), which is in turn coupled to both the methyl doublet at δ 0.96 (H₃-21) and the methylene protons at δ 1.38 and 1.03 (H-22a and H-22b). The sequence was extended to the H₃-26 and 27 methyls, taking also advantage of HSQC and TOCSY information.

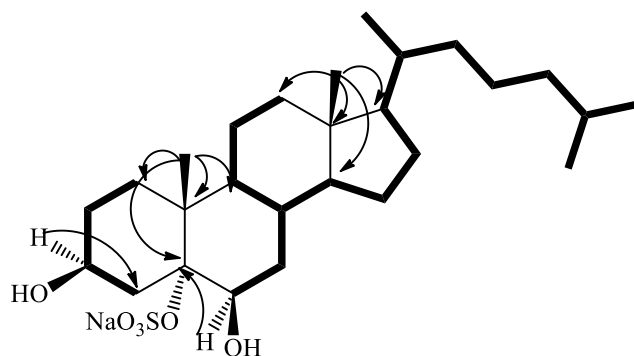


Figure 3.5. COSY connectivities (bold bonds) and selected HMBC (from H to C) correlations of **15**

The relative stereochemistry of phallusiasterol A (**15**) was established through analysis of ROESY data (**Figure 3.6**) and consideration of both coupling constants and solvent shifts ($\Delta\delta = \delta_{\text{CDCl}_3} - \delta_{\text{pyridine-}d_5}$) observed for some key signals in the ^1H NMR spectrum of **15**. The equatorial orientation of the hydroxyl group at C-3, assigned to the β face, was easily deduced by the presence of an axial-axial coupling constant ($J = 13.1$ Hz) found for the vicinal H-4 $_{\beta}$. Furthermore, a large pyridine-induced downfield shift (-0.46 ppm) was observed for the H-3 $_{\alpha}$ signal, which resonates at δ 4.33 when the proton spectrum is recorded in CDCl_3 (see experimental section). This indicated a 1,3-diaxial interaction of H-3 $_{\alpha}$ proton with the polar sulfate group linked at C-5, which therefore must be α -oriented.⁴⁴⁻⁴⁶ The axial orientation of H-8, H-9, and H-14 was apparent from the coupling constants values of these protons (**Table 3.4**). These data, combined to the observation of ROESY correlations of H₃-19 to H-4 $_{\beta}$, to H-2 $_{\beta}$, and to H-8, of H₃-18 to H-8, and of H-9 to H-14 (**Figure 3.6**), defined the A/B, B/C, and C/D *trans* ring junctions of the 5 α -cholestane nucleus of **15**.

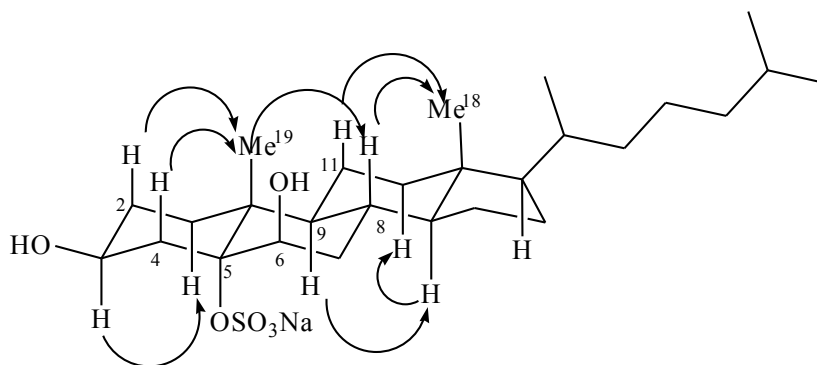


Figure 3.6. Key ROESY correlations detected for **15**

The small coupling constants showed by H-6 (δ 4.33, bs) suggested a β -orientation of the OH group at C-6. This was confirmed by the signal large pyridine-induced downfield shift observed for H-4 $_{\beta}$ (-0.75 ppm). According to Fujimoto *et al.*,⁴⁷ the resonances of H-4 protons in 3 β , 5 α , 6-cholestanetriols show a diagnostic dependence on the configurations at C-6. Their resonances are strongly influenced by a deshielding effect of the 6-OH group through a 1,3- diaxial (with the 6 β isomer) or 1,3-diequatorial (with the 6 α isomer) interaction, which is intensified in pyridine solution. Further significant pyridine-induced shifts were observed for H₃-19 (- 0.32 ppm) and H-8 (- 0.31 ppm), which supported the axial orientation of the hydroxyl group at C-6. The orientation of substituents at C-17 and C-20 in phallusiasterol A, as shown in Figure 3.4, was assumed to be the same as in related polyhydroxysterols due to the almost identical values of carbon chemical shifts around these carbon atoms.⁴⁶⁻⁴⁸ The structure of phallusiasterol A was hence established as 3 β , 6 β -dihydroxy- 5 α -cholestan -5 α -yl sodium sulfate.

Table 3.4. ^1H (700 MHz) and ^{13}C (125 MHz) NMR data for phallusiasterols A and B in pyridine- d_5 .

Pos.	Phallusiasterol A (15)			Phallusiasterol B (16)	
	δ_{C}	δ_{H} (mult., J in Hz)	HMBC	δ_{C}	δ_{H} (mult., J in Hz)
1 α /ax	34.4	1.90 (dt, 13.4, 4.2)	2, 5, 10, 19	33.8	2.10, m
1 β /eq		1.56, m	2, 3, 5, 10, 19		1.50, m
2 α /eq	31.8	2.20, m	1, 3, 10	32.5	2.22, m
2 β /ax		2.01 ^a	1, 3, 9		1.97, m
3 α /ax	67.2	4.79, m	1, 2, 4	67.4	4.72, m
4 α /eq	43.2	2.51 (dd, 13.6, 4.5)	2, 3, 5, 6, 10	43.3	2.30 (dd, 13.0, 4.0)
4 β /ax		3.10, m	2, 3		2.81, m
5	87.8	-	-	75.8	-
6 α	75.3	4.33 (bs)	4, 5, 8, 10	66.1	4.34, (d, 5.5)
7 α /ax	35.1	1.88 ^a	5, 6, 8, 9	35.7	1.93, m
7 β /eq		2.21, m	8, 14		2.45, m
8 β /ax	31.1	2.05 (qd, 11.6, 4.3)	7, 9, 14	30.9	1.99 (qd, 11.0, 3.4)
9 α /ax	46.9	1.75, (ddd, 13.6, 11.1, 3.6)	8, 10, 11, 19	45.5	1.88 (ddd, 13.5, 11.2, 3.6)
10	40.6	-	-	39.8	-
11 α /eq	21.8	1.47 (dq, 14.1, 3.8)	9, 10, 12	21.7	1.48, m
11 β /ax		1.37 ^a	9, 12, 17		1.38 ^a
12 α /ax	40.2	1.13, m	11, 14	40.8	1.17 ^a
12 β /eq		1.95 ^a	9, 13, 14		1.94 (dt, 12.4, 3.4)
13	42.9	-	-	43.4	-
14 α	56.2	1.05, m	8, 13, 15, 16, 18	56.1	1.02, m
15 α	24.4	1.57 ^a	13, 14, 16, 17	24.4	1.55, m
15 β		1.04, m	8, 14, 16		1.07, m
16 α	28.5	1.82 (ddd, 13.6, 9.5, 3.7)	13, 15, 17	29.1	1.83 (ddd, 13.6, 9.4, 3.8)
16 β		1.21 ^a	13, 17, 20		1.23, m
17	56.4	1.10, m	13, 15, 16, 20, 22	56.9	1.11, m
18	12.4	0.67, s	12, 13, 14, 17	12.3	0.71, s
19	18.7	1.60, s	1, 5, 9, 10	18.5	1.47, s
20	36	1.36, m	17, 21, 22, 23	36.8	1.35, m
21	19	0.96 (d, 6.5)	17, 20, 22	19	0.96 (d, 6.5)
22 ^a	36.5	1.38 ^a	20, 21, 24	36.5	1.37 ^a
22b		1.03, m	20, 21, 24		1.01, m
23 ^a	24.2	1.38 ^a	24	24.1	1.36 ^a
23b		1.18 ^a	24		1.17, m
24 ^a	39.7	1.13, m	23, 26, 27	39.7	1.14, m
24b		1.13, m	23, 26, 27		1.14, m
25	28.3	1.51, m	23, 24, 26, 27	28.7	1.52 ^a
26	22.7	0.88 (d, 6.6)	24, 25	22.8	0.88 (d, 6.5)
27	22.9	0.89 (d, 6.6)	24, 25	22.9	0.88 (d, 6.5)

[a] Overlapped by other signals

The molecular formula $C_{27}H_{47}SO_6Na$ established for the second metabolite phallusiasterol B (**16**) by HRESIMS and NMR data was identical to that of **15**, indicating that the compounds were isomers. The 1H and ^{13}C NMR resonances of **16** closely resembled those of **15**, except for some signals surrounding C-6 (**Table 3.4**). Interpretation of COSY, TOCSY, HSQC and HMBC 2D NMR experiments provided evidence for the same planar structure for **16** as that of **15**. The difference between **15** and **16** was traced to a different stereochemistry at C-6, with the OH group α oriented in compound **16**. This was deduced from the different shape of H-6 signal in **16** (δ 4.34, d, $J = 5.5$ Hz) when compared to that of H-6 in **15** (δ 4.33, bs). The upfield shift of C-6 in the ^{13}C NMR spectrum of **16** (δ 66.1) relative to that observed for **15** (δ 75.3) added support to this assignment.⁴⁸⁻⁵⁰ Conclusive evidence was achieved from ROESY spectrum; a strong correlation was observed between H-6 and H₃-19 and the β orientation of H-6 is the only position according with this demand. In addition, on comparison of the proton spectra of **16** recorded in $CDCl_3$ and pyridine- d_5 , a pyridine-induced deshielding was observed for H-4 $_{\alpha}$ (- 0.64 ppm), comparable to that observed for H-4 $_{\beta}$ in **15**, indicating a 1,3-diequatorial interaction of this proton with the 6 α OH group.⁴⁷ Thus, phallusiasterol B was identified as the epimer at C-6 of phallusiasterol A.

Medium pressure flash chromatography of the butanol soluble portion on a reversed phase C-18 column, followed by HPLC separations, gave phallusiasterol C (**18**) in the pure state (**Figure 3.4**).

The 1H spectrum (recorded in CD_3OD) of phallusiasterol C showed signals typical of a sterol (two upfield methyl singlets at δ_H 0.72 e a δ_H 1.03; two methyl doublets at δ_H 1.02 (d, $J= 6.2$ Hz) and at δ_H 1.03 (d, $J= 6.4$ Hz) (**Table 3.5**). Furthermore the down field region of the same spectrum contained three signals at δ_H 5.38 (m) δ_H 5.35 (dd, $J= 15.3, 8.5$) and at δ_H 5.28 (dd, $J= 15.3, 7.0$), indicated the presence of three olefinic protons. The presence of two double bonds was confirmed by the signals at δ_C 141.5 (C), 138.5 (CH), 130.2 (CH) 123.4 (CH) contained in the ^{13}C NMR.

Table 3.5. ^1H (700 MHz) and ^{13}C (125 MHz) NMR data for phallusiasterol C (**18**) in CD_3OD

Pos.	δ_{H} , mult. (J in Hz)	δ_{C}
1β	1.90, dt, (13.5, 3.6)	38.4
1α	1.10, m	
2β	1.63, m	29.9
2α	2.07, m	
3α	4.14, dddd, (11.4, 11.4, 4.8, 4.8)	80.0
4β	2.34, m	40.3
4α	2.53, ddd, (13.2, 4.7, 2.2)	
5	-	141.5
6	5.38, m	123.4
7β	1.98, m	33.0
7α	1.55, ovl	
8β	1.48, m	33.2
9α	0.96, m	51.7
10	-	37.7
11β	1.55, ovl	22.1
11α	1.51, m	
12β	2.01, dt, (12.9, 3.5)	41.0
12α	1.18, m	
13	-	43.4
14α	1.02, ovl	58.2
15β	1.07, m	25.3
15α	1.58, ovl	
16β	1.28, m	29.7
16α	1.71, m	
17	1.17, m	57.2
18	0.72, s	12.5
19	1.03, s	19.7
20	2.06, m	41.5
21	1.03, d, (6.4)	19.7
22	5.35 dd, (15.3, 8.5)	138.5
23	5.28, dd, (15.3, 7.0)	130.2
24	2.44, m	37.6
24'a	3.88, dd, (9.3, 6.0)	73.8
24'b	3.74, dd, (9.3, 7.8)	
25	1.02, d, (6.2)	21.2

A pseudomolecular ion at m/z 567.2064 $[\text{M}-\text{Na}^+]^-$ was observed in the high resolution ESI mass spectrum (negative ion mode), indicating for **18** a molecular

formula of $C_{26}H_{40}NaO_8S_2$, which indicated six unsaturation degrees. The ESI and MS/MS spectra showed pseudomolecular and fragment ions compatible with the presence of sulfate groups: 465 $[M - NaSO_3]^-$, 447 $[M - NaHSO_4 - Na]^+$, 272 (double charged species). 1H and ^{13}C spectra, together with mass data, evidenced the presence of one secondary and one primary sulfoxy groups (δ_H 4.14, dddd, $J = 11.4, 11.4, 4.8, 4.8$ Hz, δ_C 80.0, CH; δ_{Ha} 3.88, dd, $J = 9.3, 6.0$ e δ_{Hb} 3.74, dd, $J = 9.3, 7.8$ Hz, δ_C 73.8, CH₂). The location of the secondary sulfoxy group at C-3 of the steroidal nucleus was determined of 1H NMR, COSY, HSQC and HMBC spectra.

The COSY spectrum revealed useful information concerning the side chain. Starting from the methine proton at δ_H 1.17 (H-17), COSY correlations could be observed to the methine proton at δ_H 2.06 (H-20), which in turn was coupled to both of the methyl protons at δ_H 1.03 (H₃-21) and the methine proton at δ_H 5.35 (H-22). This latter proton was coupled to the methine proton at δ 5.28 (H-23). These correlations allowed us to locate the double bond between C-22 and C-23. The *E* configuration of the double bond was assigned on the basis of the coupling constant ($J \sim 15$ Hz) of H-22 and H-23. Furthermore COSY spectrum revealed that the proton at δ_H 5.28 was coupled to the methine proton at δ 2.44 (H-24), which in turn was coupled to both of the methyl protons at δ 1.02 (H₃-25) and the methylene protons at δ 3.74 and at δ 3.88 (H₂-24'), suggesting a 24'-sulfoxy-C24' side chain.

The axial orientation of H-8, H-9 and H-14 was apparent from their respective coupling constants, that of the angular methyl groups from the ROESY correlations of both H₃-18 and H₃-19 with H-8 and the axial H-11 β . On this skeleton, the coupling constants showed by H-3 with H-2 β and H-1 β illustrated their axial orientation, and therefore the equatorial orientation of the sulfate group. (**Figure 3.7**)

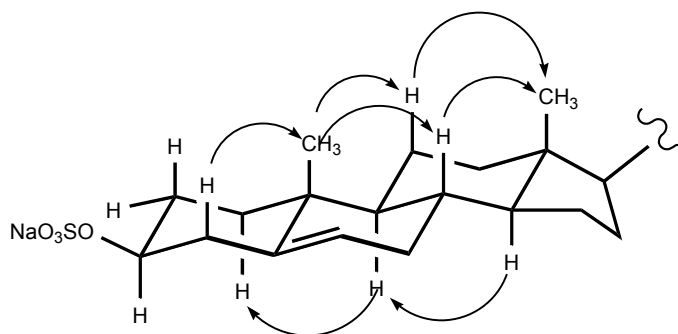


Figure 3.7. Key ROESY correlations detected for **18**

The role of marine steroids as nuclear receptor ligands has been recently highlighted⁴³ and several sulfated marine steroids have been identified as a new class of the pregnane X receptor (PXR) agonists.^{51,52} Based on this background, we have investigated a possible role of phallusiasterols A (**15**), B (**16**) and C (**18**) in regulating the PXR activity. A transactivation assay on HepG2 cells, a human hepatocarcinoma cell line, has been performed, as described in the Experimental Part. As shown in Figure 3.8A, only compound **15** acted as PXR agonist at concentration of 10 μ M; its activity was comparable to that of rifaximin, a well characterized ligand for the human PXR. As shown in Figure 3.8B, all compounds **15**, **16** and **18** failed to reverse the induction of luciferase activity caused by rifaximin, indicating that they were not PXR antagonists. Similar results have been obtained by analyzing the effect exerted by **15**, **16** and **18** in terms of regulation of PXR mediated induction of two PXR target genes, CYP3A4 (**Figure 3.8C**) and MDR1 (**Figure 3.9D**), in the same cell line. Compound **15** effectively stimulated the expression of both target genes, whereas **16** and **18** failed to induce them. These results have an important implication in terms of structure-activity relationship, because they highlight a crucial role in the ligand-receptor binding of phallusiasterols of the configuration at C-6.

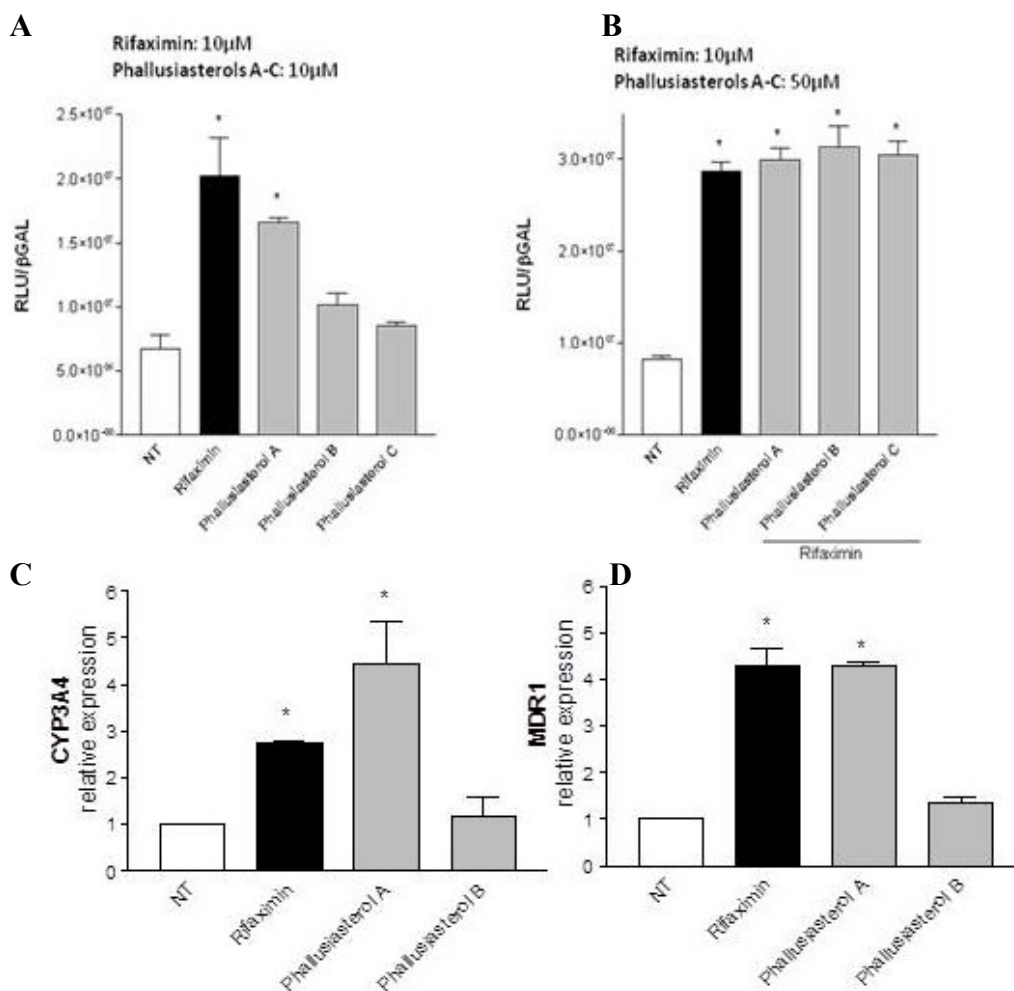


Figure 3.8 (A, B, C, D) Luciferase reporter assay.

HepG2 cells were transiently transfected with pSG5-PXR, pSG5-RXR, pCMV-βgalactosidase and p(CYP3A4)-TK-Luc vectors and then stimulated with (A) 10 μM rifaximin, phallusiasterol A (**15**) or phallusiasterol B (**16**) or phallusiasterol C (**18**) for 18 h, or (B) 10 μM rifaximin alone or in combination with 50 μM of compounds **15**, **16** or **18**. Relative Luciferase Units were normalized with β-galactosidase Units (RLU/βgal). (C, D) Real-Time PCR analysis of CYP3A4 and MDR1 expression in HepG2 cells primed with 10 μM rifaximin, compounds **15**, **16** or **18** for 18 h. Values were normalized relative to GAPDH mRNA and expressed relative to those of not treated cells, which were arbitrarily set to 1. All experiments were performed in triplicate. NT, not treated cells. R, Rifaximin. * $P < 0.05$ versus NT cells. Data are mean ± SE.

We then analyzed by means of molecular docking calculations the interactions of phallusiasterol A with hPXR. The calculations were run by Autodock4.2 software.⁵³

The hPXR presents a large ligand binding cavity, allowing the accommodation of both small and large ligands and the number of chemicals has grown rapidly,

including many drugs in use such as statins, antibiotic rifampicin and its derivative rifaxim, antihypertensive drugs nifedipine, as well as pesticides, environmental toxicant, plasticizers.

In a previous work⁵¹ the possible interactions of solomonsterols A and B with hPXR has been reported. In this model, the 2-O and 3-O sulfate groups exert hydrogen bonds with His407 and Ser247, respectively. In this study three different x-ray structures of the PXR LBD (pdb codes: 3hvl, 1nrl and 1m13) have been used. As shown in Figure 5, the OH at C-6 and the 5-O sulphate groups form hydrogen bonds with NH of His407 and OH of Ser247, respectively. The steroidal scaffold engages Van der Waals interactions with hydrophobic residues of LBD, such as Leu209, Met243 and Phe251, and the flexible side chain is settled in a hydrophobic pocket establishing several favourable contacts with Met250, Phe288, Trp299 and Tyr306 (**Figure 3.9**). Noteworthy, in this pose, the phallusiasterol A is oriented to form further hydrophobic interactions with Phe420 and Met425. These last residues are on a flexible α -helix (AF-2 helix) in the activation function 2-region (AF-2). This part of receptor is responsible for binding of the co-activator or co-repressor peptides. In conclusion the present docking analysis revealed that phallusiasterol A fitted well in the LBD of PXR and could be stabilized PXR in agonist conformation with consequent conformational change and co-activator recruitment.

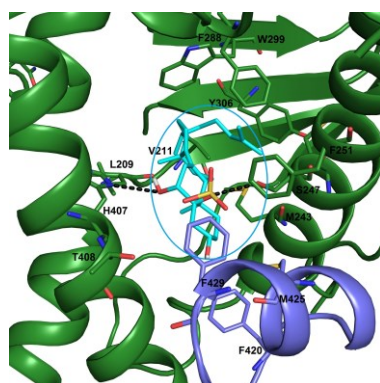


Figure 3.9. Binding mode of phallusiasterol A (**15**) (cyan sticks), predicted by docking calculations in the PXR LBD (PBD code 3HVL). PXR is shown as green cartoon, AF-2 helix is coloured in violet. Amino acids involved in ligand binding are shown as green and violet sticks. All hydrogen are omitted for clarity.

3.1.4. *Phosphoeleganin, a new cytotoxic phosphopolyketide from the ascidian *Sidnyum elegans**

Polyketides represent a large family of complex natural products built from simple carboxylic acid residues; they are produced primarily by microorganisms and find wide ranging applications as pharmaceuticals.⁵⁴ In the marine environment, they have been frequently isolated from invertebrates-associated bacteria and/or fungi.^{55,56} Most marine natural polyketides possess polyhydroxy and polyoxy substituents in their structures, but the phosphate group is a less recurring functionality. In the course of our search for cytotoxic compounds from Mediterranean ascidians, we have investigated the ascidian *Sidnyum elegans* (Giard, 1872) collected in Sardinia; this study resulted in the isolation of a potent cytotoxic phosphate-containing linear polyketide, named phosphoeleganin (**19**) whose isolation, structure determination, partial absolute stereochemistry assignment, and biological activities are reported herein (**Figure 3.10**).

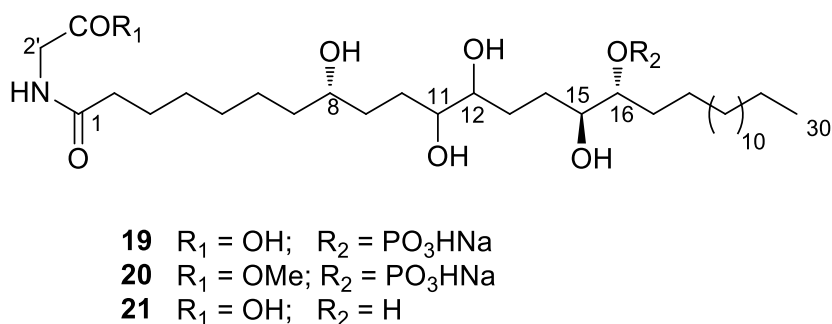


Figure 3.10 Chemical structure of phosphoeleganin (**19**) and its semisynthetic derivatives **20** and **21**

The methanol and chloroform extracts of specimens of *Sidnyum elegans* (Giard, 1872) collected in Sardinia were combined and concentrated; the resulting aqueous residue was partitioned between *n*-butanol and H₂O. Medium pressure chromatography (MLPC) over C-18 column of the *n*-butanol soluble material, followed by repeated RP-18 HPLC separation and purification steps, yielded phosphoeleganin (**19**) in the pure state.

The high resolution ESI mass spectrum of **19** (negative ion mode) displayed a pseudomolecular ion at *m/z* 668.3832 corresponding to [M-H]⁻. These MS data and

the information provided by ^{13}C NMR spectrum, which contained 32 carbon resonances, allowed the molecular formula $\text{C}_{32}\text{H}_{63}\text{NO}_{11}\text{P}$ (calculated value: 668.4049) to be established for compound **19**. The ^{13}C -NMR spectrum (CD_3OD) revealed the presence of two carbonyl signals (δ 176.6 and δ 172.0), which accounted for the only two unsaturation degrees indicated by the suggested molecular formula.

Analysis of the ^1H -NMR spectrum (CD_3OD) and HSQC data revealed the presence of five oxymethines [δ_{H} 3.38, δ_{C} 76.3 (2H, H-11 and 12); δ_{H} 3.54, δ_{C} 72.9, (H-8); δ_{H} 3.70, δ_{C} 74.7 (H-15); δ_{H} 4.19, δ_{C} 82.8 (H-16)], an aliphatic methyl at δ 0.90 (t, $J = 7.3$ Hz, Me-30), a deshielded methylene signal resonating as a singlet at δ 3.92 (δ_{C} 41.8, 2H-2'), and an aliphatic methylene at δ 2.25 (t, $J = 7.6$ Hz, 2H-2). Several unresolved methylene signals (δ 1.29-1.36), attributable to the protons of a long unbranched carbon chain, were also present. When the proton spectrum of **19** was recorded in $\text{DMSO-}d_6$, an additional signals at δ 8.05 (bs, NH) appeared, which did not display any correlations in the HSQC spectrum; on the other hand, the COSY spectrum ($\text{DMSO-}d_6$) evidenced this proton to be coupled to a methylene doublet at δ 3.70 ($J=5.8$ Hz, 2H-2') which replaced the methylene singlet at δ 3.92 present in the spectrum recorded in CD_3OD . Both the signals at δ 8.05 and 3.92 in the HMBC spectrum ($\text{DMSO-}d_6$) were correlated to the carbonyls at δ 170.8 (C-1') and 172.0 (C-1), this latter carbon being coupled to the C2 methylene protons resonating at δ 2.10. Thus, the presence of a glycine residue linked through the amide linkage at one end of the long chain of **19** was assumed. According to the remaining features of the NMR spectra and MS data, the presence of four secondary alcohol and of a phosphate groups in the molecule was supposed.

The latter hypothesis was verified by the use of ^{31}P -NMR spectroscopy. A single resonance at δ 0.90 ppm was present in the ^{31}P NMR spectrum of **19**; furthermore, a ^1H - ^{31}P -HMBC cross peak was observed from this signal and the oxymethine proton at δ 4.19 ($^3J_{\text{H,P}}=8.2$, H-16). Attachment of a phosphate group at C-16 was also deduced from the splitting of this carbon resonance (δ 82.5) by $^2J_{\text{C,P}}=6.2$ Hz in the ^{13}C NMR spectrum (**Table 3.6**).

Table 3.6. ^1H (700 MHz) and ^{13}C (125 MHz) NMR data for phosphoeleganin in CD_3OD and DMSO.

Phosphoeleganin A in CD_3OD			Phosphoeleganin A in DMSO	
Pos.	$\delta_{\text{C}}^{\text{a}}$	δ_{H} (mult, J in Hz) ^a	$\delta_{\text{C}}^{\text{a}}$	δ_{H} (mult, J in Hz) ^a
1	176.9	-	172.0	-
2	36.7	2.25 (t, 7.5)	34.4	2.10 (t, 7.5)
3	26.5	1.64 ^b	24.5	1.48
4	29.9	1.36 ^b	28.0	1.22
5	26.4	1.34 ^b	24.5	1.20 ^b
6	26.4	1.34 ^b	24.5	1.20 ^b
7	38.4	1.46 ^b 1.41 ^b	36.3	1.33 1.27
8	72.9	3.54 (m, 3.9, 3.9, 8.1)	69.5	3.34
9	34.9	1.72 ^b 1.37 ^b	33.2	1.56 ^b 1.22 ^b
10	29.7	1.81 ^b 1.37 ^b	28.3	1.64 1.20
11	76.3	3.38 ^b	73.6	3.15
12	76.3	3.39 ^b	73.6	3.15
13	29.8	1.89 1.37 ^b	28.6	1.76 1.14
14	29.7	1.83 ^b 1.44 ^b	27.5	1.60 1.22
15	74.7	3.71 (dt, 3.7, 3.7, 9.2)	72.6	3.37 ^b
16	82.8	4.18 (m, 3.7, 3.7, 8.3)	77.6	4.01 (m)
17	31.6	1.69 ^b 1.61 ^b	28.6	1.45 ^b 1.23 ^b
18	26.0	1.54 ^b 1.40 ^b	24.5	1.34 ^b 1.22 ^b
19/26	30.0	1.31 ^b	28.2	1.20
27	30.2	1.29 ^b	30.7	1.22 ^b
28	33.1	1.29 ^b	30.8	1.22 ^b
29	23.5	1.30 ^b	21.5	1.28 ^b
30	14.4	0.90 (t, 7.0)	13.3	0.85 (t, 7.0)
1'	172.0	-	170.8	-
2'	41.8	3.92 (s)	40.0	3.70 (d, 5.8)
NH	-	.	.	8.1

The whole of the 2D NMR data (COSY, TOCSY, HSQC, HMBC, and HSQC-TOCSY) allowed us to distribute these functionalities into three partial segments (A-C, **Figure 3.11**) but the severe overlapping of the remaining methylene resonances in the NMR spectra prevented the gross linear skeleton of **19** to be delineated from spectroscopic analysis.

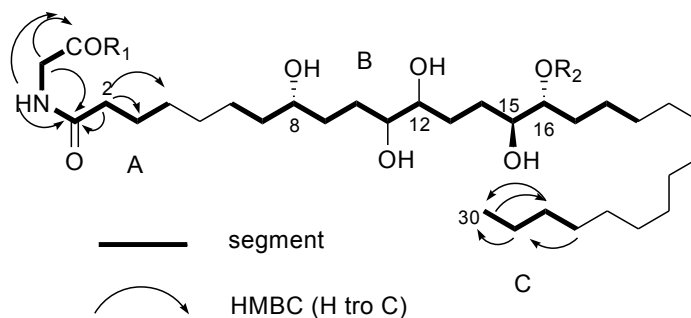


Figure 3.11. Segments A-C deduced from COSY, TOCSY, HSQC, HMBC, and HSQC-TOCSY experiments, and selected HMBC correlation

To determine the number of methylene units separating segments A and B and segments B and C, respectively, and, thus, to complete the planar structure assignment of phosphoeleganin (**19**), the natural metabolite was degraded using HIO₄ and then reduced by NaBH₄ to give the fragmentation products **22** and **23** (**Figure 3.12**) corresponding to the C1-C11 and C12-C30 portions of the molecule. Chemical characterization and, above all, ESIMS analysis of both compounds **22** and **23** (see experimental section) allowed us to complete the assignment of the planar structure of the parent compound **19**.

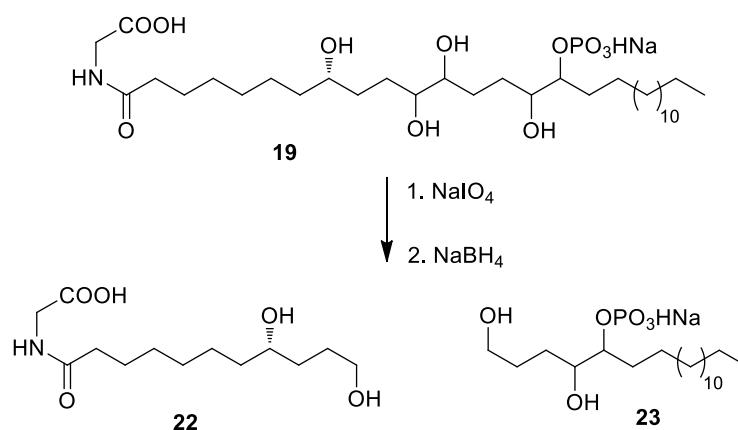


Figure 3.12. Periodate degradation reaction scheme

The effects of phosphoeleganin on the growth and viability of tumor and non-tumor cell lines have been investigated. Phosphoeleganin (**19**) showed significant cytotoxicity against different cell lines in vitro. Preliminary pharmacological studies showed that phosphoeleganin exhibited a significant and concentration-dependent cytotoxic activity toward the human epithelial cells (HaCaT cells), prostate cancer cells (DU145) and cells of neuroblastoma (N2a-APP695). To identify the biological target responsible of the pharmacological activity of phosphoeleganin, its ability to inhibit a number of kinases and phosphatase has been evaluated. In collaboration with ManRos therapeutics, the phosphoeleganin has been tested on a panel of protein kinases relevant to human disease. No correlations have been observed between the cytotoxic activity and the inhibition kinases (**Table 3.7**).

Whereas, studies aimed to explore the drug target evidenced its inhibitory effect on protein tyrosine phosphatase 1B (PTP1B), with an IC_{50} of 7.25 ± 1.55 mg / mL.

Interestingly, the preliminary cytotoxicity screening performed on the degradation products **22** and **23** revealed that the fragments were both less active or even inactive with respect to the original molecule. This suggested that both portions of phosphoeleganin molecule play an important role for the cytotoxic activity. Further studies on the effects of these derivatives as phosphatase modulators are currently in progress.

Table 3.7. Effects of phosphoeleganin (**19**) and its derivatives **22** and **23** on protein kinases.

Compound	CDK5/p25	CDK9/cyclinT	CK1	CLK1	DYRK1A	GSK3
19	110	107	90	104	98	83
22	86	91	90	111	92	103
23	96	90	111	110	114	73

3.1.5. Investigation of the Mediterranean sponge *Axinella polypoides*: isolation of a new cyclonucleoside and a new betaine

Diverse natural products found within sponges mediate many of their ecological interactions, including defense against predators and fouling organisms. Marine sponges of genus *Axinella* are an interesting target for chemo-ecological investigations. They are a well-known source of pyrrole-imidazole alkaloids (PIAs), which have been found only in the marine environment to date. Historically, this family of alkaloids has attracted the attention of natural product chemists because of their structural complexity and pharmacological activity; their role in chemically mediated interactions of Caribbean sponges has also been proven.^{57,58} In addition, the systematic recurrence of PIAs in *Axinellidae* sponges, as well as in *Agelasidae*, allowed for speculation as to their taxon-specificity and consideration of these secondary metabolites as chemical markers for phylogenetically related sponges.⁵⁹ However, the setting up of a chemical “fingerprint” of a sponge, collected from different ecosystems, requires exhaustive chemical studies. An illustrative example is the sponge *Axinella polypoides* (Schmidt 1862), widely distributed in the rock reefs of the Mediterranean Sea. Early studies are reported in literature on the chemistry of this sponge, mainly concerning its steroid and lectin content;⁶⁰⁻⁶⁴ actually, recent re-examinations of samples of *A. polypoides*, coming from different Mediterranean areas, demonstrated that the sponge has an efficient biosynthetic potential, revealing a great variety and abundance of secondary metabolites, some of them being new molecules (**Figure 3.13**). In detail, two new modified amino acids, axiphenylalaninium (**24**) and axityrosinium (**25**), were found in specimens of the sponge collected off Marseille city⁶⁵ along with the known metabolites C²- α -D-mannopyranolsyl-L-tryptophan (**29**),⁶⁵⁻⁶⁸ palythine (**27**),^{65,69,70} N³,5'-cycloxanthosine (**30**),^{65,67,71} and taurine;^{65,72} no data was reported on the presence of PIAs in the sponge. Successively, during our ongoing search for new bioactive alkaloids from *Axinellidae* sponges, my research group isolated compounds **24** and **25** in specimens of *A. polypoides* collected along Corsican coasts, together with a new betaine, polyaxibetaine (**26**).⁷³

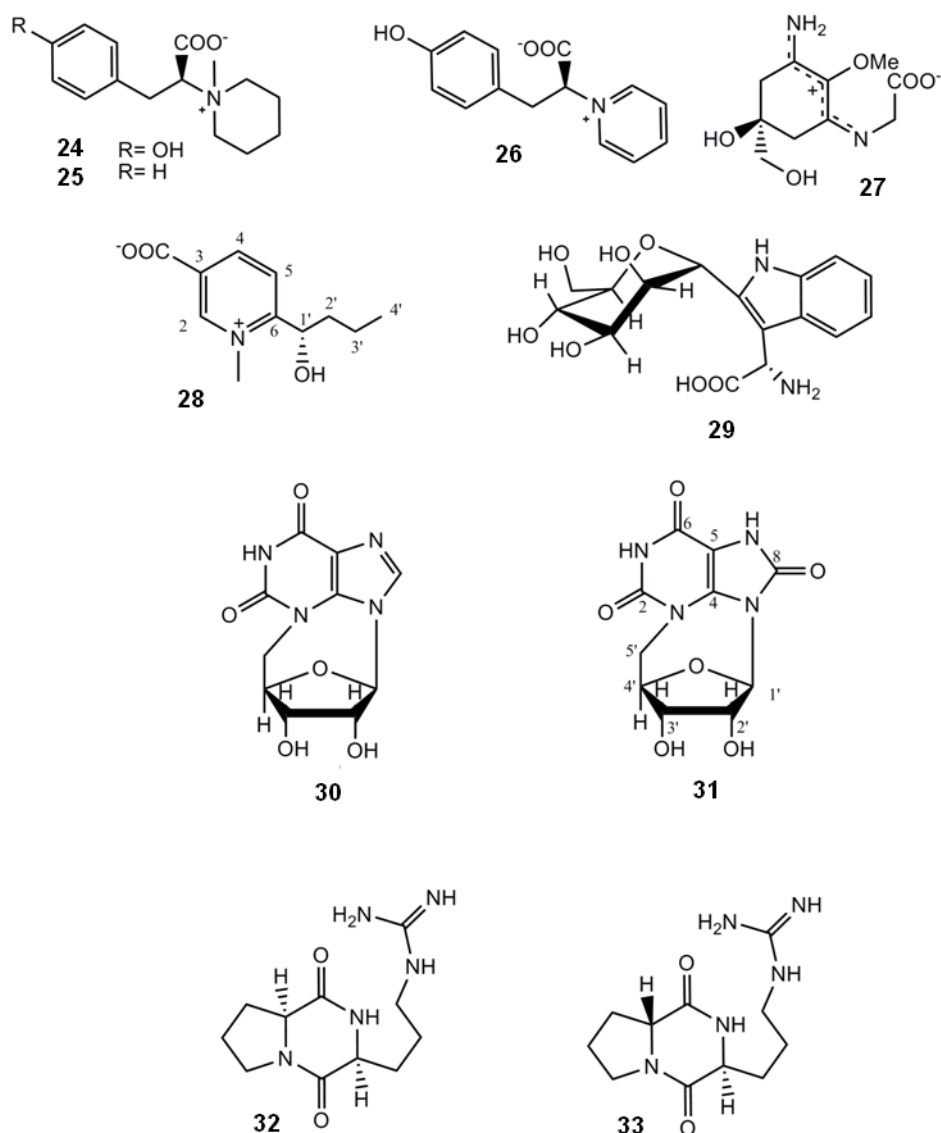


Figure 3.13. Secondary metabolites isolated from *A. polypoides*.

In the present PhD thesis, I describe the results obtained from a further and more exhaustive exploration into the metabolic content of a larger sample of *A. polypoides*, which resulted in the isolation of a new pyridinium derivative, compound **28**, and the new cyclonucleoside **31**. All the previously reported secondary metabolites from the sponge were re-isolated, except for palythine (**27**). We did not find any member of the PIAs family in the sponge extract but, interestingly, it was shown to contain the already known cyclodipeptides **32** (verpacamide A) and **33**. The cyclo(L-Arg-D-Pro) dipeptide **33** was first isolated from a marine bacterium, *Pseudomonas* sp. IZ208;⁷⁴ the relevant cyclo(L-Arg-L-Pro) stereoisomer, verpacamide A (**32**), was first reported

as a natural metabolite of the sponge *Axinella vaceleti* along with the analogues verpacamides B–D and these metabolites were considered as possible precursors of PIAs.

Specimens of *A. polypoides* were collected in the bay of Calvi (Corsica, France), they were immediately frozen after collection, and kept at $-20\text{ }^{\circ}\text{C}$ until extraction. For the extraction, fresh thawed tissues of the sponge were homogenized and exhaustively extracted at room temperature with MeOH and CHCl_3 successively. The extracts were combined and concentrated; the resulting aqueous suspension was then partitioned between butanol and H_2O . Both organic and aqueous layers were fractionated by MPLC over a reversed-phase C-18 column and by DCCC, respectively. All the fractions thus obtained were subjected to a combined NMR/ESIMS-based monitoring for the rapid identification of PIAs, also exploiting, as reference compounds, the copious chemical library of these alkaloids available in our laboratories. None of the already described PIAs was detected; fractions of interest were separated by repeated HPLC, resulting in the isolation of pure compounds **24–26** and **28–33**. Taurine, as well as compounds **24–26**, **29**, **30**, **32**, and **33** were readily identified by comparison of their spectroscopic data with those reported in literature,^{65–73} while the structures of the new compounds **28** and **31** were established as follows.

HRESI mass spectrum (positive ions) of **28** revealed two pseudomolecular ion peaks at m/z 210.1130 and 232.0950, corresponding to $[\text{M} + \text{H}]^+$ (calculated value: 210.1125), and $[\text{M} + \text{Na}]^+$ (calculated value: 232.0944), respectively. The molecular formula $\text{C}_{11}\text{H}_{15}\text{NO}_3$ was thus established for **28**, indicating five unsaturation degrees. $^1\text{H-NMR}$ spectrum of **28** (CD_3OD), interpreted on the basis of 2D experiments (HSQC, COSY) contained a set of aromatic signals, each integrating for one proton; the chemical shift and coupling constants values of these signals [δ 9.10 (bs, $\delta_{\text{C}} = 148.7$, H-2); 8.84 (bd, $J = 8.2$ Hz, $\delta_{\text{C}} = 146.3$, H-4); 8.19 (d, $J = 8.2$ Hz, $\delta_{\text{C}} = 126.6$, H-5)] were strongly indicative of a 1,2,5-trisubstituted pyridinium ring. Further proton resonances were a deshielded methine at δ 5.13 (dd, $J = 9.0, 3.3$ Hz, $\delta_{\text{C}} = 69.3$, H-1'), two AB methylene systems at δ 1.72/1.81 ($\delta_{\text{C}} = 38.9$, 2H-2') and 1.54/1.63 ($\delta_{\text{C}} = 19.9$, 2H-3'), as well as a methyl resonating as a triplet at δ 1.00 ($J = 7.5$ Hz, $\delta_{\text{C}} = 14.0$, 3H-4'), which were arranged in a single spin system on the basis of COSY connectivities. The signal at δ 5.13 was correlated in the HSQC spectrum

with a signal at δ 69.3 attributable to an oxygen bearing carbon, thus evidencing a 1-hydroxybutyl unit.

An N-methyl signal δ 4.38 ($\delta_C = 46.1$) was also present in the proton spectrum of **28**; it was correlated in the ROESY spectrum (CD₃OD) with the aromatic proton singlet at δ 9.10 (H-2) and with the oxymethine proton at δ 5.13 (H-1'). This latter information, according to the coupling constants pattern of the aromatic signals, provided convincing evidence for an N-methyl-2,5-disubstituted pyridinium ring and indicated that the 1-hydroxybutyl unit must be linked at one of the N-flanking carbons. Diagnostic C–H long range couplings, evidenced by HMBC map (CD₃OD, see Table 1), substantiated the proposed structural features and allowed to identify the third substituent, obviously linked at C-3.

Table 3.8. NMR data (CD₃OD) of compound **28**.

Pos	δ_H (mult., <i>J</i> in Hz)	δ_C	HMBC
1-NMe	4.38 (s)	46.1	2, 6
2	9.10 (bs)	148.7	1-NMe, 4, 6, COO ⁻
3	-	137.8	-
4	8.84 (bd, 8.2)	146.3	2, 6, COO ⁻ Na ⁺
5	8.19 (d, 8.2)	126.6	3, 6, 1'
6	-	163.0	-
1'	5.13 (dd, 3.3, 9.0)	69.3	6, 2'
2'	1.72 (m)	38.9	6, 1', 3', 4'
	1.81 (m)		
3'	1.54 (m)	19.9	1', 2', 4'
	1.63 (m)		
4'	1.00 (t, 7.5)	14.0	2', 3'
-COO ⁻	-	167.0	-

Particularly, the N-methyl signal at δ 4.38 was correlated to the carbon at δ 148.7 (C-2) and a quaternary carbon at δ 163.0 (C-6) which, in turn, was coupled to the signal at δ 5.13 (H-1') and 8.19 (H-5); the latter signal was correlated with the oxymethine carbon at δ 69.3 (C-1') and the quaternary carbons at δ 163.0 (C-6) and 137.8 (C-3). Moreover, both aromatic signals at δ 9.10 (H-2) and 8.84 (H-4) were coupled to a low-field carbon resonance at δ 167.0, attributable to a carbonyl; this datum, according to the mass data, allowed to locate a carboxylate function at C-3, thus accounting for the last unsaturation degree indicated by the molecular formula. Therefore, the planar structure of compound **28** was unambiguously defined as 6-(1-hydroxybutyl)-1-methylpyridinium-3-carboxylate.

A pseudomolecular peak was present in the HRESI mass -spectrum (positive ions) of **31** at m/z 283.0673 $[M + H]^+$ (calculated value: 283.0679), thus supporting the molecular formula $C_{10}H_{10}N_4O_6$. 1H - and ^{13}C -NMR spectral data of **31** strongly resembled those of the known cyclonucleoside **30** (Table 3.9). The proton spectrum of **31** (d_6 -DMSO) contained indeed resonances relevant to a sugar moiety which were nearly identical to those of **30**, with regard to the number and shape of the signals (Table 3.9); the striking difference was confined to the chemical shift value of the anomeric proton (H-1', δ 5.67 in **31** versus 6.15 in **30**). As for the heterocyclic moiety, the 1H -NMR spectrum of **31** lacked the signal due to the single aromatic proton of xanthosine present in that of **30** at δ 7.79 but a further exchangeable proton at δ 11.2 (NH-7) was present. On the other hand, ^{13}C -NMR spectrum (d_6 -DMSO), interpreted also on the basis of the HSQC experiment, contained a further deshielded quaternary carbon resonance at δ 149.6 instead of the C-8 methine carbon resonating at δ 134.5 in the ^{13}C -NMR spectrum of **30**. All these findings indicated the 8-oxo- $N^3,5$ -cycloxanthosine structure for compound **31**, according to MS data and HMBC correlations (Table 3.9).

Table 3.9. NMR data (d_6 -DMSO) of compounds **30** and **31**.

Position	30		31		
	δ_C	δ_H (J in Hz)	δ_C	δ_H (J in Hz)	HMBC ^a
1	-	-	-	-	-
2	151.0	-	150.7	-	-
3	-	-	-	-	-
4	140.7	-	136.8	-	-
5	117.8	-	98.8	-	-
6	157.4	-	153.4	-	-
7	-	-	-	-	-
8	134.5	7.79 (s)	149.6	-	-
9	-	-	-	-	-
1'	92.5	6.15 (s)	91.1	5.67 (s)	4, 8, 2', 3', 4'
2'	75.8	3.87 (dd, 5.2, 5.0)	75.0	3.90 (t, 5.3)	1', 4'
3'	70.1	4.20 (m)	70.7	4.23 (m)	5'
4'	83.7	4.55 (m)	83.6	4.46 (m)	-
5'a	51.3	4.56 (m)	52.3	4.51 (dd, 14.4, 2.4)	2, 4, 3', 4'
5'b	51.3	3.71 (dd, 15.2, 3.2)	52.3	3.72 (dd, 14.4, 2.8)	2, 4, 3', 4'
OH-2'	-	5.62 (d, 5.0)	-	5.60 (d, 5.3)	-
OH-3'	-	5.62 (bs)	-	5.35 (d, 7.1)	-
NH-1	-	11.2	-	11.3	5, 6
NH-7	-	-	-	11.2	4, 5, 8

^a HMBC correlations are from proton(s) stated to the indicated carbon.

While highlighting the uncommon chemodiversity of *A. polypoides*, these results pointed out that the sponge does not elaborate PIAs. This finding is in agreement with the results of a recent investigation on the chemical defense of *A. polypoides* and the co-occurring species *A. verrucosa*, against microbial fouling and in feeding deterrence of a potential predator,⁷⁶ activities which are believed to be mediated by PIAs.^{57,58} This study indicated in *A. polypoides* neither chemical defense against microbial fouling nor chemically mediated feeding deterrence activity. In contrast, the sympatric sponge *A. verrucosa* has a chemical defense which, as in many other species of the genera *Axinella* and *Agelas*, is mediated by its bromopyrrole compounds,⁷⁷⁻⁷⁹ such as hymenidin, which exhibits multiple defensive roles.⁷⁶ Recent studies have reported on the phylogenetic status of the genus *Axinella*,⁸⁰ which is difficult to define on the basis of its morphological character and includes a heterogeneous assemblage of species. A new phylogenetic hypothesis of Axinellidae and *Axinella*, based on two independent molecular markers (18S and 28S rRNA), has been proposed. In this taxonomic reconstruction, *A. polypoides* and *A. vaceleti* belong to a distinct clade (Axinellidae^P) than *Axinella verrucosa*; this latter sponge is now included in a new clade, named *Cymbaxinella*^P, which could be interpreted also as a new genus. The new clade *Cymbaxinella*^P constitutes a well supported clade sister-group to *Agelas*^P, according to the chemotaxonomic hypothesis proposed by Braekman *et al.*⁸¹ on the basis of the presence of pyrroles. The clades *Agelas*^P and *Cymbaxinella*^P constitute a new clade: *Agelasida*^P. Our results, thus, provide a chemotaxonomic support for the above mentioned molecular analysis, demonstrating that *A. polypoides* does not contain pyrroles, whereas it shares with *A. vaceleti* the presence of diketopiperazine derivatives.

3.1.6. Conclusions

In conclusion, the extraction and chemical analysis of different species of sea squirts (*Aplidium conicum*, *Ciona edwardsii*, *Aplidium elegans*, *Phallusia fumigata* and *Sidnyum elegans*) and of the sponge *Axinella polypoides* led to the isolation of new bioactive molecules, which are structurally different. Among these, two new meroterpenes, conithiaquinones A and B, and three alkyl sulphates with cytotoxic properties. Three sulfated sterols, phallusiasterols A-C, one of them with agonist activity on the pregnane X receptor (PXR) in HepG2 cells. The phosphoeleganin, a

potent inhibitor of protein tyrosine phosphatase 1B (PTP1B). An analysis of the metabolic content of the sponge *Axinella polypoides* has provided important chemotaxonomic information about the organism, in addition, led to the isolation of a new betaine and a new cyclonucleoside.

The structural diversity of the metabolites above reported highlighted that marine organisms continue to be rewarding sources of chemodiversity associated to a very large array of pharmacological activities. These products provide a rich source of chemical diversity that can be used to design and develop new potentially useful therapeutic agents.

3.2. THE STEREOCHEMISTRY ASSIGNMENT: A HARD CHALLENGE IN NATURAL PRODUCTS RESEARCH

Stereocomplexity often distinguishes the structures of natural products from synthetic medicinal drugs, however, many complex natural products are listed in the US and other pharmacopeia. Thus, the determination of relative and absolute configuration of a natural substance is a key step in the process of its structural characterization. Only by knowing the stereochemistry of a molecule can be traced back to its three dimensional structure and approach to biological studies, e.g. studies of drug-receptor interaction, or chemical, such as the studies related to the total synthesis of complex molecules with a good pharmacological activity. Most of the natural compounds has one or more chiral centers. Usually, in the configuration determination, we start by establishing the relative configuration of chiral centers. NMR can be very useful through the values of chemical shifts (δ), coupling constants (J) and NOE effects.

The chemical shifts of protons are influenced by their chemical around, so the protons of two diastereomers have different values.

The Karplus's equation⁸² describes the influence of relative arrangements of protons in a molecules on the values of coupling constants (J_{H-H}).

$${}^3J = A\cos\theta^2 + B\cos\theta + C$$

This equation evidences that the values of homonuclear (${}^3J_{H-H}$) and heteronuclear (${}^3J_{C-H}$) coupling constants are related to the value of the dihedral angle θ between atoms. The superscript "3" indicates that a 1H atom is coupled to another 1H atom three bonds away, via H-C-C-H bonds. The magnitude of these couplings are generally smallest (0-1,5 Hz) when the torsion angle is close to 90° and largest at angles of 0 and 180° . In some cases the axial-axial coupling constant for an antiperiplanar 180° H-C-C-H configuration may be more than 9.5 Hz. Indeed for rigid cyclohexanes it is around 9-13 Hz, because the dihedral angle is close to 180° , where the orbitals overlap most efficiently.

Additional information about relative configuration of stereogenic centers can be obtained from the so-called NOE effect (N.O.E.: "Nuclear Overhauser Enhancement").⁸³ This effect can be observed upon irradiation, during the acquisition

of the spectra, on a specific signal. In this way, the relaxation times of all the protons surrounding the irradiated proton (distance $\leq 2.5 \text{ \AA}$), even though not belonging to the same spin system, are influenced and thus, their height changes. The NOE effect establishes a spatial relationship between substituents of fixed molecules, but this effect is dependent from the dimensions of the molecule. The ROESY (Rotating-frame Overhauser Spectroscopy) experiment is a chemical shift homonuclear correlation which can detect ROEs (Rotating-frame Overhauser Effect). ROE is similar to NOE, being related to dipolar coupling between nuclei, and depending on the geometric distance between the nuclei. While NOE is positive for small molecules and negative for macromolecules, ROE is always positive. Therefore, the ROESY experiment is particularly useful for mid-size molecules, which would show a NOE close to zero. Sometimes we couldn't assign the stereochemistry of a new compound exclusively on the basis of the methods described above, so we had to appeal to other techniques, as I will describe in this chapter.

The following section describes the main stereochemical issues I have dealt with during the structure determining of the isolated compounds. They have been separately discussed also in order to highlight the diversity of methods and/or approach which can be used in stereostructure determination of new molecules, although most of them are original strategies adapted to the current problem.

3.2.1. Absolute configuration of axibetaine through ab initio calculations

Absolute configuration (AC) of compound **28** was established with the help of electronic circular dichroism (ECD) spectroscopy assisted by quantum mechanical calculations. The application of *ab initio* time-dependent density functional theory (TDDFT) to the calculation of ECD spectra has greatly enhanced the reliability with which they can be predicted and, thus, this methodology is being increasingly utilized in determining ACs of natural products.^{73,84-86} The experimental ECD spectrum of **28** was virtually compared to that predicted by TDDFT calculations for one of the two enantiomers. In detail, an initial conformational analysis of the *S* stereoisomer was performed, using the Simulated Annealing procedure (INSIGHT II Software Package). The resulting conformers were ranked on the basis of their conformational energy values and grouped into families. Twelve minima for *S*-**28**

were obtained and all conformers were optimized with the software package Gaussian 03⁸⁷ by using DFT at the RB3LYP/6-31G(d) level (the conformational families of *S*-**28**, as well as their resulting relative (ΔE) and free (ΔG) energies, are provided as Supporting Information). For all conformers of *S*-**28**, the excitation energies, as well as the oscillator and rotatory strengths of the electronic excitation were calculated, using the TDDFT methodology at the RB3LYP/6-31G(d,p) level; their ECD spectra were then simulated by the overlapping Gaussian function. To obtain the final ECD spectrum of each compound, the simulated spectra of the lowest energy conformations were averaged, by following the Boltzmann statistic, and were UV corrected. The theoretical curve was then compared to the experimental spectrum of compound **28**, recorded in MeOH. As shown in Figure 3.14, the agreement between the simulated and experimental ECD spectra of **28** was very satisfactory and, thus, the absolute configuration of **28** was established as *S*.

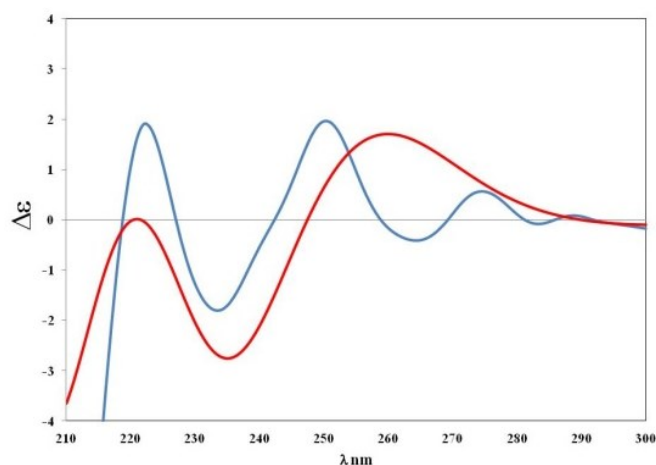


Figure 3.14. Theoretical CD curve (---) of *S*-**28** model vs. experimental curve (—) of compound **28**.

3.2.2. Ab initio calculations to determine the stereochemistry and the regiochemistry of conithiaquinone A

The whole of the NMR data recorded for conithiaquinone A (see section 3.1.1) allowed determining its planar structure but, unfortunately, they were not enough to unambiguously define the relative position of the sulfur and nitrogen atoms in the heterocyclic ring. The regiochemistry of the 1,1-dioxo-1,4-thiazine ring was thus clarified by ab initio calculation of NMR shifts, an increasingly popular tool for the stereostructure assignment of natural products.⁸⁸ By using the recently developed DP4 NMR prediction method of Smith and Goodman,⁸⁹ the experimental ¹³C and ¹H NMR chemical shifts of conithiaquinone A (**1**) were compared to those calculated for structures A1-A4 (**Figure 3.15**). Calculations were performed on both epimers at C-9 for each regioisomer in order to gain further support to the relative stereochemistry suggested by NMR data. The DP4 analysis was designed specifically for the situation where one set of experimental data is available to which one possible isomeric structure out of many must be assigned. It is based on calculated error probabilities for scaled computed chemical shifts for each hydrogen and carbon atom, assuming a statistical t distribution for these errors. A mathematical algorithm is then used to quantify the probability of the correct assignment of each structure.⁹⁰ The calculated chemical shifts for structures A1-A4 as well as those observed for conithiaquinone A were uploaded to the DP4 method online applet (<http://www-jmg.ch.cam.ac.uk/tools/nmr/DP4>). DP4 analysis identified structure A3 as the most likely, with a probability of 99.9% (the remaining 0.1% probability was assigned to structure A4). The computational evidence strongly indicated that A3 or its enantiomer is the true structure of conithiaquinone A (**Figure 3.15**).

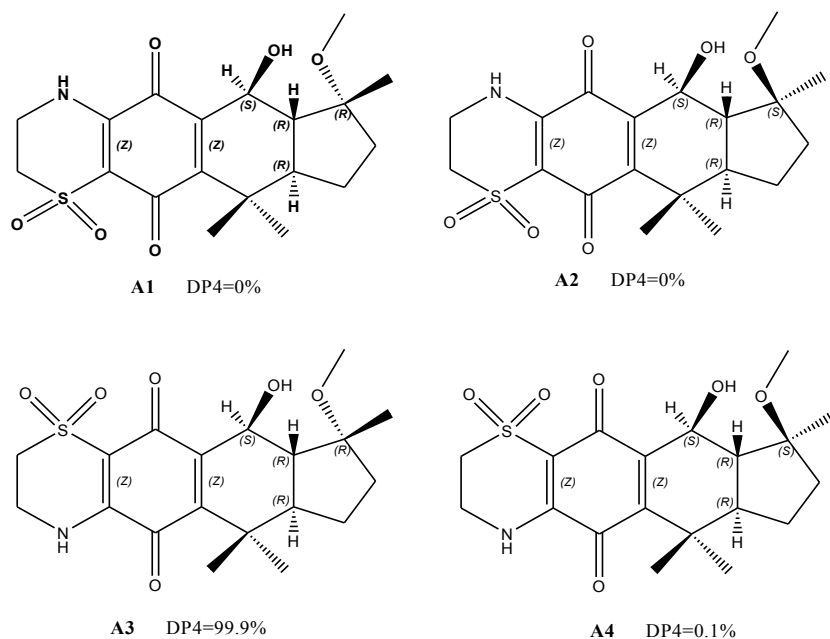


Figure 3.15 Results of DP4 analysis using both carbon and proton data.

In an effort to resolve this last ambiguity, we employed TDDFT methodology to calculate the ECD spectra for the two possible enantiomers of **1** which were then compared with the experimental data (MeOH) obtained for **1**.^{91,92} Although the calculated absorption wavelengths did not exactly fit with the experimental peak positions, the general features of ECD spectrum calculated for the 6a*R*, 9*R*, 9a*R*, 10*S* isomer showed a much better match with the experimental data than the inverted spectrum calculated for its enantiomer (**Figure 3.16**). Differences between the calculated and experimental spectra presumably resulted from an overestimation of the UV absorbance in the calculations or may be due to minor differences between calculated and solution conformers.^{93,94} These observations allowed us to propose the 6a*R*, 9*R*, 9a*R*, 10*S* absolute configuration for compound **1**. The assignment of both regiochemistry and absolute configuration of **2** was achieved following the same procedure as described for **1** (for details, see the Supporting Information).

3.2.3. Determination of phosphoeleganin stereochemistry by NMR and microscale derivatization studies

The determination of the absolute configuration of the five stereogenic centers of the phosphoeleganin (**19**) required a series of microscale derivatization reactions and spectroscopic analysis of their products.

In order to investigate the relative configuration of the 11,12 - diol system in the phosphoeleganin, the five-membered acetonide (**34**) was prepared.⁹⁵ To this purpose, phosphoeleganin (**19**) was treated with 2,2-dimethoxypropane and a catalytic amount of Dowex 50W-X8 to give the corresponding 11,12-O-isopropylidene derivative. As reported in the literature,⁹⁵ the difference in the chemical shifts of the methyl groups in the five membered acetonide is larger for the *cis*-isomer ($\Delta\delta$ 0.12–0.14) when compared to the *trans*-isomer ($\Delta\delta$ 0.01–0.04). The observed $\Delta\delta$ value of 0.09 ppm between the two methyl groups in the phosphoeleganin acetonide (see Experimental) points towards the *cis*-isomer allowing us to suggest a 11,12-*erythro* relative stereochemistry (**Figure 3.17**).

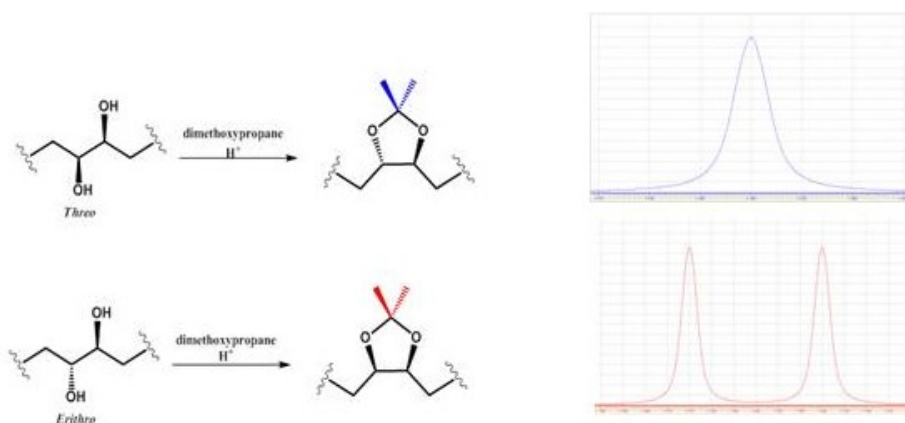


Figure 3.17. Partial ¹H NMR spectra relevant to *trans*- and *cis*- acetonides

To assign the absolute stereochemistry at C8 we used the chiral derivatizing reagent (CDA) MPA and the periodate degradation product **22**. At first the compound **22** was subjected to acidic methanolysis with 1 M HCl and then derivatized with (*R*)-(-)- and (*S*)-(+)-methoxyphenylacetic acid (MPA) using 1-ethyl-3-[3-dimethylaminopropyl]carbodiimide (EDC)⁹⁶⁻⁹⁸ (**Figure 3.18**).

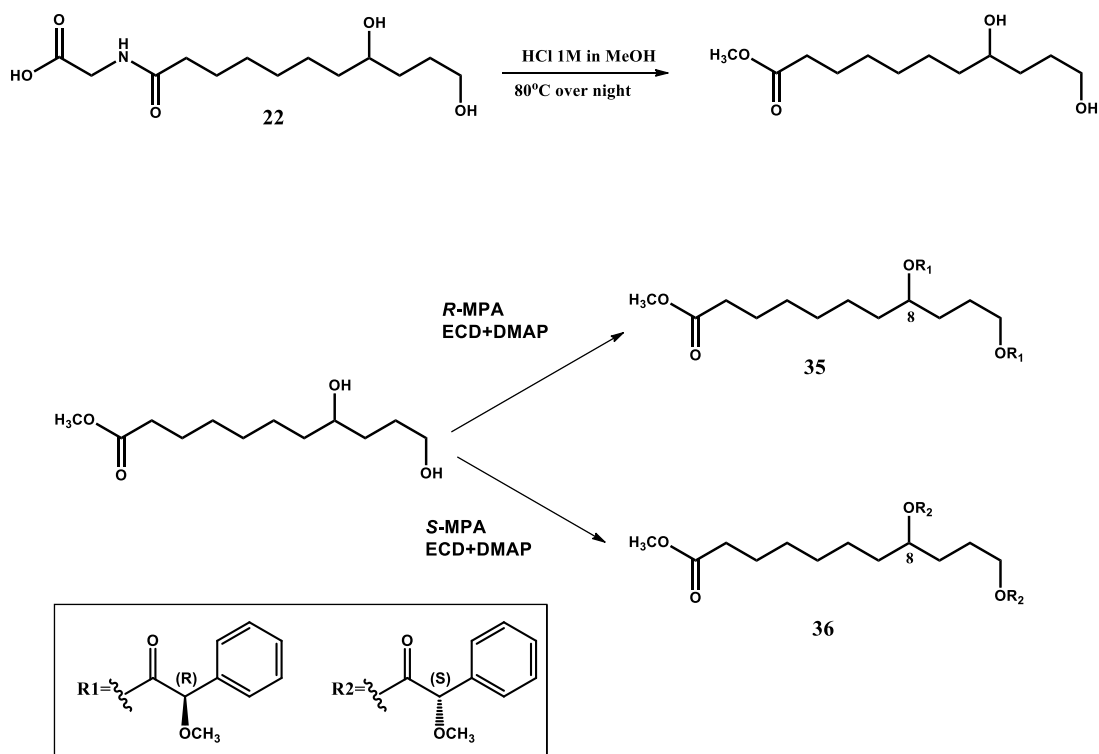


Figure 3.18. Synthesis of (*R*)-MPA (**35**) and (*S*)-MPA (**36**) esters.

The MPA may be a more reliable CDA because only two major ester conformers are present leading to $\Delta\delta$ values of greater magnitude. The model for MPA places the methoxy group, ester carbonyl, and carbinol proton in the same plane. L1 is shielded in the (*R*)-MPA ester and L2 is unaffected, and the opposite effects are observed with the (*S*)-MPA esters. The phenyl group lies on the opposite side of the CO plane with respect to the MTPA esters. For this reason, $\Delta\delta$ values are defined by a different formula ($\Delta\delta = \delta R - \delta S$). The choice of using the MPA derivate, instead of the more traditional MTPA derivate, was due to the larger anisotropic chemical shift changes observed for secondary alcohols using this chiral agent (**Figure 3.19**). The MPA derivative was chosen due to the larger anisotropic chemical shift changes observed in secondary alcohols relative to the more traditional MTPA derivative.

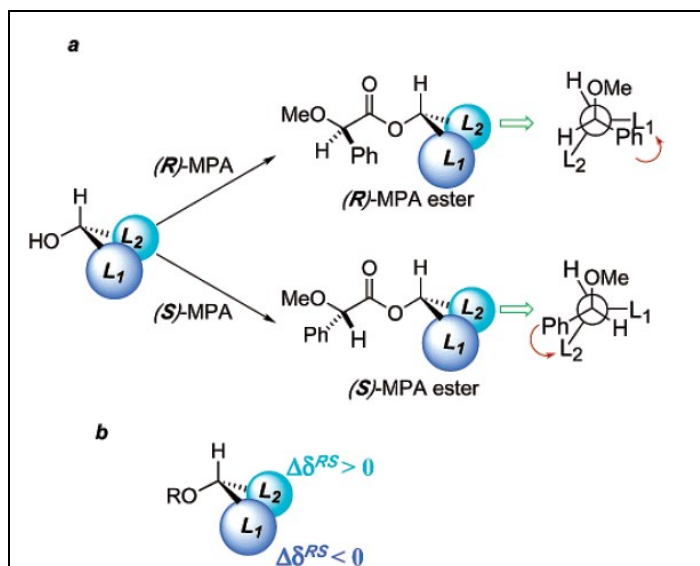


Figure 3.19. Conformers for (R)-MPA (**35**) and (S)-MPA (**36**) esters.

Thus, the analysis of the $\Delta\delta^{RS}$ ($\delta_R - \delta_S$) values in the ^1H spectrum of two esters (**35** and **36**) of phosphoeleganin allowed us to assign the configuration at C-8 as 8*S*. (**Figure 3.20**)

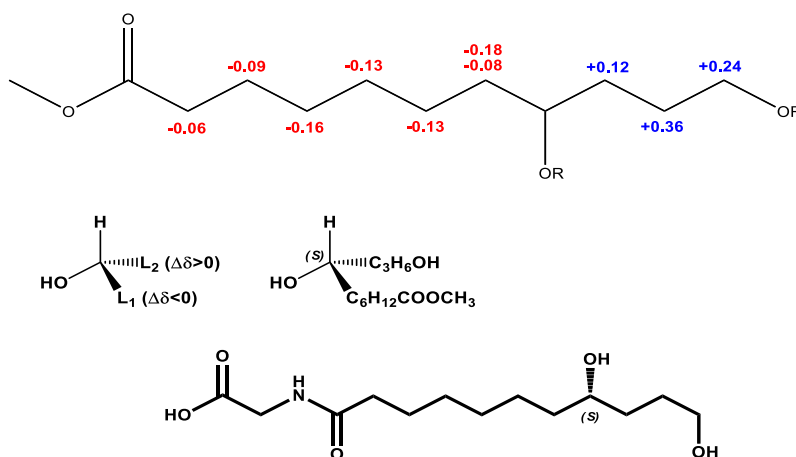


Figure 3.20. $\Delta\delta^{RS}$ ($\delta_R - \delta_S$) values in the ^1H spectrum of two esters (**35** and **36**).

The absolute stereochemistry at C15-C16 was determined through double derivatization method of **23** with a chiral auxiliary reagent developed by Riguera,⁹⁹ which is based on the use of polystyrene-bound chiral derivatizing agents (CDA-resins) specifically designed to achieve the high-yield formation of the covalent linkages (amide or ester bonds) between the substrate and the chiral auxiliary within the NMR tube, without the need for other manipulations, on a microscale level and in

a short time. We first removed the phosphate group from the molecule through an alkaline phosphatase and then we used Riguera's approach. (**Figure 3.21**)

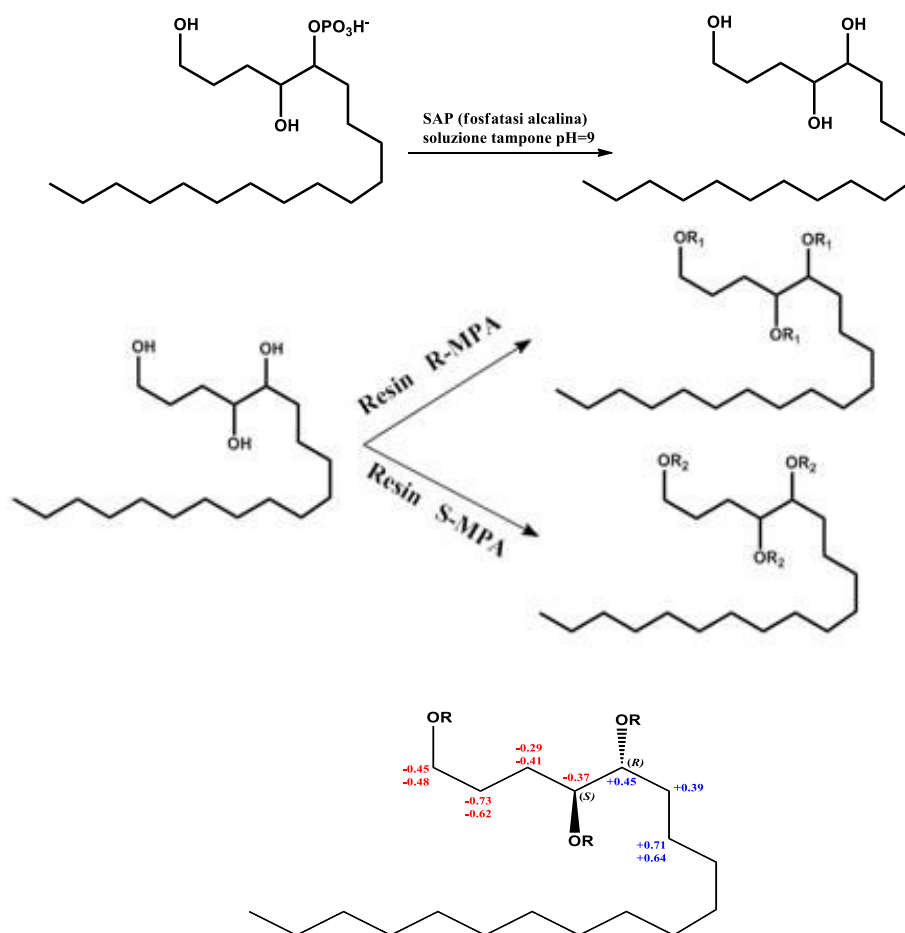


Figure 3.21. Determination of the absolute stereochemistry at C15-C16.

A consistent distribution of positive and negative $\Delta\delta$ values around C15-C16 allowed the assignment of *S*-configuration and *R*-configuration at C15-C16 respectively. (**Figure 3.21**)

In conclusion, the configuration analysis performed on phosphoeleganin allowed us to determine the stereostructure of the molecule to be one of the alternative structures **19a** and **19b** (**Figure 3.22**)

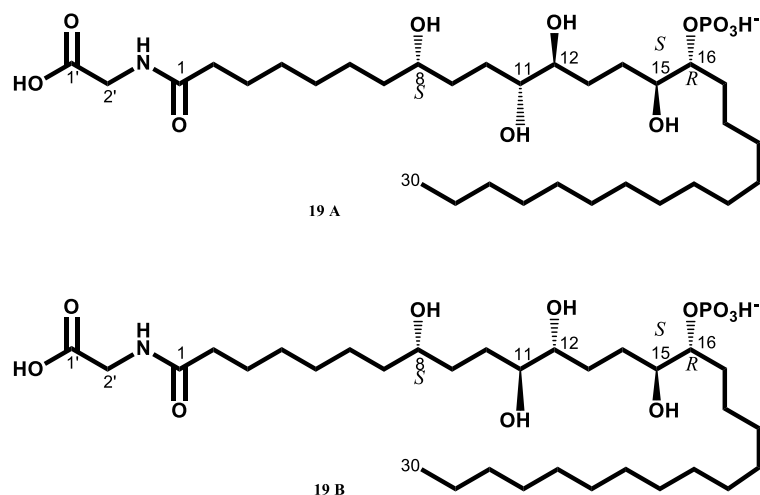


Figure 3.22. Alternative structures **19a** and **19b** of phosphoeleganin (**19**)

3.2.4 Conclusions

Although modern developments in spectroscopic techniques enable the identification of the structures of microgram samples of complex small molecules, there is no general solution to the absolute configuration (AC) of a compound, those even containing only one or a few stereocenters; absolute stereostructures are solved on a case-by-case basis. The above examples demonstrate the execution of complete solutions to stereocomplex marine natural products using modern NMR/CD instrumentation, often augmented by synthesis, requiring only a few milligrams or even micrograms of a natural product. Natural products are a significant and important source for new small molecule drug leads. The deficit in new drugs for treatments for many disease conditions, make it likely that natural products will continue to provide leads to supply pipelines of drug discovery. The foregoing examples illustrate the power of integrated structure analysis by spectroscopic techniques and chemical methods augmented by rational asymmetric synthesis. Reliable solutions to their structures are likely to be refined as current needs remain and new rare chemical entities are discovered.

3.3 NATURAL QUINONES AS LEAD COMPOUNDS IN DRUG DISCOVERY PROCESSES.

Naturally occurring prenylated 1,4-benzoquinones and hydroquinones are commonly found in a variety of organisms and play important roles in several metabolic processes, such as photosynthesis and electron transport.^{100,101} Examples of these compounds have been isolated from marine sources, mostly from tunicates belonging to the order of Aplousobranchiata (family Polyclinidae), such as ascidians of the genus *Aplidium*. They show a wide array of different structures, originated by intra- and inter-molecular cyclizations and/or rearrangements of the original terpene hydroquinone/quinone skeleton, thus giving macrocyclic or polycyclic structures; they are often linked to amino acids or taurine residues.¹⁰²⁻¹¹³ Recently, the ascidian *Aplidium conicum* has been investigated and this study yielded a large group of new prenylated quinones named conicaquinones,¹¹⁴ thiaplidiaquinones,¹¹⁵ and aplidinones (37–39).¹¹⁶ (Figure 3.23)

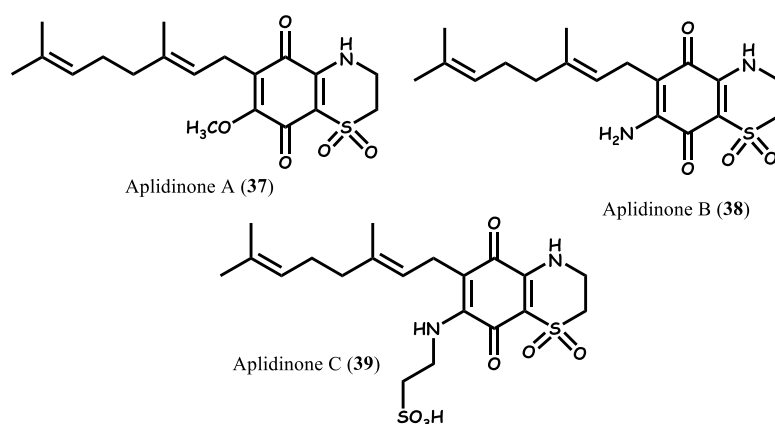


Figure 3.23. Structures of aplidinones A-C (37-39).

These compounds are structurally quite different, but they share the presence of an unusual 1,1-dioxo-1,4-thiazine ring fused to a quinone moiety. As for the aplidinones, the whole of the NMR data were not enough to unambiguously define the structure of the heterocyclic ring; an uncertainty still remained about the relative position of the sulfur and the nitrogen position in the ring. The reported regiochemistry was assigned as suggested for aplidinone A (37) by comparison of its

experimental ^{13}C NMR chemical shifts with those predicted by GIAO¹¹⁷ shielding calculations for regioisomers models A1 (40) and A2 (41). (**Figure 3.24**)

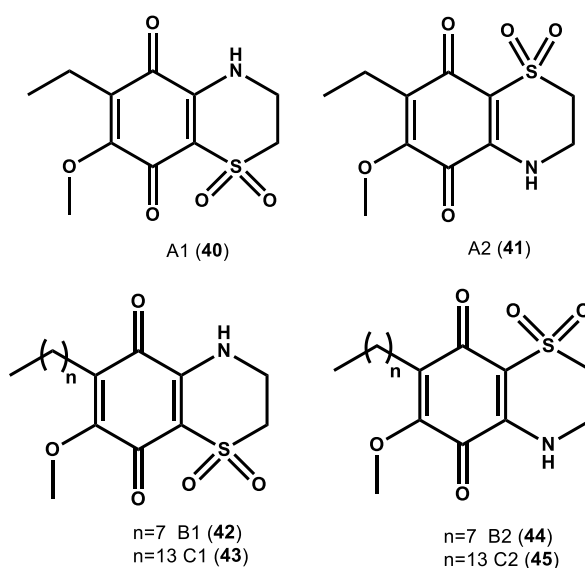


Figure 3.24. Synthetic analogues of aplidinone A

Successively, synthetic studies have been performed in order to validate the structural assignment of aplidinone A made by theoretical means. A simple and versatile synthetic strategy has been designed in order to produce the model compounds A1 and A2 (**Figure 3.24**) and to confirm the proposed regiochemistry. Heterocyclic systems like aplidinone A, having a 1,1-dioxo-1,4-thiazinic ring condensed with a benzoquinone ring, are not common in literature. This kind of compounds has been synthesized for the first time in 1988¹¹⁸ by condensation of hypotaurine with naphthoquinone using the known conjugate addition reaction of amines and sulfinic acids with naphthoquinones¹¹⁹ to give substituted naphthoquinones. Later, Harada et al. worked out the synthesis of adociaquinones A and B using the same protocol.¹²⁰ Although this route has the disadvantage of being not regioselective (**Figure 3.25**), we recognized it as a simple and versatile way to synthesize in relatively few steps aplidinone A derivatives, starting from an appropriate benzoquinone derivative.

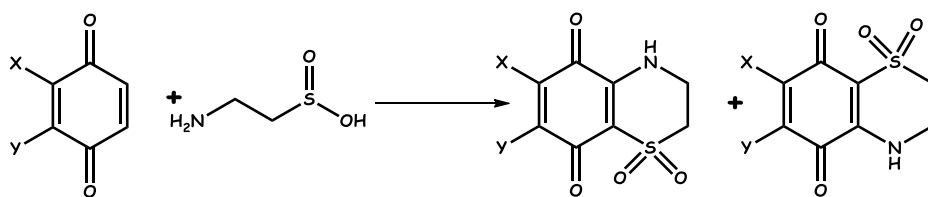


Figure 3.25. General synthetic protocol.

In addition, the designed procedure has been adapted to prepare further quinone analogues, **42-45**. (**Figure 3.24**) Both aplidinone A and its synthetic analogues were shown to possess interesting cytotoxic effects; SAR studies revealed that **44** is the most potent cytotoxic and pro-apoptotic agent against several tumor cell lines and also inhibits TNF-induced NF- κ B activation in a human leukemia T cell line.

This study well exemplifies the potential of a natural product to qualify as lead structure for medicinal chemistry campaigns, affording simplified analogues with better bioactivity and easier to synthesize.

3.3.1 Synthesis of structurally simplified analogues of aplidinone B

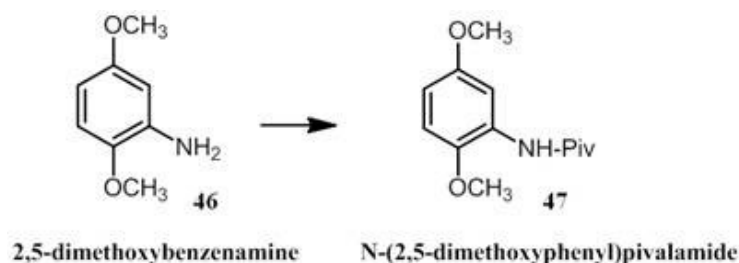
On the basis of the results obtained for the aplidinone A and its analogues, we decided to synthesise some analogues of another meroterpene isolated from the ascidian *Aplidium conicum*, the aplidinone B (**38**), both to fully confirm the regiochemistry of its heterocyclic structure, and to investigate its biological activity. In addition, this study also helped us to understand if this activity depended on the size of the hydrocarbon substituent as noted in the past among the aplidinone A analogues.¹²¹

In collaboration with the University of Rome “La Sapienza” we slightly modified the synthetic path designed for the synthesis of aplidinone A analogues. Also in this case, the key step of the synthesis was the reaction between hypotauroine and a suitable benzoquinone to give the dioxothiazine ring.

The 2,5-dimethoxy-aniline (**46**) has been chosen as starting compound, because it already contains the amino group and it is a cheap product. The first performed synthetic step (**Scheme 3.1**) was the transformation of the amino group into an amide function by treating (**46**) with pivaloyl chloride. We chose this chloride because the

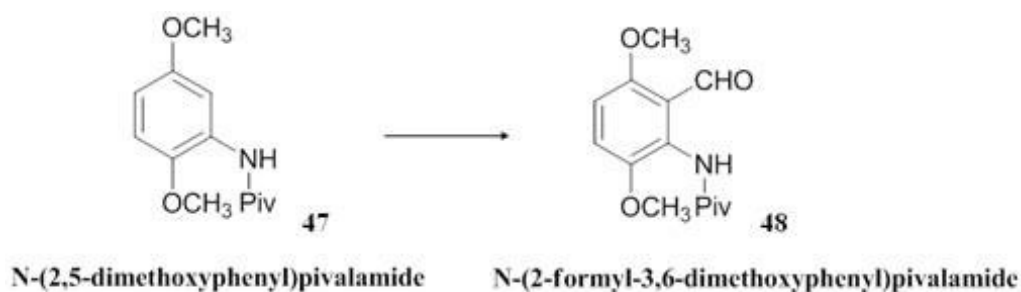
lack of α -hydrogens ensured a better stability during the next reactions. The amide (**47**) was obtained with a very good yield.

Scheme 3.1



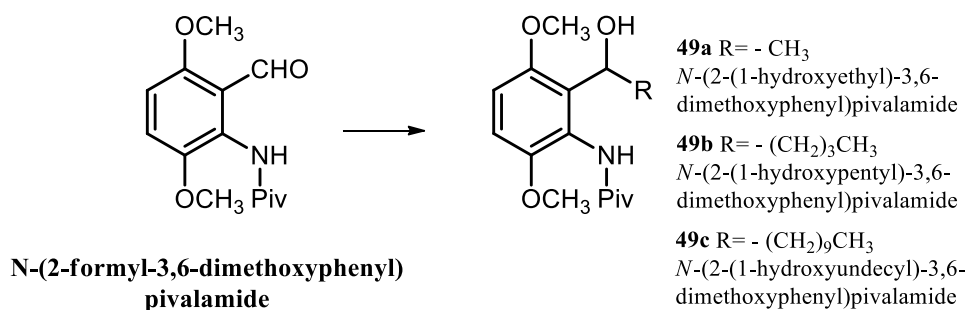
The reaction of (**47**) with *n*-BuLi and DMF afforded selectively the benzaldehyde (**48**) because the carbon between the ones linked to amide and methoxy group was the most reactive even if the direct alkylation by BuLi and alkyl bromides, analogous reaction to that performed in the aplidinone A synthesis,¹²¹ gave the alkylation product only in little quantity. The obtaining of the compound (**48**) was supported by the presence in its ¹H-NMR spectrum of the two just *ortho*-coupled aromatic protons signals (two doublets, 6.74 and 7.12 ppm respectively, $J=9.3\text{Hz}$) as well as that of the aldehyde function (singlet, 1H, 10.38 ppm). (Scheme 3.2)

Scheme 3.2



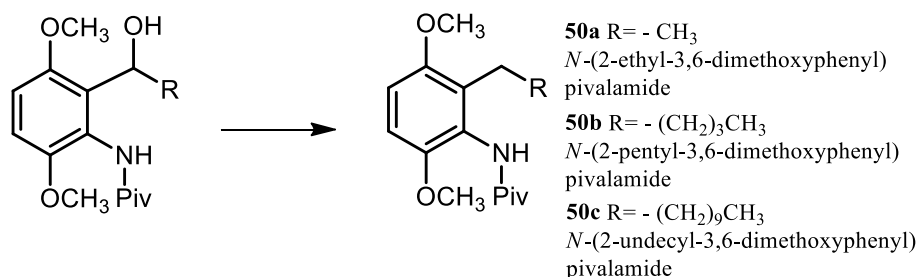
The aldehyde (**48**) is a key intermediate for the obtaining of aplidinone B analogous with hydrocarbon chains having different length; in fact the Grignard reaction between (**48**) and any alkylmagnesium iodide always afforded the corresponding benzylic alcohol (**49**) with a very good yield. (**Scheme 3.3**). The ^1H NMR spectrum of **49** showed the characteristic signal of the benzylic methyne proton (multiplet centered at 4.96 ppm) coupled both with the vicinal methylene aliphatic protons and also with the geminal alcoholic group (doublet, 3.60 ppm).

Scheme 3.3



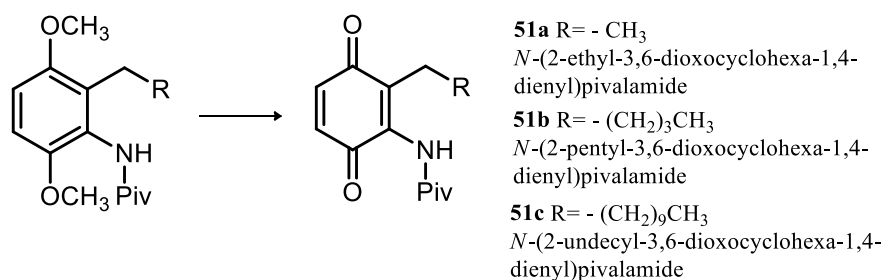
The subsequent easy hydrogenolysis of (**49**) by using Pd-C (10%) as catalyst gave the compound (**50**) with the desired hydrocarbon chain, whose ^1H NMR spectrum shows the signals of the two aromatic protons (two very close doublets between 6.67 and 6.73 ppm), those of the aliphatic protons of the chain (benzylic protons signals at 2.58ppm) and the singlet (9 protons, 1.34ppm) of the pivaloyl residue. (**Scheme 3.4**)

Scheme 3.4



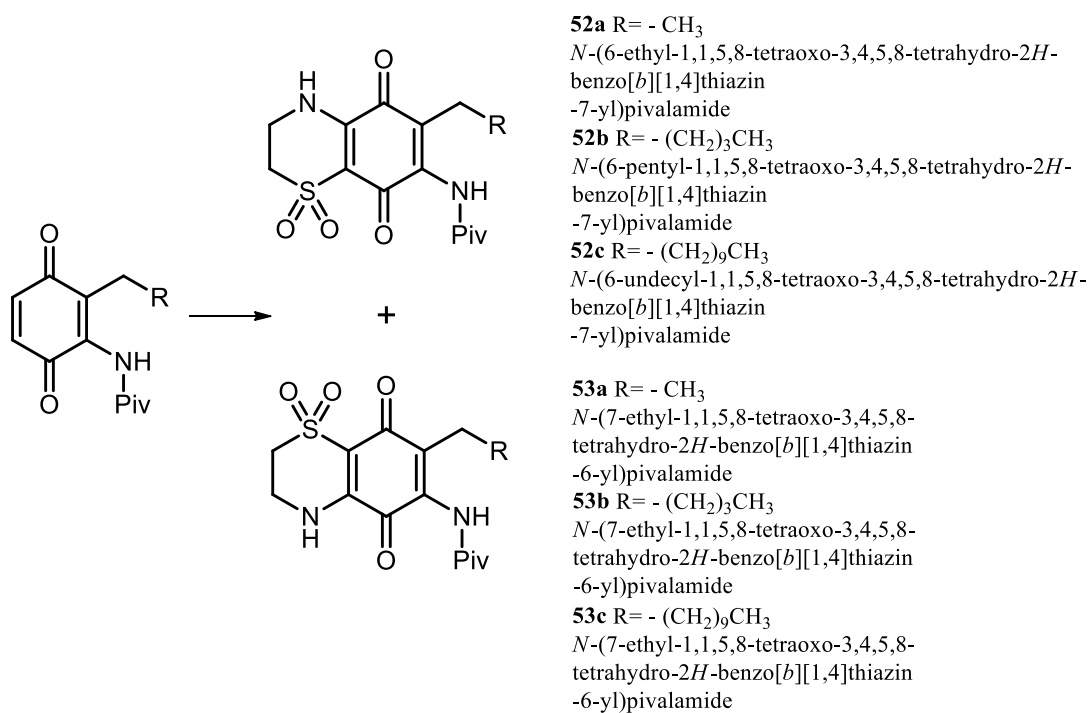
The quinone (**51**) was obtained by the oxidation of (**50**) with a large excess of CAN (molar ratio 8:1). The steps from (**49**) to (**51**) do not require any intermediate purification, so simplifying the carrying out of the whole synthesis. (**Scheme 3.5**)

Scheme 3.5



The quinone (**51**) was treated with hypotaaurine as reported in literature.¹¹⁹ Also in this reaction the two regioisomers (**52** and **53**) form in different amount. The ¹HNMR spectra of the two regioisomers are very similar, the main difference lying in the chemical shift value of the signal of the more deshielded heterocycle methylene group, 4.07ppm in the spectrum of natural regioisomer and 3.31ppm in the spectrum of non natural one. The values here reported are relative to the aplidinone B analogues with ethylic lateral chain, those of other analogous are very close to these. (**Scheme 3.6**)

Scheme 3.6



A large number of quinones, both synthetic and naturally occurring, have been screened for their antitumor activity; particularly, it has been shown that they lead to oxidative stress by means of an increase of oxygen reactive species (ROS) and the depletion of reduced glutathione (GSH) amount¹²² and this action has been related to the beginning of apoptosis.^{123,124}

In previously works it has shown that thiaplidiaquinones 3 and 4 induce generation of ROS and apoptosis in the Jurkat cell line.¹⁶ On this cell line we have now investigated the cytotoxic activity of aplidinone A (**37**), as well as that of its synthetic analogues **40-45**. Aplidinone A induced cytotoxicity with an IC₅₀ about 45 μM; the cytotoxic activity was enhanced with the modifications introduced in **44** (IC₅₀ ~ 20 μM) and decreased in **40-42**, **43**, and **45**

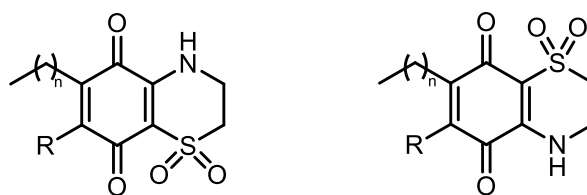
On the basis of the results reported, the analogues of aplidinone A and B have been tested on human microvascular endothelial cells (HMEC). Compound **52a** resulted the most cytotoxic of the series with an IC₅₀ about 1.50 μM.

3.3.2. *Potential of quinones as antimalarial agents*

There is an urgent need to discover new antimalarials, due to the spread of chloroquine resistance and the limited number of available drugs. A number of quinones have been shown to be effective antimalarials. In addition some have been shown to have oxidant effects on glucose-6-phosphate dehydrogenase-deficient red cells. The mitochondrial respiratory chain is an effective target for antimicrobial agents directed against *P. falciparum*. Differences between respiratory chain enzymes of mammals and pathogenic organisms have been exploited to develop compounds used for drug therapy such as atovaquone. Atovaquone is a hydroxynaphthoquinone active against different parasitic diseases including malaria and toxoplasmosis, Atovaquone inhibits the activity of the *bc1* complex activity, a central enzyme of the respiratory chain .

Antiplasmodial activity of quinone structures of marine origin has been reported. Examples are xestoquinone and halenaquinone, their derivative orlaquinone, and ketoadociaquinones, isolated from *Xestospongia* sponges, and thiaplakortones, isolated from *Plakortis lita*. It has been also evidenced that the presence of a dioxothiazine moiety enhances the antiplasmodial activity. Based on these reports, synthetic derivatives of the natural aplidinones A and B, isolated from the Mediterranean tunicate *Aplidium conicum*, have been tested in vitro against D10 (chloroquine-sensitive) and W2 (chloroquine-resistant) strains of *Plasmodium falciparum*, in collaboration with Dipartimento di Sanità pubblica, Microbiologia e Virologia of University of Milan.

Using the pLDH assay, the synthetic analogues of aplidinones A and B (**Figure 3.26**) were assayed against D10, CQ-S strain and W2, CQ-R strain of *P. falciparum*.



40	R = -OMe; n=1	41	R = -OMe; n=1
42	R = -OMe; n=7	44	R = -OMe; n=7
43	R = -OMe; n=13	45	R = -OMe; n=13
52a	R = -NHCOC(CH ₃) ₃ ; n=1	53a	R = -NHCOC(CH ₃) ₃ ; n=1
52b	R = -NHCOC(CH ₃) ₃ ; n=4	53b	R = -NHCOC(CH ₃) ₃ ; n=4
52c	R = -NHCOC(CH ₃) ₃ ; n=10	53c	R = -NHCOC(CH ₃) ₃ ; n=10

Figure 3.26. Structures of synthetic analogues of aplidinones A and B

The synthetic derivatives have shown a significant pharmacological activity and many structural requirements, critical for their activity, have been evidenced (**Table 3.10**).

Table 3.10. In vitro antiplasmodial activity compounds 1-12 against the cloroquine-sensitive (D10) and the cloroquine-resistant (W2) strains of *P. falciparum* and cytotoxicity against human microvascular endothelial (HMEC-1) cells.

Compound	D10	W2	HMEC-1
	IC ₅₀ (μM)	IC ₅₀ (μM)	IC ₅₀ (μM)
40	>28	>28	>100
41	2,4	2,4	110,29
42	>28	>28	>100
44	0,8	0,8	5,52
43	>28	>28	>100
45	1,7	1,3	4,41
52a	0.39	0,58	1,60
53a	6,15	6,31	102,72
52b	1,56	2,70	0,90
53b	6,93	7,87	41,45
52c	0,56	1,06	0,44
53c	>11	>11	6,87
CQ	0.04	0.54	>100

In particular, for methoxy derivatives it has been evidenced that:

- Compounds **41**, **44** and **45** show a very good antiplasmodial activity which do not depend on the cloroquine sensitivity of the strain tested. the compound **42** is

completely inactive, indicating that the regiochemistry of the dioxothiazine ring showed for **41**, **44**, and **45** is critical for the activity.

- **44** is the most potent in the series, with a potent antiplasmodial activity (0,8 μM); however, it resulted significantly cytotoxic (5,52 μM).
- The activity depends on the length of the side chain; it increased with the number of carbon atoms from **41** to **44** and then decreased from **44** to **45**.
- Compound **41** is not cytotoxic (>100 μM) though keeping a good antiplasmodial activity (2,4 μM)

Whereas for the amido derivatives series it has been evidenced that:

- Compound **52a** was inactive and unstable, thus the ammino-protected derivatives were tested.
- The amido derivatives were all active, although the activity depends on the thiazine ring regiochemistry: compounds **52a**, **52b**, and **52c**, sharing the same regiochemistry, resulted more active than the relevant compound in the other series of regioisomers.
- The change in the regiochemistry seems to affect more the cytotoxicity than antiplasmodial activity, especially in the absence of a side chain (**52a** vs. **53a**).
- The activity depends on the length of the side chain; it decreased with the number of carbon atoms from **52a/53a** (2 C) to **52b/53b** (5C) and then increased from **52b/53b** (5C) to **52c/53c** (11C)
- **52a** is the most potent in the series, with a potent antiplasmodial activity(0,39 μM) but it resulted significantly cytotoxic (1.6 μM).

The interesting aspect is that this antimalarial activity is due to the interaction between the quinone structures and some of the *P. falciparum* enzyme targets, such as protein farnesyl transferase (PFTasi) and Pfnk kinase-1, thus implying a mechanism different from that showed by other antimalarial agents. Based on these considerations our compounds have been tested on a platform of kinases, but no correlation was seen between the observed activities (both the antiplasmodial effects and cytotoxicity) and kinase inhibition (**Table 3.11**).

Table 3.11. Results from protein kinase assays

Compound	CDK5/p25	CDK9/cyclinT	CK1	CLK1	DYRK1A	GSK3
41	102	92	97	88	93	73
44	105	102	91	107	90	68
45	105	92	88	108	93	84
52a	106	84	86	91	93	89
53a	109	90	83	111	90	79
52b	97	82	115	101	100	100
53b	86	80	105	101	108	85
52c	102	93	92	98	94	110
53c	125	102	95	111	97	96

3.3.3 Conclusions

Interesting conclusions can be drawn by comparing the cytotoxic effects with antimalarial ones. Compound **52a** is the most active in the series, with a very potent antiplasmodial activity but also strongly cytotoxic. Compound **44** is also very potent as antiplasmodial agent, also cytotoxic but with a better therapeutic index. Compound **41** is very potent as antiplasmodial agent and not cytotoxic (**Table 3.10**).

3.4. FROM THE MACROSCOPIC TO THE MICROSCOPIC WORLD: THE HABITAT OF MICROORGANISMS

3.4.1. History of microbial drug discovery

The chemistry of marine bacteria has received increasing attention over the past twenty years. Principal reasons for this interest are their abundance and phylogenetical diversity, as well as the capacity of most of them to survive in extreme environmental conditions due to the unusual enzymatic and metabolic adaptations. In the late 1930's, stimulated by the discovery of penicillin by Alexander Fleming, terrestrial microorganisms became the focal point for one of the most prolific drug discovery efforts ever recognized. The discovery of penicillin and later actinomycin led to the "Great Antibiotic Era", which yielded more than 120 drugs for the treatment of infectious diseases, cancer, elevated cholesterol, immunomodulation and others. From the period from 1950 to 1990 most of the pharmaceutical companies invested heavily in microorganism-based drug discovery. The intensity of these explorations led to discoveries of new microorganisms from virtually all accessible terrestrial environment from arctic, and cold temperate regions to tropical environments.¹²⁵ Interestingly, although the world's ocean occupy more than 70% of the surface of the Earth, this massive resource was never explored. Convinced by some that the ocean was a simple repository for terrestrial strains, and that cultivation of true marine microbes was difficult if not impossible, this component of planet Earth never received serious consideration. However, in 2009 microorganisms are no longer the focus of most drug industries, even though marine researchers are now demonstrating the enormous drug discovery potential of microorganisms isolated from this source. Given the growth in this field, it is important to emphasize the unambiguous criteria that separate marine microorganisms from their terrestrial counterparts. Three such traits that help define some of the more distinctly marine microorganisms are their ability to display barophily (adaptation to high pressure), halophily (adaptation to high salt environments), and chemoautotrophic growth (ability to use CO₂ as a carbon source and derive energy from chemicals rather than light) properties. One tool that has been essential to define distinctions between marine and terrestrial microbes is the

use of 16S ribosomal RNA analysis (16S rRNA). Many true marine microorganisms from oceanic environments contain previously unobserved 16S signatures; this is especially true in the case of invertebrate microbial symbionts, as the phenomenon of symbiosis is prevalent in the ocean. Given the aforementioned properties, it remains difficult to prove whether a microorganism collected from an oceanic environment is truly 'marine' or whether it is simply a terrestrial strain that has been rinsed into the ocean. Over decades of study, one most simply illustrate that microbes are regularly found in the ocean and not in terrestrial environments. For example, fungi are cosmopolitan organisms that are incredibly adaptive to new environments. Several investigators mistakenly label fungi collected from the ocean as "marine fungi". This label is unwarranted until it is demonstrated that a fungal species has an obligate requirement for life in the sea. Until more can be learned, a more appropriate label is "marine-derived fungi".¹²⁶⁻¹²⁸

One very important aspect of these microorganisms is their capacity to produce secondary metabolites, but little is known about the origin, diversity, and role that secondary metabolites fulfill in their surrounding microenvironments.

3.4.2 Cytotoxic quinazolinone isolated from the fungus penicillium sp endogenous with the mangrove Bruguiera gymnorrhiza

Marine microorganisms, especially marine-derived fungi, are widely recognized as emerging sources of secondary metabolites.¹²⁹⁻¹³¹ Mangrove-associated fungi, the second largest ecological group of the marine-derived fungi, have been reported to produce a wide variety of structurally unique and biologically active compounds.¹³² In particular, many fungi were recently isolated from the mangrove *Bruguiera gymnorrhiza*. Chemical investigation of these fungi led to the isolation of an already known cytotoxic quinazolinone **54**. (**Figure 3.27**)¹³³

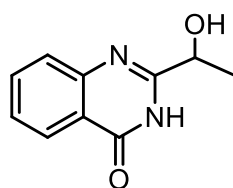


Figure 3.27. Structure of 2-(1-hydroxyethyl)-4(3H)quinazolinone (**54**).

During my PhD I have been involved in an “staff exchange” activity within the project IRSES- 7^o Framework. During my stage at Institute of Materia Medica (SIMM), Shanghai, I started the chemical analysis of a fungal strain *Penicillium sp.*, isolated from the Chinese mangrove *Bruguiera gymnorrhiza* collected from Zhanjiang.

The whole culture of *Penicillium sp.* was extracted with CH₃OH and CHCl₃ and then partitioned between EtOAc and H₂O and *n*-BuOH and H₂O. Separation of the EtOAc-soluble material (0.6 g) was achieved by gradient silica gel MPLC (ether → ethyl acetate → dichloromethane→methanol). Ten fractions were obtained. The fraction eluted with EtOAc/ether 1:1 v/v (10,0 mg) was chromatographed by HPLC on a SiO₂ column (Luna 5μ, 250 x 4.60 mm) eluting with hexane/ EtOAc 4:6 v/v, yielding the compound **54** (4.9 mg). (**Figure 3.28**).

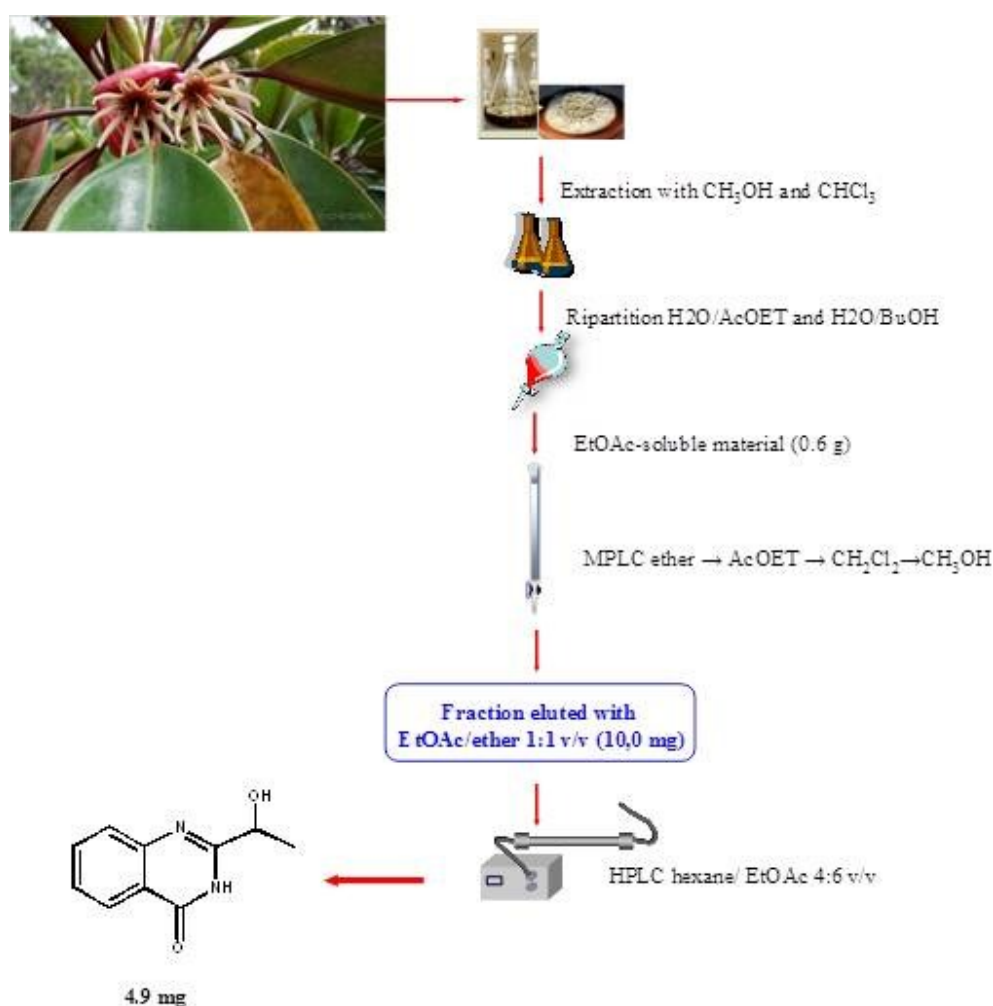


Figure 3.28. Isolation procedure of compound **54**

The analysis of the ^1H -NMR spectrum (CD_3OD) and HMBC data allowed us to identify the compound **54** as the already known cytotoxic alkaloid 2-(1-hydroxyethyl)-4(3H)quinazolinone (**Table 3.12**).¹³³

Table 3.12. NMR data (CD_3OD) of compound **54**

Pos.	δ_{H} (mult., J in Hz)	δ_{C}	HMBC
2		161.6	-
4		164.3	
5		122.2	
6		149.6	
7	7.66	127.5	122.2, 127.8
8	7.79	135.9	127.2, 149.6
9	7.49	127.8	122.2, 127.2
10	8.18	127.2	135.9, 149.6
1'	4.73	68.6	22.4, 161.6
2'	1.53	22.4	68.6, 161.6

References

1. Fenical, W. in *Food-Drugs from the Sea Proceedings*. (Eds.: H. H. Webber, G. D. Ruggieri), Marine Technology Society, Washington DC, **1976**, 4, 388-394.
2. Zubía, E.; Ortega, M. J.; Salvà, J. *Mini-Rev. Org. Chem.* **2005**, 2, 389-399.
3. Garrido, L.; Zubía, E.; Ortega, M. J.; Salvà, J. *J. Nat. Prod.* **2002**, 65, 1328-1331.
4. Aiello, A.; Fattorusso, E.; Luciano, P.; Menna, M.; Esposito, G.; Iuvone, T.; Pala, D. *Eur. J. Org. Chem.* **2003**, 898-900.
5. Aiello, A.; Fattorusso, E.; Luciano, P.; Mangoni, A.; Menna, M. *Eur. J. Org. Chem.* **2005**, 5024-5030.
6. Aiello, A.; Fattorusso, E.; Luciano, P.; Macho, A.; Menna, M.; Muñoz, E. *J. Med. Chem.* **2005**, 48, 3410-3416.
7. Fort, D. M.; Ubillas, R. P.; Mendez, C. D.; Jolad, S. D.; Inman, W. D.; Carney, J. R.; Chen, J. L.; Ianiro, T. T.; Hasbun, C.; Bruening, R. C.; Luo, J.; Reed M. J.; Iwu, M.; Carlson, T. J.; King, S. R.; Bierer, D. E.; Cooper, R. *J. Org. Chem.* **2000**, 65, 6534-6539.
8. Laird, D. W.; Poole, R.; Wikstroem, M.; Van Altena, I. A. *J. Nat. Prod.* **2007**, 70, 671-674.
9. Appleton, D. R.; Chuen, C. S.; Berridge, M. V.; Webb, V. L.; Copp, B. R. *J. Org. Chem.* **2009**, 74, 9195-9198.
10. Carbone, M.; Nunez-Pons, L.; Paone, M.; Castelluccio, F.; Avila, C.; Gavagnin, M. *Tetrahedron* **2012**, 68, 3541-3544.
11. Joshi, K. C.; Singh, P.; Taneja, S.; Cox, P. J.; Howie, R. A.; Thomson, R. H. *Tetrahedron* **1982**, 38, 2703-2708.
12. Akunyili, D. N.; Houghton, P. J. *Phytochemistry* **1993**, 32, 1015-1018.
13. Onegi, B.; Kraft, C.; Köhler, I.; Freund, M.; Jenett-Siems, K.; Siems, K.; Beyer, G.; Melzig, M. F.; Bienzle, U.; Eich, E. *Phytochemistry* **2002**, 60, 39-44.

14. Simeone, L.; Mangiapia, G.; Vitiello, G.; Irace, C.; Colonna, A.; Ortona, O.; Montesarchio, D.; Paduano, L. *Bioconjugate Chem.* **2012**, *23*, 758–770.
15. Aiello, A.; Menna, M.; Fattorusso, E. *Steroids* **1999**, *64*, 687–714.
16. Aiello, A.; Fattorusso, E.; Imperatore, C.; Luciano, P.; Menna, M.; Vitalone R. *Mar. Drugs* **2012**, *10*, 51–63.
17. Findlay, J.A.; He, Z. Q.; Calhoun, L.A. *J. Nat. Prod.* **1990**, *53*, 1015–1018.
18. Findlay, J.A.; Yayli, N.; Calhoun, L.A. *J. Nat. Prod.* **1991**, *54*, 302–304.
19. Nakao, Y.; Matsunaga, S.; Fusetani, N. *Tetrahedron Lett.* **1993**, *34*, 1511–1514.
20. Roccatagliata, A.J.; Maier, M.S.; Seldes, A.M.; Zea, S.; Duque, C. *J. Nat. Prod.* **1997**, *60*, 285–286.
21. Tsukamoto, S.; Kato, H.; Hirota, H.; Fusetani, N. *J. Nat. Prod.* **1994**, *57*, 1606–1609.
22. Fujita, M.; Nakao, Y.; Matsunaga, S.; Nishikawa, T.; Fusetani, N. *J. Nat. Prod.* **2002**, *65*, 1936–1938.
23. Crispino, A.; De Giulio, A.; De Rosa, S.; De Stefano, S.; Milone, A.; Zavodnik, N. *J. Nat. Prod.* **1994**, *57*, 1575–1577.
24. Aiello, A.; Fattorusso, E.; Menna, M.; Carnuccchio, R.; D'Acquisto, F. *Tetrahedron* **1997**, *53*, 5877–5882.
25. Aiello, A.; Fattorusso, E.; Menna, M.; Carnuccchio, R.; Iuvone, T. *Tetrahedron* **1997**, *53*, 11489–11492.
26. De Rosa, S.; Milone, A.; Crispino, A.; Jaklin, A.; De Giulio, A. *J. Nat. Prod.* **1997**, *60*, 462–463.
27. Aiello, A.; Carbonelli, S.; Esposito, G.; Fattorusso, E.; Iuvone, T.; Menna, M. *J. Nat. Prod.* **2000**, *63*, 1590–1592.
28. Aiello, A.; Carbonelli, S.; Fattorusso, E.; Iuvone, T.; Menna, M. *J. Nat. Prod.* **2001**, *64*, 219–221.
29. Aiello, A.; Fattorusso, E.; Imperatore, C.; Irace, C.; Luciano, P.; Menna, M.; Santamaria, R.; Vitalone, R. *Mar. Drugs* **2011**, *9*, 1157–1165.
30. Aiello, A.; Fattorusso, E.; Imperatore, C.; Menna, M.; Muller, W.E.G. *Mar. Drugs* **2010**, *8*, 285–291.

31. Kerr, R.G.; Baker, B.J. *Nat. Prod. Rep.* **1991**, *8*, 465–497.
32. Blunt, J.W.; Copp, B.R.; Hu, W.P.; Munro, M.H.G.; Northcote, P.T.; Prinsep, M.R. *Nat Prod Rep.* **2007**, *24*, 31–86.
33. Stonik, V.A. *Russ. Chem. Rev.* **2001**, *70*, 673–715.
34. D'Auria, M.V. *Chem. Rev.* **1993**, *93*, 1839–1895.
35. Sarma, N.S. *et al. Mar. Drugs.* **2005**, *3*, 84–111.
36. Sica, D. *et al. Steroids.* **2004**, *69*, 743–756.
37. Guyot, M.; Durgeat, M. *Tetrahedron Lett.* **1981**, *22*, 1391–1392.
38. Guyot, M.; Davoust, D. *Tetrahedron Lett.* **1982**, *23*, 1905–1906.
39. Gunatilaka, A.L.; Gopichand, Y.; Schmitz, F.J.; Djerassi, F.J. *J. Org. Chem.* **1981**, *46*, 3860–3866.
40. Tam Ha, T.B.; Kokke, W.C.; Djerassi, C. *Steroids.* **1982**, *40*, 433–453.
41. Palermo, J.A.; Rodriguez Brasco, M.F.; Hughes, E.A.; Seldes, A.M.; Balzaretto, V.T.; Cabezas, E. *Steroids.* **1996**, *61*, 2–6.
42. Aiello, A.; Esposito, G.; Fattorusso, E.; Iuvone, T.; Luciano, P.; Menna, M. *Steroids.* **2003**, *68(9)*, 719–723.
43. Fiorucci, S.; Distrutti, E.; Bifulco, G.; D'Auria, M.V., Zampella, A. *Trends Pharm. Sci.* **2012**, *33*, 591–600.
44. Demarco, P.V.; Farkas, E.; Doddrell, D.; Mylari, B.V.; Wenkert, E. *J. Am. Chem. Soc.* **1968**, *90*, 5480–5486.
45. Migliuolo, A.; Notaro, G.; Piccialli, V.; Sica, D. *J. Nat. Prod.* **1990**, *53*, 1414–1429.
46. Aiello, A.; Fattorusso, E.; Menna, M.; Carnuccio, R.; Iuvone, T. *Steroids.* **1995**, *60*, 660–673.
47. Fujimoto, Y.; Yamada, T.; Ikekawa, N. *Chem. Pharm. Bull. (Tokyo).* **1985**, *33*, 3129–3133.
48. Notaro, G.; Piccialli, V.; Sica, D.; Corriero, G. *J. Nat. Prod.* **1991**, *54*, 1570–1575.
49. Das, B.; Srinivas, N.S. *J. Nat. Prod.* **1992**, *55*, 1310–1312.
50. Das, B.; Padma Rao, S.; Srinivas, N.S. *J. Nat. Prod.* **1993**, *56*, 2210–2211.
51. Festa, C.; De Marino, S.; D'Auria M.V.; Bifulco, G.; Renga, B.; Fiorucci, S.; Petek, S.; Zampella, A. *J. Med. Chem.* **2011**, *54*, 401–405.

52. Sepe, V.; Ummarino, R.; D'Auria, M.V.; Mencarelli A.; D'Amore, C.; Renga, B.; Zampella, A.; Fiorucci, S. *J. Med. Chem.* **2011**, *54*, 4590–4599.
53. Morris, G.M.; Huey, R.; Lindstrom, W.; Sanner, M.F.; Belew, R.K.; Goodsell, D.S.; Olson, A.J. *J Comput Chem* **2009**, *30*, 2785–91.
54. a) Katz, L. *Chem. Rev.* **1997**, *97*, 2557–2575. b) Weissman, K. J.; Leadlay, P. F. *Nat. Rev. Microbiol.* **2005**, *3*, 925–936.
55. Fushimi S, Nishikawa S, Shimazu A, Seto H. *J. Antibiot.* **1989**,*42*,1019–1025.
56. a) Stampwala, S. S.; Bunge, R. H.; Hurley, T. R.; Willmer, N. E.; Brankiewicz, A. J.; Steinman, C. E.; Smitka, T. A.; French, J. C. *J. Antibiot.* **1983**, *36*, 1601–1605. b) Tunac, J. B.; Graham, B. D.; Dobson, W. E. *J. Antibiot.* **1983**, *36*, 1595–1600. c) M. Ghatge, N. Palaniappan, S. D. Choudhuri, K. Reynolds, *J. Ind. Microbiol. Biotechnol.* **2006**, *33*,589–599. d) A. E. Fagerholm, D. Habrant, A. M. P. Koskinen, *Mar. Drugs* **2010**, *8*, 122-172.
57. Kelly, S.R.; Jensen, P.R.; Henkel, T.P.; Fenical, W.; Pawlik, J.R. *Aquat. Microb. Ecol.* **2003**, *31*, 175–182.
58. Richelle-Maurer, E.; De Kluijver, M.J.; Feio, S.; Gaudencio, S.; Gaspar, H.; Gomez, R.; Tavares, R.; Van de Vyver, G.; Van Soest, R.W.M. *Biochem. Syst. Ecol.* **2003**, *31*, 1073–1091.
59. Forte, B.; Malgesini, B.; Piutti, C.; Quartieri, F.; Scolaro, A.; Papeo, G. *Mar. Drugs* **2009**, *7*, 705–753.
60. Cimino, G.; De Stefano, S.; Minale, L. *Biochem. Physiol. Part B* **1974**, *47*, 895–897.
61. Minale, L.; Sodano, G. *J. Chem. Soc. Perk. T. 1* **1974**, *15*, 1888–1892.
62. De Rosa, M.; Minale, L.; Sodano, G. *Experientia* **1975**, *31*, 758–759.
63. Crist, B.V.; Djerassi, C. *Steroids* **1983**, *42*, 331–343.
64. Buck, F.; Schulze, C.; Breloer, M.; Strupat, K.; Bretting, H. *Comp. Biochem. Physiol. Part B* **1998**, *121*, 153–160.
65. Gabant, M.; Martin, M.; Moriou, C.; Ermolenko, L.; Guerineau, V.; Retailleau, P.; Thoison, O.; Boury-Esnault, N.; Perez, T.; Al-Mourabit, A. *J. Nat. Prod.* **2009**, *72*, 1875–1878.

66. Hofsteenge, J.; Mueller, D.R.; de Beer, T.; Loeffler, A.; Richter, W.J.; Vliegthart, J.F.G *Biochemistry* **1994**, *33*, 13524–13530.
67. Capon, R.J.; Trotter, N.S. *J. Nat. Prod.* **2005**, *68*, 1689–1691.
68. Garcia, A.; Lenis, L.A.; Jimenez, C.; Debitus, C.; Quiñoa, E.; Riguera, R. *Org. Lett.* **2000**, *2*, 2765–2767.
69. Tsujino, I.; Yabe, K.; Sekikawa, I.; Hamanaka, N. *Tetrahedron Lett.* **1978**, *16*, 1401–1402.
70. Takano, S.; Uemura, D.; Hirata, Y. *Tetrahedron Lett.* **1978**, *26*, 2299–2300.
71. Chen, G.S.; Chen, C.S.; Chien, T.C.; Yeh, J.Y.; Kuo, C.C.; Talekar, R.S.; Chern, J.W. *Nucleos. Nucleot. Nucl.* **2004**, *23*, 347–359.
72. Broberg, A.; Kenne, L.; Pedersen, M. *Planta* **1998**, *206*, 300–307.
73. Aiello, A.; Fattorusso, E.; Luciano, P.; Menna, M.; Vitalone, R. *J. Nat. Prod.* **2010**, *73*, 620–622.
74. Izumida, H.; Imamura, N.; Sano, H. *J. Antibiot.* **1996**, *49*, 76–80.
75. Vergne, C.; Boury-Esnault, N.; Perez, T.; Martin, M.; Adeline, M.; Tran Huu Dau, E.; Al-Mourabit, A. *Org. Lett.* **2006**, *8*, 2421–2424.
76. Haber, M.; Carbone, M.; Mollo, E.; Gavagnin, M.; Ilan, M. *Mar. Ecol. Prog. Ser.* **2011**, *422*, 113–122.
77. Cimino, G.; De Stefano, S.; Minale, L.; Sodano, G. *Comp. Biochem. Physiol.* **1975**, *50B*, 279–285.
78. Aiello, A.; D'Esposito, M.; Fattorusso, E.; Menna, M.; Muller, W.E.G.; Perovic-Ottstadt, S.; Schroder, H.C. *Bioorg. Med. Chem.* **2006**, *14*, 17–24.
79. Haber, M.; Carbone, M.; Ilan, M.; Gavagnin, M. *Arkivoc* **2010**, *2*, 233–239.
80. Gazave, E.; Carteron, S.; Chenuil, A.; Richelle-Maurer, E.; Boury-Esnault, N.; Borchiellini, C. *Mol. Phylogenet Evol.* **2010**, *57*, 35–47.
81. Braekman, J.C.; Dalozze, D.; Stoller, C.; Van Soest, R.W.M. *Biochem. Syst. Ecol.* **1992**, *20*, 417–431.
82. Karplus, M.; *J. Chem. Phys.*, **1959**, *11*.
83. Sanders, J. K. M.; Mersh, J. D.; *Prog. NMR Spectrosc.*, **1982**, *353*.
84. McCann, D.M.; Stephens, P.J. *J. Org. Chem.* **2006**, *71*, 6074–6098.

85. Aiello, A.; Fattorusso, E.; Imperatore, C.; Luciano, P.; Menna, M.; Vitalone, R. *Mar. Drugs* **2012**, *10*, 51–63.
86. Petrovic, A.G.; Navarro-Vazquez, A.; Alonso-Gomez, J.L. *Curr. Org. Chem.* **2010**, *14*, 1612–1628.
87. Frisch, M.J.; Trucks, G.W.; Schlegel, H.B.; Scuseria, G.E.; Robb, M.A.; Cheeseman, J.R. Jr.; Montgomery, J.A.; Vreven, T.; Kudin, K.N.; Burant, J.C. et al. *Gaussian 03, Revision B.05*; Gaussian: Inc., Wallingford, CT, USA, 2004.
88. Lodewyk, M. W.; Tantillo, D. J. *J. Nat. Prod.* **2011**, *74*, 1339-1343.
89. Smith, S. G.; Goodman, J. M. *JACS* **2010**, *132*, 12946-12959.
90. Aiello, A.; Fattorusso, E.; Imperatore, C.; Luciano, P.; Menna, M.; Vitalone, R. *Mar. Drugs* **2012**, *10*, 51-63.
91. Aiello, A.; Fattorusso, E.; Luciano, P.; Menna, M.; Vitalone, R. *J. Nat. Prod.* **2010**, *73*, 620-622.
92. . Smith, M. T *J. Toxicol. Environ. Health* **1985**, *16*, 665-672.
93. Kamel, H. N.; Ding, Y.; Li, X. C.; Ferreira, D.; Fronczek, F. R.; Slattery, M. *J. Nat. Prod.* **2009**, *72*, 900-905.
94. Tayone, W. C.; Honma, M.; Kanamaru, S.; Noguchi, S.; Tanaka, K.; Nehira, T.; Hashimoto, M. *J. Nat. Prod.* **2011**, *74*, 425–429.
95. Lombardo, M.; Morganti, S.; Trombini, C. *J. Org. Chem.* **2003**, *68*, 997-1006.
96. Latypov, Sh. K.; Seco, J. M.; Quinoa, E.; Riguera R. *J. Org. Chem.* **1996**, *61*, 8569-8577.
97. Freire, F.; Seco, J. M.; Quinoa, E.; Riguera R. *J. Org. Chem.* **2005**, *70*, 3778-3790.
98. Freire, F.; Seco, J. M.; Quinoa, E.; Riguera R, *Chem. Eur. J.* **2005**, *11*, 5509 – 5522
99. Porto, S.; Seco, J. M.; Espinosa, J. F.; Quinoa, E.; Riguera, R. *J. Org. Chem.* **2008**, *73*, 5714–5722
100. Thomson, R. H. *Naturally Occurring Quinones*; Academic Press: London, **1971**.
101. Pennock, J. F. In *Terpenoids in Plants*; Pridham, J. B., Ed.; Academic Press: London, **1967**; 129–146.

102. Fenical, W. *Food-Drugs Sea, Proc. Conf. 4th* **1976**, 4, 388.
103. Howard, B. M.; Clarkson, K.; Berstein, R. L. *Tetrahedron Lett.* **1979**, 4449.
104. Targett, N. M.; Keeran, W. S. *J. Nat. Prod.* **1984**, 47, 556.
105. Guella, G.; Mancini, I.; Pietra, F. *Helv. Chim. Acta* **1987**, 70, 621.
106. Benslimane, A. F.; Pouchus, Y. F.; Le Boterff, J.; Verbist, J. F.; Roussakis, C.; Monniot, F. *J. Nat. Prod.* **1988**, 51, 582.
107. Sato, A.; Shindo, T.; Kasanuki, N.; Hasegawa, K. *J. Nat. Prod.* **1989**, 52, 975.
108. Fu, X.; Houssain, M. B.; van der Helm, D.; Schmitz, F. J. *J. Am. Chem. Soc.* **1994**, 116, 12125. this reference has been corrected in *J. Am. Chem. Soc.* **1995**, 117, 9381.
109. Rochfort, S. J.; Metzger, R.; Hobbs, L.; Capon, R. *Aust. J. Chem.* **1996**, 49, 1217.
110. Fu, X.; Houssain, B. M.; Schmitz, F. J.; van der Helm, D. *J. Org. Chem.* **1997**, 62, 3810.
111. Davis, R. A.; Carroll, A. R.; Quinn, R. J. *J. Nat. Prod.* **1999**, 62, 158.
112. Garrido, L.; Zubia, E.; Ortega, M. J.; Salva, J. *J. Nat. Prod.* **2002**, 65, 1328.
113. Shubina, L. K.; Fedorov, S. N.; Radchenko, O. S.; Balaneva, N. N.; Kolehnikova, S. A.; Dmitrenok, P. S.; Bode, A. M.; Dong, Z.; Stonik, V. A. *Tetrahedron Lett.* **2005**, 46, 559.
114. Aiello, A.; Fattorusso, E.; Luciano, P.; Menna, M.; Esposito, G.; Iuvone, T.; Pala, D. *Eur. J. Org. Chem.* **2003**, 898.
115. Aiello, A.; Fattorusso, E.; Luciano, P.; Macho, A.; Menna, M.; Munoz, E. *J. Med. Chem.* **2005**, 48, 3410.
116. Aiello, A.; Fattorusso, E.; Luciano, P.; Mangoni, A.; Menna, M. *Eur. J. Org. Chem.* **2005**, 5024.
117. (a) Barone, G.; Gomez-Paloma, L.; Duca, D.; Silvestri, A.; Riccio, R.; Bifulco, G. *Chem. Eur. J.* **2002**, 8, 3233; (b) Barone, G.; Duca, D.; Silvestri, A.; Gomez-Paloma, L.; Riccio, R.; Bifulco, G. *Chem. Eur. J.* **2002**, 8, 3240.
118. Schmitz, F. J.; Bloor, S. J. *J. Org. Chem.* **1988**, 53, 3922.

119. Scribner, R. M. *J. Org. Chem.* **1966**, *31*, 3671.
120. Harada, N.; Sugioka, T.; Soutome, T.; Hiyoshi, N.; Uda, H.; Kuriki, T. *Tetrahedron: Asymmetry* **1995**, *6*, 375.
121. Aiello A. et al. *Bioorg. Med. Chem.* **2010**, *18*, 719–727.
122. Inbaraj, J. J.; Gandhidasan, R.; Murugesan, R. *Free Radical Biol. Med.* **1999**, *26*, 1072.
123. Obberhammer, F.; Fritsch, G.; Schmied, M.; Pavelka, M.; Printz, D.; Purchio, T.; Lassman, H.; Schulte-Hermann, R. *J. Cell Sci.* **1993**, *104*, 317.
124. Ott, M.; Robertson, J. D.; Gogvadze, V.; Zhivotovsky, B.; Orrenius, S. *Proc. Natl. Acad. Sci. U.S.A.* **2002**, *99*, 1259.
125. Murphy, B. T.; Maloney, K. N.; Fenical, W. *Phytochemistry and pharmacognosy*.
126. Arp, A. J. *Encyclopedia of ocean sciences*, second edition, **2008**, 1242-1246.
127. Biers, E. J.; Sun, S.; Howard, E. C. *Appl. Environ. Microbiol.* **2009**, *75*, 2221-2229.
128. Bowman, J. P.; Mccammon, S. A.; Brown, M. V.; Nichols, D. S.; Mcmeekin, T. A. *Appl. Environ. Microbiol.* **1997**, *63*, 3068-3078.
129. Bugni, T. S.; Ireland, C. M., *Nat. Prod. Rep.* **2004**, *21*, 143-163.
130. Rateb, M. E.; Ebel, R., *Nat. Prod. Rep.* **2011**, *28*, 290-344
131. Saleem, M.; Ali, M. S.; Hussain, S.; Jabbar, A.; Ashraf, M.; Lee, Y. S., *Nat. Prod. Rep.* **2007**, *24*, 1142-1152.
132. Cheng, Z.-S.; Pan, J.-H.; Tang, W.-C.; Chen, Q.-J.; Lin, Y.-C. *Journal of Forestry Research* **2009**, *20*, 63-72.
133. Tsantrizos Y. S. et al. *Can. J. Chem.*, **1993**, *71*, 1362-1367.

CHAPTER 4

EXPERIMENTAL.

4.1 *Aplidium conicum*

Extraction and Isolation Procedures: Specimens of *A. conicum* were collected in November 2007 at Porto Cesareo (Lecce, Italy). They were frozen immediately after collection and kept frozen until extraction. A reference specimen is deposited at the Dipartimento di Chimica delle Sostanze Naturali, University of Naples. The fresh thawed animals (6,7 g of dry weight after extraction) were homogenized and extracted twice with methanol and then twice with chloroform (4 x 200 mL). The combined extracts were concentrated in vacuo, and then partitioned between H₂O and EtOAc and, subsequently, between H₂O and n-BuOH. Separation of the EtOAc soluble material (2,24 g) was achieved by gradient silica gel MPLC (hexane → EtOAc → MeOH). The fraction eluted with EtOAc 100% (v/v) was chromatographed by HPLC on a SiO₂ column (Luna 5 μm, 250 x 4.60 mm) eluting with EtOAc/hexane 75:25 (v/v), yielding a fraction (4.2 mg) which has been further purified by reverse HPLC on a Luna 3 μm PFP 100 Å column, eluting with MeOH/H₂O 8:2, thus affording conithiaquinones A (1.2 mg) and B (0.7 mg) as pure compounds.

Conithiaquinone A (1): Colorless amorphous solid. $[\alpha]_D^{25} = + 3.2$ (c=0.11 in methanol). ¹H NMR (700 MHz, CD₃OD) and ¹³C NMR (175 MHz, CD₃OD): see Table 3.1. HRESI-MS (positive ion mode, MeOH): calcd. for C₁₉H₂₅NO₆SNa [M+Na]⁺ 418.1295; found 418.1290. ¹H NMR (700 MHz, CDCl₃): δ 6.56 (H, br s, 4-NH), 5.16 (10-H, d, J = 9.1 Hz), 4.06 (3-2H, m), 3.65 (H, br s, OH), 3.29 (2-2H, m), 3.23 (13-3H, s), 2.04 (8-H_b, m), 1.84 (6a-H, dt, J= 13.6 and 9.1 Hz), 1.68 (7-H_b, m), 1.60 (9a-H, dd, J= 13.6 and 9.1 Hz), 1.49 (7-H_a, m), 1.42 (12-3H, s), 1.41 (8-H_a, overlapped), 1.22 (15-3H, s), 1.21 (14-3H, s).

Conithiaquinone B (2): Colorless amorphous solid. $[\alpha]_D^{25} = +9.5$ ($c=0.06$ in methanol). ^1H NMR (700 MHz, CD_3OD) and ^{13}C NMR (175 MHz, CD_3OD): see Table 3.1. HRESI-MS (positive ion mode, MeOH): calcd. for $\text{C}_{20}\text{H}_{27}\text{NO}_6\text{SNa}[\text{M}+\text{Na}]^+$ 432.1451; found 432.1449.

Computational calculations: DFT calculations were performed on a Pentium-4 processor at 3.0 GHz using the Gaussian03 package (Multiprocessor). DP4 NMR prediction analysis was carried out as described by Smith and Goodman. Gaussian 03 was used to calculate both the carbon and proton GIAO NMR shielding tensors at the mPW1PW91 functional and 6-31G(d,p) basis set, using as input the geometry previously optimized at the mPW1PW91/6-31G(d) level. For these calculations, the IEF-PCM solvent continuum model, as implemented in Gaussian (methanol solvent), was used. TDDFT calculations were run using the functional B3LYP and the basis sets TZVP including at least 30 excited states in all cases, and using IEF-PCM for MeOH. ECD spectra were generated.

Cell cultures and microcultures bioassay: Biological activity was investigated on tumour MCF-7 human breast adenocarcinoma cells and non-tumour HaCaT human skin keratinocytes, purchased from ATCC[®] (American Type Culture Collection, Manassas, Virginia, USA). HaCaT cells were grown in Dulbecco's modified Eagle's medium (DMEM, Invitrogen, Paisley, UK) containing high glucose (4.5 g/l), while MCF-7 cells were grown in RPMI 1640 medium (Invitrogen, Paisley, UK). Media were supplemented with 10% fetal bovine serum (FBS, Cambrex, Verviers, Belgium), L-glutamine (2 mM, Sigma, Milan, Italy), penicillin (100 units/ml, Sigma) and streptomycin (100 $\mu\text{g}/\text{ml}$, Sigma), according to ATCC recommendations. All cells were cultured in a humidified 5% CO_2 atmosphere at 37°C. For bioactivity and cytotoxicity studies, cells were seeded in a 96-microwell culture plates at density of 10^4 cells/well. Cells were allowed to grow for 24 h, then the medium was replaced with fresh medium and cells were treated for further 48 h with different concentrations of the tested compounds. In detail, both compounds (1) and (2) were dissolved in dimethyl sulphoxide (DMSO, Sigma) and 1 or 2 μL of DMSO solutions were added to cell culture medium to give various concentration ranging from 1 to 250 μM ; 1 or 2 μL of DMSO alone (vehicle) were added into control cells (0.5 and 1% v/v final concentrations, respectively). Positive control for cytotoxicity was

performed using cisplatin (CDDP, Sigma). Live/death cell number was determined by the trypan blue dye exclusion test. After the treatments, the medium was removed and the cells were washed twice with PBS buffer solution (Sigma) and then incubated with a trypsin-EDTA solution (Sigma) at 37°C for 5 min. Trypsin was inactivated by re-suspending the cells in medium containing 10% FBS (Cambrex). The cells were pelleted at 250 x g and resuspended in PBS. Viable cells, cells that excluded 0.4% trypan blue (Sigma), were then counted with a Burker haemocytometer chamber.¹ Concurrently, cell viability was evaluated with an MTT assay procedure, which measures the level of mitochondrial dehydrogenase activity using 3-(4,5-dimethyl-2-thiazolyl)-2,5-diphenyl-2H-tetrazolium bromide (MTT, Sigma) as substrate. The assay was based on the redox ability of living mitochondria to convert dissolved MTT into insoluble formazan. Briefly, after treatments with the test compounds, the medium was removed and the cells were incubated with 20 µL/well of an MTT solution (5 mg/mL) for 1 h in a humidified 5% CO₂ incubator at 37°C. The incubation was stopped by removing the MTT solution and by adding 100 µL/well of DMSO to solubilize the formazan. Finally, the absorbance was monitored at 550 nm by using a Perkin-Elmer LS 55 Luminescence Spectrometer (Perkin-Elmer Ltd, Beaconsfield, UK).² The calculation of the concentration required to inhibit the net increase in the 48 h cell count and viability by 50% (IC₅₀) is based on plots of data carried out in triplicates and repeated three times. IC₅₀ values were obtained using a dose response curve by nonlinear regression using a curve fitting program, GraphPad Prism 5.0, and are expressed as mean ± SEM.

4.2 *Ciona edwardsii* and *Aplidium elegans*

Extraction and Isolation Procedures: Specimens of *A. elegans* were collected at -40 m depth in the autumn of 2003 in the Bay of Naples (Bacoli) and kept frozen until used. The freshly thawed tunicate was homogenized and extracted at room temperature with methanol (3×1 L) and, subsequently, with chloroform (3×1 L) (31.8 g dry weight of the tunicate after air drying). The combined extracts were concentrated *in vacuo* to give an aqueous suspension that was subsequently partitioned initially with EtOAc and then with *n*-BuOH. The butanol-soluble material obtained after evaporation of the solvent (4.1 g of a dark brown oil), was chromatographed on a RP-18 silica gel flash column using a gradient elution (H₂O/MeOH 9:1 → H₂O/MeOH 7:3 → H₂O/MeOH 1:1 → H₂O/MeOH 3:7 → MeOH 100% → MeOH/CHCl₃ 9:1 → MeOH/CHCl₃ 7:3 → MeOH/CHCl₃ 1:1 → CHCl₃ 100%). The fractions eluted with H₂O/MeOH 1:1 were rechromatographed by HPLC on an RP-18 column (Luna, 3 μm, 150 × 4.60 mm), using H₂O/MeOH 7:3 containing TFA 0.1% as the eluent (flow 0.5 mL/min). This separation afforded pure compound **10** (1.2 mg) and pure compound **11** (1.0 mg). Specimens of *C. edwardsii* were collected at -75 m depth in the autumn of 2006 in the Bay of Naples (at -65/-75 meter in Meta di Sorrento Punta Gradelle) and kept frozen until used. The freshly thawed tunicate was homogenized and treated at room temperature with methanol (3×1 L) and, subsequently, with chloroform (3×1 L) (21.9 g dry weight of the tunicate after air drying). The combined extracts were concentrated *in vacuo* to give an aqueous suspension that was subsequently partitioned initially with EtOAc and then with *n*-BuOH. The butanol-soluble material obtained after evaporation of the solvent (5.4 g of a dark brown oil), was chromatographed on a RP-18 silica gel flash column using a gradient elution (H₂O/MeOH 9:1 → H₂O/MeOH 7:3 → H₂O/MeOH 1:1 → H₂O/MeOH 3:7 → MeOH 100% → MeOH/CHCl₃ 9:1 → MeOH/CHCl₃ 7:3 → MeOH/CHCl₃ 1:1 → CHCl₃ 100%). The fractions eluted with H₂O/MeOH 3:7 were rechromatographed by HPLC on an RP-18 column (Luna, 3 μm, 150 × 4.60 mm), using H₂O/MeOH 72:28 containing TFA 0.1% as the eluent (flow 0.5 mL/min). This separation afforded 2.4 mg of pure compound **12**.

Compound 10: colorless amorphous solid; $[\alpha]_D^{25} = +2.5$ ($c = 0.002$, CH₃OH). ESI-MS (negative ion mode): $m/z = 511$ [M-Na]⁻; HRESIMS (negative ion mode): $m/z = 511.1987$; the molecular formula C₂₀H₄₀NaO₉S₂⁻ requires 511.2006; ¹H-NMR and ¹³C-NMR data (CD₃OD, 500/125 MHz) are reported in Table 3.3.

Compound 11: colorless amorphous solid; $[\alpha]_D^{25} = +3.4$ ($c = 0.002$, CH₃OH). ESI-MS (negative ion mode): $m/z = 497$ [M-Na]⁻; HRESIMS (negative ion mode): $m/z = 497.1825$; the molecular formula C₁₉H₃₈NaO₉S₂⁻ requires 497.1849; ¹H-NMR and ¹³C-NMR data (CD₃OD, 500/125 MHz) are reported in Table 3.3.

Compound 12: Colorless amorphous solid; $[\alpha]_D^{25} = +1.8$ ($c = 0.002$, CH₃OH). ESI-MS (negative ion mode): $m/z = 379$ [M-Na]⁻; ESI-MS (positive ion mode): $m/z = 403$ [M+H]⁺; HRESIMS (negative ion mode): $m/z = 379.2522$; the molecular formula C₁₉H₃₉O₅S⁻ requires 379.2513; ¹H-NMR and ¹³C-NMR data (CD₃OD, 500/125 MHz) are reported in Table 3.3.

Cell Culture: J774A.1 cell line (BALB/c murine macrophages) was cultured in Dulbecco's modified Eagle's medium (DMEM) supplemented with 4.4% NaHCO₃ (HyClone), penicillin (100 U/mL), streptomycin (100 µg/mL), 2 mM glutamine, 25 mM Hepes, 130 µg/mL Na pyruvate and 10% foetal calf serum (FCS) (Hy Clone). The rat astrocytic glioma C6 cell line was cultured in DMEM supplemented with 10% FCS, penicillin (100 U/mL), streptomycin (100 µg/mL), and L-glutamine 2 mM. All cells were cultured in plastic tissue culture flasks and kept at 37 °C under 5% CO₂ atmosphere.

Cytotoxicity Assay: cytotoxicity studies in both tumour cell lines were performed in a 96-well plate ^{3,4} J774A.1 were mechanically scraped, while C6 cells were enzymatically detached. The cells were plated 12.5 × 10⁴/well (J774A.14) or 2.5 × 10³/well (C6) to a final volume of 200 µL. After 4 h J774A.1, cells were incubated with compounds **10–12** at increasing concentrations (10–100 µM) for 22 h; conversely, after 3 days C6 cells were incubated with compounds **10–12** (10–300 µM) for 22 h. Then, 25 µL of 3-(4,5-dimethylthiazol-2-yl)-2,5-diphenyltetrazolium bromide (MTT, 5 mg/mL) was added in each well, 3 h later the cells were lysated with 100 µL of lysis buffer (20% SDS and 50% DMF, pH 4.7). After an incubation

of 22 h at 37 °C the optical densities (OD₆₂₀) for the serial dilutions of both compounds were compared with the OD of the control wells to assess the cytotoxicity⁵ LC₅₀ for each cell line was obtained by statistical computer program.

Data Analysis: data are reported as mean ± SEM values of three independent determinations. All experiments were performed at least three times, each time with three or more independent observations. Statistical analysis was performed by ANOVA test, and multiple comparisons were made by Dunnett.

4.3 *Phallusia fumigata*

Collection, Extraction, and Isolation: specimens of *Phallusia fumigata* were collected in April 2008 at in the bay of Pozzuoli (Napoli, Italy). The samples were frozen immediately after collection and stored at -20 °C until extraction. A reference specimen is deposited at the Dipartimento di Farmacia, University of Naples. The fresh thawed animals (424 g of dry weight after extraction) were homogenized and extracted twice with methanol and then twice with chloroform (4 x 200 mL). The combined extracts were concentrated in vacuo, and the resulting aqueous residue was extracted with EtOAc and subsequently with *n*-BuOH. Separation of the EtOAc soluble material (1,04 g) was achieved by gradient silica gel MPLC (hexane → EtOAc → MeOH). The fraction eluted with hexane/EtOAc 3:7 v/v, (37.0 mg) was chromatographed by HPLC on a SiO₂ column (Luna 5 μm, 250 x 4.60 mm) eluting with hexane/EtOAc 55:45 (v/v), yielding a fraction (3.3 mg) which has been further purified by HPLC on a SiO₂ column (Luna 5 μm, 250 x 4.60 mm), eluting with hexane/propan-2-ol 93:7, thus affording phallusiasterol A (2.0 mg) and B (1.1 mg) as pure compounds. Separation of the BuOH soluble material (2,0 g) was achieved by reversed-phase silica gel (RP18) MPLC, using a gradient elution (H₂O→MeOH→CHCl₃). The fraction eluted with H₂O/MeOH 3:7 v/v, (170.4 mg) was chromatographed by HPLC on a Synergi 4μ Polar-RP 80 Å (250 x 4.60 mm) column, eluting with MeOH/H₂O 65:35 (v/v) and 0.1 % of trifluoroacetic acid, yielding a fraction (40.6 mg) which has been further purified by HPLC on a Synergi 4μ Hydro-RP 80 Å (250 x 4.60 mm) column, eluting with MeOH/H₂O 7:3 (v/v) and

0.1 % of trifluoroacetic acid, thus affording phallusiasterol C (4.7 mg) as pure compound.

Phallusiasterol A (15): colorless amorphous solid, $[\alpha]_D^{25}$ -3.5 (c 0.1, CHCl_3); HRESIMS (positive ion mode, CH_3OH) m/z 545.2858 ($[\text{M} + \text{Na}]^+$, calcd. for $\text{C}_{27}\text{H}_{47}\text{SO}_6\text{Na}_2^+$ 545.2889); ^1H and ^{13}C NMR ($\text{C}_5\text{D}_5\text{N}$): see Table 3.4 ^1H NMR (CDCl_3): δ 4.33 (1H, m, H-3), 3.96 (1H, br s, H-6), 2.34 (1H, dd, $J = 13.1, 10.5$ Hz, H-4 β), 2.02 (1H, m, H-7 β), 1.99 (1H, overlapping, H-4 α), 1.98 (1H, overlapping, H-12 β), 1.90 (1H, m, H-2 α), 1.83 (1H, ddd, $J = 13.6, 9.5, 3.7$, H-16 α), 1.74 (1H, qd, $J = 12.0, 4.3$ Hz, H-8 β), 1.68 (1H, dt, $J = 13.4, 4.2$ Hz, H-1 α), 1.60 (1H, overlapping, H-7 α), 1.57 (1H, overlapping, H-2 β), 1.57 (1H, overlapping, H-15 α), 1.54 (1H, m, H-9 α), 1.51 (1H, m, H-25), 1.48 (1H, ddd, $J = 13.4, 4.5, 2.3$, H-1 β), 1.41 (1H, dq, $J = 14.1, 3.8$, H-11 α), 1.37 (1H, m, H-20), 1.35-1.33 (2H, overlapping, H-22a and H-23a), 1.29 (1H, overlapping, H-11 β), 1.28 (3H, s, Me-19), 1.26 (1H, overlapping, H-16 β), 1.25 (1H, m, H-14 α), 1.24 (1H, overlapping, H-23b), 1.18 (1H, m, H-12 α), 1.15-1.10 (3H, m, H-17, H-24a, and H-24b), 1.07 (1H, m, H-15 β), 1.00 (1H, m, H-22b), 0.91 (3H, d, $J = 6.5$ Hz, Me-21), 0.87 (3H, d, $J = 6.6$ Hz, Me-26), 0.86 (3H, d, $J = 6.6$ Hz, Me-27), 0.67 (3H, s, Me-18). ^{13}C NMR (CDCl_3): δ 84.2 (C-5), 75.8 (C-6), 67.8 (C-3), 56.0 (C-17), 55.8 (C-14), 46.0 (C-9), 42.8 (C-13), 41.3 (C-4), 39.8 (C-10 and C-12), 39.6 (C-24), 36.2 (C-22), 35.8 (C-20), 34.0 (C-7), 33.6 (C-1), 30.5 (C-2), 30.4 (C-8), 28.2 (C-16), 28.0 (C-25), 24.0 (C-15), 23.8 (C-23), 21.3 (C-11), 22.7 (Me-26), 22.5 (Me-27), 18.8 (Me-21), 18.2 (Me-19), 12.1 (Me-18).

Phallusiasterol B (16): colorless amorphous solid, $[\alpha]_D^{25}$ +7.9 (c 0.1, CHCl_3); HRESIMS (positive ion mode, CH_3OH) m/z 545.2870 ($[\text{M} + \text{Na}]^+$, calcd. for $\text{C}_{27}\text{H}_{47}\text{SO}_6\text{Na}_2^+$ 545.2889); ^1H and ^{13}C NMR ($\text{C}_5\text{D}_5\text{N}$): see Table 3.4. ^1H NMR (CDCl_3): δ 4.05 (1H, m, H-3), 3.84 (1H, d, $J = 5.4$, H-6), 2.25 (1H, t, $J = 13.2$, H-4 β), 1.99 (1H, dt, $J = 12.4, 3.4$, H-12 β), 1.96 (1H, m, H-7 β), 1.67 (1H, dd, $J = 13.2, 2.1$, H-4 α), 1.87-1.84 (3H, overlapping, H-2 α , H-7 α , H-8 β , H-16 α), 1.68 (1H, dd, $J = 13.1, 4.7$, H-9 α), 1.56-1.54 (3H, overlapping, H-1 α , H-2 β , and H-15 α), 1.51 (1H, m, H-25), 1.42-1.41 (2H, m, H-1 β and H-11 α), 1.37 (1H, m, H-20), 1.33 (2H, overlapping, H-22a and H-23a), 1.30 (1H, overlapping, H-11 β), 1.28 (3H, s, Me-19), 1.27-1.24 (3H, overlapping, H-14 α , H-16 β , and H-23b), 1.12 (1H, m, H-12 α), 1.20-

1.11 (3H, m, H-17, H-24a, and H-24b), 1.07 (1H, m, H-15 β), 1.00 (1H, m, H-22b), 0.91 (3H, d, $J = 6.5$ Hz, Me-21), 0.87 (3H, d, $J = 6.6$ Hz, Me-26), 0.86 (3H, d, $J = 6.6$ Hz, Me-27), 0.70 (3H, s, Me-18). ^{13}C NMR (CDCl_3): δ 77.2 (C-5), 67.3 (C-3), 63.5 (C-6), 56.4 (C-17), 55.6 (C-14), 46.1 (C-9), 42.9 (C-13), 41.6 (C-4), 40.2 (C-12), 39.6 (C-24), 39.4 (C-10), 36.1 (C-22), 35.8 (C-20), 35.2 (C-7), 32.6 (C-1), 30.6 (C-2), 29.7 (C-8), 29.1 (C-16), 27.9 (C-25), 24.0 (C-15), 23.8 (C-23), 21.1 (C-11), 22.7 (Me-26), 22.5 (Me-27), 18.5 (Me-21), 18.2 (Me-19), 12.0 (Me-18).

3 β , 6 β -diacetate-5 α -cholestan-5 α -yl sodium sulfate (17): to a stirred solution of 0.5 mg of pure **15** in 0.5 mL of dry pyridine was added 0.3 mL of Ac_2O . After the mixture was stirred for 12 h at room temperature, evaporation under vacuum gave 0.7 mg of **17** as a white solid: HRESIMS (positive ion mode, CH_3OH) m/z 629.3089 ($[\text{M} + \text{Na}]^+$, calcd. for $\text{C}_{31}\text{H}_{51}\text{SO}_8\text{Na}_2^+$ 629.3100); ^1H NMR (C_6D_6): δ 0.61 (3H, s, Me-18), 0.94 (6H, d, $J = 6.6$ Hz, Me-26 and Me-27), 0.98 (3H, d, $J = 6.6$ Hz, Me-21), 1.14 (3H, s, Me-19), 1.52 (3H, s, COMe), 1.70 (3H, s, COMe), 5.43 (1H, br s, H-6 α), 5.72 (1H, m, H-3 α); ^{13}C NMR (C_6D_6): δ 11.9 (C-18), 17.2 (C-19), 18.5 (C-21), 20.1 (COMe), 20.4 (COMe), 22.4 (C-26 and C-27), 69.9 (C-3), 75.1 (C-6), 168.8 (CO), 169.4 (CO).

Phallusiasterol C (18): colorless amorphous solid; HRESI-MS (negative ion mode CH_3OH) m/z 567.2064 $[\text{M}-\text{Na}^+]^-$; calcd. for $\text{C}_{26}\text{H}_{40}\text{NaO}_8\text{S}_2$ 567.2062. ESIMS: 465 $[\text{M}-\text{NaSO}_3]^-$, 447 $[\text{M}-\text{NaHSO}_4-\text{Na}^+]^-$, 272 (double charged species).

Transactivation Experiments: HepG2 cells were plated in a 24-wells plate, at 5×10^4 cells/well, and transfected with 75 ng of pSG5-PXR, 75 ng of pSG5-RXR, 125 ng of pCMV- β -galactosidase, and with 250 ng of the reporter vector pCYP3A4promoter-TKLuc, using Fugene HD transfection reagent (Roche). At 24 hours post-transfection, cells were primed with Rifaximin, **15**, **16** and **18** (10 μM) or with the combination of Rifaximin (10 μM) plus compounds **15**, **16** and **18** (50 μM). After treatments, cells were lysed in 100 μL Lysis Buffer (25 mM TRIS-phosphate pH 7.8; 2mM DTT; 10% glycerol; 1% Triton X-100) and 20 μL cellular lysate was assayed for Luciferase activity using the Luciferase Assay System (Promega). Luminescence was measured using an automated luminometer (Glomax 20/20, Promega). Luciferase activities were normalized for transfection efficiencies by

dividing the Luciferase relative light units (RLU) by β -galactosidase activity (β gal) expressed from cells co-transfected with pCMV β gal. All experiments were performed in triplicate.

Cells culture, RNA extraction and Real-Time PCR: HepG2 cells were maintained at 37 °C in E-MEM supplemented with 10% FBS, 1% L-glutamine and 1% penicillin/streptomycin. To evaluate PXR target genes expression, serum starved HepG2 cells were stimulated for 18 h with Rifaximin and compound **15**, **16** and **18** (10 μ M). Total RNA was extracted using the TRIzol reagent (Invitrogen), purified of the genomic DNA by DNAase I treatment (Invitrogen) and random reverse-transcribed with Superscript II (Invitrogen). 10 ng template was amplified using the following reagents: 0.2 μ M of each primer and 10 μ l of KAPA SYBR FAST Universal qPCR Kit (KAPA BIOSYSTEMS). All reactions were performed in triplicate and the thermal cycling conditions were: 3 min at 95 °C, followed by 40 cycles of 95 °C for 15 s, 58 °C for 20 s and 72 °C for 30 s. The relative mRNA expression was calculated and expressed as $2^{-(\Delta\Delta C_t)}$. Primers used for qRT-PCR were:

hGAPDH: GAAGGTGAAGGTCGGAGT and
CATGGGTGGAATCATATTGGAA;

hCYP3A4: CAAGACCCCTTTGTGGAAAA and CGAGGCGACTTTCTTTCATC;

hMDR1: gtggggcaagtcagttcatt and tcttcacctccaggctcagt.

Statistical Analysis: all values are expressed as means \pm standard error (SE) of n observations/group. Comparisons of two groups were made with a one-way ANOVA with post hoc Tukey's test. Differences were considered statistically significant at values of $P < 0.05$.

Computational Details: molecular docking of phallusiasterol A in the three-dimensional X-ray structures of the PXR LBD (PDB codes: 3hvl, 1nrl and 1m13) without the co-crystallized inhibitor and waters were carried out using the AutoDock software package (version 4.2). Ligands and receptor structures were converted to AutoDock format files using the ADT software, and the Gesteiger-Marsili partial charges were then assigned. A box around the binding pocket has defined the docking area and grids points of 48 \times 40 \times 38 with 0.375 Å spacing were calculated

within the this area for all the ligand atom types using AutoGrid4. For each ligand, 100 separate docking calculations were performed. Each docking run consisted of 25 million energy evaluations using the Lamarckian genetic algorithm local search (GALS) method. Otherwise default docking parameters were applied. The docking conformations were clustered on the basis of the root-mean square deviation values (rmsd tolerance = 1.5 Å) between the cartesian coordinates of the ligand atoms and were ranked based on the AutoDock scoring function.

4.4 *Sydneyia elegans*

Collection, Extraction, and Isolation: Specimens of *S. elegans* were collected at Capo Caccia (Alghero, Italy). They were frozen immediately after collection and kept frozen until extraction. The fresh thawed animals (39.7 g of dry weight after extraction) were homogenised and at room temperature with methanol (3 × 300 mL) and then with chloroform (3 × 300 mL). The combined extracts were concentrated in vacuo and the resulting aqueous residue was extracted with EtOAc and, subsequently, with *n*-BuOH. The *n*-butanol-soluble material was chromatographed by MLPC over a C-18 column followed using a gradient elution (H₂O→MeOH→CHCl₃). The fraction eluted with MeOH:H₂O 7:3 (v/v) was further purified by RP-HPLC (Synergi RP-MAX 4 μm column, MeOH/H₂O 8:2 and 0.1% of trifluoroacetic acid) and yielded phosphoeleganin (**19**) (80.0 mg) in a pure state.

Phosphoeleganin (19): HRESI-MS (negative ion mode): m/z =668.3832, C₃₂H₆₃NO₁₁P requires 668.4049. ¹H and ¹³C NMR data (CD₃OD and DMSO): see Table 3.6.

Preparation of acetonide: A solution of phosphoeleganin (3.5 mg) in 2,2-dimethoxypropane (1.5 mL) was treated with Dowex 50W-X8 (H⁺ form, 20 mg), and the mixture was stirred at room temperature for 3 h. The resin was removed by filtration and the solvent from the filtrate was dried obtaining compound **34** (4.5 mg).

Periodate degradation: phosphoeleganin (6.3 mg) was dissolved in 2 mL of 0.012 M NaIO₄ and stirred at room temperature for 3 h. Then the solution was cooled to 0 °C, excess amount of NaBH₄ was added and kept for 1 hr. The reaction solution was partitioned between water and butanol. The butanol extract was purified by reverse phase HPLC (Luna C18 3μ, MeOH/H₂O 8:2 with 0.1%TFA) yielded compounds **22** and **23** in the pure state.

4.5 *Axinella Polypoides*

Collection, Extraction and Isolation: specimens of *A. polypoides* were collected in the Bay of Calvi (Corsica, France), frozen immediately and kept frozen until extraction. A reference specimen was deposited at the Dipartimento di Chimica delle Sostanze Naturali, University of Naples “Federico II”. Fresh thawed animals (105.2 g dry weight after extraction) were homogenized and extracted twice with MeOH and, then, twice with CHCl₃ (4 × 500 mL). Extracts were combined and concentrated; the resulting aqueous residue was then partitioned between H₂O and n-BuOH. Separation of the organic phase (13.0 g) was achieved by reversed-phase silica gel (RP18) MPLC, using a gradient elution (H₂O→MeOH→CHCl₃). Ten fractions (A–L) were obtained, each of them was subjected to a rapid ¹H-NMR/ESIMS-based analysis. Fraction B, eluted with H₂O/MeOH 9:1 v/v, (3.4 g) was re-chromatographed under medium pressure on a RP18 column eluting with a linear gradient of MeOH (from 2% to 100%) in H₂O, thus affording twelve fractions (1–12). Fraction 8 (219 mg), eluted with H₂O/MeOH 92:8 v/v, was separated by HPLC on a Synergy Polar-RP 4 μm column (250 × 4.60 mm) eluting with H₂O/MeOH (98:2, v/v) and 0.1% TFA, to give compounds **30** (22.3 mg) and **31** (4.0 mg). Fraction 10 (55.8 mg), eluted with H₂O/MeOH (85:15, v/v) was separated by HPLC in the same conditions as above, to give **32** (7.8 mg) and **33** (4.8 mg). Fractions C and D, both eluted with H₂O/MeOH 7:3 v/v, were combined (524.5 mg) separated by HPLC on a Synergy Polar-RP 4 μm column (250 × 4.60 mm) eluting with H₂O/MeOH (98:2, v/v), to give axityrosinium (**24**, 52.0 mg), axiphenylalaninium (**25**, 19.2 mg), polyaxibetaine (**26**, 6.0 mg) and compound **29** (9.1 mg). The hydrophilic extract (42.7 g) was subjected to Droplet Counter Current Chromatography (DCCC), using a mixture of BuOH-Acetone-H₂O (3:1:5) as the solvent, in the ascending mode. The flow rate of the mobile phase was adjusted to 25 mL/h; a total of 150 fractions of 8 mL each were collected and, as for the organic extract, analyzed by ¹H-NMR/ESIMS for the rapid detection of PIAs. Fractions 40–50 were combined, the solvent was evaporated, and the residue (300 mg) was chromatographed by HPLC on a Synergy Polar-RP 4 μm column (250 × 4.60 mm) eluting with H₂O/MeOH (98:2, v/v) and 0.1% TFA, thus affording pure **28** (16.4 mg).

Compound 28: $[\alpha]_D +7.59$ (MeOH, $c = 0.005$); HRESI-MS (positive ion mode): $m/z = 210.1130 [M+H]^+$, $232.0950 [M+ Na]^+$; 1H and ^{13}C NMR data (CD_3OD) are reported in Table 3.8.

Compound 31: $[\alpha]_D +1.70$ (MeOH, $c = 0.003$); HRESI-MS (positive ion mode): $m/z = 283.0673 [M+H]^+$, $265.0567 [M-H_2O+H]^+$; 1H and ^{13}C NMR data (d_6 -DMSO) are reported in Table 3.9.

Computational Details: A preliminary conformational search for one of the two enantiomers of **28** was performed by Simulated Annealing in the INSIGHT II package. The MeOH solution phases were mimicked through the value of the corresponding dielectric constant. Using the steepest descent followed by quasi-Newton-Raphson method (VA09A) the conformational energy was minimized. Restrained simulations were carried out for 500 ps using the CVFF force field as implemented in Discover software (Accelrys, San Diego, USA). The simulation started at 1000 K, and then the temperature was decreased stepwise to 300 K. The final step was again the energy minimization, performed in order to refine the structures obtained, using the steepest descent and the quasi-Newton-Raphson (VA09A) algorithms successively. Both dynamic and mechanic calculations were carried out by using 1 (kcal/mol)/Å² flat well distance restraints. One hundred structures were generated. To simulate the solvent chosen for NMR analysis, a distance-dependent dielectric constant set to the value of MeOH ($\epsilon=32.63$) was used during the calculations. All optimizations were performed with the software package Gaussian 03, by using the DFT functional RB3LYP and the basis set 6-31G(d). The B3LYP/6-31G(d) harmonic vibrational frequencies were further calculated to confirm their stability. Rotatory strength values for the electronic transitions from the ground state to the singly excited states for all conformers of *S*-28 were obtained by TDDFT calculations RB3LYP/6-31G(d,p) with Gaussian 03. The rotatory strength values were summed after a Boltzmann statistical weighting and $\Delta\epsilon$ values were calculated by forming sums of Gaussian functions centered at the wavelengths of the respective electronic transitions and multiplied by the corresponding rotatory strengths. The ECD spectra that was obtained was UV-corrected and compared with the experimental one.

4.6 Synthesis of quinone derivatives

General experimental procedures: ^1H and ^{13}C NMR spectra were recorded with a Varian Gemini 200 MHz or a Varian Mercury 300 MHz or a Bruker Avance 400 MHz.

Reagents: Sigma–Aldrich. Solvents: Carlo Erba. TLC: Silica Gel 60 F254 (plates 5 x 20, 0.25 mm) Merck. Preparative TLC: Silica Gel 60 F254 plates (20 x 20, 2 mm). Spots revealed by UV lamp then by spraying with 2 N sulfuric acid and heating at 120 °C. ‘Acidic’ silica gel was prepared by treating Silica Gel 60 Merck with 1 N HCl for 24 h, washing with water until the chlorine test was negative, activating for 48 h at 120 °C, then equilibrating with 10% of water. Anhydrous solvents: Sigma–Aldrich or prepared by distillation according to standard procedures.

Synthesis of compound 47: To 25 mL of dichloromethane/water 1:1, 3 g (19.6 mmol) of **46** and 5 g (47 mmol) of Na_2CO_3 , were added under stirring 2.5 mL of pivaloylchloride (0.02 mmol) were then added dropwise and the mixture was stirred for 3 hours at room temperature (the end of the reaction was checked by TLC, eluent: hexane/ethyl acetate 7:3). The dark liquid was then poured into cold water and extracted three times with dichloromethane. The combined organic layers were washed with brine, dried with sodium sulfate and filtered; solvent removal under reduced pressure afforded gave **47** (4.38 g, 95%) sufficiently pure for the following reaction. ^1H NMR 200 MHz (CDCl_3): δ 1.31 (9H, s, $-\text{C}(\text{CH}_3)_3$); 3.77 (3H, s, $-\text{OCH}_3$); 3.84 (3H, s, $-\text{OCH}_3$); 6.55 (1H, Dd, $J_1 = 8.8$ Hz, $J_2 = 2.8$ Hz, H-4); 6.78 (1H, d, $J = 8.8$ Hz, H-3); 8.17 (1H, d, $J = 2.8$ Hz, H-6).

Synthesis of compound 48: 4.00 g (16.88 mmol) of **47** were dissolved in 60 mL of anhydrous THF and 32.0 mL of a n-BuLi 1.6 M solution (50.64 mmol) were added, under argon atmosphere at 0 °C; the mixture was stirred for 2 h. Then, 5.12 mL of DMF (65.84 mmol) were added dropwise and the mixture was left under stirring for 16 h (the end of the reaction was checked by TLC, eluent: hexane/ethyl acetate 9:1). The mixture was poured into cold water (150 mL) and extracted three times with ethyl acetate. The combined organic layers were washed with brine, dried over sodium sulfate, and filtered. The solvent removal under reduced pressure gave crude product **48** (4.1 g), which were purified by chromatography on ‘acidic’ silica gel

(SiO₂/crude 3 50:1; eluent: hexane/ethyl acetate 9:1) to give pure **48** (3.064 g, 11.56 mmol, 68.5%). ¹H NMR 300 MHz (CDCl₃): δ 1.32 (9H, s, -C(CH₃)₃); 3.83 (3H, s, -OCH₃); 3.85 (3H, s, -OCH₃); 6.74 (1H, d, *J* = 9.3 Hz, H-5); 7.12 (1H, d, *J* = 9.3 Hz, H-4); 9.20 (1H, bs, NH); 10.38 (1 H, s, -CHO).

Synthesis of compounds 49a-c: To a suspension of 73 mg of Mg powder (3 mmol) in 2 mL of anhydrous diethyl ether, 2.28 mmol of iodoalkane (0.14 ml of iodomethane or 0.44 ml of iodobutane or 2.05 ml of iododecane respectively) in 5 ml of anhydrous diethyl ether were added slowly under stirring at room temperature. After completion, the reaction mixture was refluxed for 1 h and then a solution of compound **48** (150 mg, 0.57 mmol) in anhydrous diethyl ether (10 mL) was added dropwise. The reaction was refluxed for 4 hours (the end of the reaction was checked by TLC, eluent: chloroform/ethyl acetate 9:1) and quenched with 6 ml of saturated NH₄Cl. The mixture was poured into water (20 mL) and extracted three times with ethyl acetate. The combined organic layers were washed with brine, dried over sodium sulfate, and filtered; solvent removal under reduced pressure gave products **49a** (158.6 mg, 99%), **49b** (182.5 mg, 99%) as a colorless crystals sufficiently pure for the following reaction and crude product **49c** (400 mg), which were purified by chromatography on silica gel (SiO₂/crude 3 50:1; eluent: hexane/ethyl acetate 6:4) to give pure **49c** (174.3 mg, 75%).

¹H NMR 300 MHz (CDCl₃) **49a**: δ 1.32 (9H, s, -C(CH₃)₃); 1.58 (3H, d, *J* = 6.6 Hz, -CHOHCH₃); 3.65 (1H, d, *J* = 8.7 Hz, -OH); 3.75 (3H, s, -OCH₃); 3.83 (3H, s, -OCH₃); 4.96 (1H, m, -CHOHCH₃); 6.75 (2H, s*, H-4 and H-5); 7.32 (1H, bs, NH).

¹H NMR 300 MHz (CDCl₃) **49b**: δ 0.85 (3H, t, *J* = 6.8 Hz, -(CH₂)₃CH₃); 1.15 - 1.44 (13H, -CH₂(CH₂)₂CH₃ and -C(CH₃)₃); 1.74 - 1.97 (2H, m, -CHOHCH₂-); 3.55 (1H, bs, -OH); 3.74 (3H, s, -OCH₃); 3.78 (3H, s, -OCH₃); 4.80 (1H, m, -CHOH-); 6.73 (2H, s*, H-4 and H-5); 7.42 (1H, bs, NH).

¹H NMR 300 MHz (CDCl₃) **49c**: δ 0.87 (3H, t, *J* = 6.5 Hz, -(CH₂)₉CH₃); 1.14 - 1.30 (16H, -CH₂(CH₂)₈CH₃); 1.32 (9H, s, -C(CH₃)₃); 1.77 - 1.99 (2H, m, -CHOHCH₂-); 3.30 (1H, bs, -OH); 3.75 (3H, s, -OCH₃); 3.81 (3H, s, -OCH₃); 4.79 (1H, m, -CHOH-); 6.75 (2H, s*, H-4 and H-5); 7.34 (1H, bs, NH).

Synthesis of compounds 50 a-c: to a suspension of 38 mg of 10% Pd-on-charcoal in EtOH (5 mL) and HCl conc. (0.2 mL) under atmosphere of H₂ (balloon) at rt, 0.31 mmol of **49** (87 mg of **49a**, 100 mg of **49b**, 126 mg of **49c**) were added. After stirring under the same conditions for 2.5 hours (the end of the reaction was checked by TLC, eluent: hexane/ethyl acetate 7:3), the hydrogen atmosphere was replaced by a argon atmosphere and then the mixture was filtered through a fluted filter paper washing the catalyst several times with EtOH (total volume 100 mL). The filtrate was concentrated under reduced pressure and 20 mL of saturated NaHCO₃ solution were added to the residue and extracted three times with ethyl ether. The ethereal solution was washed with brine, dried over sodium sulfate, and filtered. The solvent removal under reduced pressure afforded **50a** (80 mg, 97%), **50b** (91.5 mg, 96%) and **50c** (112 mg, 92%) sufficiently pure for the following reaction.

¹H NMR 300 MHz (CDCl₃) **50a**: δ 1.08 (3H, t, $J = 7.5$ Hz, -CH₂CH₃); 1.34 (9H, s, -C(CH₃)₃); 2.58 (2H, q, $J = 7.5$ Hz, -CH₂CH₃); 3.74 (3H, s, -OCH₃); 3.78 (3H, s, -OCH₃); 6.67 (1H, d, $J = 9.0$ Hz, H-5); 6.73 (1H, d, $J = 9.0$ Hz, H-4); 6.87 (1H, bs, NH).

¹H NMR 200 MHz (CDCl₃) **50b**: δ 0.87 (3H, t, $J = 7.5$ Hz, -(CH₂)₄CH₃); 1.18 - 1.49 (15H, s, -CH₂(CH₂)₃CH₃ and -C(CH₃)₃); 2.54 (2H, m, -CH₂(CH₂)₃CH₃); 3.74 (3H, s, -OCH₃); 3.76 (3H, s, -OCH₃); 6.68 (1H, d, $J = 9.0$ Hz, H-5); 6.74 (1H, d, $J = 9.0$ Hz, H-4); 6.87 (1H, bs, NH).

¹H NMR 300 MHz (CDCl₃) **50c**: δ 0.88 (3H, t, $J = 7.5$ Hz, -(CH₂)₁₀CH₃); 1.25 - 1.45 (27H, s, -CH₂(CH₂)₉CH₃ and -C(CH₃)₃); 2.54 (2H, m, -CH₂(CH₂)₉CH₃); 3.74 (3H, s, -OCH₃); 3.77 (3H, s, -OCH₃); 6.68 (1H, d, $J = 8.7$ Hz, H-5); 6.73 (1H, d, $J = 8.7$ Hz, H-4); 6.86 (1H, bs, NH).

Synthesis of compounds 51 a-c: 0.91 mmol of **50** (240 mg of **50a**, 280 mg of **50b**, 356 mg of **50c**) dissolved in 50 mL of acetonitrile were added dropwise to a solution of CAN (1.5 g, 2.72 mmol) in water (16 mL) at rt. The mixture was stirred for 5 minutes at room temperature (the end of the reaction was checked by TLC, eluent: chloroform/ethyl acetate 7:3). The orange liquid was then poured into 100 mL of cold water and extracted three times with ethyl acetate. The combined organic layers were washed with brine, dried over sodium sulfate, and filtered. The solvent removal

under reduced pressure afforded **51a** (210 mg, 99%), **51b** (250 mg, 99%) and **51c** (326 mg, 99%) sufficiently pure for the following reaction.

¹H NMR 300 MHz (CDCl₃) **51a**: δ 1.07 (3H, t, *J* = 7.5 Hz, -CH₂CH₃); 1.32 (9H, s, -C(CH₃)₃); 2.47 (2H, q, *J* = 7.5 Hz, -CH₂CH₃); 6.73 (1H, d, *J* = 9.9 Hz, H-5); 6.77 (1H, d, *J* = 9.9 Hz, H-4); 7.66 (1H, bs, NH).

¹H NMR 400 MHz (CDCl₃) **51b**: δ 0.86 (3H, t, *J* = 7.0 Hz, -(CH₂)₄CH₃); 1.25 - 1.45 (15H, m, -CH₂(CH₂)₃CH₃ and -C(CH₃)₃); 2.48 (2H, m, -CH₂(CH₂)₃CH₃); 6.73 (1H, d, *J* = 9.9 Hz, H-5); 6.76 (1H, d, *J* = 9.9 Hz, H-4); 7.62 (1H, bs, NH).

¹H NMR 300 MHz (CDCl₃) **51c**: δ 0.86 (3H, t, *J* = 6.6 Hz, -(CH₂)₁₀CH₃); 1.15 - 1.42 (27H, m, -CH₂(CH₂)₉CH₃ and -C(CH₃)₃); 2.47 (2H, m, -CH₂(CH₂)₉CH₃); 6.72 (1H, d, *J* = 9.9 Hz, H-5); 6.76 (1H, d, *J* = 9.9 Hz, H-4); 7.62 (1H, bs, NH).

Synthesis of compounds 52 a-c and 53a-c: 0.53 mmol of quinone **51** (125 mg of **51a**, 147 mg of **51b**, 192 mg of **51c**) were dissolved in 7 mL of a mixture of EtOH/CH₃CN 1:1 and heated in a water bath under stirring; then, a solution of hypotaurine (173 mg, 1.59 mmol) in 8 mL of water was added in portions. The mixture was stirred for 5 minutes at room temperature (the end of the reaction was checked by TLC, eluent: ethyl acetate/hexane 10:3). The yellow solution became orange/red. Most of the ethanol was removed in vacuo and the residue was poured into water. The mixture was extracted with ethyl acetate (three times) and the organic phase was washed with brine, dried over sodium sulfate, and filtered. The solvent removal under reduced pressure afforded a crude mixture of the isomers **52** and **53** (157 mg of **52a/53a**, 159 mg of **52b/53b**, 270 mg of **52c/53c**) which were separated by chromatography on 'acidic' silica gel previously treated with 5% w/w of water (SiO₂/crude 50:1; eluent: ethyl acetate/hexane 5:1) to give pure **52a** (14.5 mg, 8%), **52b** (3.9 mg, 2%), **52c** (8.9 mg, 3.6 %), **53a** (28 mg, 15.5 %), **53b** (8.1 mg, 4%) and **53c** (27 mg, 11%).

¹H NMR 300 MHz (C₃D₆O) **52a**: δ 1.01 (3H, t, *J* = 7.4 Hz, -CH₂CH₃); 1.30 (9H, s, -C(CH₃)₃); 2.39 (2H, q, *J* = 7.4 Hz, -CH₂CH₃); 3.31 (2H, m, -CH₂ NH-); 4.07 (2H, m, -CH₂ SO₂-); 8.40 (1H, bs, -NHCO-).

^{13}C NMR 300 MHz ($\text{C}_3\text{D}_6\text{O}$) **52a**: δ 181.53 (C8'); 176.78 (C5'); 174.44 (C1); 146.82 (C4a'); 139.21 (C7'); 133.86 (C8a'); 109.04 (C6'); 49.54 (C2'); 40.95 (C3'); 40.92 (C2); 27.55 (3C3); 21.20 (C1''); 11.83 (C2'').

^1H NMR 300 MHz (CD_3OD) **53a**: δ 1.04 (3H, t, $J = 7.5$ Hz, $-\text{CH}_2\text{CH}_3$); 1.28 (9H, s, $-\text{C}(\text{CH}_3)_3$); 2.46 (2H, q, $J = 7.5$ Hz, $-\text{CH}_2\text{CH}_3$); 3.35 (2H, m, $-\text{CH}_2\text{NH}-$); 3.95 (2H, m, $-\text{CH}_2\text{SO}_2-$).

^{13}C NMR 300 MHz (CD_3OD) **53a**: δ 181.23 (C8'); 178.29 (C5'); 177.34 (C1); 150.40 (C4a'); 146.70 (C6'); 136 (C8a'); 109.09 (C7'); 49.55 (C2'); 40.95 (C3'); 40.88 (C2); 28.05 (3C3); 21.30 (C1''); 13.19 (C2'').

^1H NMR 400 MHz (CD_3OD) **53b**: δ 0.89 (3H, m, $-(\text{CH}_2)_4\text{CH}_3$); 1.23 – 1.48 (15H, m, $-\text{CH}_2(\text{CH}_2)_3\text{CH}_3$ and $-\text{C}(\text{CH}_3)_3$); 2.45 (2H, m, $-\text{CH}_2(\text{CH}_2)_3\text{CH}_3$); 3.36 (2H, m, $-\text{CH}_2\text{NH}-$); 3.96 (2H, m, $-\text{CH}_2\text{SO}_2-$).

^{13}C NMR 400 MHz (CD_3OD) **53b**: δ 181.12 (C8'); 178.47 (C5'); 177.09 (C1); 149.44 (C4a'); 146.71 (C6'); 137.04 (C8a'); 110.57 (C7'); 49.73 (C2'); 40.74 (C3'); 40.28 (C2); 33.21 (C1''); 29.30 (C2'' or C3'' or C4''); 27.72 (3C3); 26.95 (C2'' or C3'' or C4''); 23.42 (C2'' or C3'' or C4''); 14.22 (C5'').

References

1. Santamaria, R.; Fiorito, F.; Irace, C.; De Martino, L.; Maffettone, C.; Granato, G. E.; Di Pascale, A.; Iovane, V.; Pagnini, U.; Colonna, A. *Biochim. Biophys. Acta* **2011**, *1813*, 704-712.
2. Maffettone, C.; De Martino, L.; Irace, C.; Santamaria, R.; Pagnini, U.; Iovane, G.; Colonna, A. *J. Cell. Biochem.* **2008**, *104*, 213-223.
3. Ferrante, M. C.; Mattace Raso, G.; Esposito, E.; Bianco, G.; Iacono, A.; Clausi, M.T.; Amero, P.; Santoro, A.; Simeoli, R.; Autore, G.; Meli, R. *Toxicol. Lett.* **2011**, *202*, 61–68.
4. Meli, R.; Mattace Raso, G.; Cicala, C.; Esposito, E.; Fiorino, F.; Cirino, G. *J. Neurochem* **2001**, *79*, 556–563.
5. Mosmann, T. *J. Immunol. Methods* **1983**, *65*, 55–63.

CHAPTER 5

SUPPORTING DATA

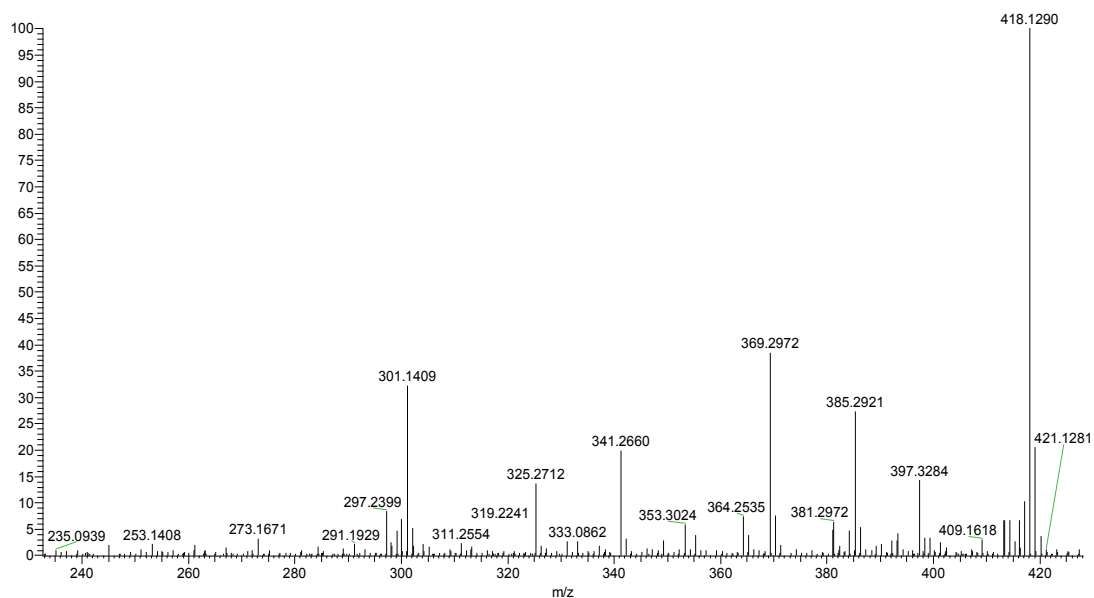
5.1. *General methods*

This paragraph describes the chromatographic and spectroscopic methods employed for the execution of the research. This techniques have been applied for all the projects.

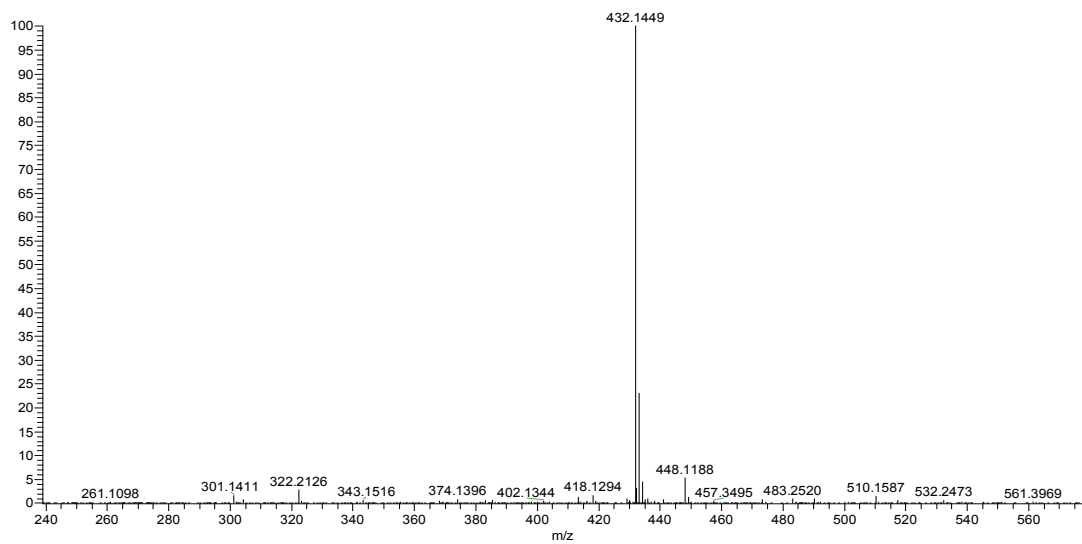
Low and high resolution ESI-MS spectra were performed on a LTQ Orbitrap XL (Thermo Scientific) mass spectrometer. Optical rotations (CHCl₃) were measured at 589 nm on a Jasco P-2000 polarimeter using a 10 cm microcell. UV spectra were measured on a Thermo Scientific (mod. Nanodrop 2000c) instrument. CD spectra were registered on a Jasco J-710 spectropolarimeter (Jasco, Tokyo, Japan) with J-710 for Windows software (Jasco). ¹H (700 and 500 MHz) and ¹³C (175 and 125 MHz) NMR spectra were measured on Varian Unity Inova spectrometers. Chemical shifts were referenced to the residual solvent signal (C₅D₅N: δ_{H} 8.71, 7.55, 7.19, δ_{C} 149.9, 135.5, 123.5; CDCl₃: δ_{H} 7.26, δ_{C} 77.0; C₆D₆: δ_{H} 7.15, δ_{C} 128.0; CD₃OD: δ_{H} 3.31, δ_{C} 49.0; *d*6-DMSO: δ_{H} 2.50, δ_{C} 39.0). ¹H connectivities were determined by homonuclear COSY experiment. Through-space ¹H connectivities were evidenced using a ROESY experiment with a mixing time of 500 ms. One-bond heteronuclear ¹H-¹³C connectivities was determined by the HSQC experiment; two- and three-bond ¹H-¹³C connectivities by gradient 2D HMBC experiments optimized for a ^{2,3}*J* of 8 Hz. Medium pressure liquid chromatography was performed on a Büchi apparatus using a silica gel (230-400 mesh) column. HPLC were achieved on a Knauer and Shimazu apparatuses equipped with a refractive index detector and Synergy Polar-RP 4 μ (250 \times 4.6 mm), LUNA 5 μ (Phenomenex) SiO₂ or C18 (250 \times 4 mm), Luna 3 μ m RP-18 (150 \times 4.60 mm) and Synergi RP-MAX 4 μ m columns.

5.2. Mass spectra

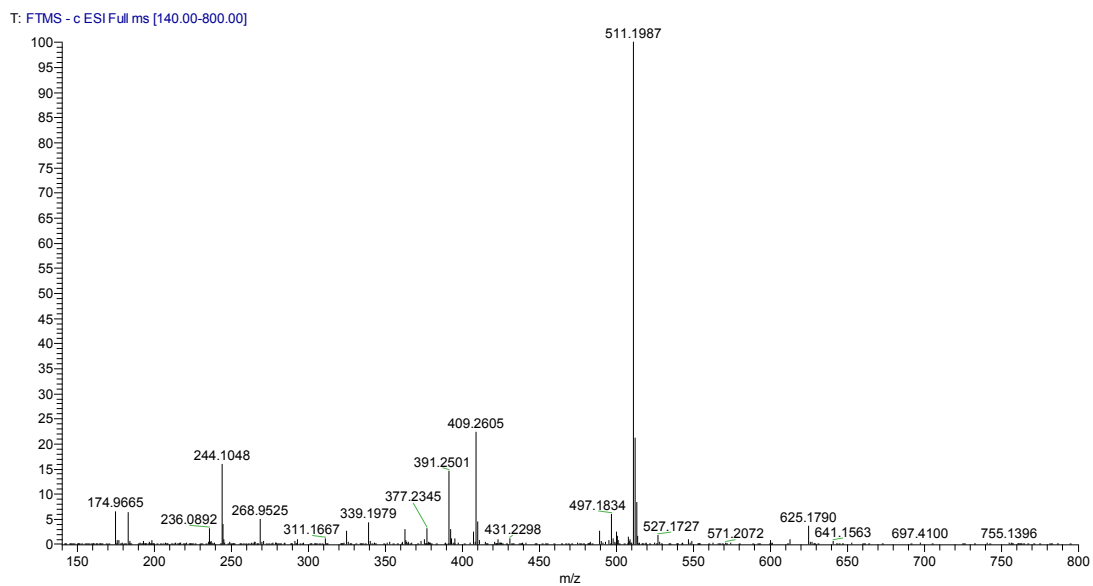
HRESI MS spectrum of conithiaquinone A (1)



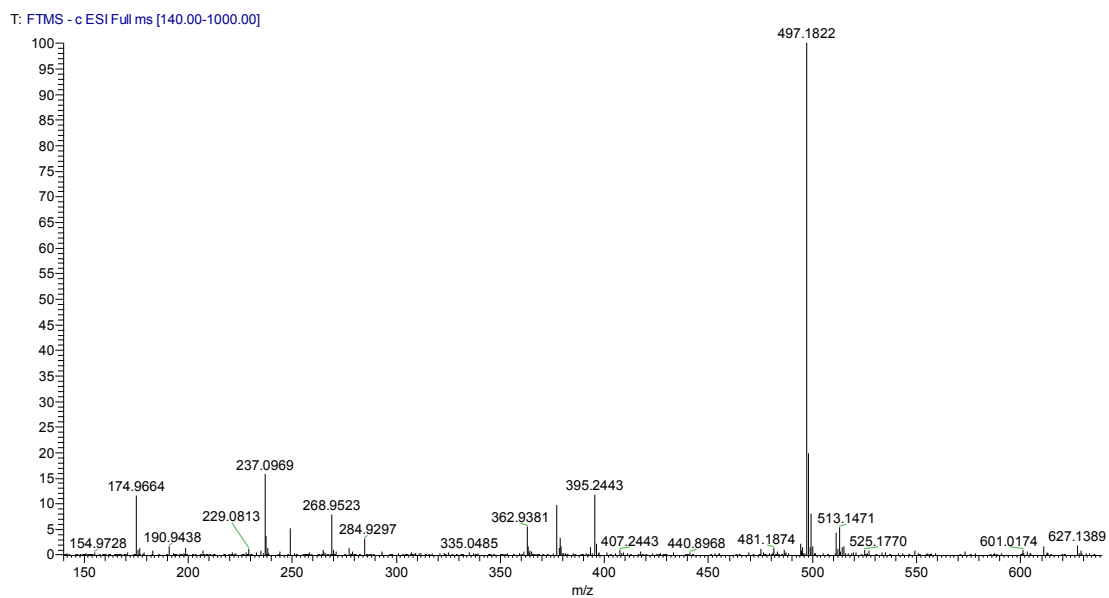
HRESI MS spectrum of conithiaquinone B (2)



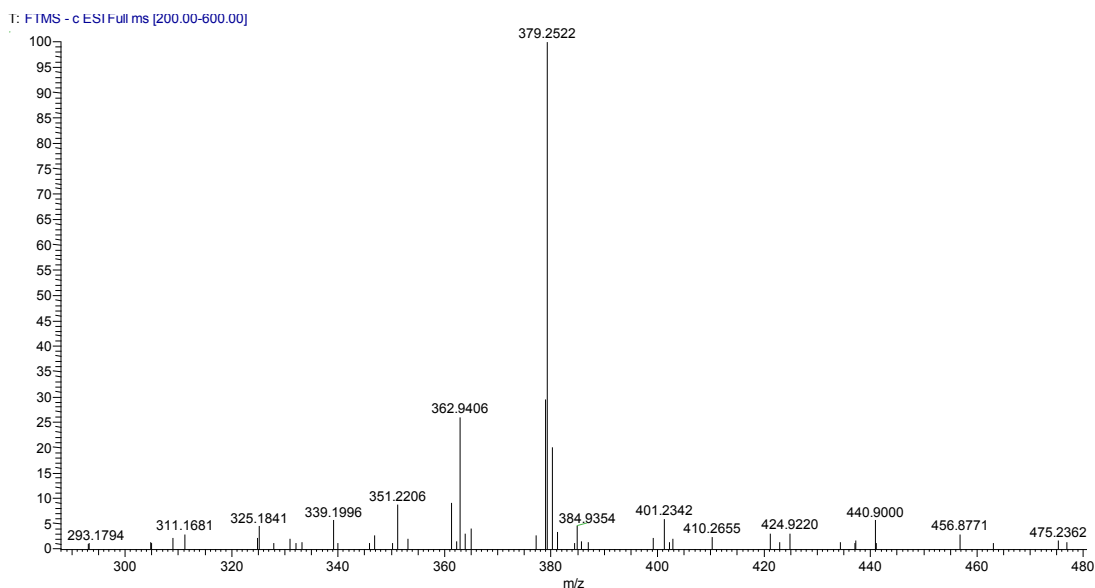
HRESI MS spectrum of compound 10



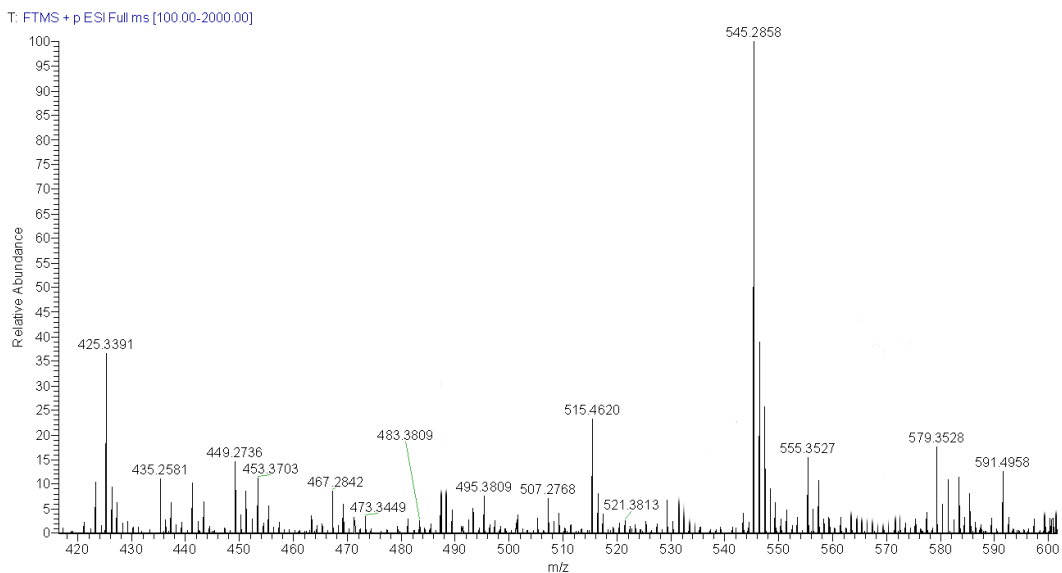
HRESI MS spectrum of compound 11



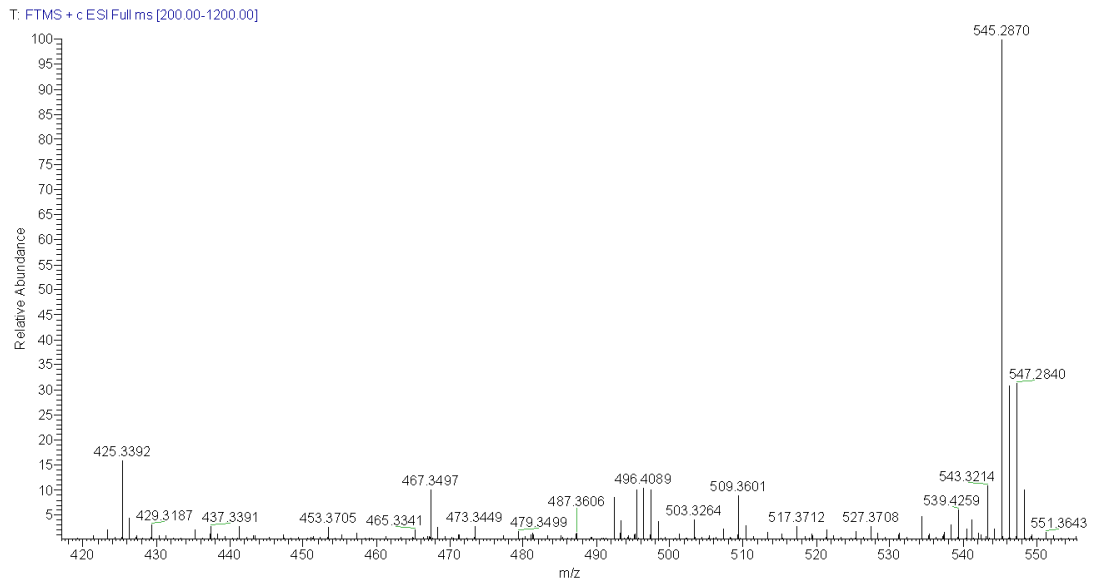
HRESI MS spectrum of compound 12



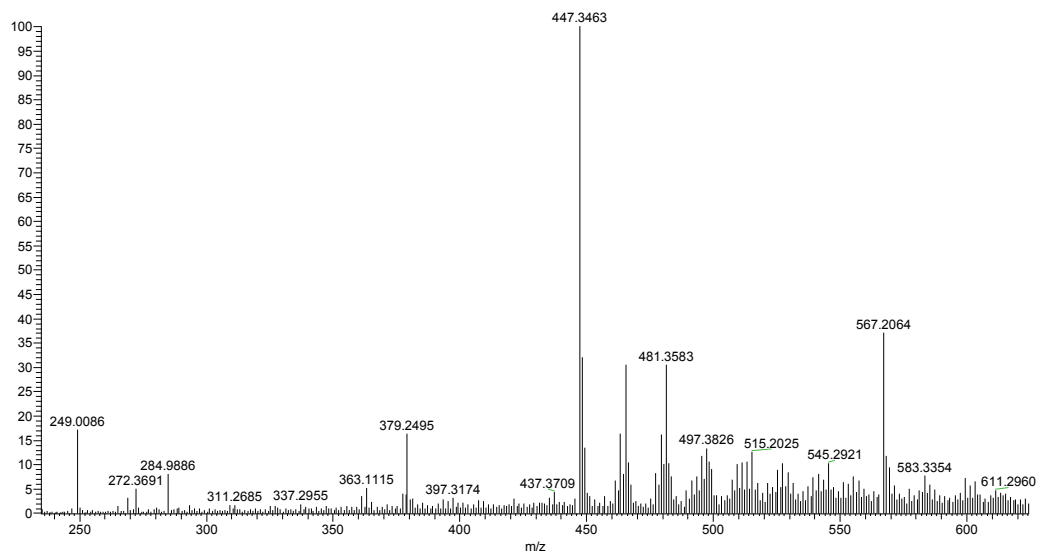
HRESI MS spectrum of phallusiasterol A (15)



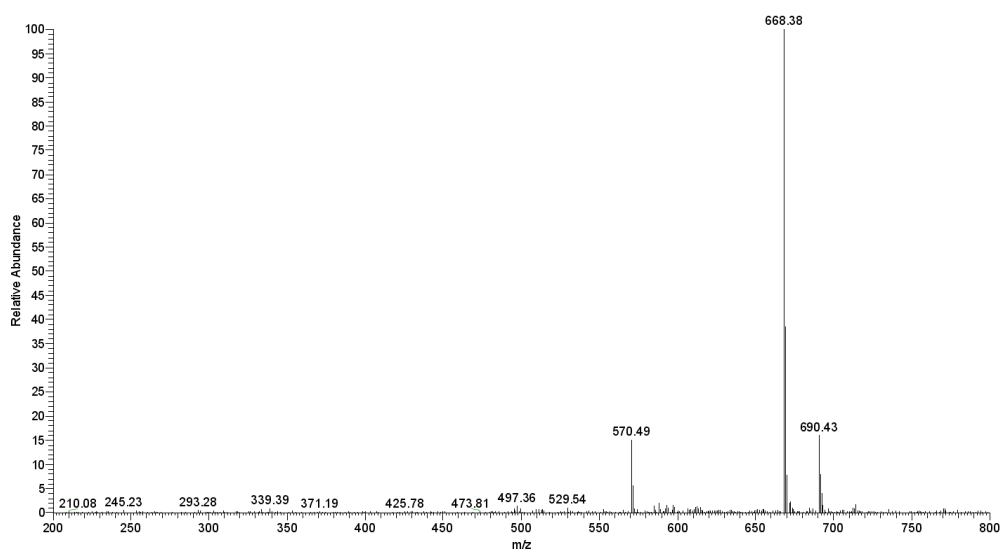
HRESI MS spectrum of phallusiasterol B (16)



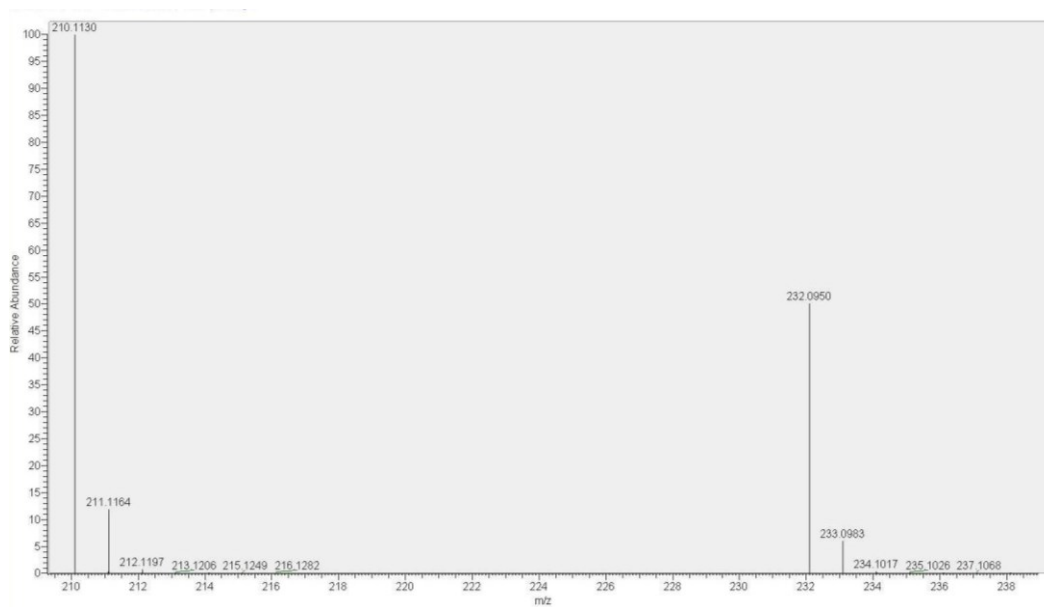
HRESI MS spectrum of phallusiasterol C (18)



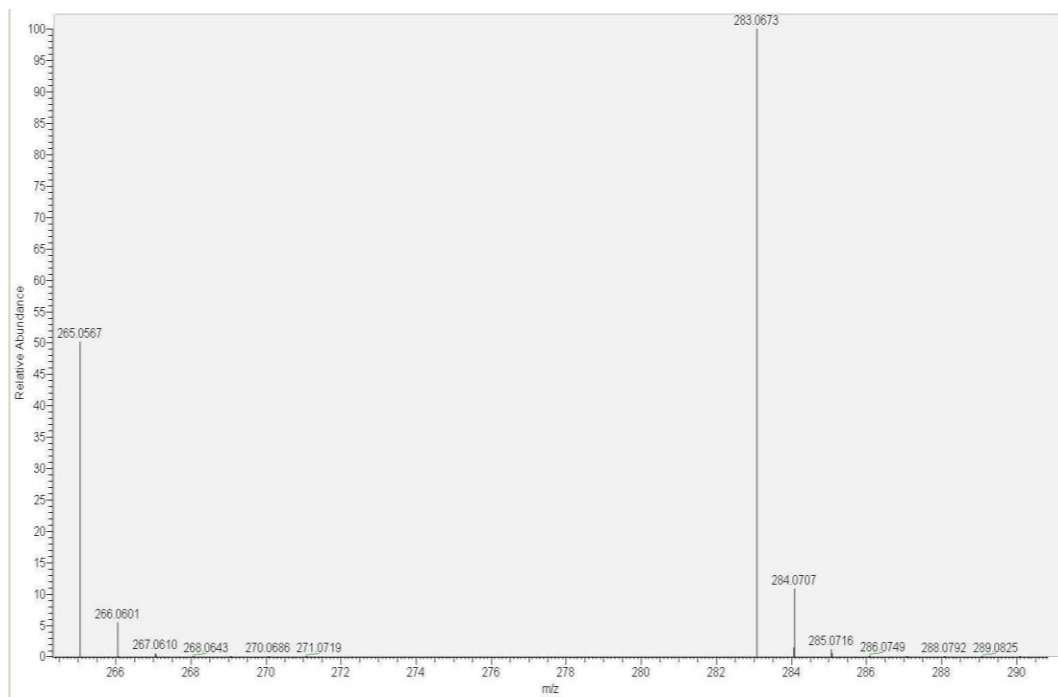
HRESI MS spectrum of phosphoeleganin (19)



HRESI MS spectrum of betaine (28)

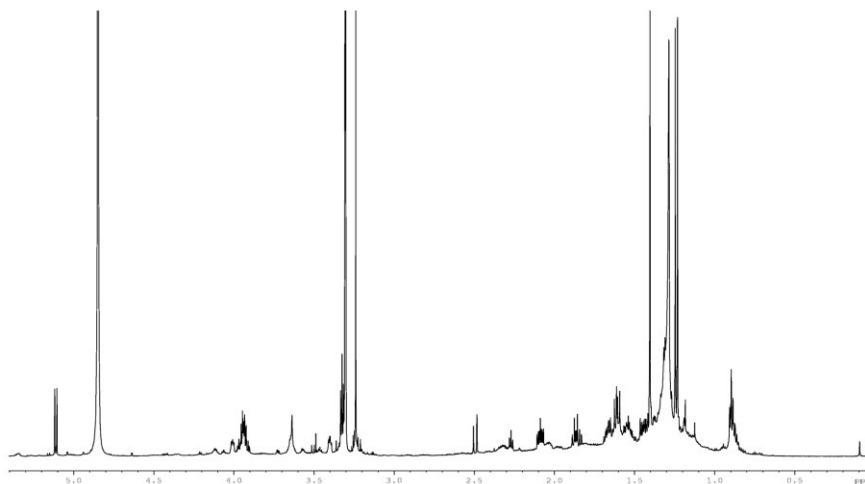


HRESI MS spectrum of cyclonucleoside (31)

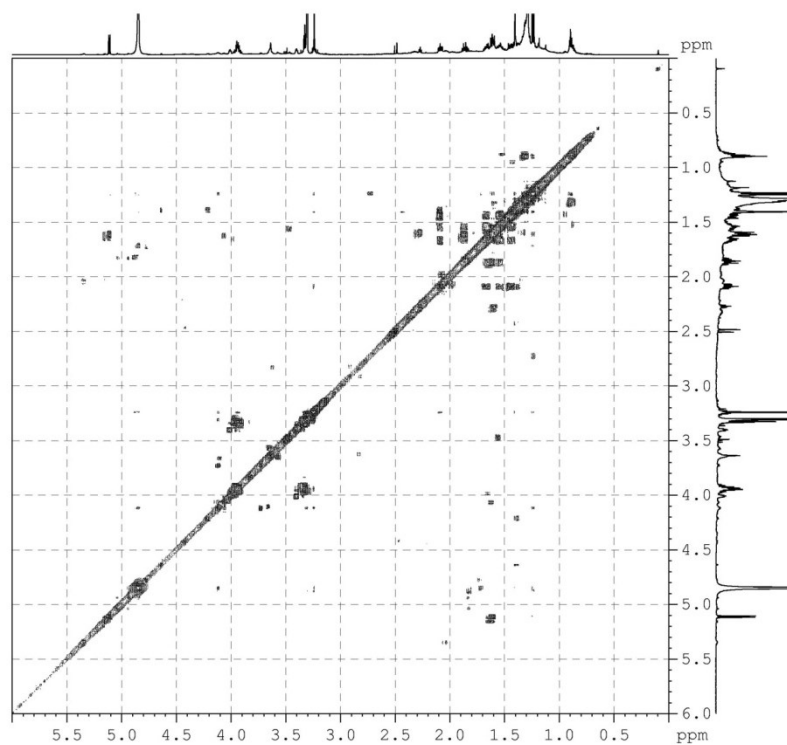


5.3. NMR spectra

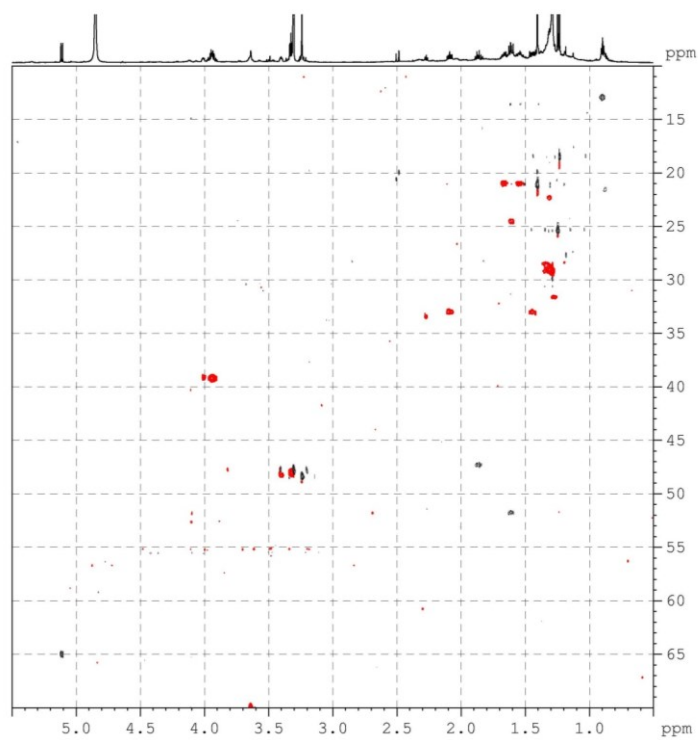
^1H NMR spectrum (700 MHz) of conithiaquinone A (**1**) in CD_3OD



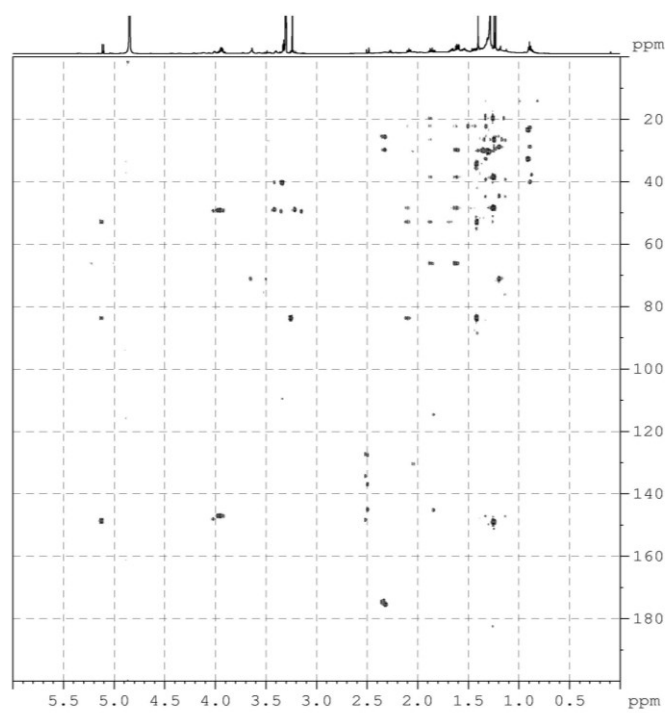
COSY 2D NMR spectrum (700 MHz) of conithiaquinone A (**1**) in CD_3OD



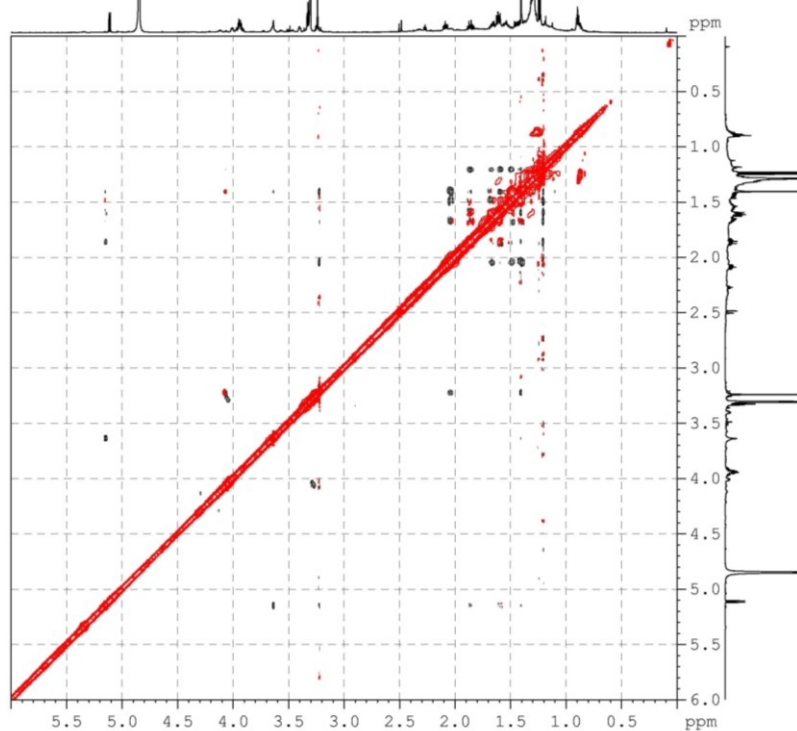
HSQC 2D NMR spectrum (700 MHz) of conithiaquinone A (**1**) in CD₃OD



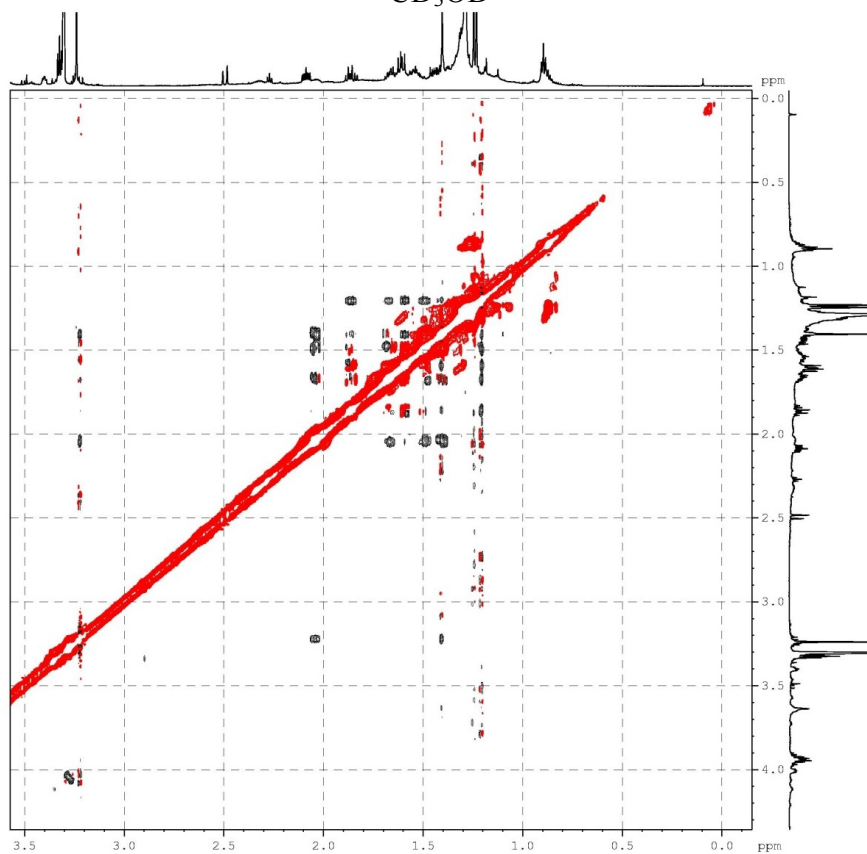
HMBC 2D NMR spectrum (700 MHz) of conithiaquinone A (**1**) in CD₃OD



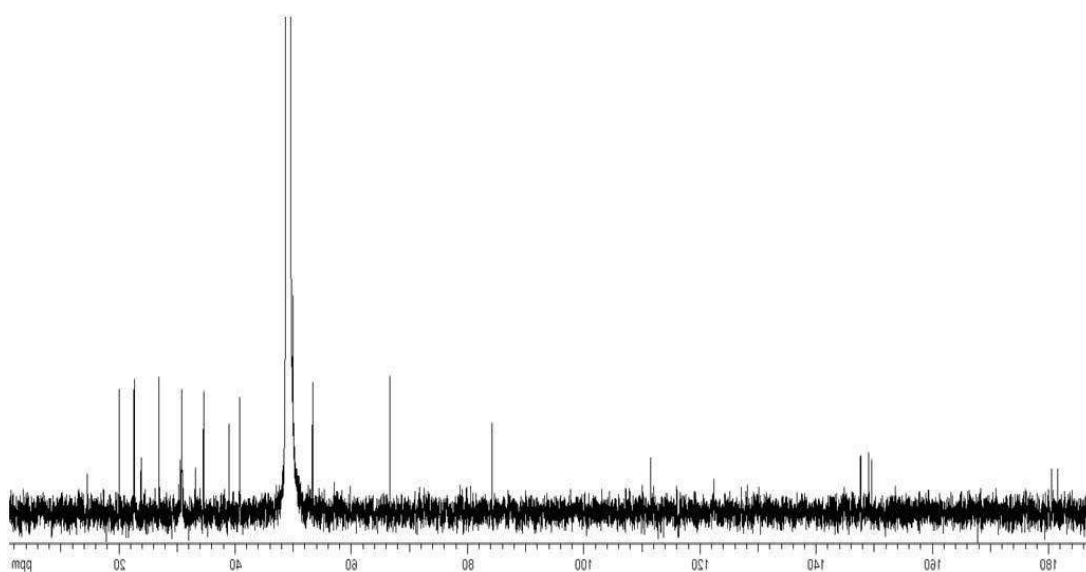
ROESY 2D NMR spectrum (700 MHz) of conithiaquinone A (**1**) in CD₃OD



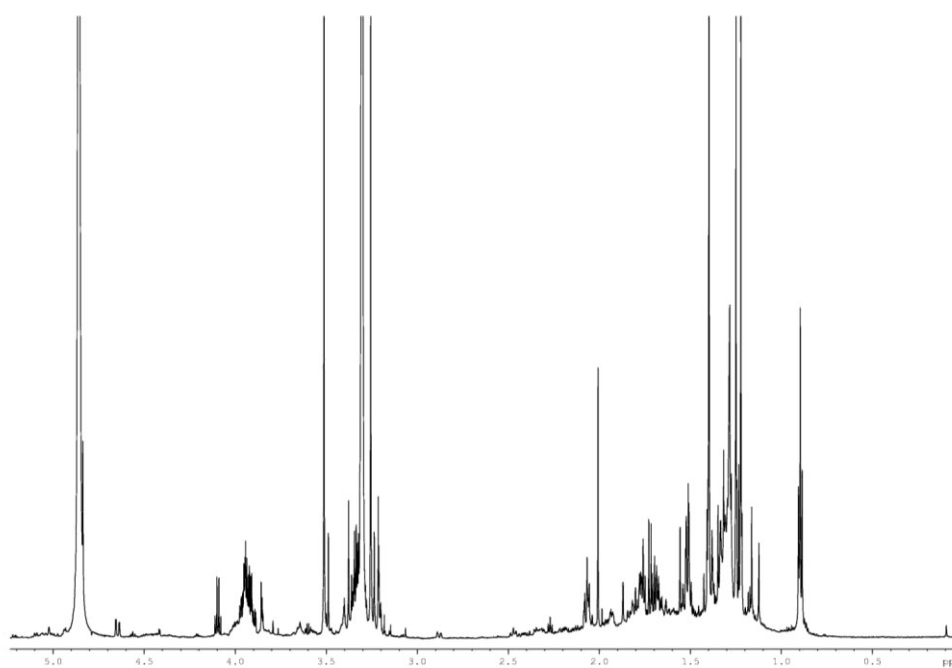
ROESY 2D NMR spectrum (700 MHz) enlargement of conithiaquinone A (**1**) in CD₃OD



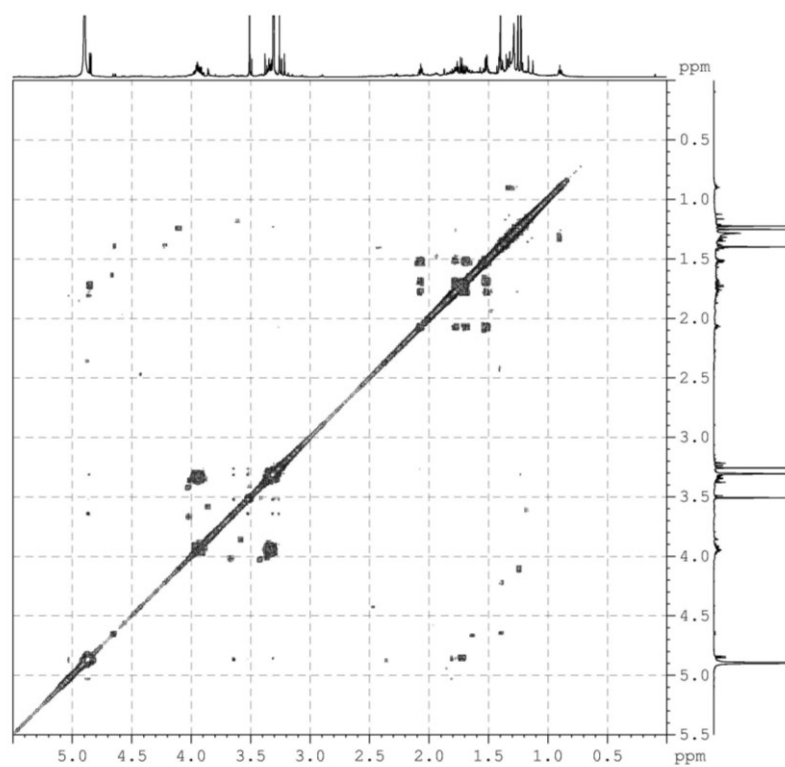
^{13}C NMR spectrum (125 MHz) of conithiaquinone A (**1**) in CD_3OD .



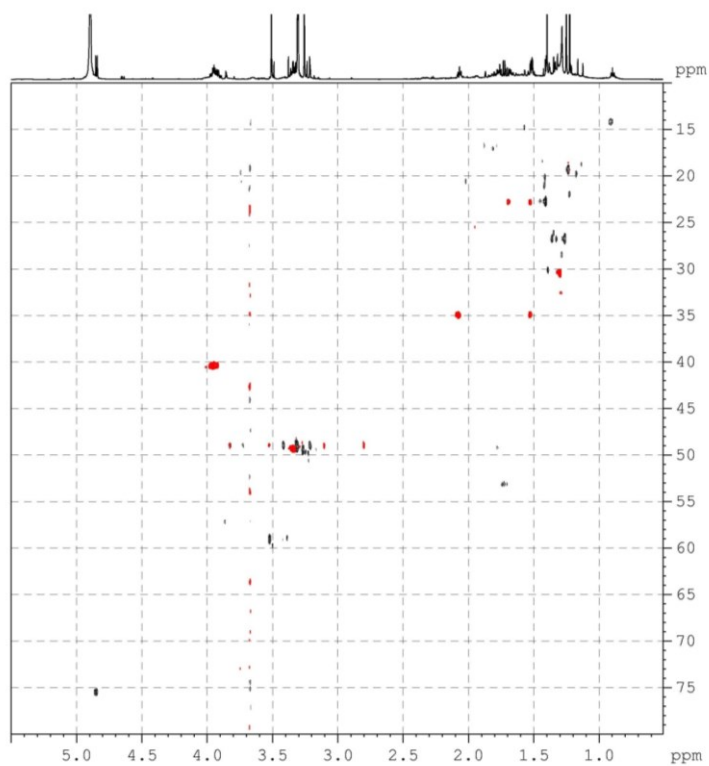
^1H NMR spectrum (700 MHz) of conithiaquinone B (**2**) in CD_3OD .



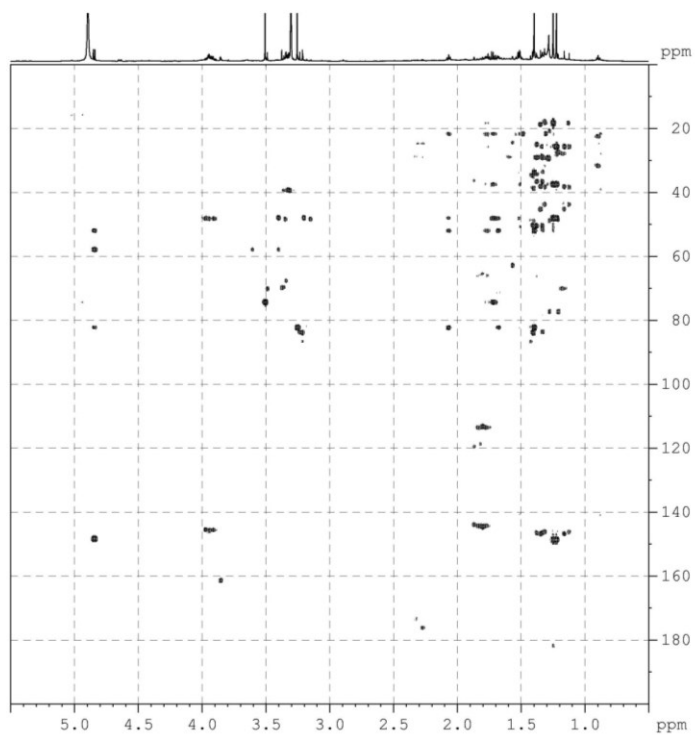
COSY 2D NMR spectrum (700 MHz) of conithiaquinone B (**2**) in CD₃OD



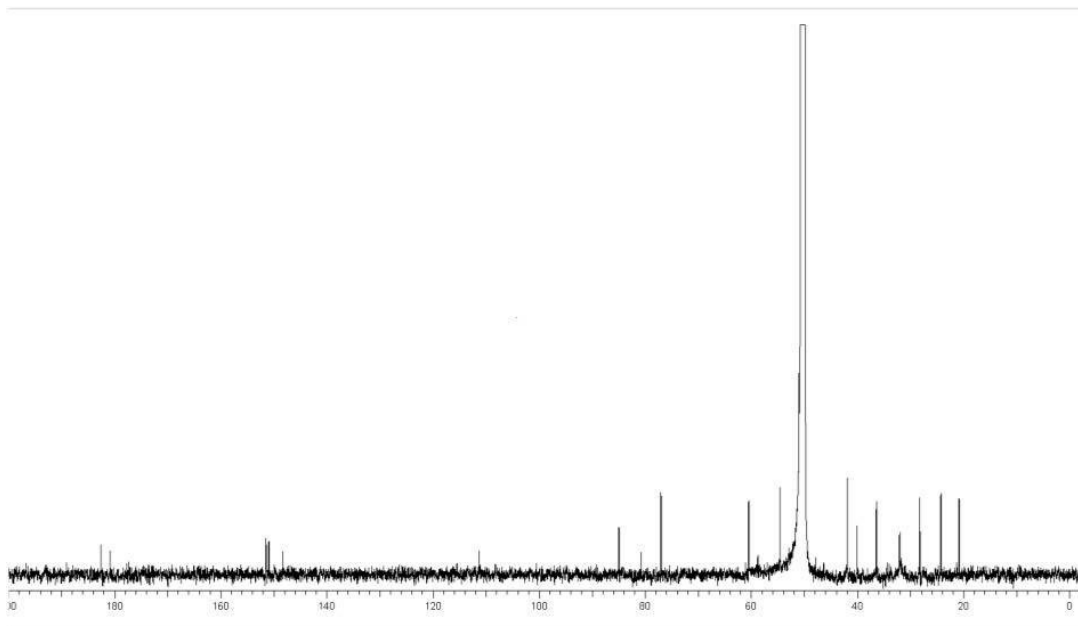
HSQC 2D NMR spectrum (700 MHz) of conithiaquinone B (**2**) in CD₃OD



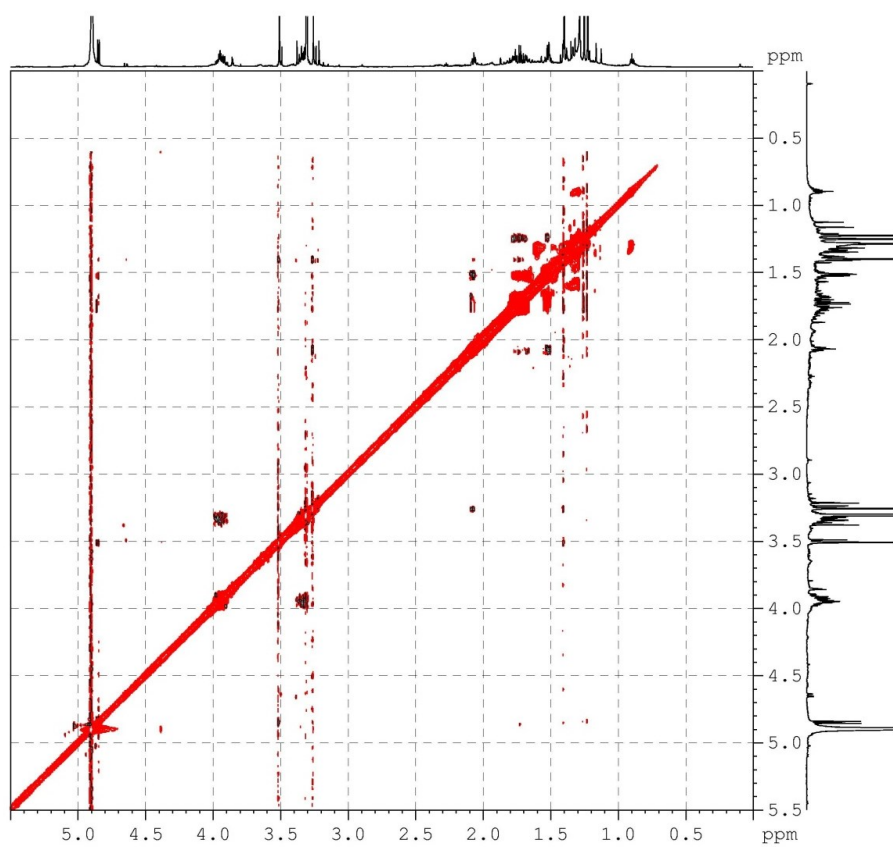
HMBC 2D NMR spectrum (700 MHz) of conithiaquinone B (**2**) in CD₃OD



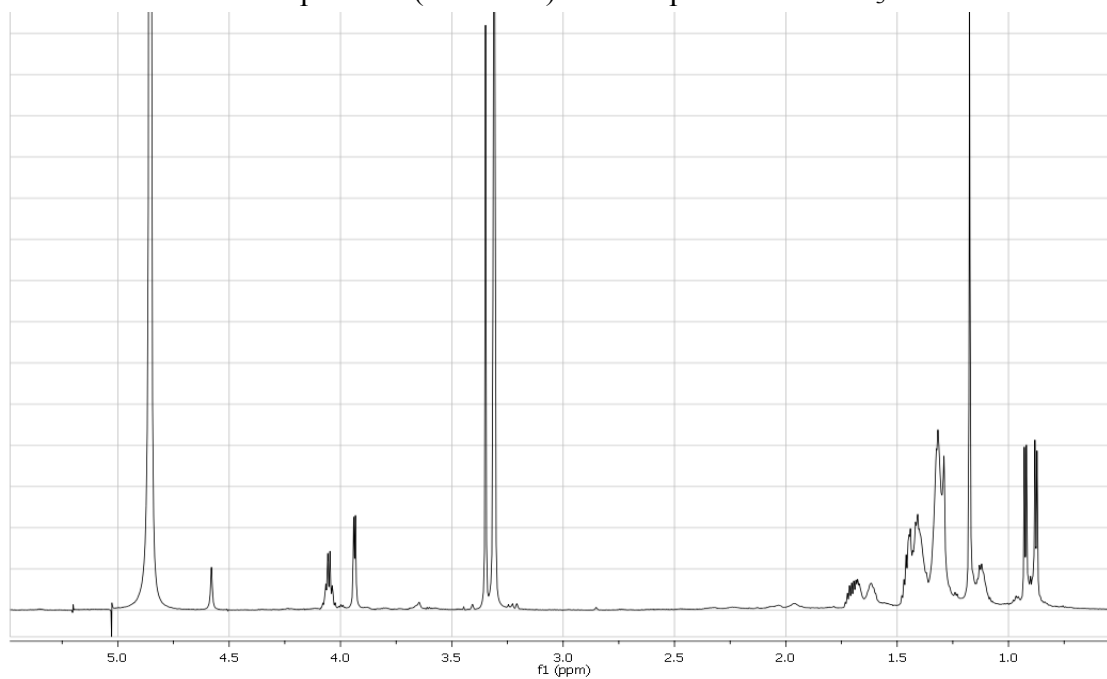
¹³C NMR spectrum (125 MHz) of conithiaquinone B (**2**) in CD₃OD



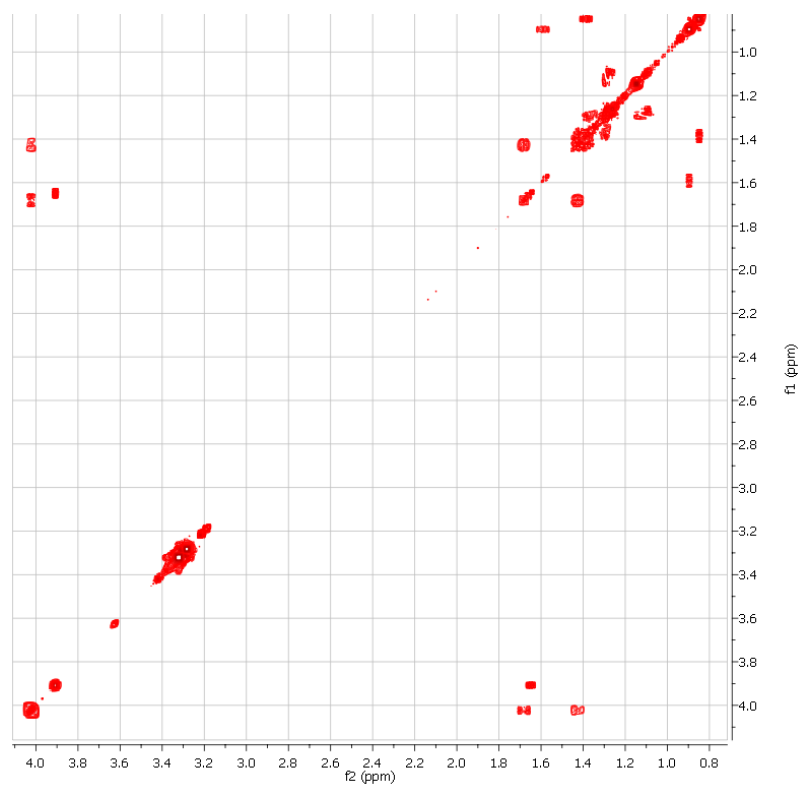
ROESY 2D NMR spectrum (700 MHz) of conithiaquinone B (**2**) in CD₃OD



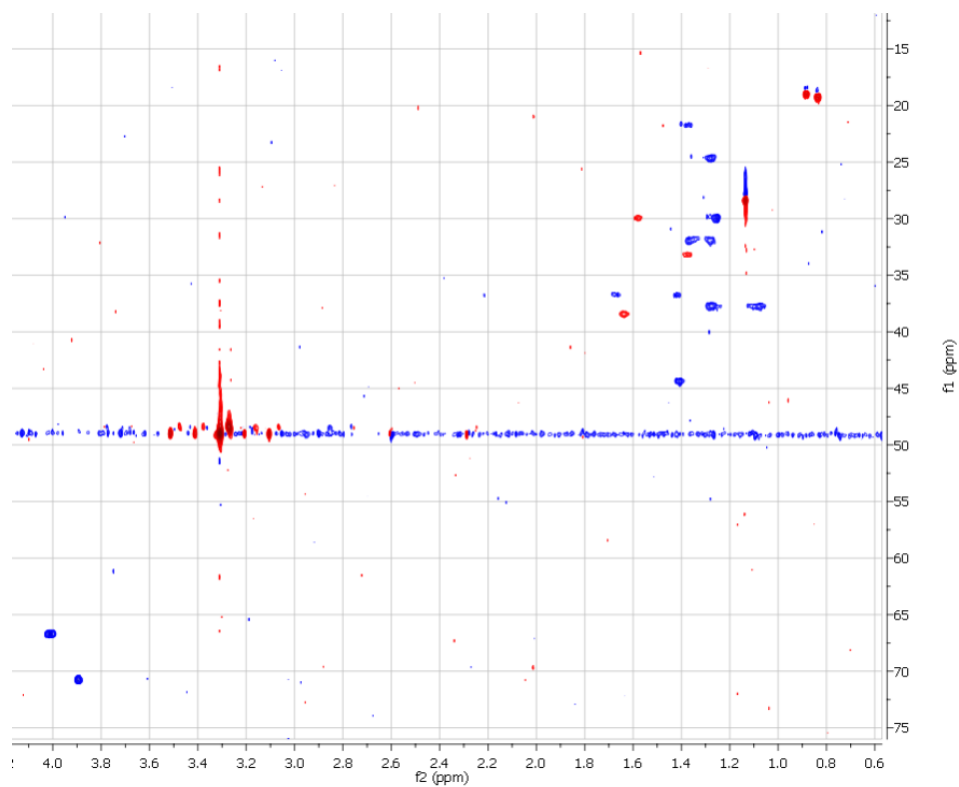
¹H NMR spectrum (500 MHz) of compound **10** in CD₃OD



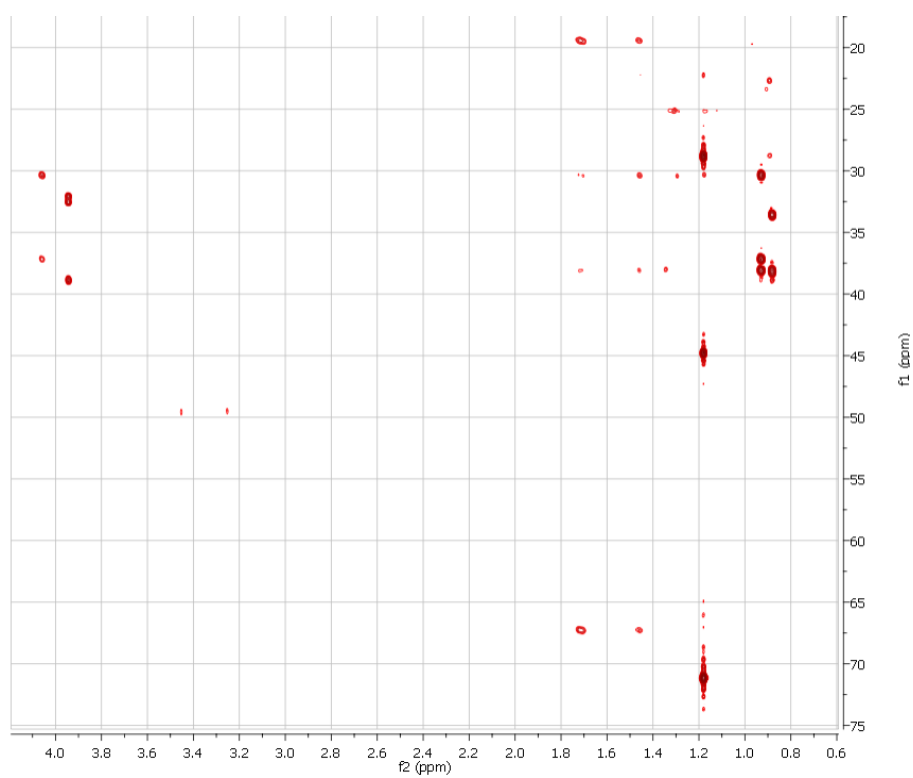
COSY 2D NMR spectrum (500 MHz) of compound **10** in CD₃OD



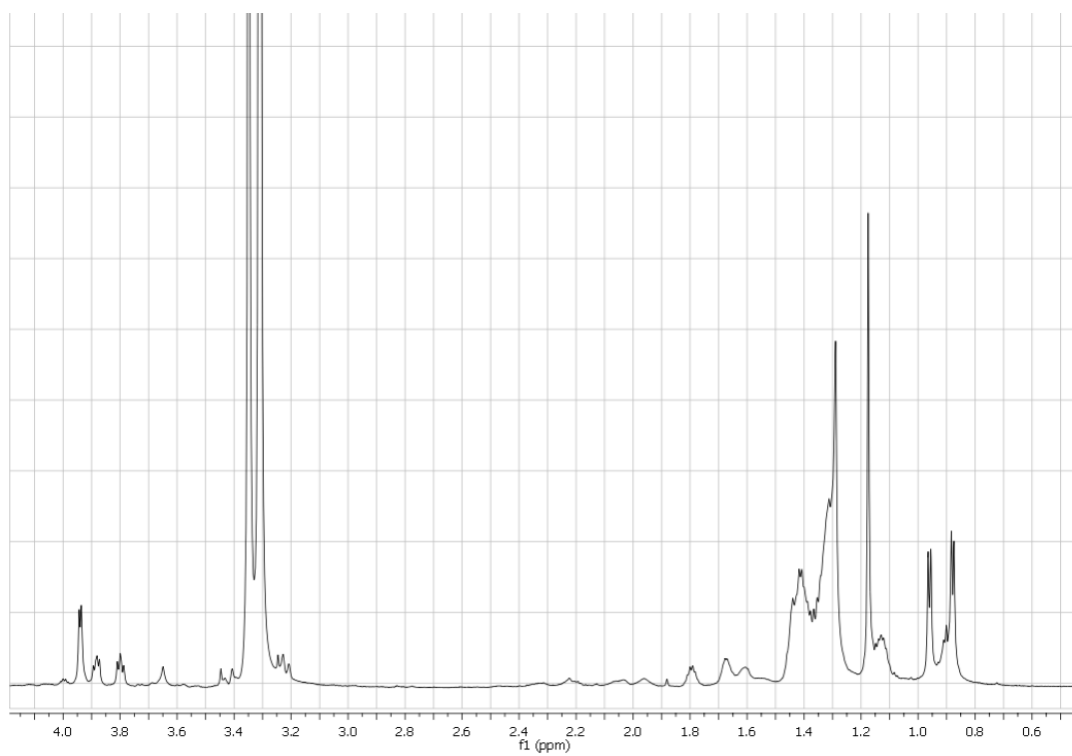
HSQC 2D NMR spectrum (500 MHz) of compound **10** in CD₃OD



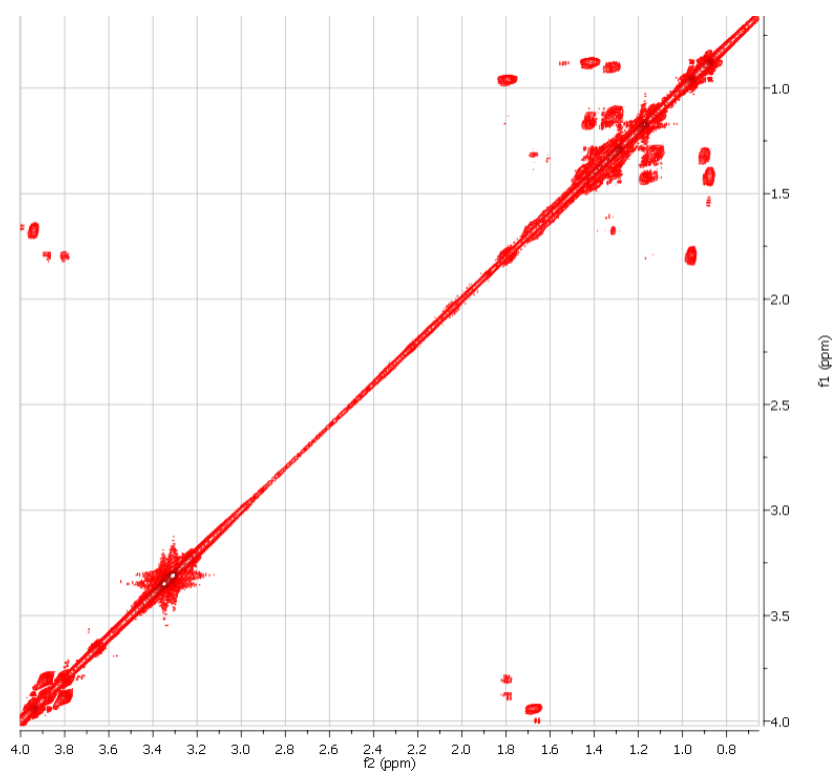
HMBC 2D NMR spectrum (500 MHz) of compound **10** in CD₃OD



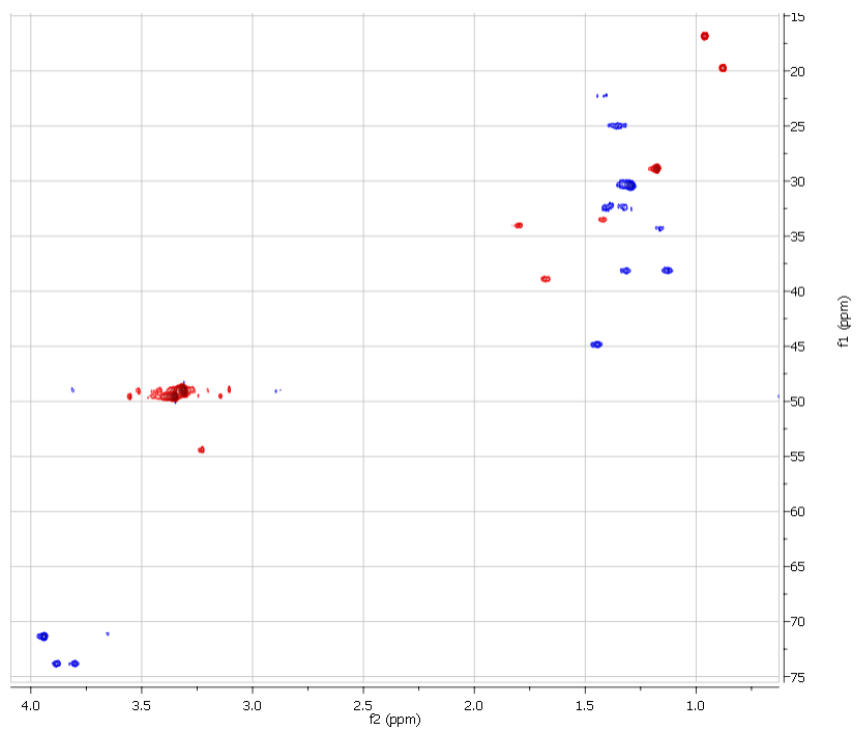
¹H NMR spectrum (500 MHz) of compound **11** in CD₃OD



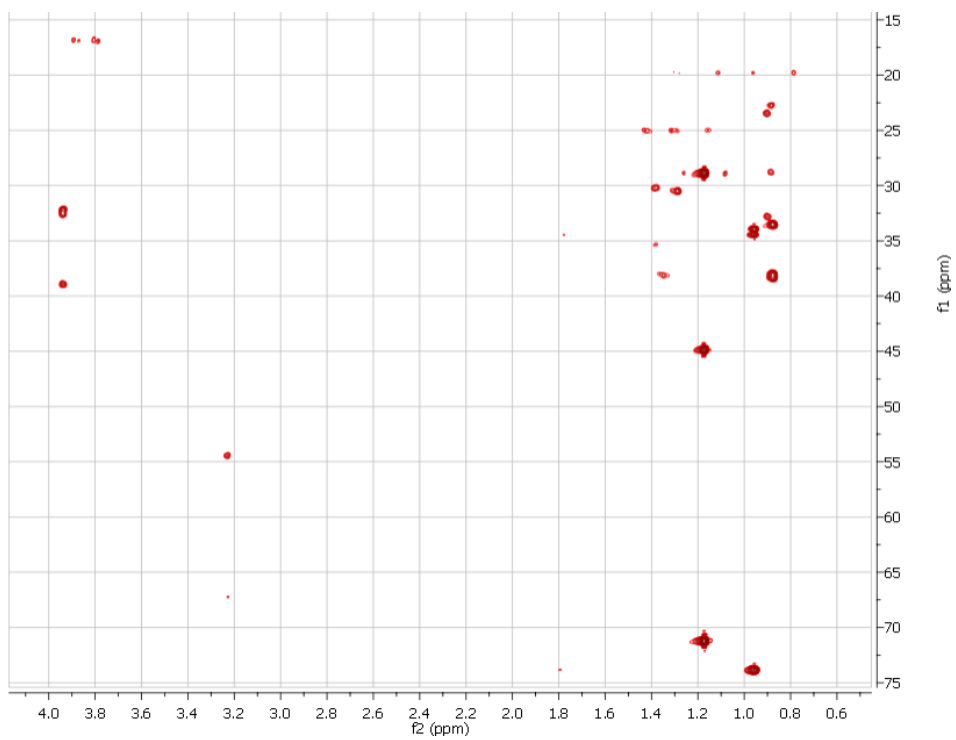
COSY 2D NMR spectrum (500 MHz) of compound **11** in CD₃OD



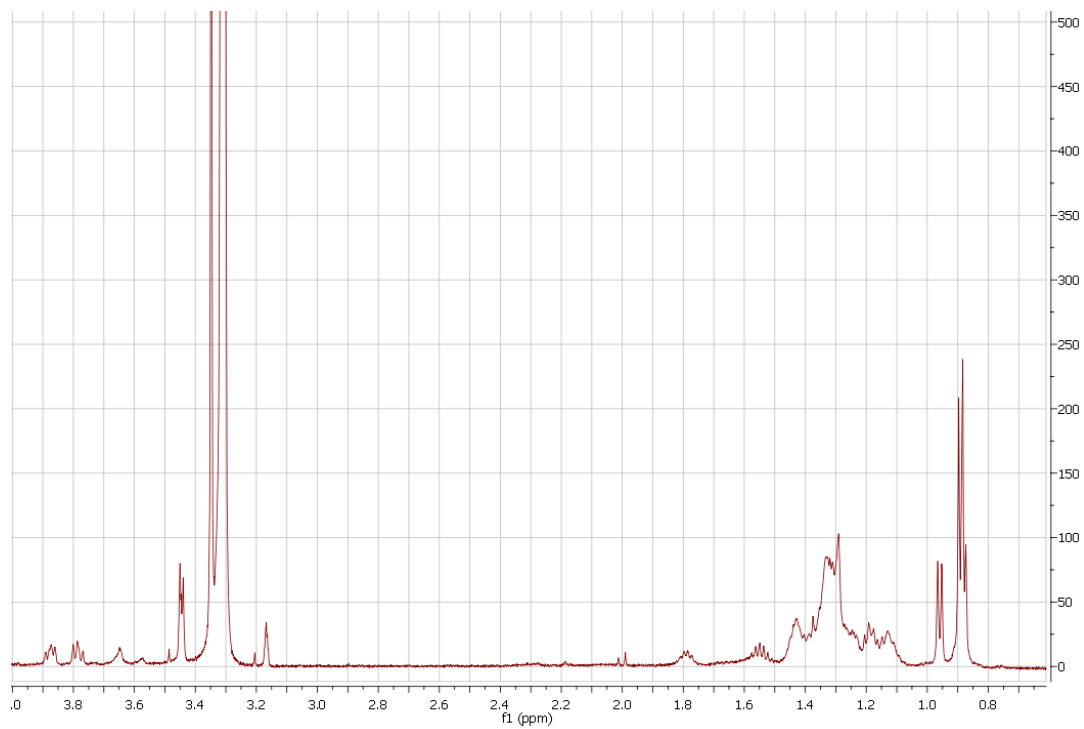
HSQC 2D NMR spectrum (500 MHz) of compound **11** in CD₃OD



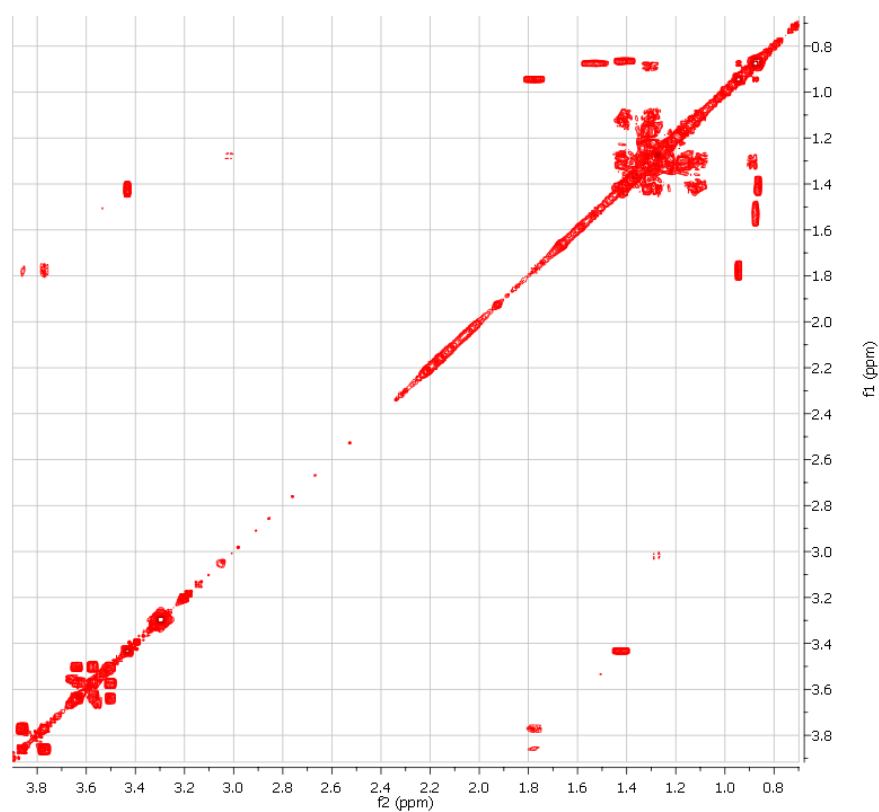
HMBC 2D NMR spectrum (500 MHz) of compound **11** in CD₃OD



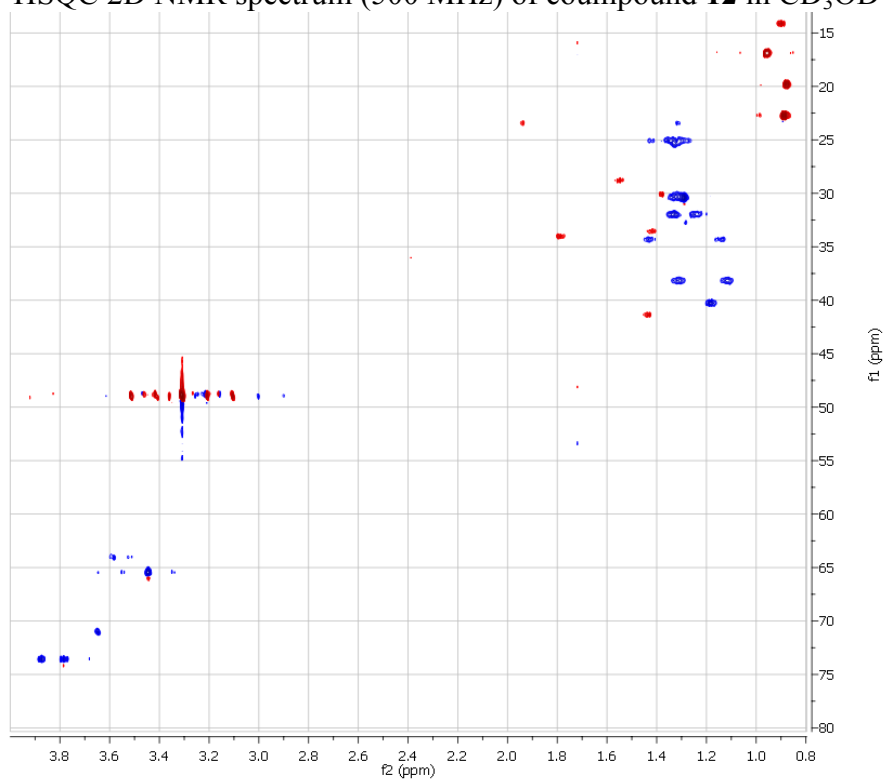
¹H NMR spectrum (500 MHz) of compound **12** in CD₃OD



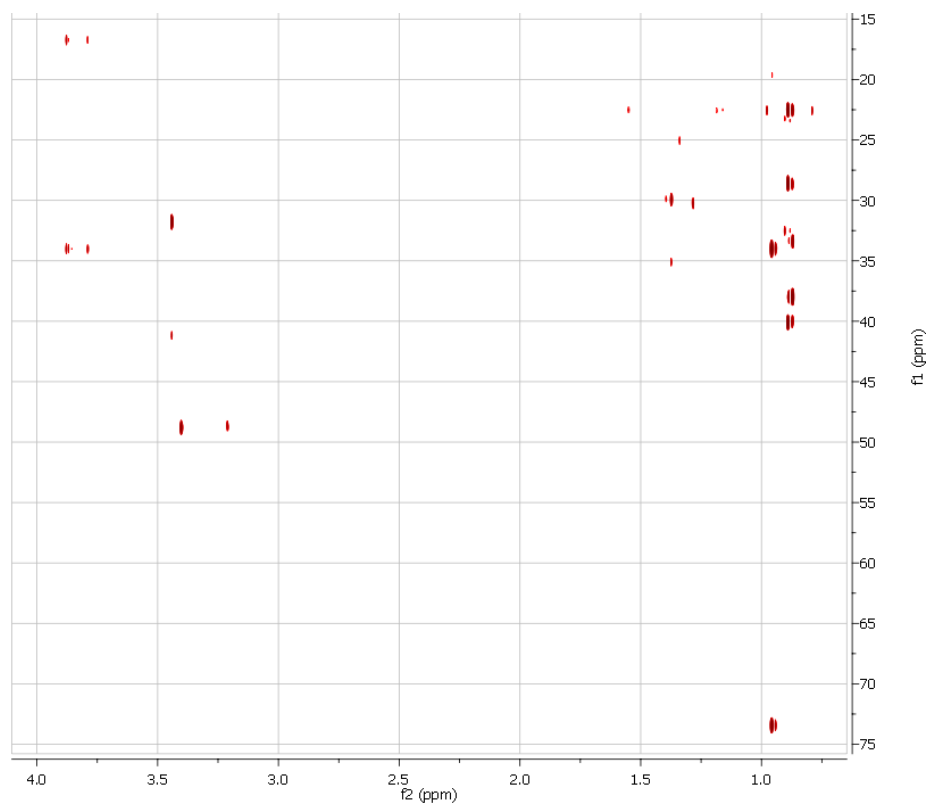
COSY 2D NMR spectrum (500 MHz) of compound **12** in CD₃OD



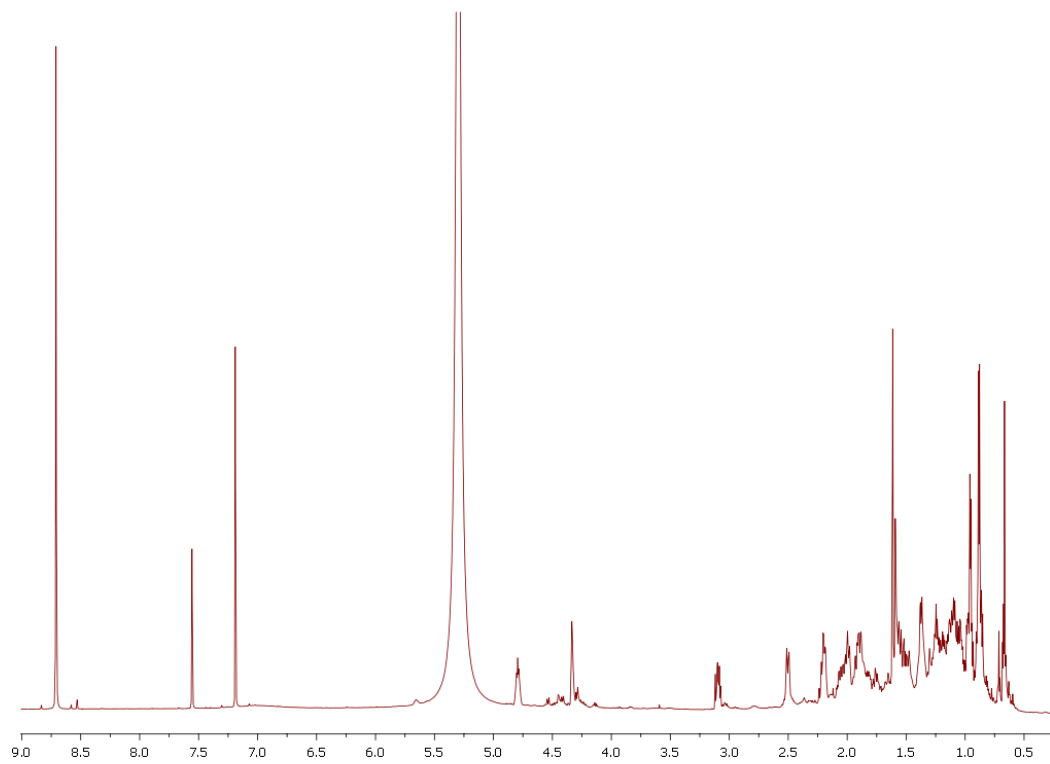
HSQC 2D NMR spectrum (500 MHz) of compound **12** in CD₃OD



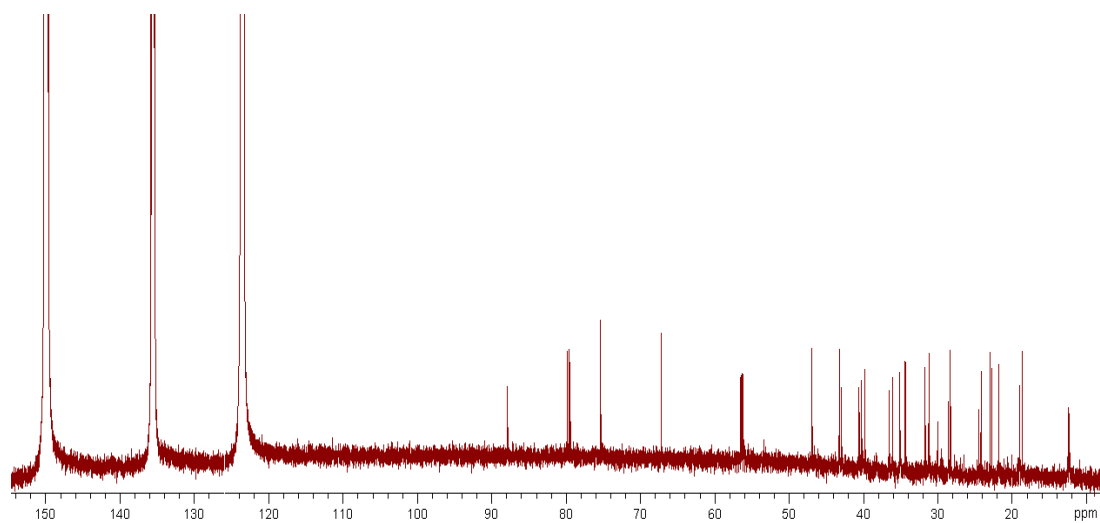
HMBC 2D NMR spectrum (500 MHz) of compound **12** in CD₃OD



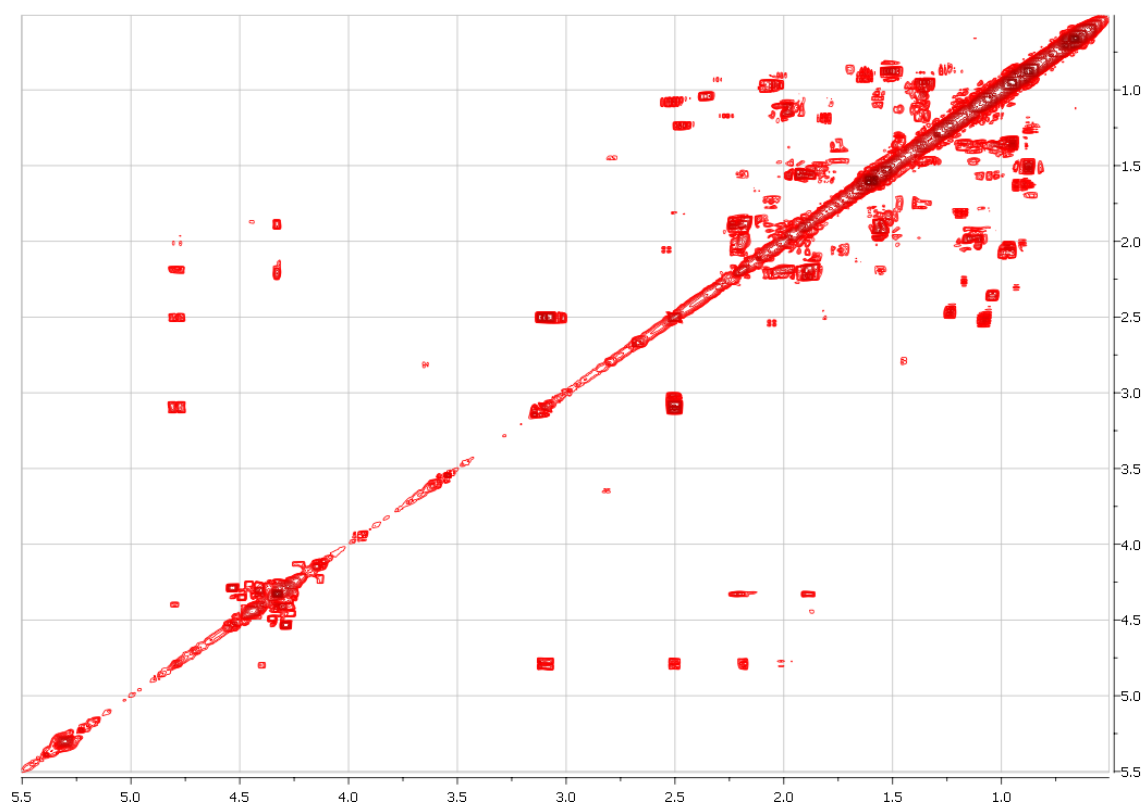
¹H NMR spectrum (700 MHz) of phallusiasterol A (**15**) in C₅D₅N



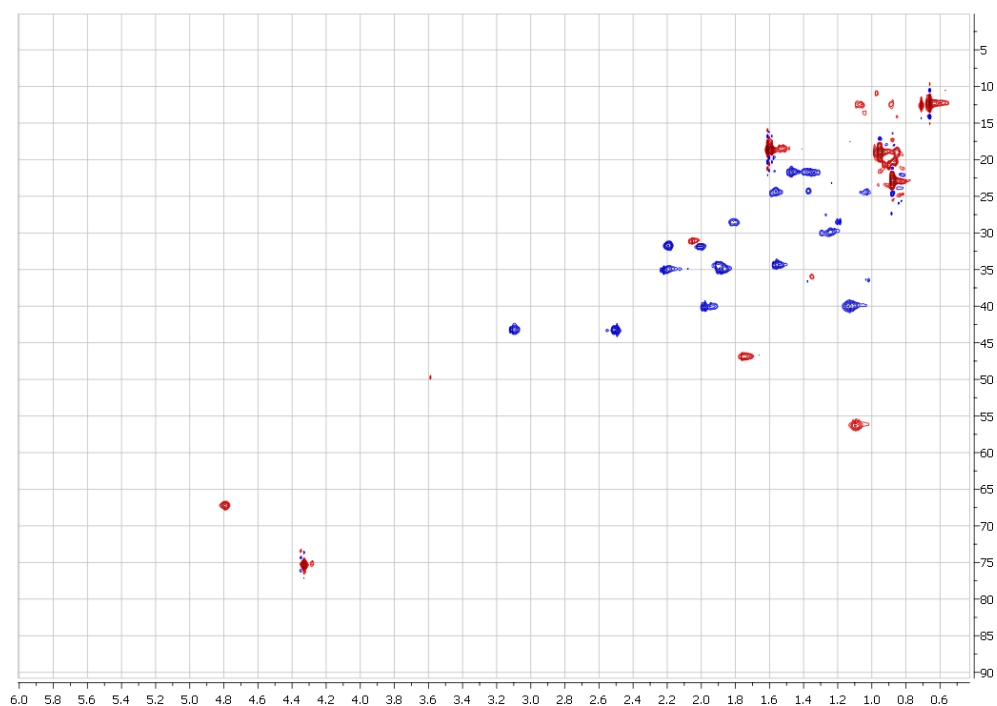
^{13}C NMR spectrum (125 MHz) of phallusiasterol A (**15**) in $\text{C}_5\text{D}_5\text{N}$



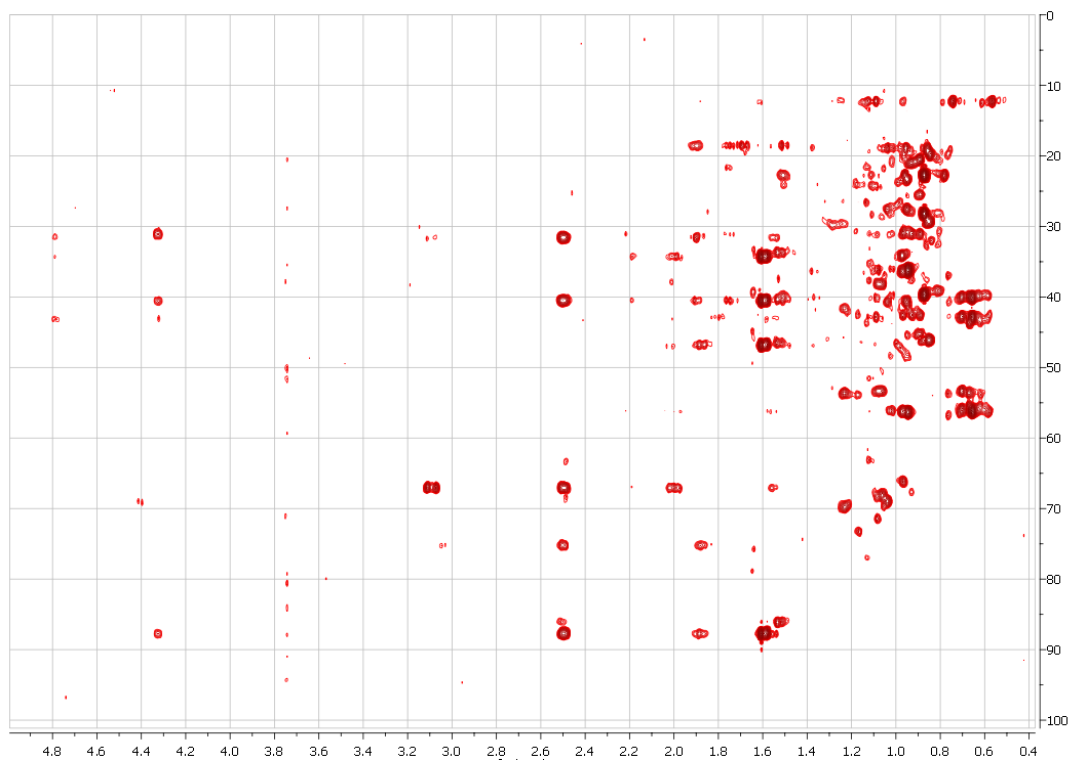
COSY 2D NMR spectrum (700 MHz) of phallusiasterol A (**15**) in $\text{C}_5\text{D}_5\text{N}$



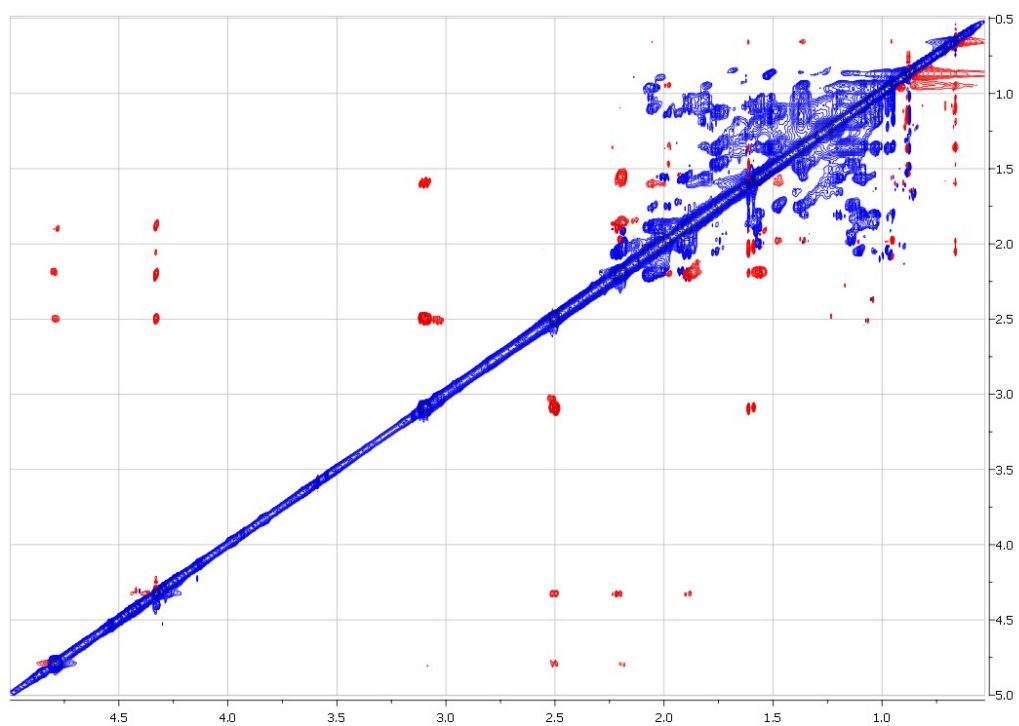
HSQC 2D NMR spectrum (700 MHz) of phallusiasterol A (**15**) in C₅D₅N



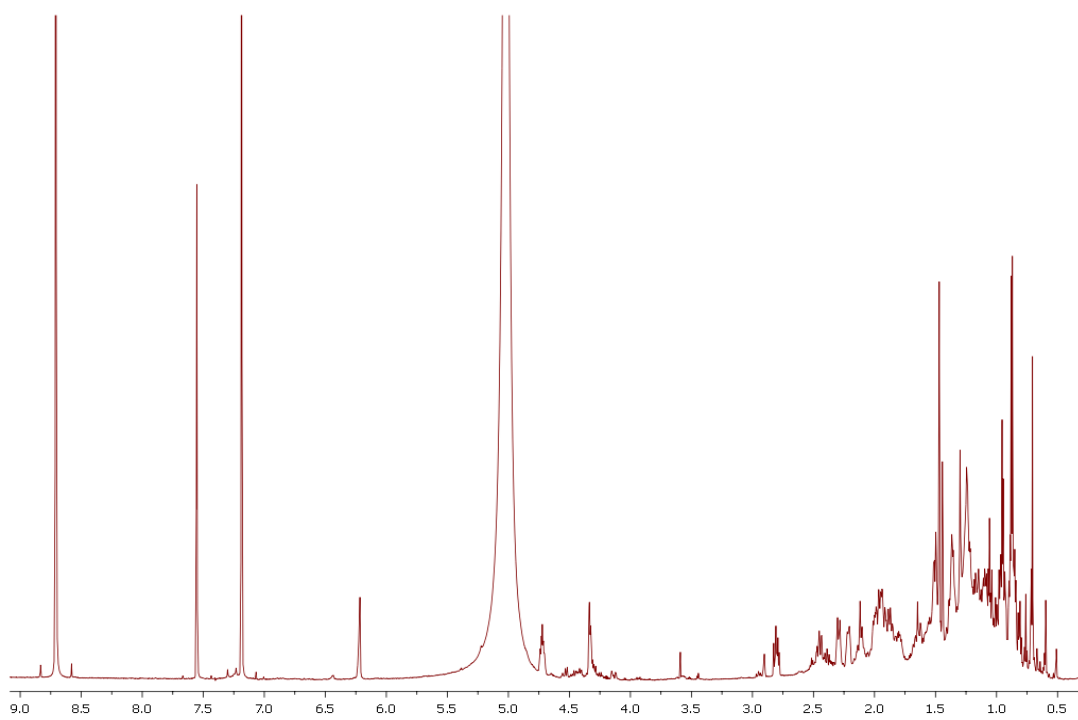
HMBC 2D NMR spectrum (700 MHz) of phallusiasterol A (**15**) in C₅D₅N



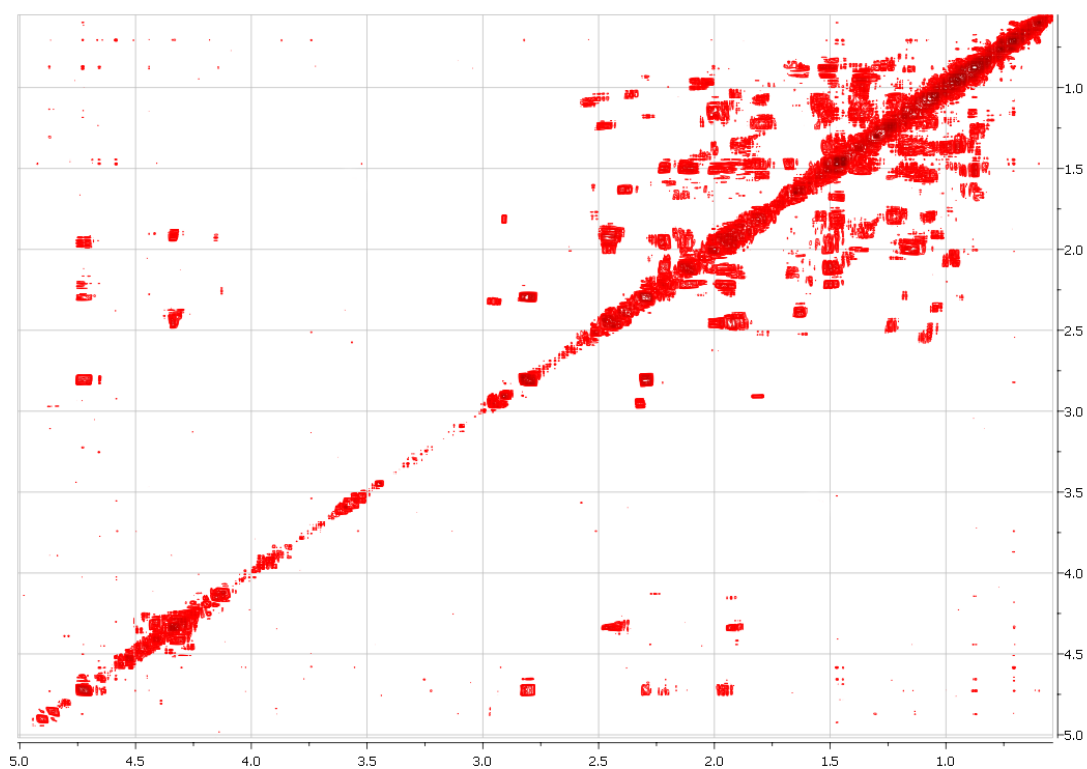
ROESY 2D NMR spectrum (700 MHz) of phallusiasterol A (**15**) in C_5D_5N



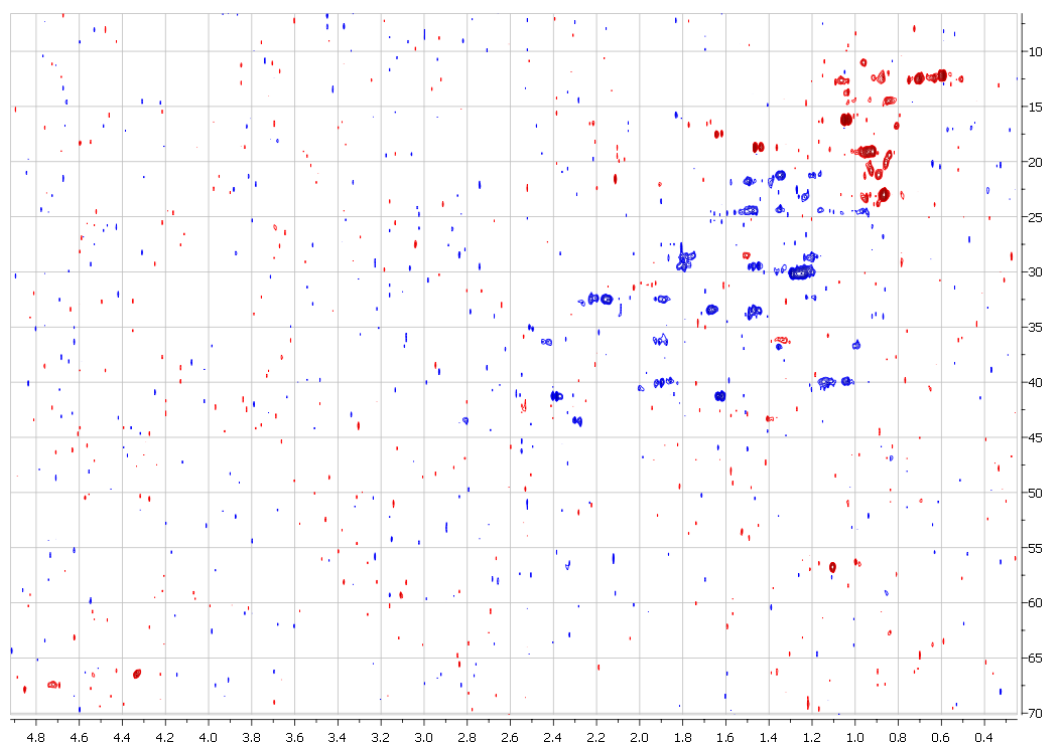
1H NMR spectrum (700 MHz) of phallusiasterol B (**16**) in C_5D_5N



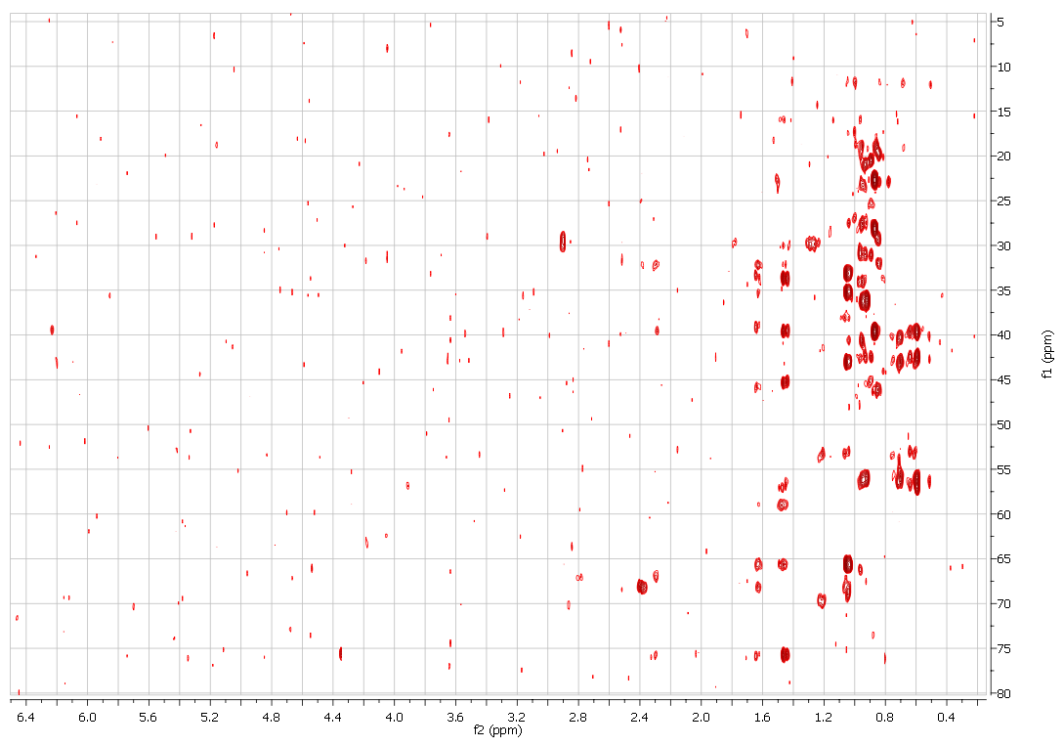
COSY 2D NMR spectrum (700 MHz) of phallusiasterol B (**16**) in C₅D₅N



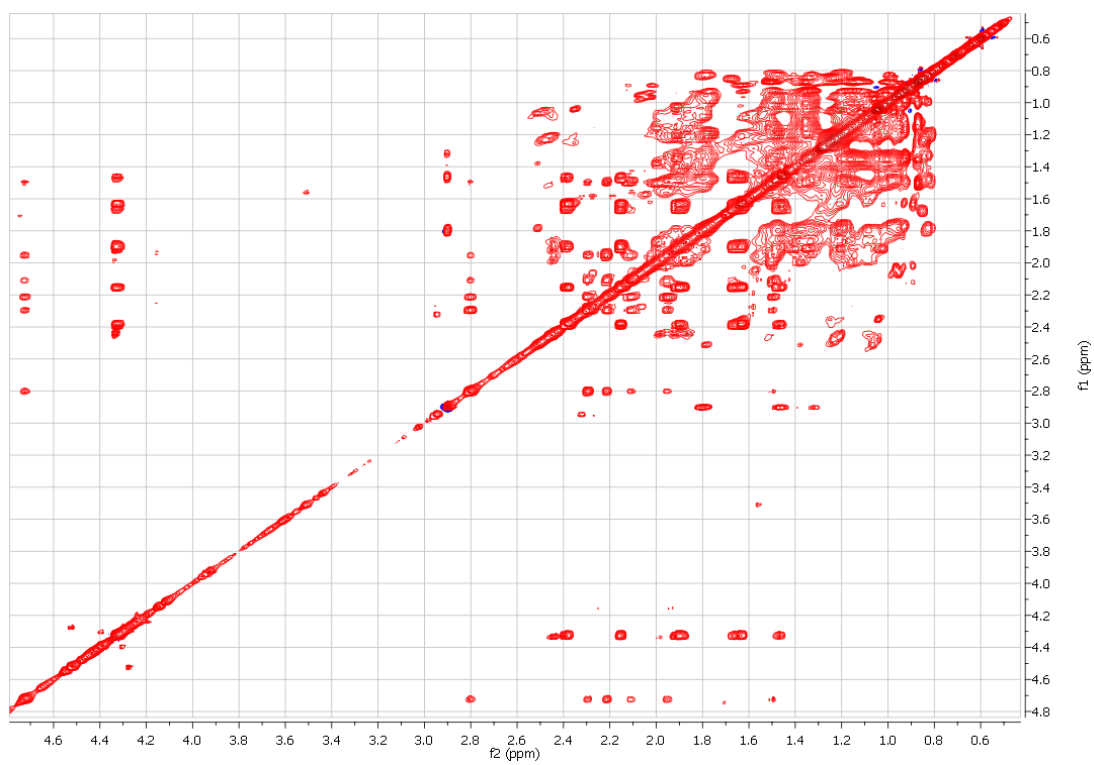
HSQC 2D NMR spectrum (700 MHz) of phallusiasterol B (**16**) in C₅D₅N



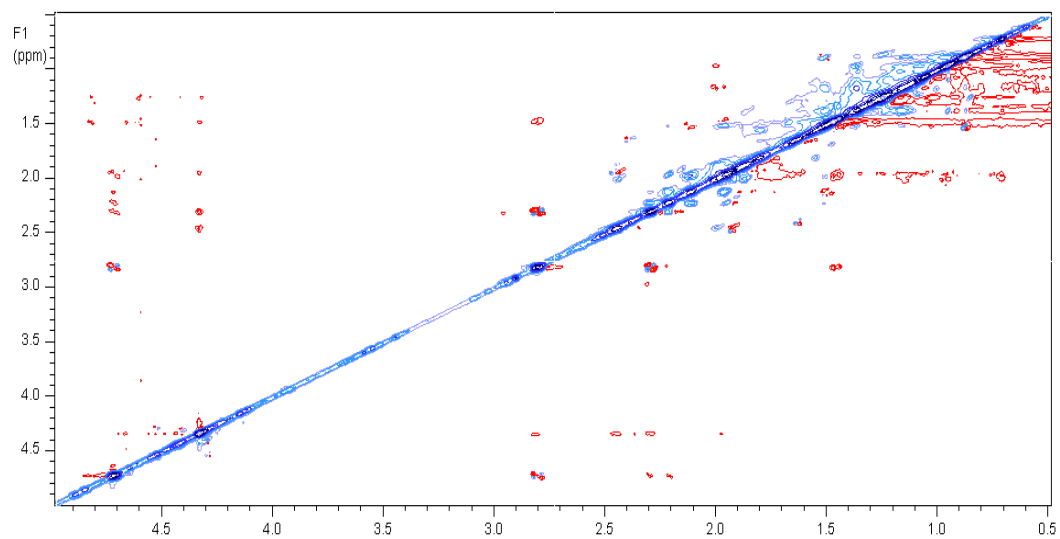
HMBC 2D NMR spectrum (700 MHz) of phallusiasterol B (**16**) in C₅D₅N



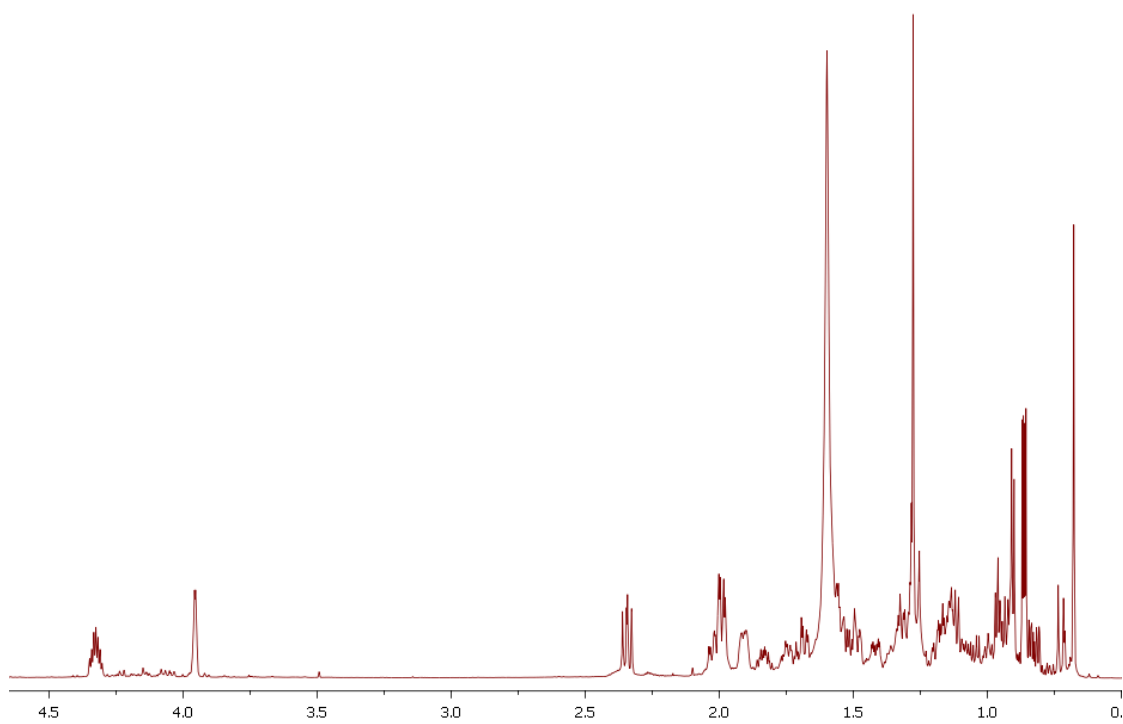
TOCSY 2D NMR spectrum (700 MHz) of phallusiasterol B (**16**) in C₅D₅N



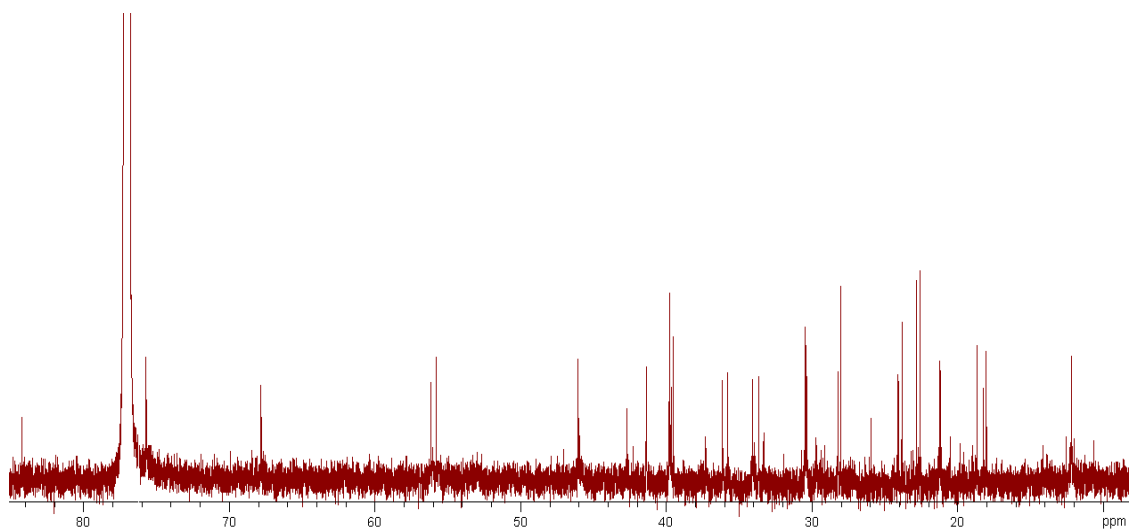
ROESY 2D NMR spectrum (700 MHz) of phallusiasterol B (**16**) in C_5D_5N



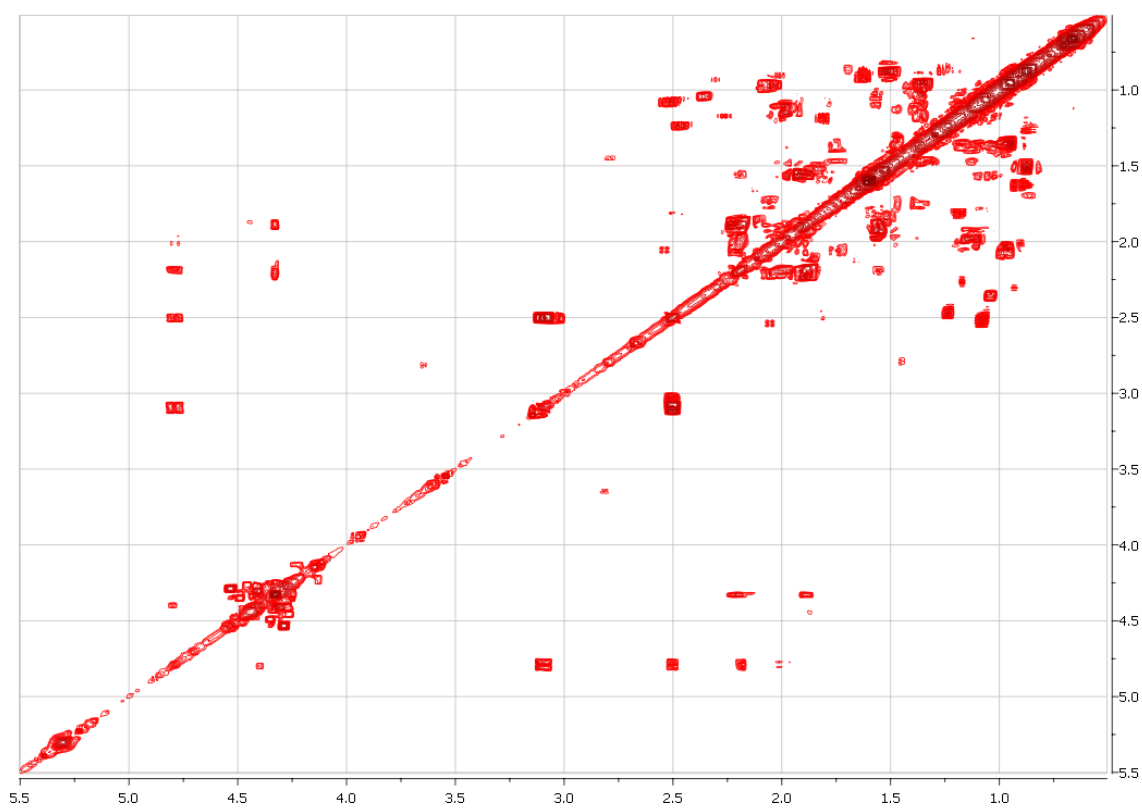
¹H NMR spectrum (700 MHz) of phallusiasterol A (**15**) in $CDCl_3$



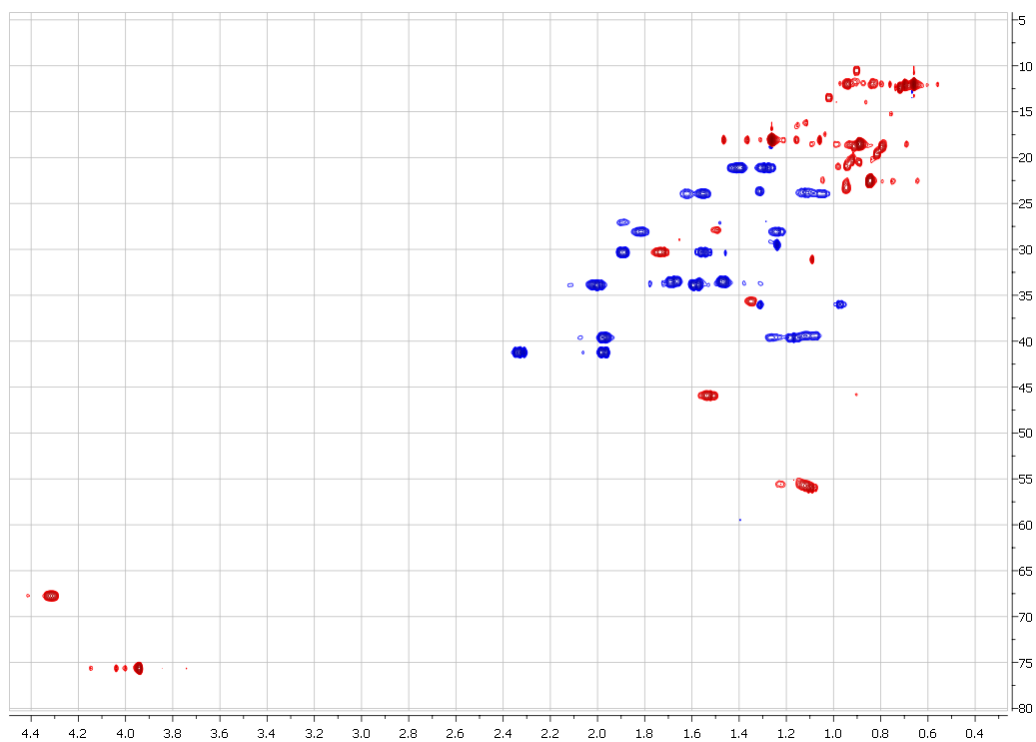
^{13}C NMR spectrum (125 MHz) of phallusiasterol A (**15**) in CDCl_3



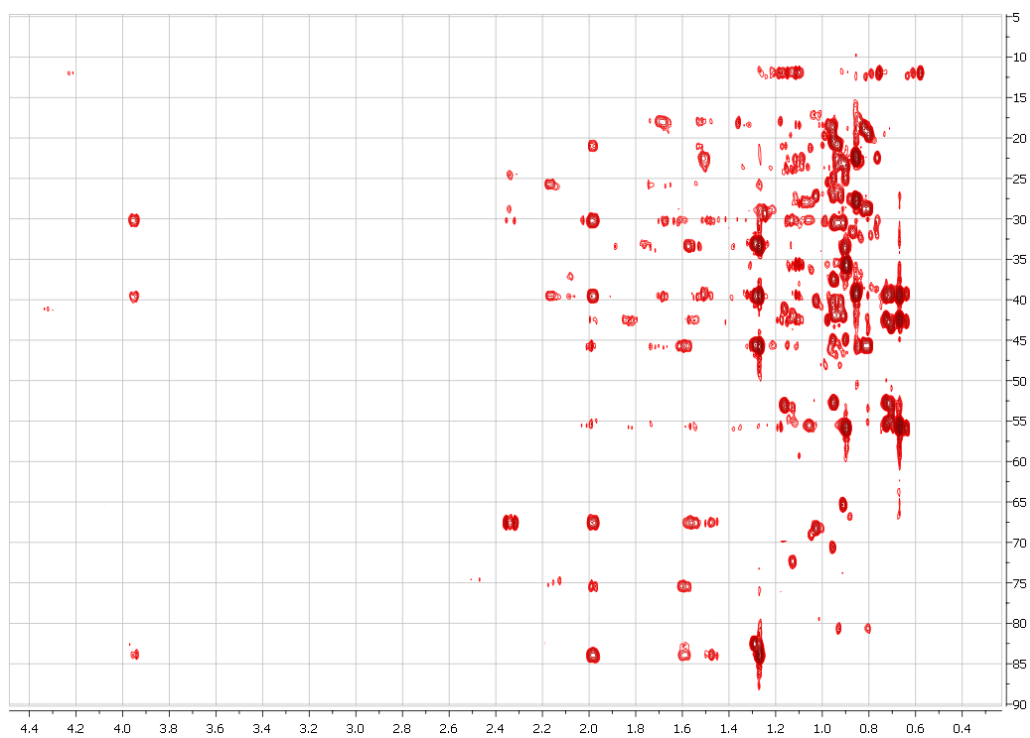
COSY 2D NMR spectrum (700 MHz) of phallusiasterol A (**15**) in CDCl_3



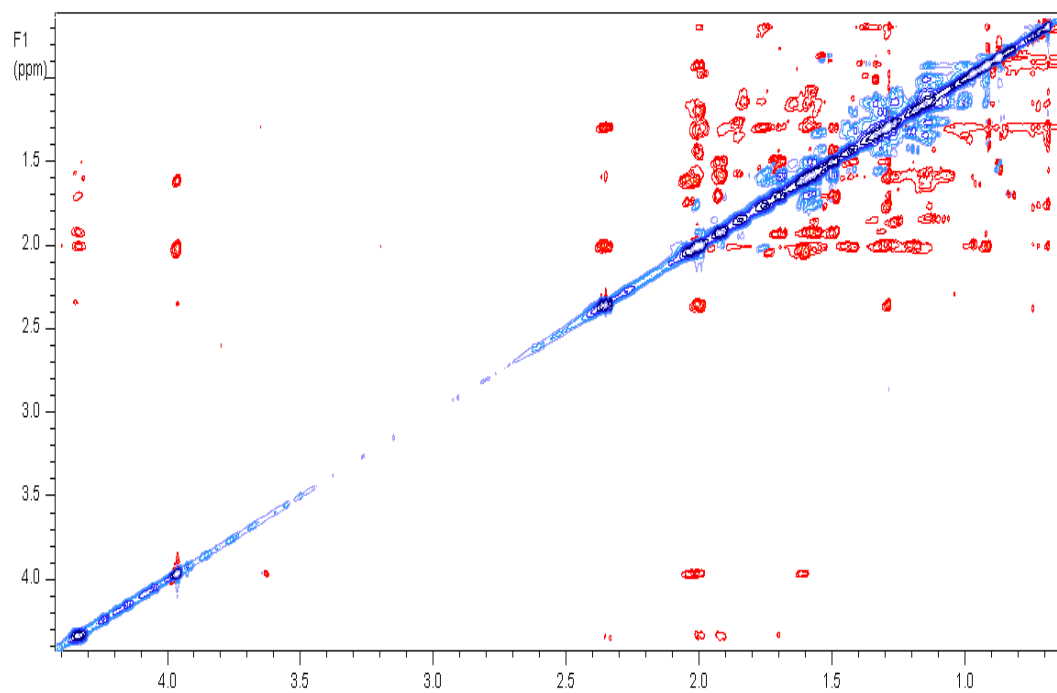
HSQC 2D NMR spectrum (700 MHz) of phallusiasterol A (**15**) in CDCl₃



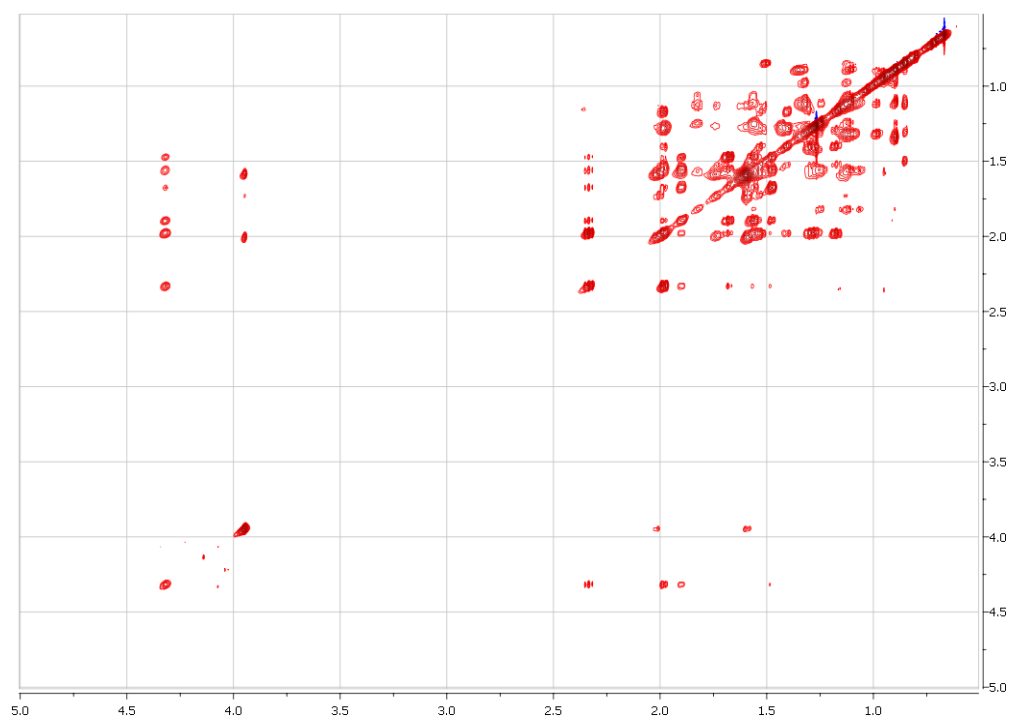
HMBC 2D NMR spectrum (700 MHz) of phallusiasterol A (**15**) in CDCl₃



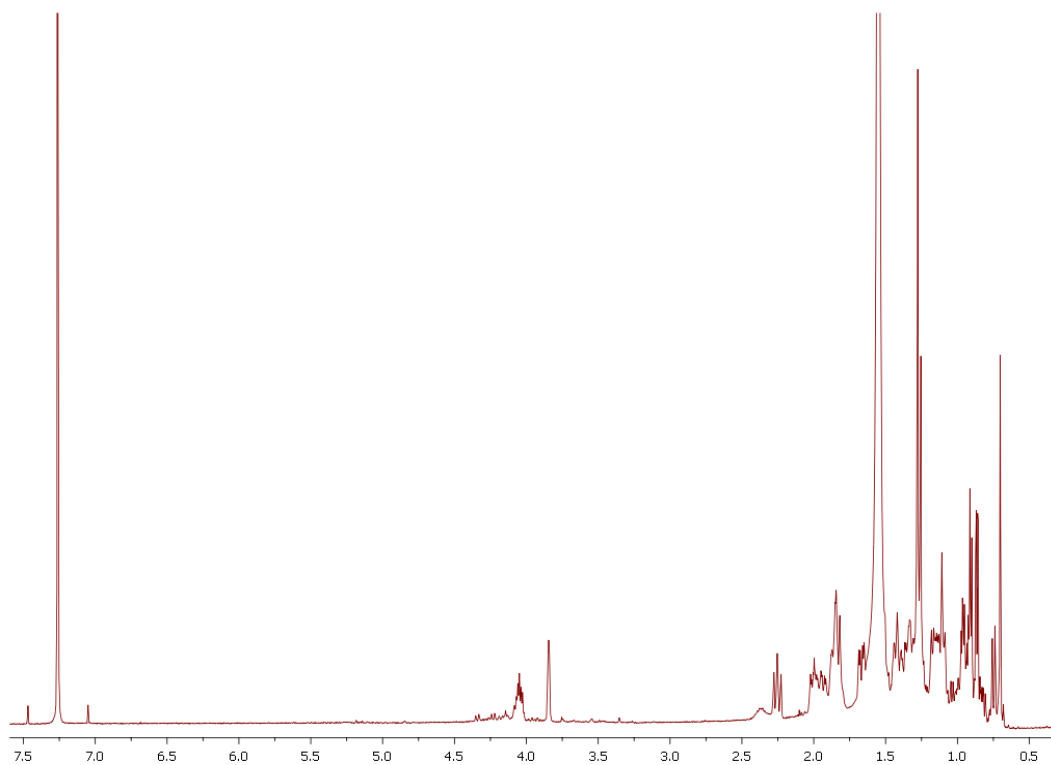
ROESY 2D NMR spectrum (700 MHz) of phallusiasterol A (**15**) in CDCl₃



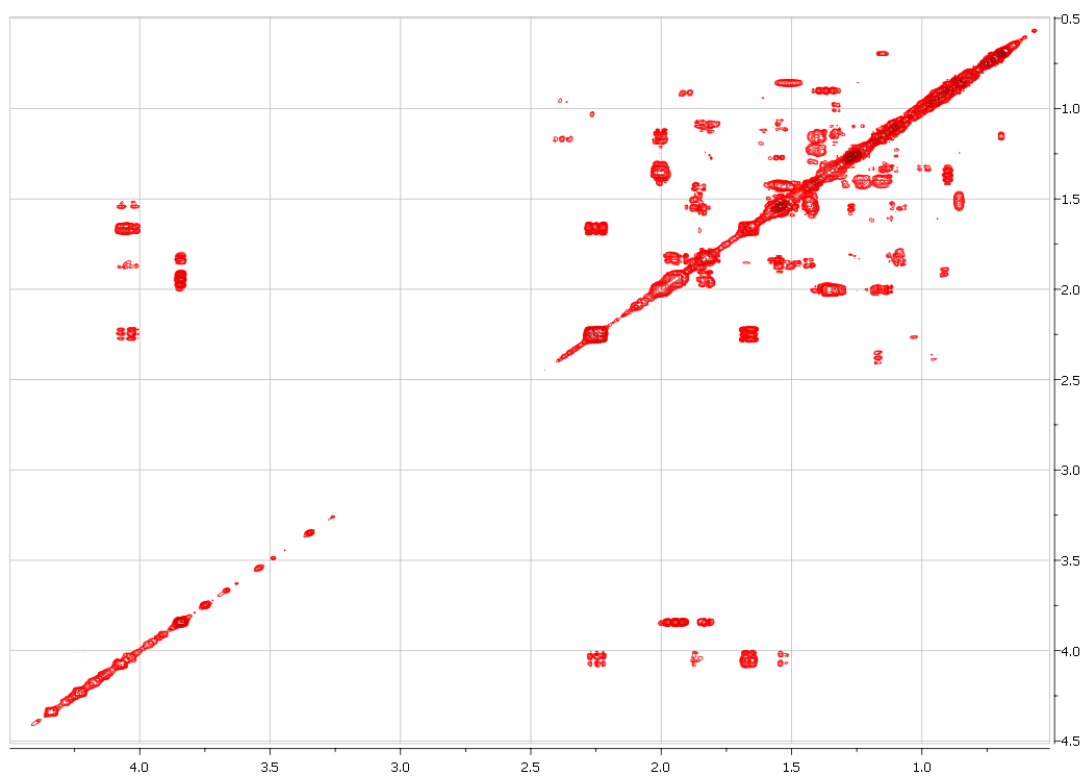
TOCSY 2D NMR spectrum (700 MHz) of phallusiasterol A (**15**) in CDCl₃



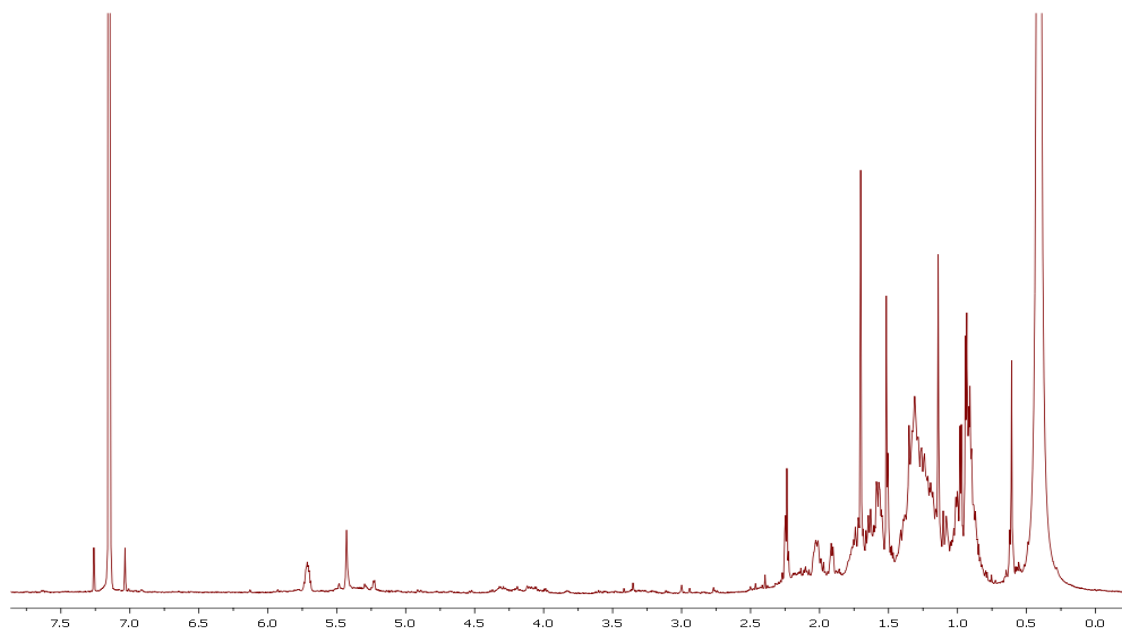
^1H NMR spectrum (700 MHz) of phallusiasterol B (**16**) in CDCl_3



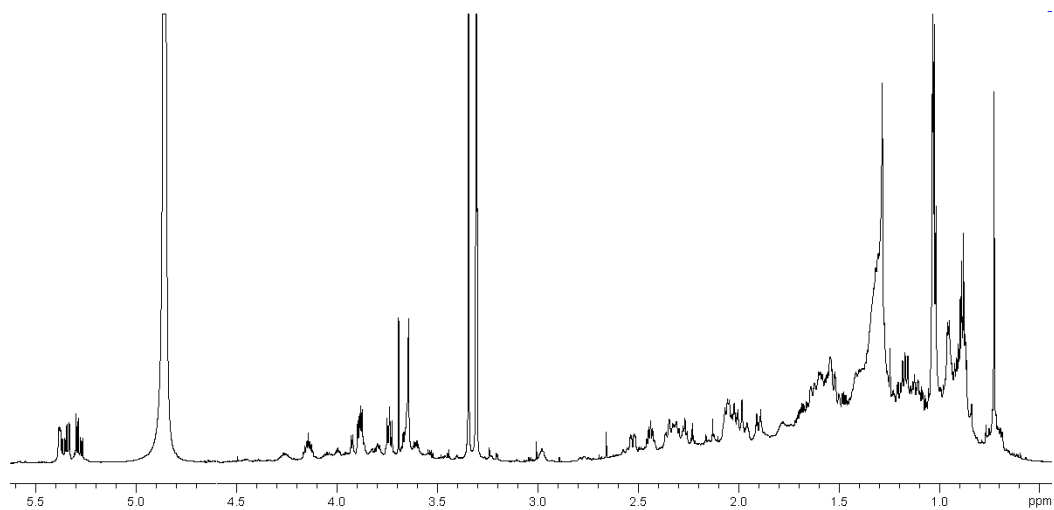
COSY 2D NMR spectrum (700 MHz) of phallusiasterol B (**16**) in CDCl_3



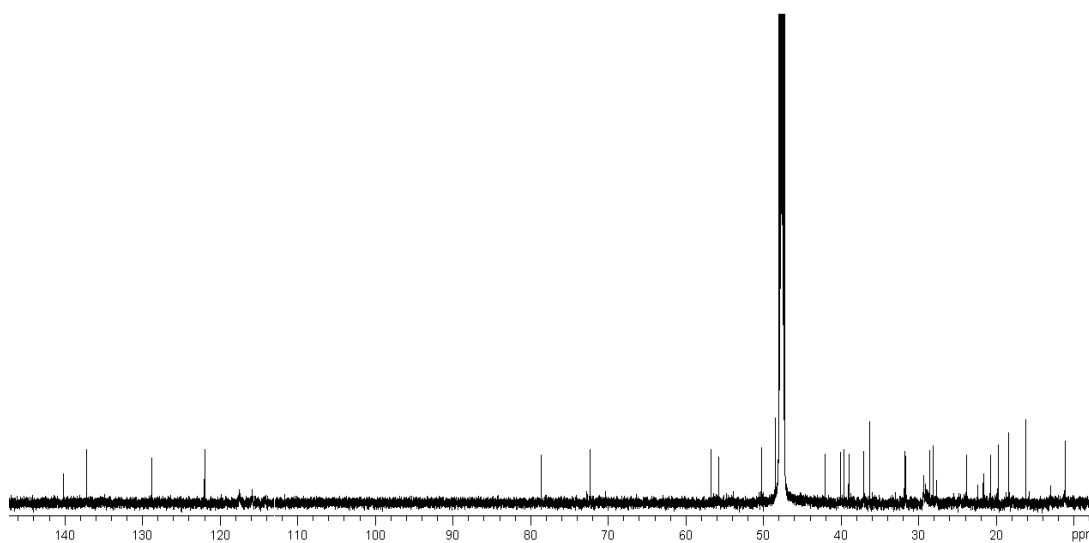
^1H NMR spectrum (700 MHz) of compound **17** in C_6D_6



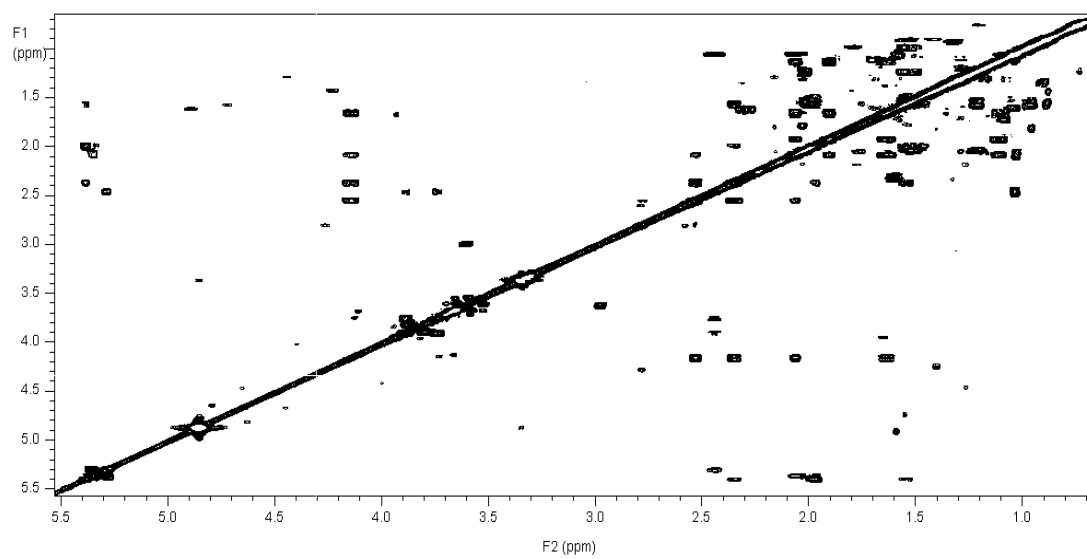
^1H NMR spectrum (700 MHz) of phallusiasterol C (**18**) in CD_3OD



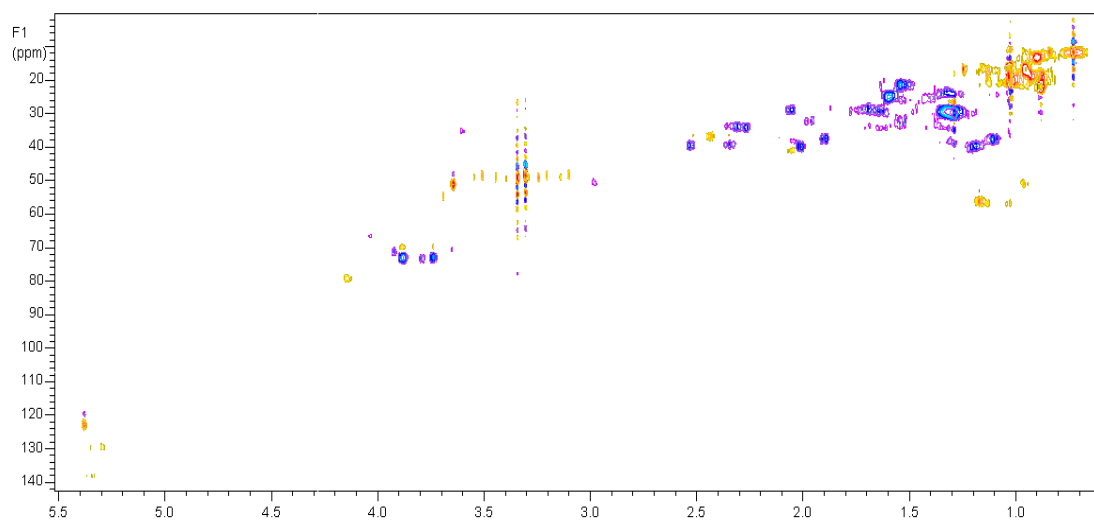
^{13}C NMR spectrum (700 MHz) of phallusiasterol C (**18**) in CD_3OD



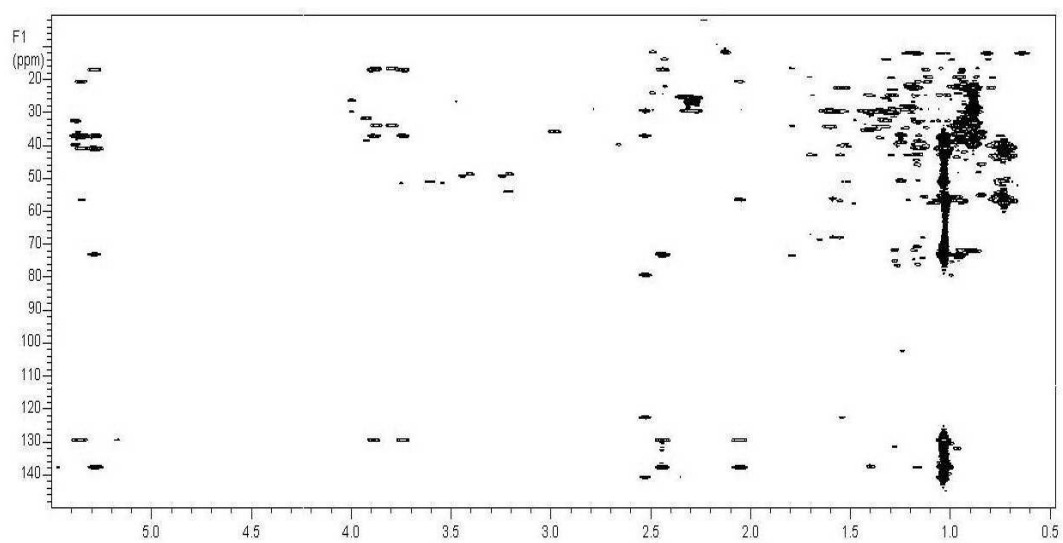
COSY 2D NMR spectrum (700 MHz) of phallusiasterol C (**18**) in CD_3OD



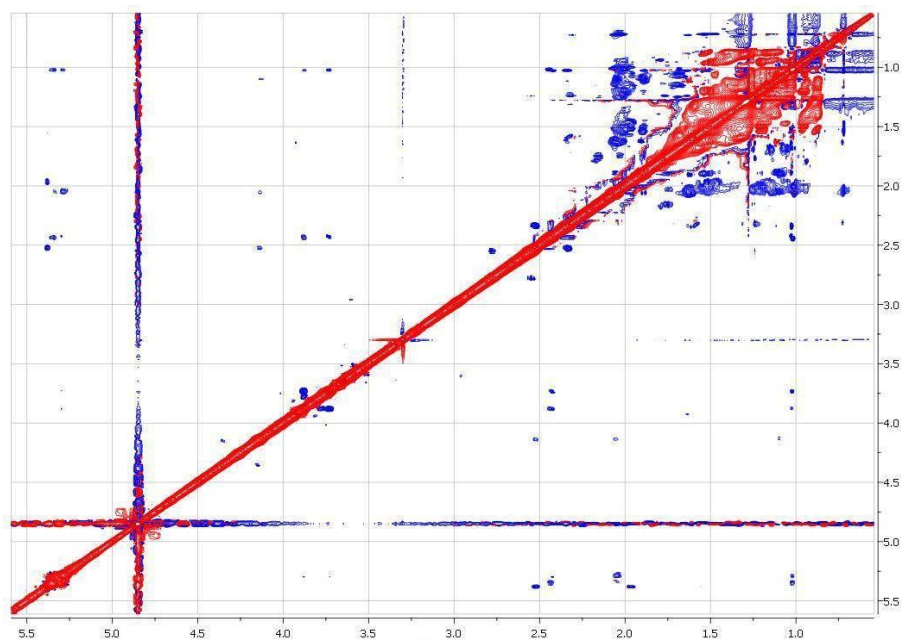
HSQC 2D NMR spectrum (700 MHz) of phallusiasterol C (**18**) in CD₃OD



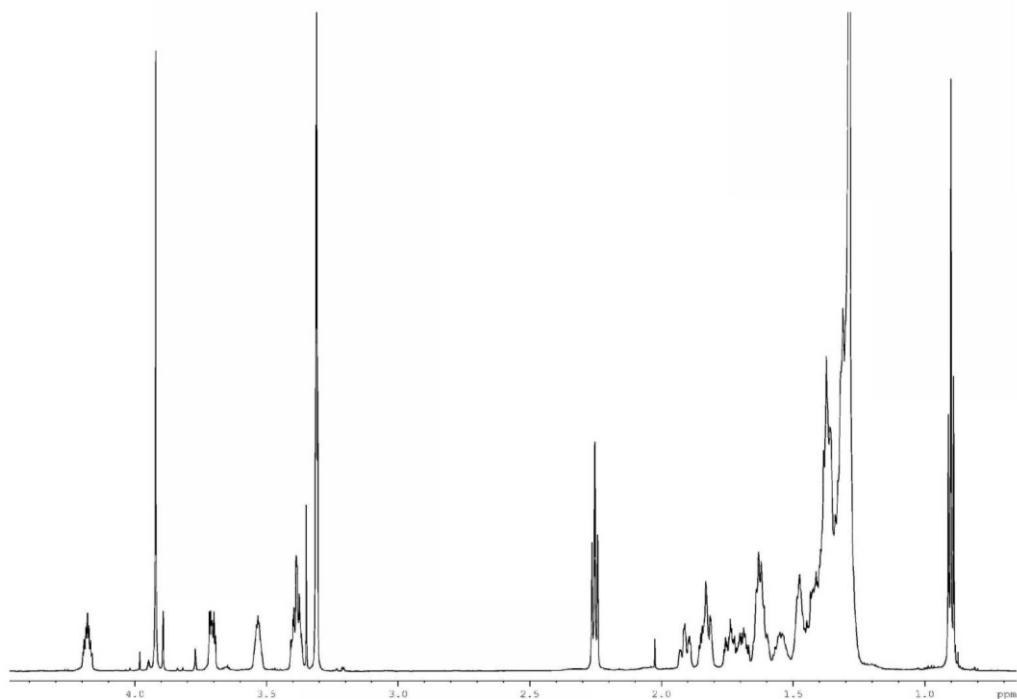
HMBC 2D NMR spectrum (700 MHz) of phallusiasterol C (**18**) in CD₃OD



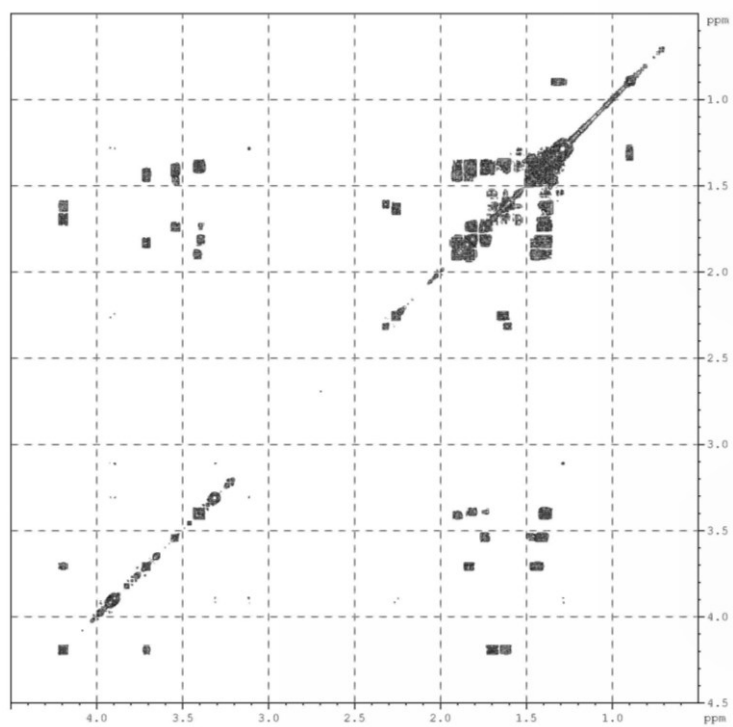
ROESY 2D NMR spectrum (700 MHz) of phallusiasterol C (**18**) in CD₃OD



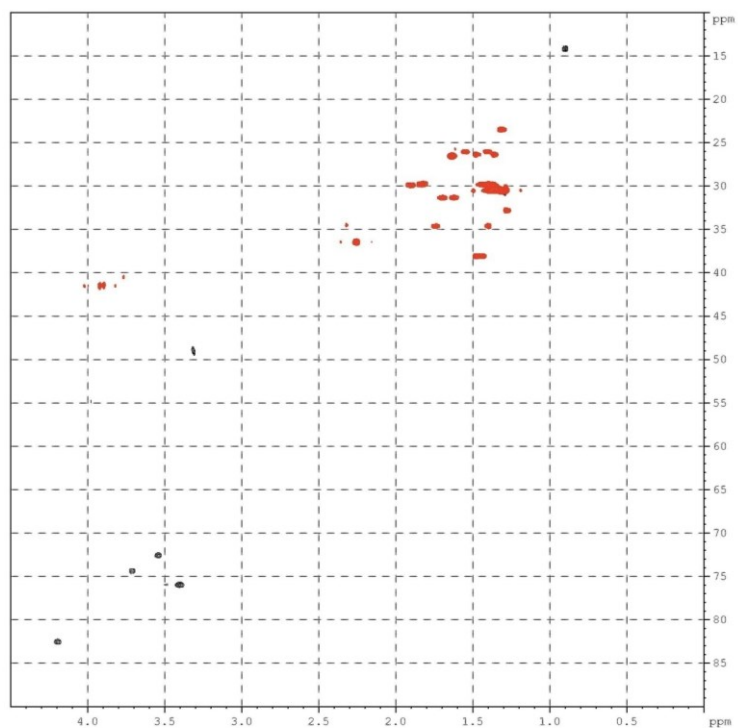
¹H NMR spectrum (700 MHz) of phosphoeleganin (**19**) in CD₃OD



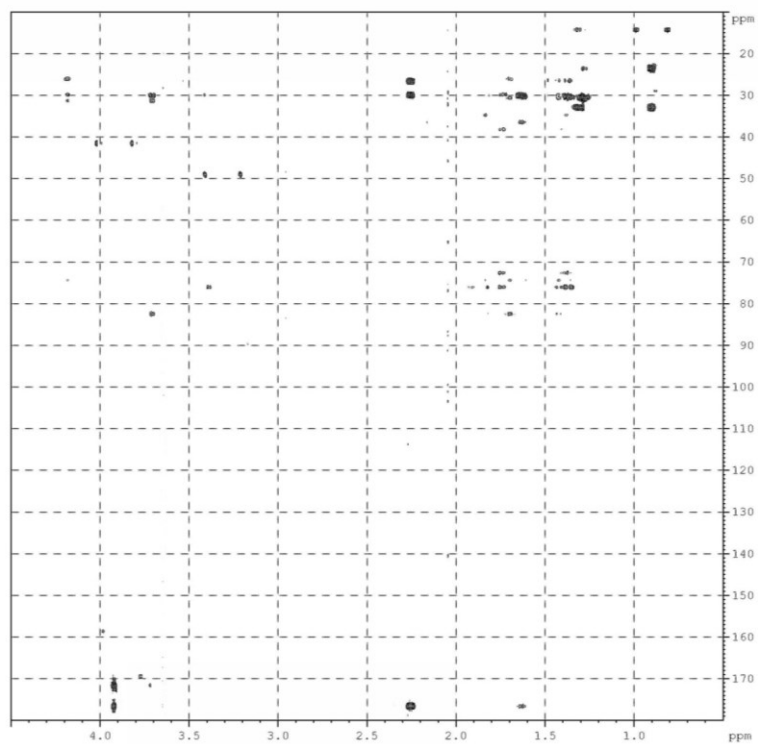
COSY 2D NMR spectrum (700 MHz) of phosphoeleganin (**19**) in CD₃OD



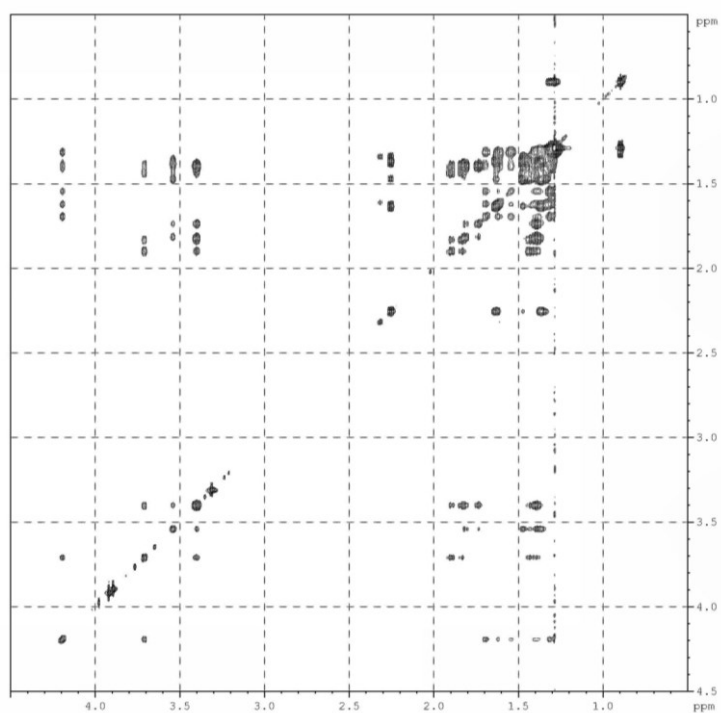
HSQC 2D NMR spectrum (700 MHz) of phosphoeleganin (**19**) in CD₃OD



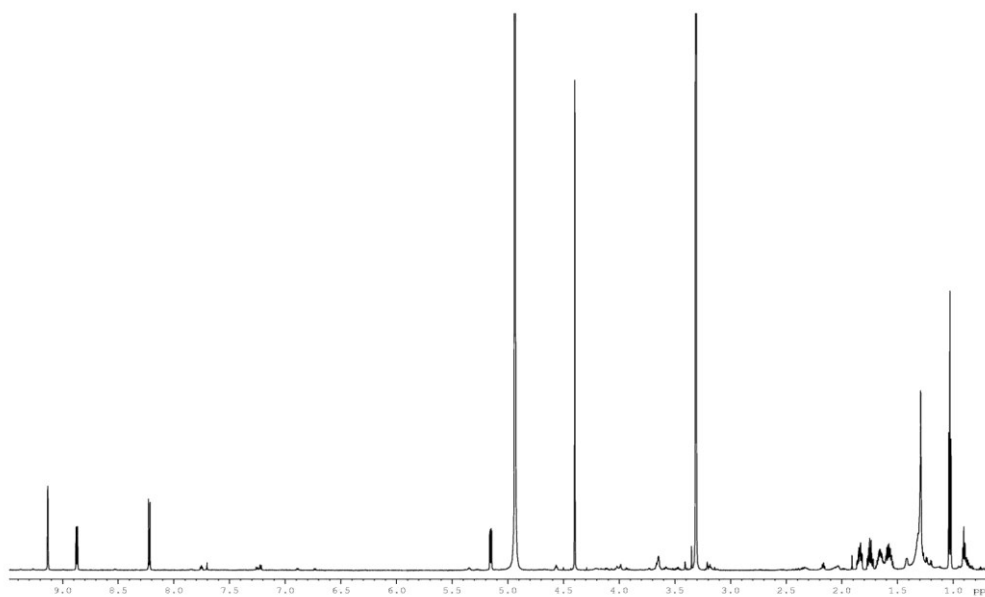
HMBC 2D NMR spectrum (700 MHz) of phosphoeleganin (**19**) in CD₃OD



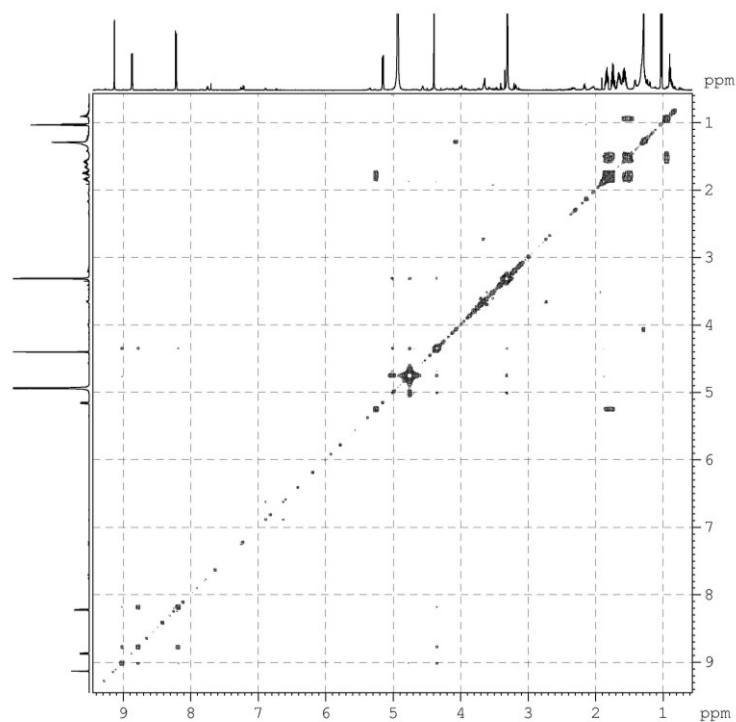
TOCSY 2D NMR spectrum (700 MHz) of phosphoeleganin (**19**) in CD₃OD



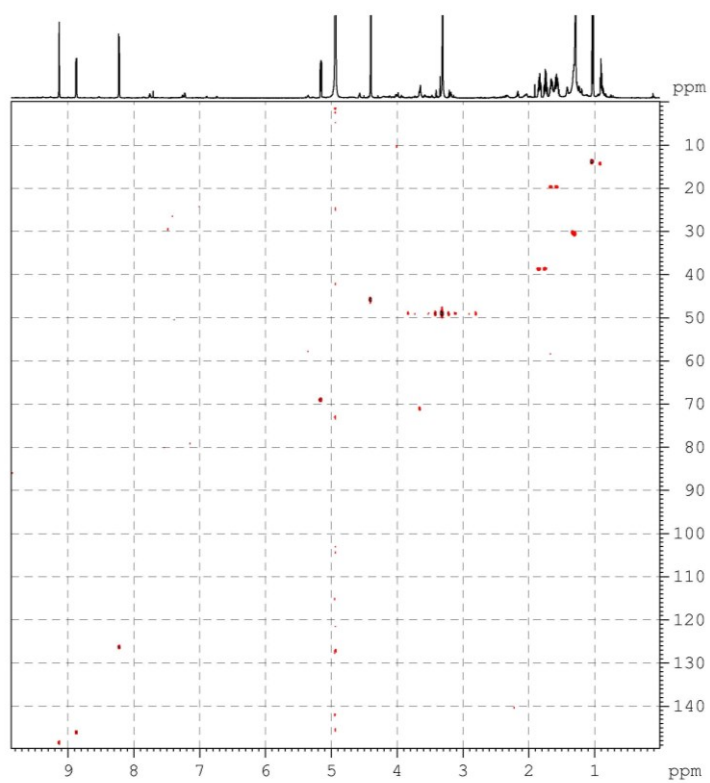
^1H NMR spectrum (700 MHz) of betaine (**28**) in CD_3OD



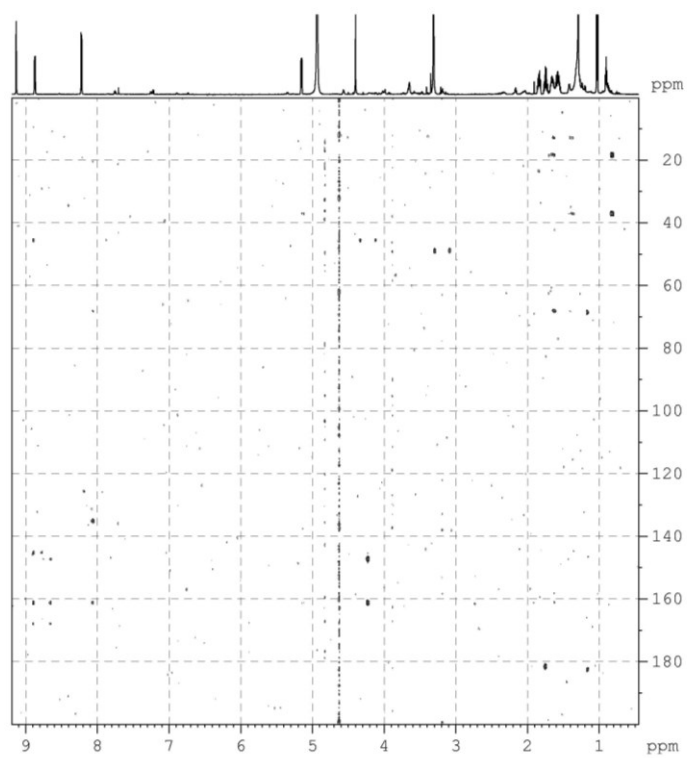
COSY 2D NMR spectrum (700 MHz) of betaine (**28**) in CD_3OD



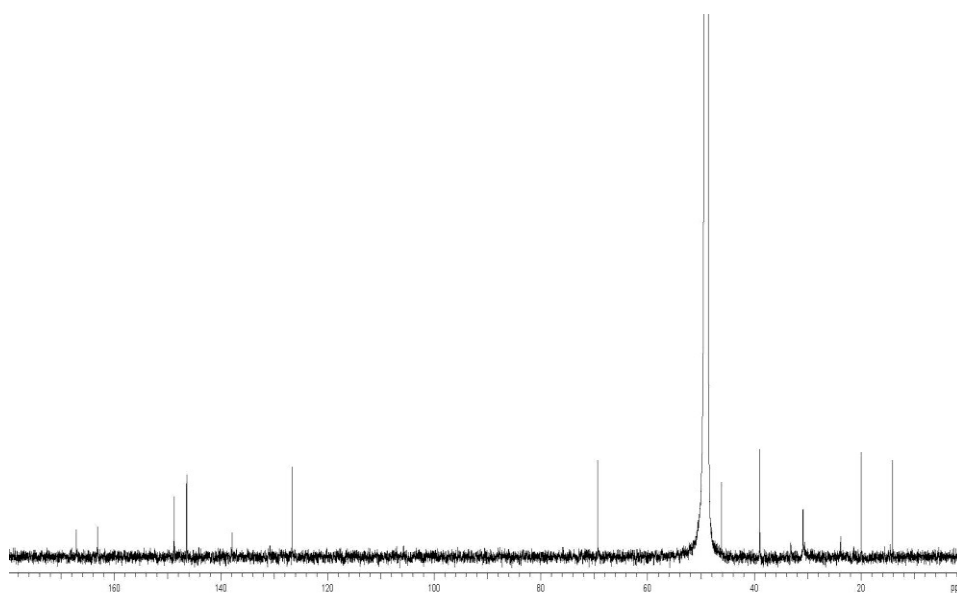
HSQC 2D NMR spectrum (700 MHz) of betaine (**28**) in CD₃OD



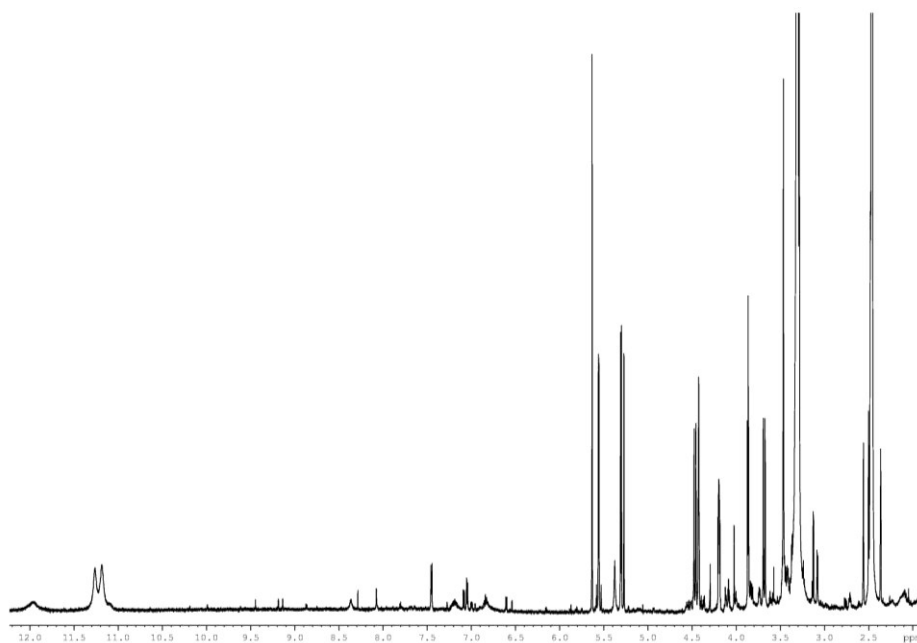
HMBC 2D NMR spectrum (700 MHz) of betaine (**28**) in CD₃OD



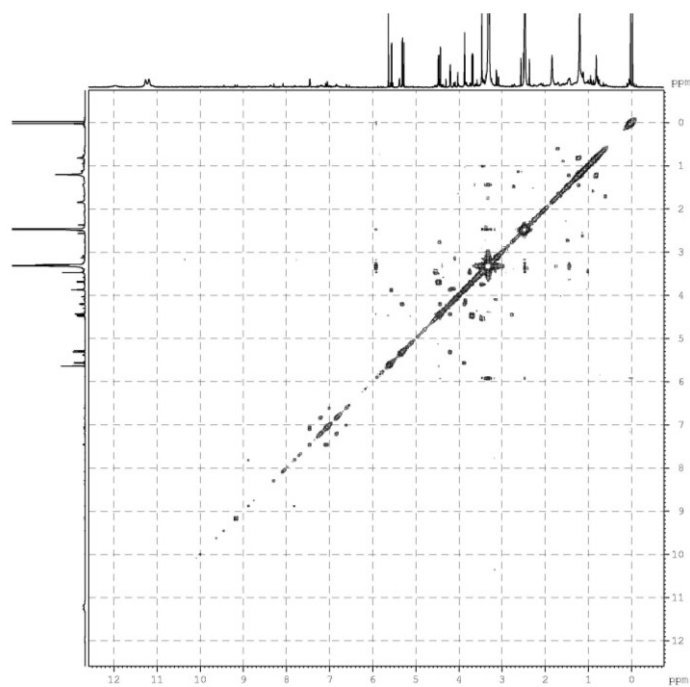
^{13}C NMR spectrum (125 MHz) of betaine (**28**) in CD_3OD



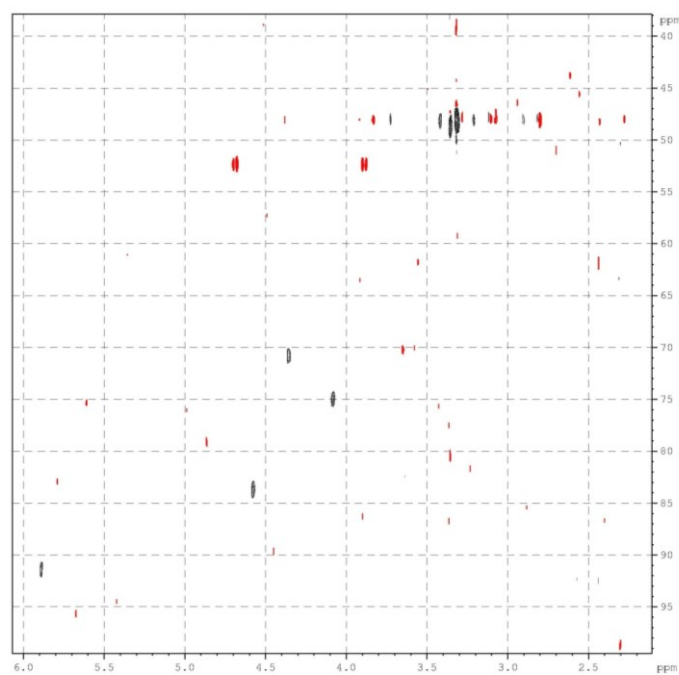
^1H NMR spectrum (700 MHz) of cyclonucleoside (**31**) in d_6 -DMSO



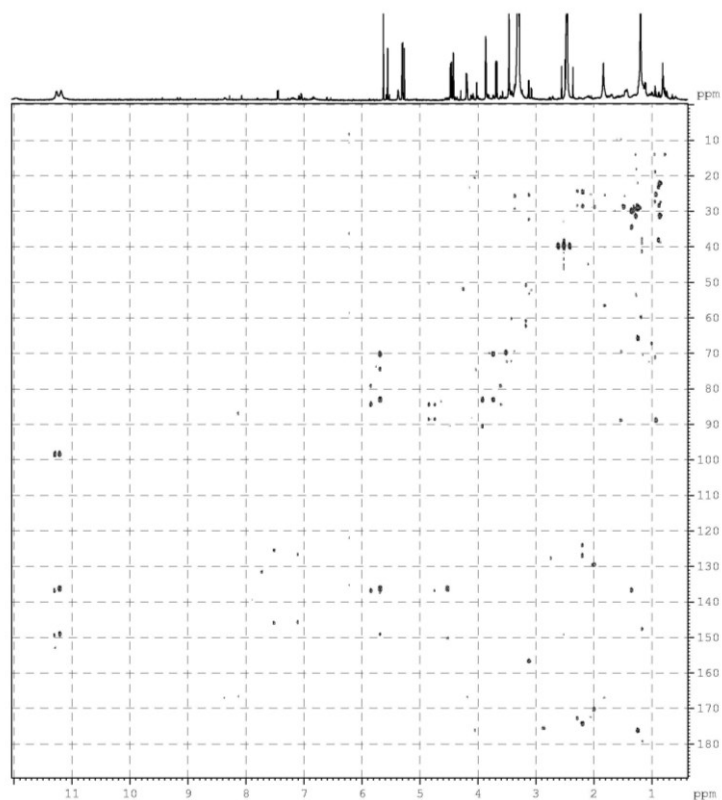
COSY 2D NMR spectrum (700 MHz) of cyclonucleoside (**31**) in *d*₆-DMSO



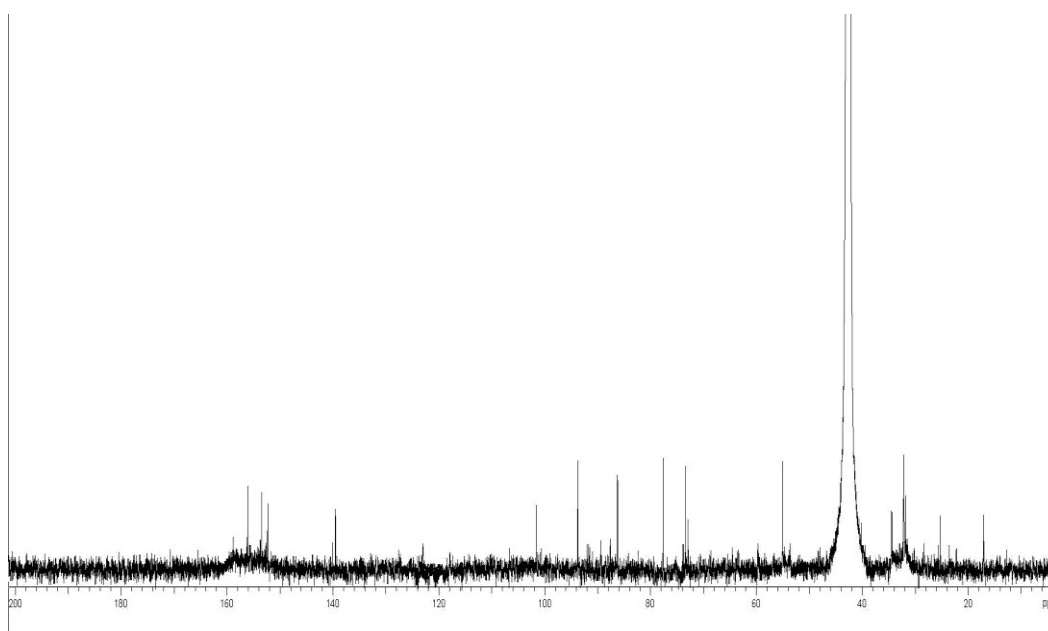
HSQC 2D NMR spectrum (700 MHz) of cyclonucleoside (**31**) in *d*₆-DMSO



HMBC 2D NMR spectrum (700 MHz) of cyclonucleoside (**31**) in *d6*-DMSO



¹³C NMR spectrum (125 MHz) of cyclonucleoside (**31**) in *d6*-DMSO



5.4. Computational details of conithiaquinones A and B

Optimized Z-Matrixes of model A1

C 0	-5.134261	0.668195	-0.229577	H 0	-4.780889	0.456603	-1.265746
C 0	-6.451732	-0.056444	0.063127	H 0	-4.344676	0.299345	0.466515
S 0	-7.761221	0.658546	-0.934958	H 0	-6.366772	-1.147227	-0.148100
C 0	-7.541432	2.435388	-0.813438	H 0	-6.717143	0.071071	1.138902
C 0	-6.350786	2.924993	-0.374273	H 0	-4.403243	2.659707	0.266965
N 0	-5.248754	2.129205	-0.062811	H 0	-9.227163	7.335088	-0.307723
C 0	-8.636026	3.361870	-1.174684	H 0	-7.567622	7.303691	-2.873556
C 0	-8.380528	4.836797	-1.223085	H 0	-6.785594	7.172959	0.127984
C 0	-7.174315	5.318555	-0.824545	H 0	-10.426665	8.048904	-3.024866
C 0	-6.168579	4.395413	-0.226923	H 0	-10.913972	8.557174	-1.378134
C 0	-9.496744	5.744554	-1.761876	H 0	-9.477587	10.422486	-1.590193
C 0	-9.162400	7.214921	-1.420029	H 0	-9.100971	9.862351	-3.246568
C 0	-7.728990	7.583253	-1.805752	H 0	-8.682798	5.700367	-3.828337
C 0	-6.764473	6.790802	-0.917971	H 0	-9.860413	4.411957	-3.493715
C 0	-10.034368	8.327546	-2.022691	H 0	-10.442153	6.058931	-3.750033
C 0	-9.112806	9.548027	-2.176181	H 0	-10.778320	5.487839	0.023487
C 0	-7.708774	9.116607	-1.731712	H 0	-11.317700	4.496375	-1.372715
O 0	-7.525879	0.261173	-2.310539	H 0	-11.619336	6.226589	-1.381227
O 0	-9.014940	0.242383	-0.335817	H 0	-4.344017	7.012733	0.288490
O 0	-9.703809	2.863566	-1.516374	H 0	-4.910879	8.601461	-0.366483
O 0	-5.171043	4.794779	0.363793	H 0	-3.590009	7.693907	-1.201571
C 0	-9.622497	5.476618	-3.278319	H 0	-7.596043	10.467812	-0.333453
C 0	-10.861744	5.466744	-1.086920	H 0	-5.606271	9.538219	-2.260592
O 0	-5.468006	6.920107	-1.472543	H 0	-6.732133	10.900443	-2.530979
C 0	-4.543912	7.589326	-0.638052	H 0	-6.721620	9.496465	-3.655643
O 0	-7.533507	9.512225	-0.397400				
C 0	-6.636450	9.791985	-2.585606				

Optimized Z-Matrixes of model A2

C 0	1.287443	5.880124	-0.581787	H 0	0.655365	7.831093	-0.310881
N 0	0.321030	6.885015	-0.624545	H 0	-1.664839	6.434911	-0.053694
C 0	-1.104018	6.728220	-0.971656	H 0	-1.495897	7.722207	-1.291579
C 0	-1.312572	5.710731	-2.097508	H 0	-0.833555	6.085808	-3.032472
S 0	-0.540273	4.154768	-1.644408	H 0	-2.396423	5.550312	-2.300956
C 0	1.055641	4.589930	-0.948583	H 0	3.340639	1.536295	1.005233
C 0	2.122255	3.572242	-0.823461	H 0	5.091134	1.332175	1.270113
C 0	3.475209	3.964539	-0.320932	H 0	4.221741	2.738765	1.973681
C 0	3.689373	5.243240	0.080502	H 0	5.501351	1.267238	-1.382863
C 0	2.632692	6.279404	-0.085539	H 0	3.753592	1.219889	-1.447504
C 0	4.572509	2.898935	-0.212733	H 0	4.634083	2.478965	-2.384331
C 0	4.303423	2.090984	1.073411	H 0	5.986080	4.184210	-1.206995
C 0	4.607441	1.927982	-1.417056	H 0	5.912329	4.135759	1.840456
C 0	5.931019	3.635060	-0.232830	H 0	5.330643	6.575498	0.089906
C 0	6.057022	4.680204	0.875446	H 0	6.275589	7.488593	2.270925
C 0	4.972684	5.748503	0.741098	H 0	4.748548	8.270483	1.659881
O 0	4.638814	6.225641	2.033881	H 0	4.875909	7.745848	3.382878
C 0	5.168473	7.496794	2.338210	H 0	7.603569	2.503058	-1.115777
C 0	7.226962	2.813254	-0.113384	H 0	7.073558	1.888508	0.486636
C 0	8.239513	3.725452	0.604145	H 0	8.495377	3.276541	1.593874
C 0	7.541233	5.076923	0.812041	H 0	9.193681	3.822677	0.039071
C 0	7.923621	6.070428	-0.286395	H 0	7.631359	5.717236	-1.299468
O 0	7.953558	5.615851	2.038739	H 0	7.466006	7.071014	-0.124646
O 0	-0.375469	3.401123	-2.873054	H 0	9.025357	6.233187	-0.303374
O 0	-1.355388	3.552819	-0.605957	H 0	8.912501	5.608193	2.084469
O 0	2.846988	7.466128	0.144044				
O 0	1.829803	2.411350	-1.090828				

Optimized Z-Matrixes of model A3

C 0	1.305856	6.152216	-0.267925	H 0	-1.379308	5.736622	-1.890694
S 0	-0.027974	7.285001	-0.662370	H 0	-2.391898	6.876904	-0.921366
C 0	-1.472506	6.247475	-0.903548	H 0	-1.755134	5.667898	1.196144
C 0	-1.538311	5.196412	0.209123	H 0	-2.372289	4.486187	-0.001520
N 0	-0.289159	4.418527	0.321790	H 0	-0.354663	3.416451	0.632918
C 0	1.012744	4.886155	0.136620	H 0	5.559123	1.622583	0.499338
C 0	2.114211	3.922485	0.433152	H 0	5.125299	2.754661	-0.832051
C 0	3.504883	4.435164	0.614124	H 0	3.894334	1.772452	-0.039387
C 0	3.777358	5.701741	0.220565	H 0	4.870718	2.246549	2.990172
C 0	2.715887	6.579417	-0.361462	H 0	3.248494	2.081036	2.319024
C 0	4.573104	3.497692	1.187543	H 0	3.672627	3.568916	3.215566
C 0	4.810586	2.368696	0.158226	H 0	5.666663	4.661904	2.640982
C 0	4.059563	2.820168	2.487274	H 0	6.963476	6.070428	1.420729
C 0	5.858683	4.262909	1.611827	H 0	5.368155	6.863541	-0.603616
C 0	6.273529	5.473771	0.767910	H 0	6.776996	8.342446	0.973118
C 0	5.120535	6.388534	0.373584	H 0	5.307525	9.055807	0.152939
O 0	4.959629	7.397066	1.356451	H 0	5.555154	9.273601	1.927857
C 0	5.693861	8.570593	1.076747	H 0	7.065492	2.396541	1.917639
C 0	7.172462	3.458452	1.610810	H 0	7.870339	3.919247	2.352755
C 0	7.776437	3.644536	0.207028	H 0	8.889275	3.656320	0.261358
C 0	7.205971	4.962576	-0.337760	H 0	7.509826	2.790834	-0.455520
C 0	8.304482	5.964864	-0.696368	H 0	8.957846	6.189902	0.177008
O 0	6.465701	4.722938	-1.503405	H 0	7.870979	6.927250	-1.051068
O 0	2.985442	7.677531	-0.840900	H 0	8.955736	5.567439	-1.507724
O 0	1.794749	2.751347	0.609417	H 0	7.016575	4.285087	-2.155702
O 0	0.210979	7.964295	-1.921481				
O 0	-0.279631	8.120227	0.497208				

Optimized Z-Matrixes of model A4

C 0	1.025298	6.169174	-0.026752	H 0	-1.598360	5.544423	-1.693620
S 0	-0.245605	7.247838	-0.690894	H 0	-2.609133	6.869392	-0.995673
C 0	-1.715905	6.226890	-0.819057	H 0	-2.110035	6.050622	1.334012
C 0	-1.870613	5.399690	0.461152	H 0	-2.722163	4.689525	0.340268
N 0	-0.659573	4.616282	0.773177	H 0	-0.777867	3.685725	1.247899
C 0	0.666590	5.000603	0.572493	H 0	3.004984	1.485061	1.589889
C 0	1.710693	4.050922	1.057117	H 0	4.665530	1.176186	1.138271
C 0	3.151951	4.359116	0.835954	H 0	3.515094	1.751341	-0.115850
C 0	3.496937	5.562717	0.313503	H 0	4.673599	4.525641	3.077620
C 0	2.452603	6.521432	-0.160245	H 0	5.206992	2.810278	3.169042
C 0	4.215347	3.339243	1.257466	H 0	3.483009	3.230522	3.332793
C 0	3.821670	1.875099	0.947619	H 0	5.194986	3.496508	-0.665441
C 0	4.414953	3.485901	2.779942	H 0	6.220007	5.174975	1.667621
C 0	5.477605	3.622455	0.410664	H 0	5.036287	6.311414	-0.912433
C 0	5.997661	5.050313	0.579573	H 0	6.717068	8.021304	-0.037364
C 0	4.932959	6.067460	0.167082	H 0	5.088682	8.659091	-0.546425
O 0	5.073501	7.230082	0.965718	H 0	5.800545	9.141576	1.041829
C 0	5.703606	8.308396	0.310411	H 0	6.688891	1.800815	0.083219
C 0	6.730087	2.762739	0.644194	H 0	6.849946	2.522359	1.724698
C 0	7.915895	3.630264	0.185512	H 0	8.671227	3.688561	1.004607
C 0	7.354848	5.023128	-0.144470	H 0	8.431069	3.175523	-0.690909
C 0	7.304706	5.249180	-1.656991	H 0	6.615526	4.538554	-2.164750
O 0	8.208002	5.993540	0.401826	H 0	6.989505	6.283721	-1.916326
O 0	2.756424	7.576708	-0.709609	H 0	8.313119	5.113703	-2.110111
O 0	1.324267	3.040422	1.634987	H 0	9.101257	5.848981	0.080785
O 0	0.085968	7.668192	-2.039158				
O 0	-0.524520	8.293547	0.275343				

Optimized Z-Matrixes of model B1

C 0	-5.769599	1.391478	-0.221508	H 0	-5.915142	1.872972	-1.216478
C 0	-6.163454	-0.088296	-0.260604	H 0	-6.428241	1.928716	0.500571
S 0	-4.988290	-0.988847	-1.275137	H 0	-6.135538	-0.511274	0.771076
C 0	-3.370554	-0.401318	-0.767235	H 0	-7.193046	-0.221880	-0.665204
C 0	-3.275758	0.774822	-0.089795	H 0	-4.131220	2.468080	0.730359
N 0	-4.369157	1.593005	0.198079	H 0	1.756081	0.106408	-1.533442
C 0	-2.153771	-1.182924	-1.073602	H 0	1.540353	-0.817054	1.358738
C 0	-0.811600	-0.695420	-0.621726	H 0	0.798105	1.907160	0.118778
C 0	-0.726955	0.440600	0.118465	H 0	3.033446	-2.301214	-0.041941
C 0	-1.946302	1.258923	0.375644	H 0	3.356633	-1.821205	-1.754628
C 0	0.418350	-1.529005	-1.010276	H 0	4.364341	0.221974	-1.078987
C 0	1.701245	-0.704779	-0.764074	H 0	4.904841	-0.838389	0.261772
C 0	1.723686	-0.017194	0.600713	H 0	1.226130	-3.528607	-0.509427
C 0	0.575433	0.989055	0.708410	H 0	0.449600	-2.686931	0.881189
C 0	3.046715	-1.444688	-0.754453	H 0	-0.536885	-3.433449	-0.399324
C 0	4.006717	-0.379169	-0.209546	H 0	-0.343997	-2.593430	-2.830955
C 0	3.182210	0.484941	0.768952	H 0	1.389282	-2.317647	-2.836736
O 0	-5.160838	-2.394520	-0.961300	H 0	0.279537	-0.939694	-3.139797
O 0	-5.210256	-0.591327	-2.653045	H 0	0.121195	3.352685	1.842021
O 0	-2.303940	-2.233390	-1.689470	H 0	1.796973	2.823930	2.303191
O 0	-1.899789	2.355231	0.924745	H 0	0.464881	2.757979	3.511444
C 0	0.393249	-2.852656	-0.216720	H 0	4.432199	3.439615	0.016087
C 0	0.426730	-1.856385	-2.524689	H 0	5.317850	1.881980	0.234265
O 0	0.400728	1.293118	2.082033	H 0	4.567166	2.742738	1.665335
C 0	0.713501	2.624721	2.435158	H 0	3.525885	-0.766081	2.541619
O 0	3.228908	1.823441	0.368443	H 0	4.731433	0.519455	2.351628
C 0	4.455644	2.485543	0.589261	H 0	3.076291	0.926199	2.926754
C 0	3.651022	0.291659	2.217024				

Optimized Z-Matrixes of model B2

C 0	1.691375	6.065476	-0.339936	H 0	0.825454	7.861940	-0.887095
N 0	0.587819	6.880371	-0.594731	H 0	-1.132408	6.108502	-1.555228
C 0	-0.835051	6.491804	-0.551741	H 0	-1.439031	7.409669	-0.359897
C 0	-1.119475	5.459454	0.544105	H 0	-2.180620	5.120907	0.514922
S 0	-0.022550	4.054486	0.333983	H 0	-0.924824	5.912811	1.544690
C 0	1.600415	4.763442	0.045063	H 0	4.667658	1.685634	0.053354
C 0	2.825027	3.959016	0.251466	H 0	6.384881	1.907178	-0.253388
C 0	4.169878	4.613279	0.183794	H 0	5.191960	2.601461	-1.400339
C 0	4.250459	5.935631	-0.116772	H 0	6.303407	2.794923	2.267373
C 0	3.030016	6.692749	-0.513422	H 0	4.532911	2.874303	2.301744
C 0	5.412017	3.756320	0.475571	H 0	5.474765	4.349257	2.616249
C 0	5.403696	2.427861	-0.320468	H 0	6.566157	4.587956	-1.136804
C 0	5.440135	3.435131	1.984857	H 0	6.565063	5.912220	1.600701
C 0	6.659231	4.520054	-0.022649	H 0	5.751404	7.033528	-1.150760
C 0	6.704214	5.958181	0.492441	H 0	5.460519	9.952687	0.786782
C 0	5.542173	6.757332	-0.093579	H 0	5.107199	9.277811	-0.850239
O 0	5.347460	7.909754	0.708856	H 0	6.780292	9.156254	-0.147098
C 0	5.694635	9.125239	0.080342	H 0	8.475034	3.452969	-0.630840
C 0	8.060549	3.955941	0.274701	H 0	8.067050	3.202362	1.091536
C 0	8.930575	5.163621	0.668937	H 0	9.947021	5.105128	0.218730
C 0	8.154732	6.421915	0.243390	H 0	9.056964	5.161156	1.778784
C 0	8.441585	6.777073	-1.221109	H 0	8.093444	5.988991	-1.922863
O 0	8.406584	7.497461	1.100624	H 0	9.530925	6.884540	-1.419056
C 0	9.713907	8.024650	1.049042	H 0	7.955565	7.729428	-1.525368
O 0	-0.053199	3.312198	1.579748	H 0	9.885912	8.560734	0.090915
O 0	-0.443427	3.351184	-0.863270	H 0	10.474883	7.231651	1.209553
O 0	3.090221	7.824072	-0.984572	H 0	9.807819	8.770345	1.870232
O 0	2.681467	2.770994	0.521257				

Optimized Z-Matrixes of model B3

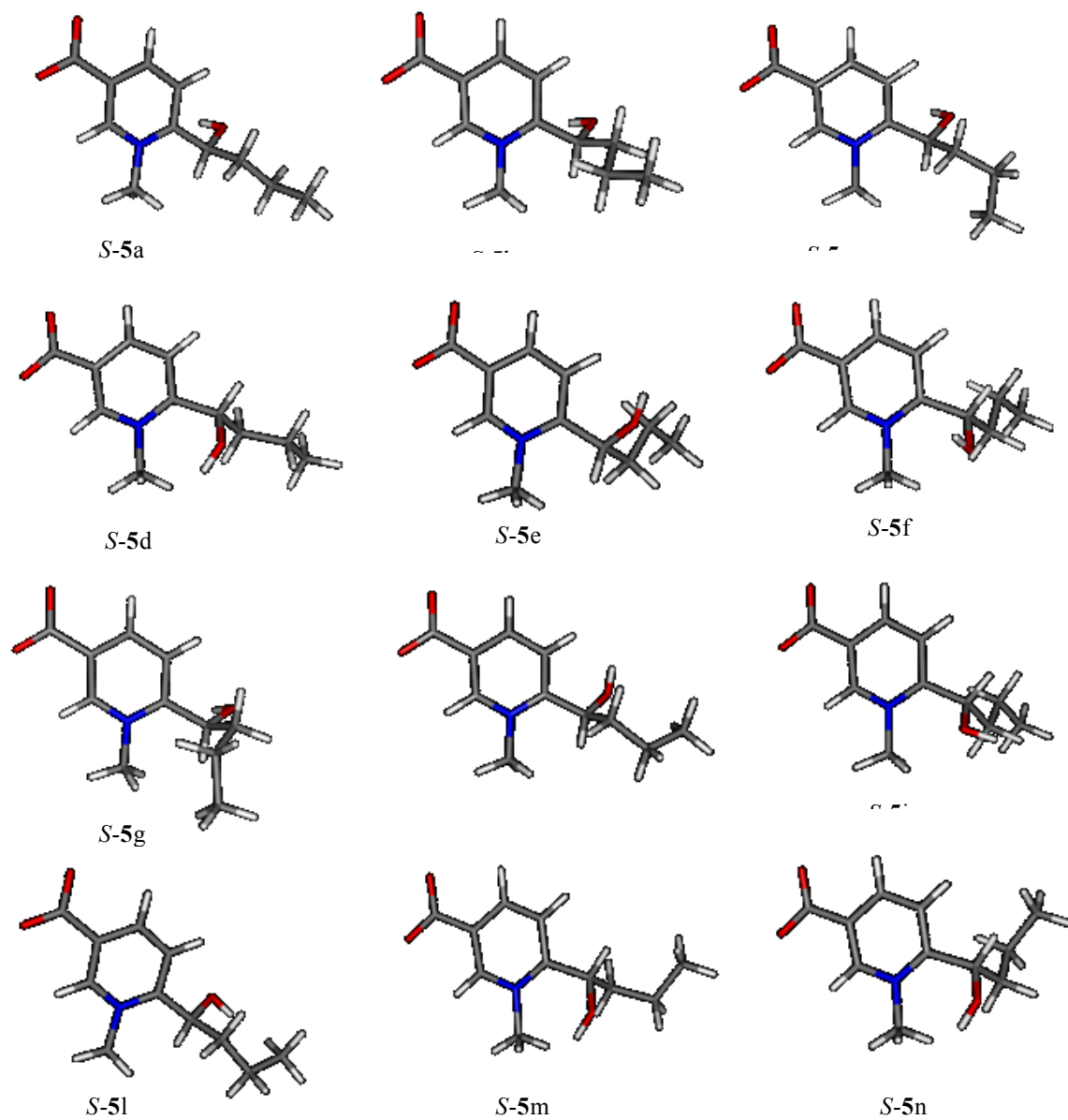
C 0	1.507815	6.107003	-0.075037	H 0	-0.885444	5.200465	-1.923811
S 0	0.024804	6.973224	-0.595343	H 0	-2.183704	6.130262	-1.078196
C 0	-1.169694	5.683828	-0.959284	H 0	-1.808534	3.788103	-0.112166
C 0	-1.149107	4.643803	0.165852	H 0	-1.547668	5.069273	1.116022
N 0	0.205577	4.114761	0.414116	H 0	0.298310	3.117501	0.733957
C 0	1.412300	4.809175	0.321515	H 0	5.993496	1.842775	-0.223290
C 0	2.642805	4.046883	0.675696	H 0	4.758051	2.626369	-1.262976
C 0	3.983087	4.657166	0.437948	H 0	4.292228	1.737156	0.222654
C 0	4.072073	5.974647	0.110582	H 0	4.547446	2.850492	2.504798
C 0	2.827195	6.770437	-0.126170	H 0	5.514200	4.325288	2.715640
C 0	5.212001	3.746230	0.590790	H 0	6.299509	2.776555	2.267552
C 0	5.047570	2.428435	-0.205746	H 0	6.229375	4.540228	-1.139242
C 0	5.408827	3.415266	2.086453	H 0	6.482985	5.882379	1.594223
C 0	6.428269	4.457469	-0.038770	H 0	5.518000	6.836473	-1.184801
C 0	6.567399	5.891116	0.481834	H 0	6.599719	8.950652	-0.853989
C 0	5.404993	6.711220	-0.083638	H 0	5.666106	9.989251	0.294827
O 0	5.419054	7.970542	0.560908	H 0	4.813519	9.150745	-1.057941
C 0	5.633752	9.059573	-0.315822	H 0	8.149697	3.406794	-0.896498
C 0	7.824266	3.823270	0.086492	H 0	7.880919	2.990822	0.819943
C 0	8.751793	4.974491	0.501441	H 0	9.768009	4.877120	0.063133
C 0	8.021452	6.280011	0.140600	H 0	8.882809	4.932381	1.609969
C 0	8.556138	7.443593	0.981680	H 0	9.664569	7.521091	0.914652
O 0	8.070783	6.526935	-1.234498	H 0	8.320654	7.307520	2.061116
C 0	9.286834	7.040137	-1.731700	H 0	8.132192	8.424454	0.681876
O 0	2.853831	7.954865	-0.443563	H 0	9.433974	8.091205	-1.401806
O 0	2.491593	2.911456	1.115295	H 0	9.219525	7.043936	-2.842907
O 0	0.250632	7.690773	-1.835534	H 0	10.148736	6.405147	-1.439357
O 0	-0.492254	7.737658	0.524104				

Optimized Z-Matrixes of model B4

C 0	1.418371	6.123099	-0.053290	H 0	-0.976211	5.192575	-1.868625
S 0	-0.049951	6.998227	-0.598557	H 0	-2.269374	6.170172	-1.070209
C 0	-1.262440	5.715305	-0.925376	H 0	-1.937902	3.862112	-0.014348
C 0	-1.263516	4.715090	0.235266	H 0	-1.656231	5.179338	1.169653
N 0	0.081997	4.171092	0.502070	H 0	0.157484	3.183568	0.855144
C 0	1.301394	4.839930	0.385285	H 0	5.869881	1.803846	0.020561
C 0	2.517579	4.063601	0.761185	H 0	4.612663	2.520400	-1.041036
C 0	3.868953	4.653254	0.538200	H 0	4.179594	1.714647	0.502566
C 0	3.974447	5.960106	0.181450	H 0	4.410112	2.979968	2.696744
C 0	2.749003	6.761564	-0.123132	H 0	5.409326	4.444073	2.824526
C 0	5.092138	3.747331	0.738694	H 0	6.162888	2.854350	2.465006
C 0	4.921308	2.385385	0.020797	H 0	6.069540	4.455873	-1.041100
C 0	5.285332	3.500923	2.249766	H 0	6.493258	5.863121	1.620776
C 0	6.302321	4.419367	0.053716	H 0	5.397687	6.958409	-1.038998
C 0	6.488427	5.867797	0.503203	H 0	6.657255	9.028665	-0.224372
C 0	5.302167	6.713881	0.042397	H 0	5.510354	9.925627	0.837501
O 0	5.266575	7.891884	0.830037	H 0	4.922855	9.240216	-0.727044
C 0	5.607152	9.070861	0.131522	H 0	7.959975	3.224405	-0.738104
C 0	7.695510	3.780995	0.191958	H 0	7.765431	3.055163	1.030965
C 0	8.673494	4.946736	0.423403	H 0	9.616841	4.813955	-0.152901
C 0	7.919037	6.235806	0.055360	H 0	8.944448	4.969452	1.506897
C 0	8.033096	6.532407	-1.445267	H 0	7.567325	7.504459	-1.718054
O 0	8.341613	7.317188	0.834331	H 0	7.551556	5.748279	-2.068052
C 0	9.661135	7.757608	0.600808	H 0	9.091965	6.565941	-1.784758
O 0	2.818937	7.921965	-0.516824	H 0	10.387071	6.922466	0.695532
O 0	2.346985	2.939943	1.223142	H 0	9.902627	8.519315	1.375746
O 0	0.184339	7.677361	-1.858753	H 0	9.742006	8.253004	-0.390496
O 0	-0.554469	7.802865	0.498266				

5.5. Computational details of compound 28

Minimum Energy Conformations for S-28



Conformational Analysis of *S*-28 conformers in methanol

	ΔE^a	ΔG^b	P% ^c
<i>S</i> -28a	0.00	0.00	45.75
<i>S</i> -28b	0.25	0.52	18.91
<i>S</i> -28c	0.79	0.69	14.29
<i>S</i> -28d	0.91	1.01	8.32
<i>S</i> -28e	1.05	1.25	5.55
<i>S</i> -28f	1.24	1.57	3.23
<i>S</i> -28g	1.26	1.62	2.97
<i>S</i> -28h	1.47	3.08	0.25
<i>S</i> -28i	1.47	3.08	0.25
<i>S</i> -28l	1.81	3.25	0.19
<i>S</i> -28m	1.81	3.25	0.19
<i>S</i> -28n	1.94	3.69	0.09

^aRelative energy (kcal/mol). ^bRelative Gibbs free energy (kcal/mol).
^cConformational distribution calculated at the at the B3LYP/6-31G(d) level in methanol.

Calculated ECD of S-28 at the B3LYP/6-31G**

